The Pennsylvania State University

The Graduate School

John and Willie Leone Family Department of Energy and Mineral Engineering

CONTINUOUS CO_2 INJECTION DESIGN IN NATURALLY FRACTURED RESERVOIRS USING NEURAL NETWORK BASED PROXY MODELS

A Dissertation in

Energy and Mineral Engineering

by

Hassan H. Hamam

Submitted in Partial Fulfillment
of the Requirements
for the Degree of

Doctor of Philosophy

August 2016

The dissertation of Hassan H. Hamam was reviewed and approved* by the following:

Turgay Ertekin
Head of John and Willie Leone Family Department of Energy and Mineral Engineering
Professor of Petroleum and Natural Gas Engineering
George E. Trimble Chair in Earth and Mineral Sciences
Undergraduate Program Chair of Petroleum and Natural Gas Engineering
Dissertation Advisor
Chair of Committee

Eugene Morgan
Assistant Professor of Petroleum and Natural Gas Engineering

Sanjay Srinivasan
Professor of Petroleum and Natural Gas Engineering
John and Willie Leone Family Chair in Energy an Mineral Engineering

Sridhar Anandakrishnan
Associate Professor of Geosciences

Luis F. Ayala
William A. Fustos Family Professor
Professor of Petroleum and Natural Gas Engineering
Associate Department Head for Graduate Education
FCMG Chair in Fluid Behavior and Rock Interactions

*Signatures are on file in the Graduate School

ABSTRACT

More than 60% of the original oil in place (OOIP) is left in the ground after the primary and secondary recovery processes. With the introduction of enhanced oil recovery (EOR), that number goes down to about 40% of the OOIP. Carbon dioxide (CO_2) injection is one of the most effective EOR methods in naturally fractured reservoirs. The fracture network provides a faster means for fluid flow due to its high conductivity but it is also the cause of premature breakthrough of the injected fluids. However, if employed efficiently, fractures can help push the injected CO_2 to the reservoir boundaries so that a large portion of the reservoir fluid interacts with the injected CO_2. Zones swept by miscible CO_2 reported the lowest residual oil saturation.

Continuous CO_2 injection is becoming more and more preferred to the popular cyclic pressure pulsing. Continuous CO_2 injection has no down time and could potentially provide better CO_2 interaction with the reservoir fluid which provides a higher recovery.

In this research, artificial neural networks (ANNs) are used to construct robust proxy models with highly predictive capabilities for naturally fractured reservoirs undergoing continuous CO_2 injection. The main purpose of this research is to shed more light and understanding on continuous CO_2 injection in naturally fractured reservoirs and provide a tool that empowers engineers to make decisions on the fly while evaluating uncertainty and mitigating risk rather than wait months or years to do so.

In light of the above, various ANN designs and configurations undergo development and evolution to ultimately be able to provide valuable insights regarding reservoir performance, history matching, and injection design for naturally fractured reservoirs undergoing CO_2 injection. Initial ANN designs targeted specific reservoirs using specific fluid compositions from the literature. The designed ANNs were able to provide predictions with a low degree of error. ANN designs went over many complex adjustments, variations, and enhancements until final

configurations were reached. The final ANN designs developed in this research surpass previously developed ANNs in similar projects with its capability to handle a huge range of reservoir properties, relative permeability, capillary pressure, and fluid compositions under uncertainty.

The reservoir simulation model used in this research is a two-well, two-layer, miscible compositional simulation model working in a dual-porosity system. Critical parameters affected the accuracy and predictability of the ANN designs and they were an essential part of the final ANN configurations. The parameters that a major effect on continuous CO_2 injection are reservoir fluid composition, fracture permeability, well spacing, bottomhole flowing pressure (BHFP), thickness, and CO_2 injection amount under miscible conditions had the highest impact on recovered oil.

The final ANN designs were encompassed inside a graphical user interface that equipped the ANN with uncertainty evaluation capabilities. The ease to use nature of the GUI allows anyone to use the developed ANNs in this research, as well as provide a simple intuitive interface to manipulate input data, run simultaneous sensitivity and uncertainty analysis.

The developed ANNs in this research bring us a step closer to achieving real-time simulation for naturally fractured reservoirs undergoing CO_2 injection. The correlations embedded in the ANNs were able to overcome reservoir fluid, relative permeability, and capillary pressure limitations that existed in the previous ANN studies.

TABLE OF CONTENTS

LIST OF FIGURES

APPENDIX F

APPENDIX G

LIST OF TABLES

APPENDIX H

APPENDIX I

NOMENCLATURE

A:	Drainage Area (Acres)
H:	Formation Thickness (ft)
I:	Characteristic Lengths
Lx:	Fracture spacing in the x-direction
Ly:	Fracture spacing in the y-direction
Lz:	Fracture spacing in the z-direction
K_{xm}:	Effective Matrix Permeability in the x-direction (Md)
K_{ym}:	Effective Matrix Permeability in the y-direction (Md)
K_z:	Effective Matrix Permeability in the z-direction (Md)
K_f:	Fracture Permeability (Md)
K_m:	Matrix Permeability (Md)
Kr:	Relative Permeability
Kro:	Relative Permeability to Oil
Krwiro:	Relative Permeability to Water at Irreducible Oil
Krocw:	Relative Permeability to Oil at Connate Water
Krogcg:	Relative Permeability to Oil at Connate Gas
Krgcl:	Relative Permeability to Gas at Connate Liquid
MC_{5+} :	Molecular weight of C5+
n:	Set of Normal Fractures
Ng:	Exponent for Calculating Krg
Now:	Exponent for Calculating Krow
Nog:	Exponent for Calculating Krog

Nw:	Exponent for Calculating Krw
P:	Reservoir Pressure (Psia)
Pc:	Capillary Pressure (Psia)
$P_{CO2\text{-}LO}$:	Minimum miscibility pressure for CO2 with a live oil
Pcew:	Entry Capillary Pressure Oil Water (Psia)
Pcog:	Oil Gas Capillary Pressure (Psia)
Pcow:	Oil Water Capillary Pressure (Psia)
Sg:	Gas Saturation (Fraction)
Sgcon:	Connate Gas Saturation (Fraction)
Sgcrit:	Critical Gas Saturation (Fraction)
Sl:	Liquid Saturation (Fraction)
So:	Oil Saturation (Fraction)
Soirg:	Irreducible Oil Saturation for Gas-Liquid Table (Fraction)
Soirw:	Irreducible Oil Saturation for Water-Oil Table (Fraction)
Sw:	Water Saturation (Fraction)
Sorg:	Residual Oil Saturation for Gas-Liquid Table (Fraction)
Sorw:	Residual Oil Saturation (Fraction)
Swcrit:	Critical Water Saturation (Fraction)
Swcon:	Connate Water Saturation (Fraction)
S_w^*:	Normalized Water Saturation.
T:	Reservoir Temperature (^{o}Fahrenheit)
TR:	Alston's Reservoir temperature in ^{0}F
t:	Time (Days)
X_{vol}:	The oil volatile fraction, C1 and N2.
X_{int}:	The oil intermediate fraction, C2, C3, C4, CO_2, and H_2S.

Greek:

ϕ_f:	Fracture Porosity (Fraction)
ϕ_m:	Matrix Porosity (Fraction)
ω:	Acentric Factor
ɣ:	Parameter related to pore size distribution.
Ϭ:	Shape Factor

Abbreviations:

ANN:	Artificial Neural Networks
BBL:	Barrels
BHFP:	Bottomhole Flowing Pressure
CO_2:	Carbon Dioxide
CP:	Critical Pressure
CT:	Critical Temperature
EOR:	Enhanced Oil Recovery
EOS:	Equation of State
FCM:	First Contact Miscibility
H_2S:	Hydrogen Sulfide
MCM:	Multiple Contact Miscibility
MMP:	Minimum Miscibility Pressure (Psia)
MW:	Molecular Weight
N_2:	Nitrogen
OOIP:	Original Oil In Place
PI:	Initial Reservoir Pressure
SCF:	Standard Cubic Feet
SG:	Specific Gravity

STB:	Stock-Tank Barrels
WAG:	Water Alternating Gas

ACKNOWLEDGEMENTS

I thank GOD Almighty, for all the countless blessings, strength, protection, and guidance HE grants me every single day of my life. I thank my amazing parents, Hasan and Fawzeyah, who served as my role models and continued to push me and support me throughout all my life.

I would like to express my deep appreciation and gratitude to my advisor, Professor Turgay Ertekin for giving me the opportunity to work with him. I would like to thank him for opening a new door to me and providing me with guidance and support academically and personally. I am honored to have worked with him.

I would like to extend my gratitude to Professor Eugene Morgan, Professor Sanjay Srinivasan, and Professor Sridhar Anandakrishnan who served as my committee members and provided help and guidance.

I would like to express my thanks to Saudi Aramco for aiding me in getting the best education in my Bachelor, Masters, and PhD programs.

I dedicate this work to my wife Roaa who followed me everywhere and provided me with unconditional love and support, and my kids, Abdulelah, Maan, Miral, and Mayar.

Chapter 1

INTRODUCTION

In the past decade, the world witnessed a technology leap that continues to grow and evolve every single day. This jump in technology has changed the way we do things in all aspects of life. Enhanced oil recovery (EOR) methods have become the main focus for the oil and gas industry lately. While there are many different types of EOR techniques, the success of these projects depends on careful consideration and evaluation of their design.

Carbon Dioxide (CO_2) injection is a popular EOR technique when it comes to fractured reservoirs. Continuous CO_2 injection has yet to show its full potential due to it being overshadowed by cyclic pressure pulsing. Continuous CO_2 injection is the less popular and less researched form of CO_2 injection.

Conventional oil reservoirs go through different recovery techniques that are applied to accommodate reservoir changes and maximize recovery. There are three main recovery methods; primary, secondary, and enhanced. During primary recovery, natural drive mechanisms, such as solution gas drive, gas cap drive, and gravity drainage, are responsible for releasing the reservoir's natural energy to produce oil. Primary recovery method has a unique pressure decline signature at the start of the field production. Secondary recoveries are employed when natural drive mechanisms are exhausted and there is not enough energy to produce the hydrocarbons. This method depends on the injection of a fluid to re-pressurize the reservoir using an artificial drive. Enhanced oil recovery (EOR), also known as tertiary oil recovery, is then used to recover more hydrocarbons as a last resort.

In the recent years, EOR methods have become very important due to their major contribution to recovery and the number of fields going through this stage. While there are different techniques, careful and thorough studies must be conducted in order to choose the most appropriate way to maximize recovery. CO_2 flooding is one of the most important EOR methods. It basically depends on injecting CO_2 in the reservoir under miscible or immiscible conditions which would then interact with the reservoir fluid and enhance its mobility. The most popular form of CO_2 injection is cyclic pressure pulsing, also known as huff 'n' puff. Another important, but less used, CO_2 injection technique is the continuous CO_2 injection. It is often less used due to the amount of CO_2 required to be injected during the project duration. Continuous CO_2 injection undergoes one stage with no down-time unlike cyclic pressure pulsing that typically requires three stages and have extensive down-time. The process is described by a dedicated injector that continuously injects CO_2 while a dedicated producer is on full production from the other end as can be seen in Figure 1-1. Many projects have shown that continuous CO_2 injection can be very rewarding especially when alternating with water in a process called Water Alternating Gas (WAG). WAG was initially a method proposed to improve gas injection sweep. The first CO_2 injection application was in the 1950s, while the first WAG application was reported from Canada in 1957 (Christensen et al., 1998).

The purpose of this study is not to approve or disapprove of which EOR method or CO_2 injection method is better than the other. While this EOR method will definitely and absolutely not work for significant types of reservoirs and reservoir fluids, it would be very beneficial to know how, when, and where it might work. This can be done through the coupling of smart technology and EOR techniques. One of the products of this coupling is a tool that is capable of providing decisions on the fly that conventionally takes months or years to make. In this dissertation, a comprehensive research is conducted on the performance of continuous CO_2 injection in naturally fractured reservoirs, its applicability, and limitations.

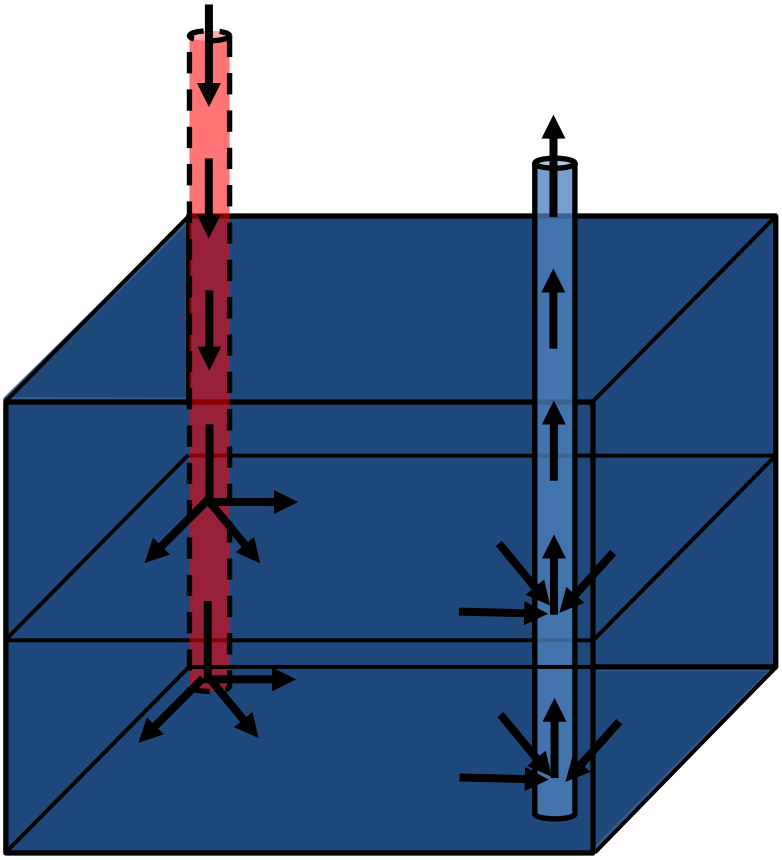

Figure 1-1: Conceptualized continuous CO_2 injection model in this study

The chapters of this dissertation are prepared in a sequential order as the following:

- In Chapter 2, a literature review is conducted to highlight the most important milestones around carbon dioxide injection, continuous carbon dioxide injection, naturally fractured reservoirs, and artificial neural networks.
- Chapter 3 describes the problem statement and the scope of this research.
- Chapter 4 explains the artificial neural networks theory and the back propagation algorithm used in this research.

- Chapter 5, detailed methodology is described in this section regarding all the components in this research from data generation and validation to constructing the artificial neural network models.
- Chapter 6 contains detailed descriptions about all the variables used to construct the various artificial neural networks in this research.
- Chapter 7 shows the development of the artificial neural networks starting from very basic artificial neural network designs to very complicated ones. Also, full details and description about each design is included as well as the blind testing results.
- Chapter 8 shows a step by step reservoir mechanism analysis for a sample case along with plots and illustrations of the mechanism in the particular example and expected artificial neural network behavior in terms of reservoir performance.
- Chapter 9 describes the graphical user interface (GUI) and provides a quick guide on how to use the GUI for any of the developed ANNs.
- Chapter 10 contains discussion and concluding remarks about this work as well as future work suggestions for enhancements.

Chapter 2

LITERATURE REVIEW

EOR recovery methods are implemented when primary and recovery methods are exhausted in order to recover as much additional production as possible. While there are many EOR methods with different mechanics, CO_2 injection is considered to be one of the most important ones. The aim behind CO_2 injection is basically to lower oil viscosity due to interaction between CO_2 and the reservoir fluid. CO_2 injection is not new as there are studies done using CO_2 injection as a mean to improve mobility dating back to 1950s. Different CO_2 injection methods were used in different scenarios such as cyclic pressure pulsing, and continuous CO_2 injection. This chapter covers previous CO_2 injection studies as well as other relevant components that are crucial to this project from 1950s until today.

2.1 Continuous Carbon Dioxide (CO_2) Injection

Since its initial use back in the early 1950's and its wide growth between the 1970s and 1980s, field and laboratory experiments have proven the strong applicability of carbon dioxide as a major displacement component (Murray et al., 2001). Carbon dioxide injection encompasses different ways to inject CO_2 to improve mobility during tertiary recovery, each with its own unique mechanism and applications. Cyclic pressure pulsing depends on injecting CO_2 for a specific period of time and then shut-in, followed by production from the same injection well and so forth. CO_2 could also be injected continuously from one well while a dedicated producer is on production throughout the whole process. Continuous CO_2 injection is sometimes alternated with water in a method known as water alternating gas (WAG) and all gas injection methods in general could be done under either miscible or immiscible conditions.

Cyclic pressure pulsing has been the most popular method of CO_2 injection than continuous injection for various reasons such as not requiring large amount of carbon dioxide. However, many studies in the literature have shown that continuous CO_2 injection is better in certain scenarios. So, when designing a CO_2 EOR project, it is very important to evaluate all the factors equally. Zhou et all, showed that cyclic CO_2 injection performed better for tight formations and required relatively low investment while continuous CO_2 injection has higher recovery at early stages but was highly situational due to the high amount of CO_2 it requires. (Zhou et al., 2012)

In the 1960's, CO_2 was used as a way to improve water flooding displacement efficiency in highly fractured reservoirs. The importance of CO_2 as an injected fluid appears at high reservoir pressure and temperature where CO_2 is injected in a critical state to mix with the reservoir fluid and form a single low viscosity and low interfacial tension fluid. Since CO_2 has higher mobility than water and oil, it can contact areas that were previously bypassed by previous primary and secondary recovery methods. Surguchev et al. (1992) reported that swept residual oil zones are the lowest when displaced by miscible injected gas thus leading to high oil recoveries.

In 1964, a pilot test by Holm and O'Brien (1970) reported 53%-82% more oil production using a large slug of CO_2 alternating with carbonated water. The first CO_2 commercial EOR project, and the world's largest miscible project, was initiated in January 1972 at Snyder Field in Scurry County in West Texas. (Langston et al., 1988).

Since its remarkable success back then, the number of CO_2 projects has been growing progressively and many applications and techniques were developed for different conditions.

2.2 Miscibility

Miscibility is considered as the key phenomenon when it comes to carbon dioxide injection. Surguchev et al. (1992) referred to the pressure of the maximum curvature on an oil recovery vs

pressure plot as miscibility, while Holm (1986) described miscibility as “the ability of two or more substances to form a single homogenous phase when mixed in all proportions”. Miscibility between fluids could be achieved by either first contact miscibility (FCM) or multiple contact miscibility (MCM). When an injected fluid mixes in all proportions with another fluid to form a single mixture, then the process is called FCM. The process is called MCM when the fluids require more mixing before they become miscible. Otherwise, if the fluids don’t mix at all, the process is called immiscible.

Miscibility has a huge impact on the success of EOR projects. EOR miscible injection projects reported very high oil recoveries in contrast to immiscible injection where large amounts of residual oil remained. There are four types of miscibility that could develop inside the reservoir between the injected fluid and the reservoir fluid:

1) First Contact Miscibility Injection
2) Dynamic Miscibility Injection due to Vaporizing Drive (MCM)
3) Dynamic Miscibility Injection due to Condensing Drive (MCM)
4) Immiscible Injection

2.2.1 First Contact Miscibility

An injection process is called first contact miscible when injected gas mixes with the reservoir fluid at all proportions and forms a single mixture. Figure 2-1 shows an illustration on a ternary diagram for a first contact miscibility process where injected gas has pure 100% light component. Typically, first contact miscibility occurs at high reservoir temperature and pressures.

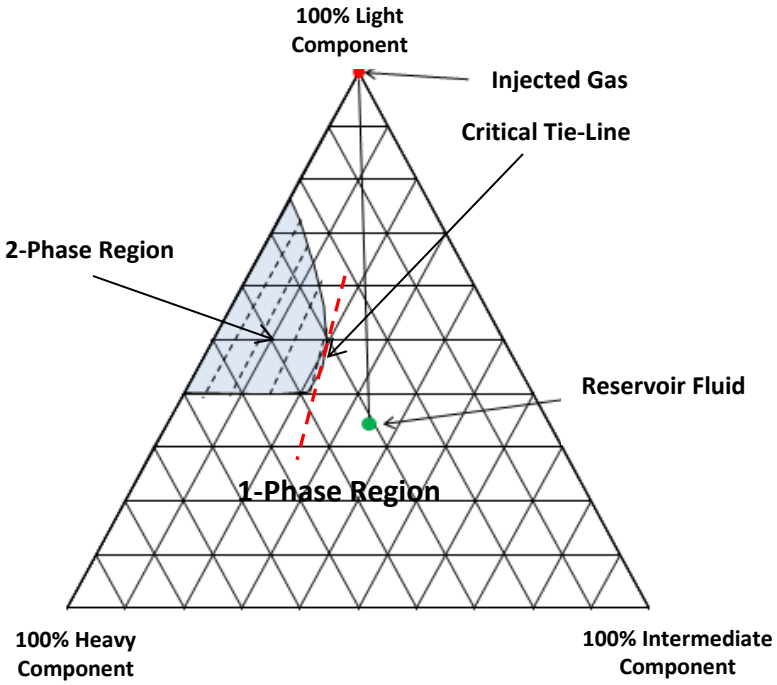

Figure 2-1: First Contact Miscibility

2.2.2 Dynamic Miscibility Due to Vaporizing Drive (Multiple Contact Miscibility)

Multiple contact miscibility occurs when the fluids require more mixing before they become miscible. For multiple contact miscibility due to vaporizing drive miscibility, reservoir fluid has to fall on the right hand side of the critical tie line on the ternary diagram. The injected gas at the trailing edge mixes with the reservoir oil at the leading edge. This partial mixture has a new vapor composition (V1) and new liquid composition (O1). Since vapor has very high mobility, V1 goes

to the leading edge while O1 lags behind at the trailing edge. Now, at the leading edge, the new vapor composition mixes with reservoir oil to and forms a newer partially mixture with vapor composition (V2) and liquid compositions (O2). The process repeats itself until a vapor composition becomes miscible with the reservoir oil at the leading edge, figure 2-2. Figure 2-3: Vaporizing Drive Miscibility shows a typical multiple contact miscibility due to vaporizing gas drive on a ternary diagram.

Trailing Edge			**Leading Edge**		
Injected Gas (IG)	+		Reservoir Fluid (RF)		
IG +	(O1	+ V1)	+ RF		
	+	(O2	+	V2) + RF	
	+		+	(O3 +	V3) + RF
	+		+		(Oc + **Vc) + RF**

Figure 2-2: Multiple contact miscibility due to vaporizing drive

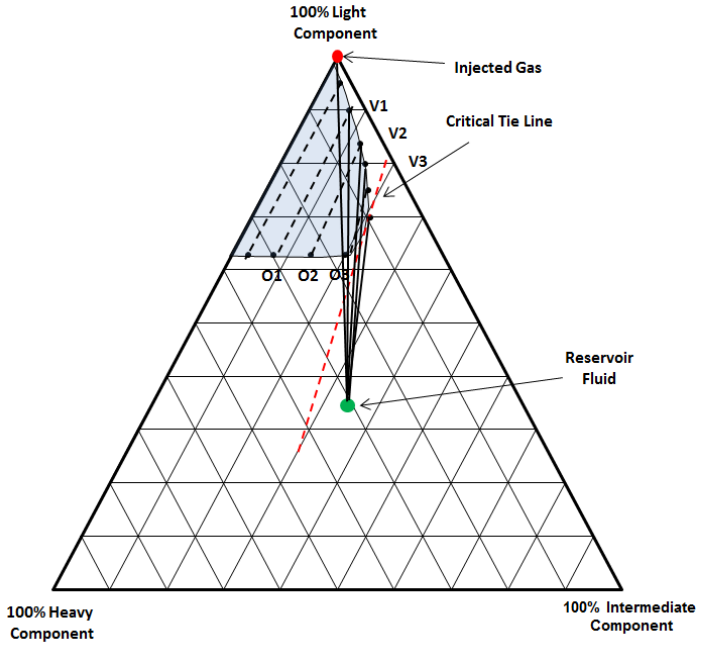

Figure 2-3: Vaporizing Drive Miscibility

2.2.3 Dynamic Miscibility Due to Condensing Drive (Multiple Contact Miscibility)

In multiple contact miscibility due to condensing drive, injected fluid falls on the right hand side of the critical tie line on the ternary diagram. The injected gas at the trailing edge mixes with the reservoir oil at the leading edge. This partial mixture has a new vapor composition (V1) and new liquid composition (O1). Since it has very high mobility, V1 goes to the leading edge while O1 lags behind at the trailing edge. With additional injection, Injected gas at the trailing edge mixes with the partial mixture liquid composition O1 which leads to a newer partial mixture with newer vapor (V2) and liquid compositions (O2). The process repeats itself until a liquid composition becomes miscible with the injected gas at the trailing edge, Figure 2-4. Figure 2-5 shows a typical multiple contact miscibility due to condensing gas drive on a ternary diagram.

Note: One of the major differences between vaporizing drive and condensing drive multiple contact miscibility is where the mixing happens. In vaporizing drive, the mixing happens at the leading edge between the partial mixture vapor composition and the reservoir fluid. While in condensing drive, the mixing happens at the trailing edge between the injected gas and the partial mixture liquid composition.

Trailing Edge			**Leading Edge**			
Injected Gas (IG)	+	Reservoir Fluid (RF)				
IG +	(O1 +	V1)	+ RF			
IG+	(O2 +	V2)	+	+ RF		
IG+	(O3 +	V3)	+	+	+ RF	
IG+	(Oc +	Vc)	+	+	+	**+ RF**

Figure 2-4: Multiple contact miscibility due to condensing drive

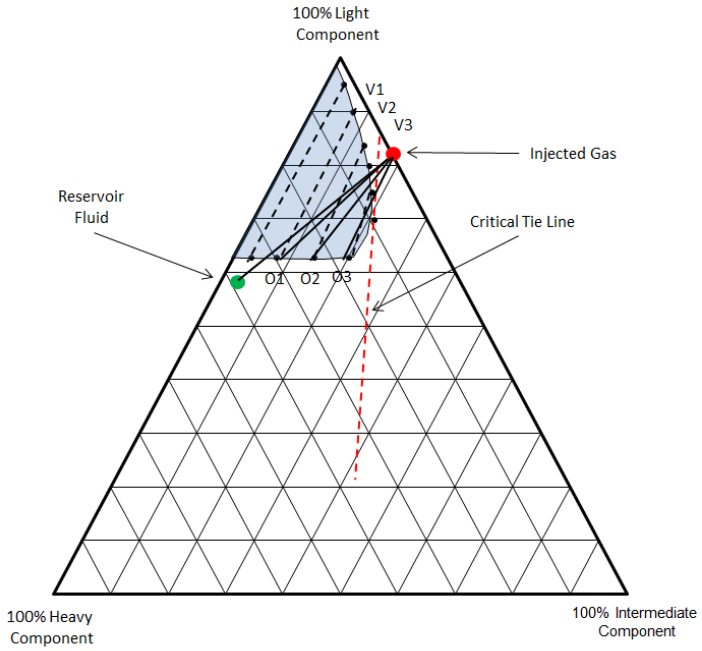

Figure 2-5: Condensing Drive Miscibility

Minimum Miscibility Pressure Determination

Experimentally, there are many tests that are used to determine miscibility behavior such as raising bubble and slim tube experiments. Raising bubble experiment depends on the visual observation of the disappearance between fluids to determining miscibility. In slim tube experiment, a 40 feet spiral tube is filled with glass beads or some other materials and then saturated with reservoir oil. CO_2 is then injected at various incremental pressure steps while recording oil recovery at every pressure after injecting 1.2 PV of CO_2. Oil recovery is then plotted against injection pressure. Miscibility is then determined as the break over point on the plot (Orr, 1982).

Outside the traditional laboratory experiments, Mogensen et al (2009) divided MMP determination methods into:

1) Empirical correlations.

2) 1D compositional simulation.
3) Analytical gas flooding theory based on the method of characteristics combined with key-tie-line.
4) Mixing-cell models.

Empirical Correlations typically use temperature, plus fraction molecular weight, and light component mole fraction. Cronquist (1977) used C5+ as the main parameter to determine MMP while Yellig and Metcalfe (1980) developed a temperature based correlation. Johnson and Pollin (1981) focused on injected gas properties in their correlation while Yuan et al. (2005) had more emphases on the intermediate components C_2-C_6.

The analytical solution provided by the method of characteristics (MOC) defines the path between the injection composition and the reservoir fluid composition (Orr, 2007). In a multi-component system, the key tie-line method was developed by Johns and Orr (1996), Wang and Orr (1997) and Jensen et al. (1998). The key tie-line method depends on three types of key tie-lines (Mogensen et al, 2009):

1) Tie-line through the initial reservoir fluid composition
2) Tie-line through initial injection composition.
3) Crossover tie-lines.

Ahmadi and Johns (2008) extended their previous MOC and came out with the mixing-cell models.

2.3 Naturally Fractured Reservoirs

Naturally fractured reservoirs constitute the majority of oil and gas reservoirs in the world. Although fractures provide major highways for fluid flow, the impact of their existence is yet to

be fully understood. Nelson (2001) defined a reservoir fracture as "*a naturally occurring macroscopic planar discontinuity in rock due to deformation or physical diagenesis*". The formation of fractures through brittle or ductile rock failure plays a major positive or negative effect on fluid flow (Nelson, 2001). While a very large percentage of hydrocarbon reservoirs are fractured, not all fractured reservoirs act as fractured reservoirs. For a reservoir with naturally occurring fractures to be qualified as a fractured reservoir, the fractures must have a significant impact on fluid flow (Nelson, 2001).

Barenblatt et al. (1960) introduced the dual-porosity model in 1960 to model matrix and fracture flow using transfer functions. Warren and Root then introduced the famous Sugar-Cube-Model, which is an idealized version of Barenblatt's work (Warren and Root, 1963), Figure 2-6. Warren and Root described their shape factor as:

$$Warren\ \&\ Root\ Shape\ Factor\ \sigma = \frac{4n(n+2)}{I^2}$$

Where:

σ is the Shape Factor

I is the characteristic lengths

n is the set of normal fractures

In 1976, Kazemi et al. suggested a modification to the Sugar-Cube-Model to account for two-phase flow which Thomas et al. (1983) extended to a three-phase model. Kazemi's shape factor is described by:

$$Kazemi's\ Shape\ Factor\ \sigma = 4\left[\frac{1}{L_x^2} + \frac{1}{L_y^2} + \frac{1}{L_z^2}\right]$$

Where:

σ is the Shape Factor

Lx is the fracture spacing in the x-direction

Ly is the fracture spacing in the y-direction

Lz is the fracture spacing in the z-direction

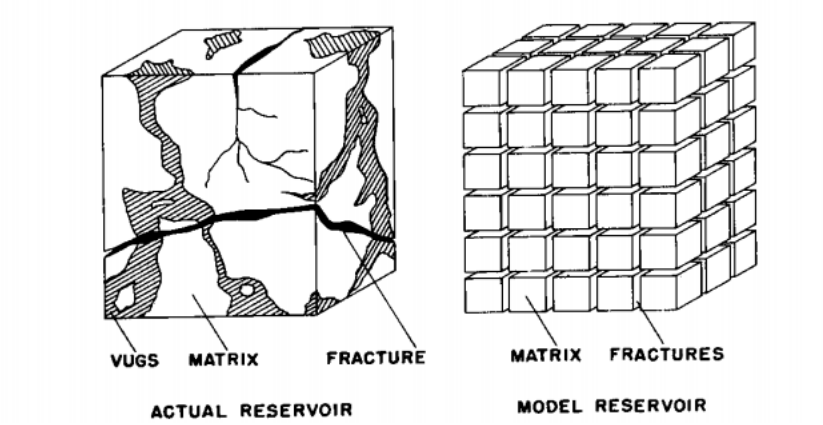

Figure 2-6: Warren and Root Sugar-Cube-Model (Warren and Root, 1963)

Most of the recent studies are an extension of the work that was initiated by Barenblatt back in the 1960's. Dykhuizen (1990), Zimmerman et al. (1993), and Sarma and Aziz (2004) introduced modifications to improve the fluid flow between the matrix and the fracture among a few others. Fractures in a fractured reservoir affect every recovery stage. They provide high permeability zones that very often cause anomalies and unexpected reservoir performance. That is one of the mains reasons why naturally fractured reservoirs are generally not considered to be good candidates for EOR. The complications added by the fractures and the fracture network highly impacts the fluid performance allowing fluids to breakthrough much earlier than desired and lower the sweep efficiency. However, with proper modeling and understanding of fractures, they could improve the efficiency of CO_2 injection by providing a large contact surface for the injected gas.

2.4 Artificial Neural Networks (ANNs)

Artificial neural networks first saw the light with the coupling of neurophysiological knowledge and networking. They are intelligent systems that were created in an attempt to mimic the biological nervous system through transmitting impulses and signals between cell bodies. These biological systems differ between living organisms, for example, humans have very complex neural networks compared to other organisms. The human brain contains an average of 100 billion neurons that are interconnected through synapses. A biological neuron consists of (Mohaghegh, 2000):

- Cell body
- Axon: Carry cell bodies signals.
- Synaptic connections
- Dendrites

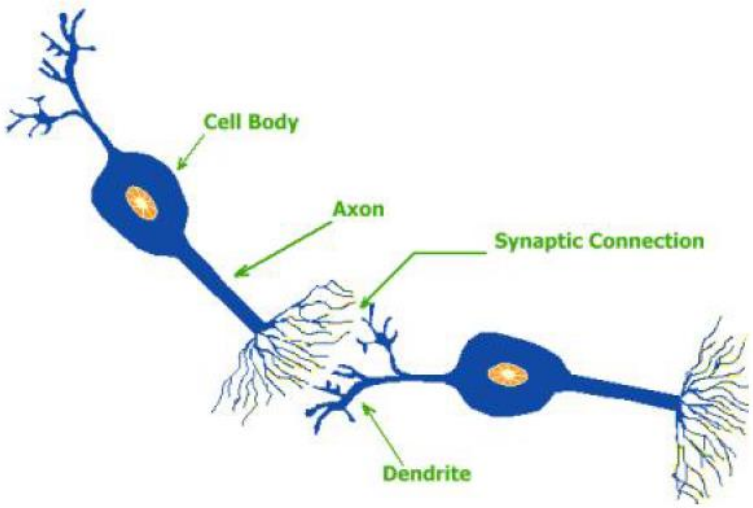

Figure 2-7: A biological Neuron as illustrated by Mohaghegh (2000).

Artificial neural networks are different than regular networks and simulation algorithms. One striking difference between ANNs and regular networks is that ANNs work without any regard to the system or the process in a model best known as black box. What that means is that only inputs

and outputs matter to the ANN without needing any other piece of information (Graupe, 2007). Typical algorithms follow a sequential approach, while ANNs excel in that area as they follow a parallel method. Parallel methods are better, faster, and are very forgiving where mistakes can be adjusted without stopping and repeating the whole process like sequential methods (Graupe, 2007).

2.5 Carbon Dioxide Injection Artificial Neural Networks

There are a limited number of CO_2 ANN projects in the literature. Surguchev et al. (2000) provided a basic screening tool for EOR processes. In his study, only 12 input parameters were studied for gas injection, steam injection, and cyclic water flooding. Parada (2008) created an ANN based tool-box for screening and designing IOR methods. One of the methods inside the tool-box was miscible CO_2 injection. Artun (2008) designed a CO_2 and N_2 cyclic pressure pulsing (huff''n'puff) tools in fractured reservoirs using ANN. Artun's work was followed closely and his work marks the starting point for this research but using a different CO2 injection technique.

Chapter 3

PROBLEM STATEMENT

Enhanced oil recovery projects such as continuous CO_2 injection and Water Alternating Gas (WAG) injection are often considered to be not very good candidates in naturally fractured reservoirs. That is because of the early breakthrough of injected fluids due to poor implementation in the highly conductive fracture system. While that is not always true, it remains a major concern when conducting such projects. For any CO_2 injection project, miscibility plays the main role in determining the injection method and all the injection design parameters.

To have a successful EOR design, major efforts and through investigation are to be fully utilized. For any continuous CO_2 or WAG project, the following questions should be addressed in the early stages of the project. Is it going to be a miscible or immiscible gas injection as the mechanisms are completely different in both designs. What amounts of gas to inject, or gas and water in case of WAG, and what is the water to gas ratio as well as deciding whether these gas and water amounts are fixed or vary per month.

It is the responsibility of the reservoir engineer to study each of the parameters and design an appropriate design that is economically viable and fits the project appropriately. Reservoir engineers normally study all the available recovery techniques for a particular reservoir ahead of time. Then, based on the reservoir unique characteristics some methods are excluded and the other methods are extensively exhausted. A cheap and very effective method to do that is through numerical reservoir simulators.

Reservoir simulators have become the first step in any study regardless of its purpose. Consistent and representative simulation models that are thoroughly constructed always yield better reliable answers than those that are poorly built. Various analysis and designs are tested using the reservoir simulation model, and then an efficient design is suggested. For full field scale models,

it is often very difficult to explore every single possible scenario due to time, computational power, and human power limitations.

Artificial neural networks are capable of correlating inputs and outputs and finding non-linear relations through complicated systems. For that reason, ANNs are often used to overcome the heavy computational requirements through proxy-models. However, developing a reliable robust proxy model that is capable of mimicking full field models requires careful design, development, and optimization of the best scenario that would maximize efficiency.

In this study, proxy-based models are designed and used for continuous CO_2 and WAG injection. Keeping that in mind, the aim of this research is to gain good understanding of continuous CO_2 injection in naturally fractured reservoirs as well as concluding if and when continuous CO_2 injection is the answer. Also, an optimized universal proxy-model for continuous CO_2 and WAG injection using ANN would be provided for certain reservoirs and fluid compositions.

Chapter 4

ARTIFICIAL NEURAL NETWORKS THEORY

Every system faces challenges of various natures and shapes. The best way to overcome these challenges is through disintegrating it into smaller parts. Hence, networks and networking come into play. Every network, regardless of its nature, consists of nodes and connectors. The nodes typically get the inputs and process them to compute outputs while connectors basically carry everything between nodes in different directions. Figure 4-1 shows a simple illustration of a network consisting of nodes and connectors.

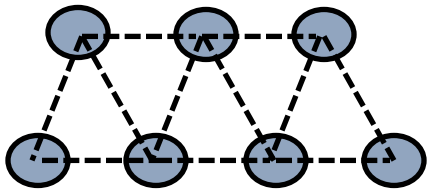

Figure 4-1: A Simple Network of Nodes and Connectors

Artificial Neural Networks are considered superior networks due to their powerful adaptive capabilities. The ANN nodes are conceived as artificial neurons, hence the name.

The ANN strength lies in the fact that they learn from data and then use what they learn which makes ANNs intelligent systems. ANN capabilities include describing a system by a set of inputs and outputs without needing any information about the system itself and this is called a black box, Figure 4-2.While a lot of researchers do not like the black box model idea, this is a very powerful tool. This means that, any number of inputs of a specific system can be used to relate any number of outputs of a different system that have no connection whatsoever. However, such ANN mapping have no use at all. For example, an ANN can be built using inputs from a phone's

component and outputs from an oil well as long as inputs and outputs are described in numbers. The ANN will not distinguish between any specification of any input or output; it only tries to find relationships between them. Also, the outputs don't have to look like or behave in any specific way. ANN's capabilities in drawing non-linear and complex relationships made them the tool of the decade.

Figure 4-2: Black Box Model Concept

Since artificial neurons were inspired from the biological nervous system, the way it works also tries to mimic a biological neuron but in a much basic way. So, an artificial neuron works by receiving inputs (inputs could be outputs coming from another artificial neuron) these inputs are then multiplied by weight functions and then summed. Now, on the inside of the artificial neuron, the previous summation is then processed through an activation function and transferred as an output to another artificial neuron (Gershenson, 2014).

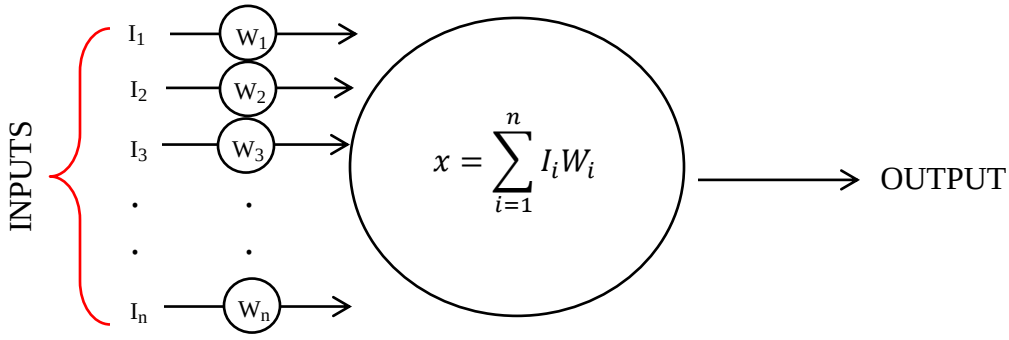

Figure 4-3: A Feedforward Typical Artificial Neuron Mechanism

Typically, any ANN has three components: architecture (connection design between neurons), inputs weights method (also known as the training algorithm), and the activation functions (or transfer functions). Table 4-1 shows the most common transfer functions used in ANN.

Table 4-1: Common Transfer Functions in Artificial Neural Networks (Hagan et al., 1996)

Name	Function
Hard Limit	$a = 0 \quad n < 0$ $a = 1 \quad n \geq 0$
Symmetrical Hard Limit	$a = -1 \quad n < 0$ $a = +1 \quad n \geq 0$
Linear	$a = n$
Saturating Linear	$a = 0 \quad n < 0$ $a = n \quad 0 \leq n \leq 1$ $a = 1 \quad n \geq 0$
Symmetric Saturating Linear	$a = -1 \quad n < -1$ $a = n \quad -1 \leq n \leq 1$ $a = 1 \quad n \geq 1$
Log-Sigmoid	$a = \frac{1}{1 + e^{-n}}$
Hyperbolic Tangent Sigmoid	$a = \frac{e^{n} - e^{-n}}{e^{n} + e^{-n}}$
Positive Linear	$a = 0 \quad n < 0$ $a = n \quad n \geq 0$
Competitive	$a = 0$ neuron with max n $a = n$ all other neurons

It is important to note that any basic ANN, there are input neurons forming the input layer, hidden neurons engulfed in the hidden layer, and output neurons displaying the output layer. In many advanced systems, there could be more than one hidden layer in the middle each with its separate neurons. Figure 4-4 shows a system with an input layer, 2 hidden layers each with different number of neurons, and an output layer.

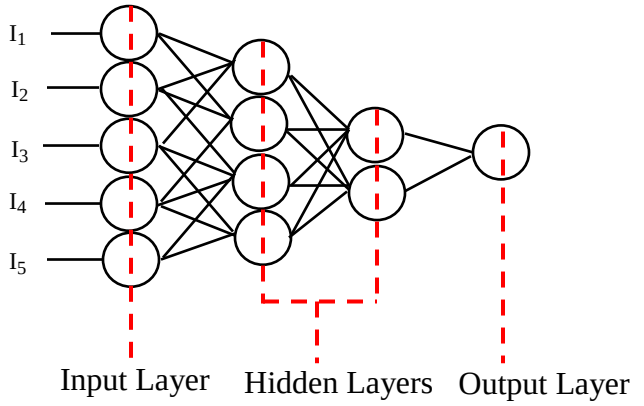

Figure 4-4: An ANN with Two Hidden Layers

Artificial Neural Networks Mathematical Model

Nielsen (2015) provided an overview of the simple mathematical models as well as advanced ANN concepts in his online book.

The concept of artificial neurons were developed back in the 1950s-1960s by Frank Rosenblatt were they were known as perceptrons (Nielsen, 2015). A perceptron produces a simple input by using several inputs.

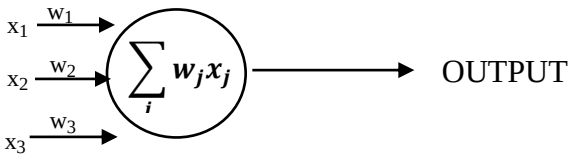

Figure 4-5: Basic Perceptron

Rosenblatt calculated the output by introducing weights to each of the inputs based on their importance. The output of the artificial neuron would be either 0 or 1 and is assigned based on the value of the weighted sum of the inputs and their respective weights in relation to a predefined value known as the threshold value (Nielsen, 2015).

$$if \sum_j w_j x_j \leq Threshold \rightarrow Output = 0$$

$$if \sum_j w_j x_j > Threshold \rightarrow Output = 1$$

The basic perceptron's mathematical model makes decisions by weighing up all the provided inputs. The perceptron's mathematical model can be applied to real life situations (Nielsen, 2015).

In feed-forward configurations, there is no way to calibrate the weights other than starting over with new weights and manually adjust the new weights.

Perceptrons Network

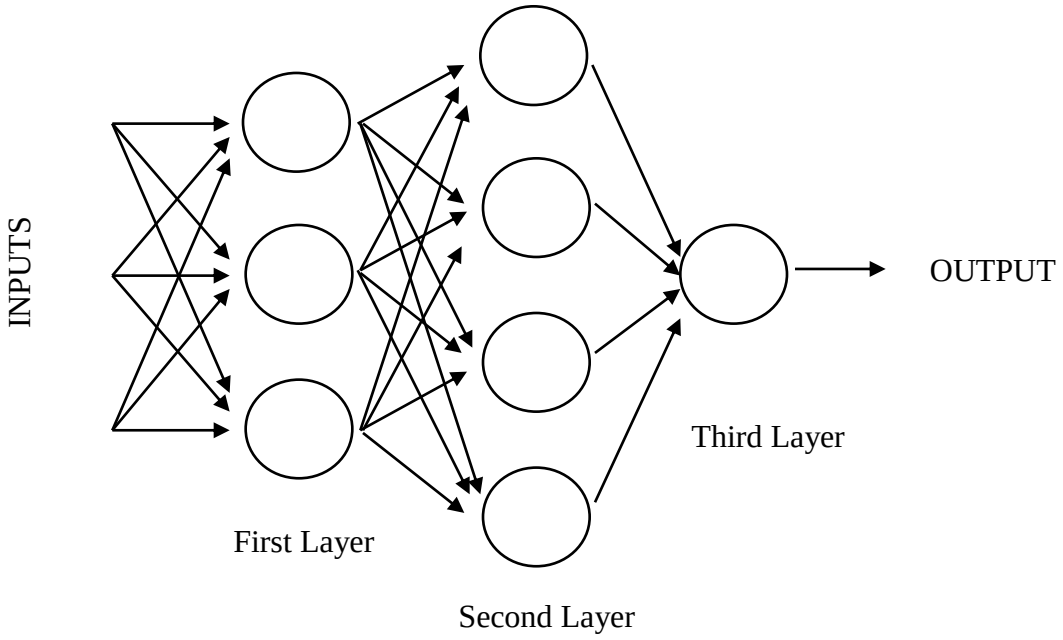

Figure 4-6: Example of a complex Network of Perceptrons

ANNs are often used to solve complex problems through various layers of perceptrons:

1) Each perceptron in the first layer performs as previously shown in in the simple perceptron model.

2) Perceptrons in the second layer also follow the basic model. However, outputs from first layer perceptrons are summed appropriately and used as inputs of the second layer and new weights are assigned to them before sending them to the next layer.
3) Perceptrons in advanced layers make more complex conclusions than the ones in the previous layers.

The complex network learns and converges gradually through applying small changes to the weights or biases of perceptrons so that only a small change in output would happen (Nielsen, 2015). Figure 4-7 shows the desired network changes that would allow for the network to learn. The optimal value for the weight is one that minimizes the mismatch with the actual outputs.

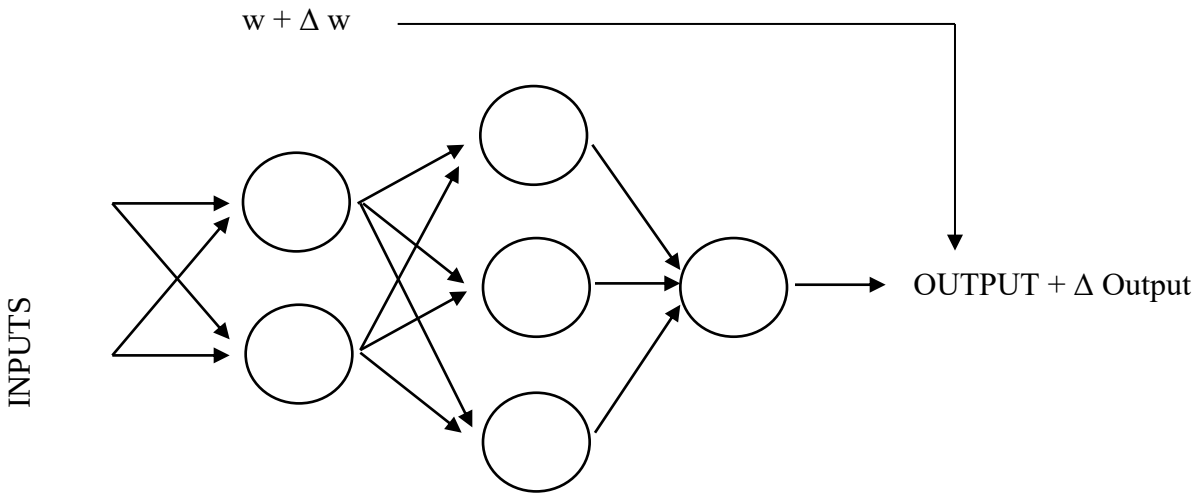

Figure 4-7: A small change in weight cause a small change in the Output (Nielsen 2015)

Newer perceptron models replaced the basic one as the simple model couldn't handle complex network changes and often caused the entire network to misbehave (Nielsen 2015). One of the famous models is the sigmoid neuron which is capable of handling small changes and performs in

the right direction. The main difference between a perceptron and a sigmoid neuron is the output where it is not 0 or 1 anymore, but is represented by a function (Nielsen, 2015).

$$\boldsymbol{\sigma}\,(\boldsymbol{w}.\boldsymbol{x}+\boldsymbol{b})$$

$$\boldsymbol{\sigma}(\boldsymbol{z}) = \frac{\mathbf{1}}{\mathbf{1}+\boldsymbol{e}^{-\boldsymbol{z}}}$$

The Back Propagation Algorithm

There are many different types of ANNs which often have different names. However, there are some that are considered to be the main ones, such as back propagation which is considered the most common one.

The main target of the back propagation algorithm method is to minimize the total squared error produced by the network through the gradient descent algorithm.

The back propagation algorithm works in a simple way. It requires a set of inputs that are linked to real outputs as the network learns by example. At the start, the ANN is initialized through the inputs with randomly assigned weights. Then, everything is processed through the network to be processed through the activation functions to produce some outputs. The ANN then compares the calculated outputs against the real outputs and calculates a mean-squared error. The mean-squared error is sent backward through the network and adjusts the weights in each layer. The ANN starts over using the newly adjusted weights and the process repeats itself until it reaches the desired threshold. Figure 4-8, Figure 4-9, and Figure 4-10 show the mechanism of a back propagation algorithm.

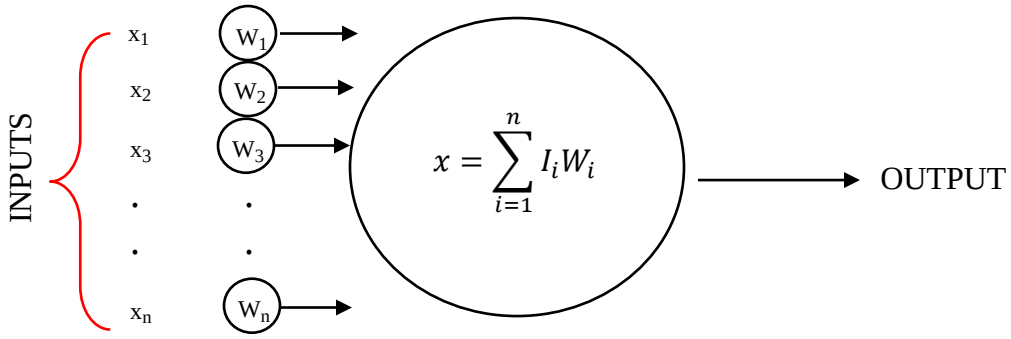

Figure 4-8: Step 1, Data Feed-forward

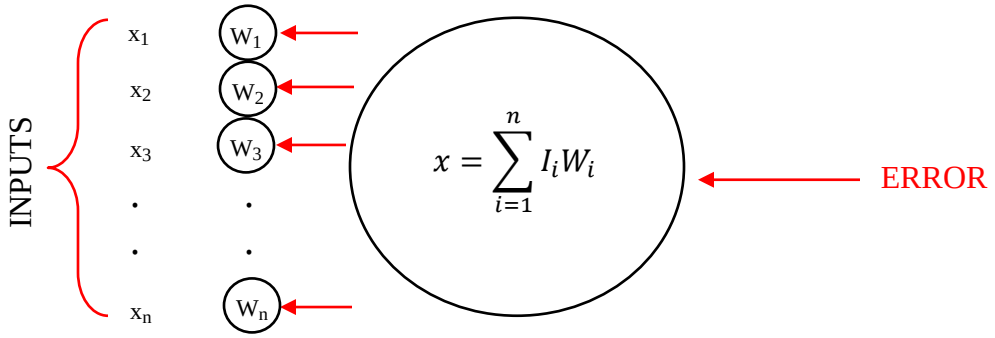

Figure 4-9: Step 2, Error Propagation Backward

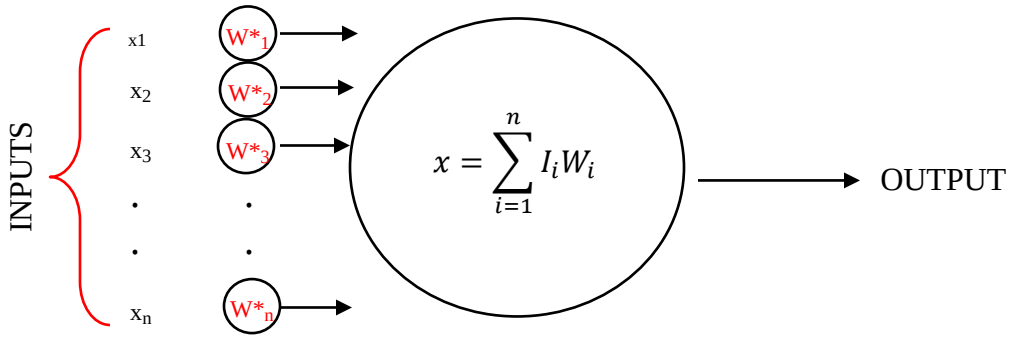

Figure 4-10: Step 3, Feed-forward with Adjusted Weights

It is important to note that forward-feed ANNs go in one direction, from input layer to hidden layers to output layer. The complexity of the design allows for outputs to be tied closely to the

inputs allowing the network to recognize trends and patterns along with inputs as well as novel behaviors that were not seen before. In a feed-back type ANN, the process goes back and forth between nodes and connections in a loop until it finds an equilibrium point. The strength of this non-linear dynamic system lies within its ability to optimize and find the best set of interconnected factors for any set of inputs.

The following steps summarize the back propagation algorithms steps:

1) Weights are assigned randomly for all the inputs.
2) Input layer sends its values and their corresponding weights to the first hidden layer where each neuron sums the incoming signals.

$$z_{in,j=}w_{oj}+\sum_{i=1}^{n} x_i w_{ij}$$

3) The desired activation function is applied on every neuron in the first hidden layer.

$$z_j = f\left(z_{in,j}\right)$$

4) The previous steps continue through all the hidden layers until they reach the output layer.

$$y_{in,k=}w_{ok}+\sum_{j=1}^{p} z_i w_{jk}$$

5) Similar to step 3, the desired activation function is applied on every neuron on the output layer.

$$y_k = f\left(y_{in,k}\right)$$

6) Now that the ANN completed the feed-forward algorithm, the backpropagation part starts by calculating the difference (error) between the calculated value y_k and the actual target output t_k. The error then is used to find weight adjustments and bias corrections.

$$e_k = t_k - y_k$$

$$\delta_k = e_k f'\left(y_{in,k}\right)$$

$$\Delta w_{jk} = \alpha \delta_k z_j$$

$$\Delta w_{ok} = \alpha \delta_k$$

7) The last step in the backpropagation algorithm is to find the new weights for the input layer and the output layer.

$$Input\ Layer \qquad w'_{ij} = w_{ij} + \Delta w_{ij}$$

$$Output\ Layer \qquad w'_{jk} = w_{jk} + \Delta w_{jk}$$

8) The algorithm repeats itself until it reaches the specified tolerance.

Neuro-Simulation

In the absence of huge data sets consisting of inputs and outputs, neuro-simulation becomes a viable solution for constructing an ANN provided it is done and defined correctly. In this project, a commercial simulator with heavy computational requirement is used to provide data sets for constructing the ANN. Data sets generated are directly related to the problem in hand. On the other hand, data validity and accuracy in depicting real life fields become an issue. So, to overcome any problems that could potentially jeopardize the accuracy of the ANN, thorough setup for data generation algorithms are tested and parameter ranges cover a wide range of real life reservoirs.

Initially, a simple base case for a specific reservoir is constructed, and then it would be modified and adjusted to fit the problem in hand. Next, sensitivity analysis and grid size analysis are performed. Finally, appropriate ranges for the parameters are used in order to generate enough data sets to build the ANN. Once the ANN is constructed, tested, and verified, no more data are required for it. It can be used right away for the goal it was constructed to do given that its error is within the acceptable range during construction.

Chapter 5

METHODOLOGY

This chapter will go over the methodology and process in this dissertation. A well-established, multi-purpose, and cross-discipline tool is employed to correlate reservoir properties and injection design to reservoir performance. In this section, reservoir model construction as well as data availability and generation will be shown since it is the main part of building a solid ANN.

5.1 Reservoir Model Construction

In this section, all the steps for constructing the reservoir model and parameters for generating more reservoir cases are explained. In this step, heavy computational power is required and it is used to generate data sets that eventually shape the ANN. Since no real data that cover the whole spectrum of the problem at hand are available, this part of the project becomes critically important in understanding the data sets and how they are generated.

Reservoir simulators are used extensively in the oil and gas industry. Instead of going with trial and run in the field and lose millions of dollars for lost opportunities, reservoir simulation becomes a game-changing tool if used wisely. In the oil and gas industry, we deal with challenges that we do not see. The best technology today can get us very close to explaining the processes occurring in the subsurface, but falls short a lot of time and we have to deal with a lot of uncertainty. Reservoir simulation is not an answer, but it is a tool that enables us to evaluate all the possible scenarios and act accordingly.

To be able to construct a reservoir model there are a lot of parts that have to be thoroughly studied and then provided for the simulator. The main parts of any reservoir simulator include the unique rock properties for the specific reservoir in question as well as the fluid properties. Then, there are some additional parameters that are imposed by engineers to account for various decisions concerning the reservoir and its development.

In this project, a specific design is studied relating continuous carbon dioxide injection in naturally fractured reservoirs. So, before jumping to construct a reservoir model, there are some essential parts that have to be explained in details such as grid size, reservoir layering, miscibility, fluid composition, relative permeability, injection design, and if gas injection is alternating with water.

5.1.1 Compositional Reservoir Modeling Vs. Black Oil Modeling

Reservoir simulators are composed of two parts; the governing physics of flow in porous media and the computational power that is capable of conducting numerous calculations in a timely manner. Reservoir modeling can typically be divided into compositional or black-oil simulation. In black-oil modeling, reservoir fluid is modeled as three components; water, oil, and gas. On the same note, gas can be present in the oil phase as a dissolved gas and oil can be vaporized in the gas phase. Oil, water, and gas formation volume factors (B_o, B_w, B_g) as well as solution-gas ratio (R_s) describes the fluid phase behavior in black-oil formulation.

In compositional modeling, reservoir fluid is represented by the hydrocarbon components and any impurities. Compositional formulation is used when the reservoir fluid experiences compositional changes which are described by different models of cubic equation of state. Every component is described distinctively from the other ones and this results in a very long computational time than

the typical black-oil modeling since flash calculations are conducted at every time-step at every grid block.

Black oil formulation application differs from compositional formulation application. For example, black-oil modeling is typically used to describe primary recovery mechanisms and water flooding projects while carbon dioxide injection, especially miscible injection, is modeled compositionally.

In this research, heavy-computational compositional formulation is used to run all the reservoir simulation cases that formed the ANN's database.

5.1.2 Grid Size Sensitivity

Before carrying any simulation cases, simulation grid dimensions must be carefully selected to avoid grid size error. This exercise is simple, yet very important when conducting any reservoir simulation runs. The idea of this exercise is to run different grid dimensions but on the same reservoir size. So, the goal would be to go as fine as possible until we reach a point where going with smaller grids doesn't account for much difference at all. Why not go with the smallest grid possible from the start? Because every time we go with finer grids, runs take more time to complete, so a balance between grid size error and computational time is required.

In this step, a single 3-layer simulation case was used to test various grid dimensions ranging from 16x16 ft. to 264x264 ft. in a drainage area of 1 acre. Figure 5-1 displays the comparisons between the grid dimensions. It would be ideal to run with the smallest grid size but that would impact the run time of every case. So, since grid size error stabilizes around 44 ft. and below it would be used as the optimal grid size for the final ANNs.

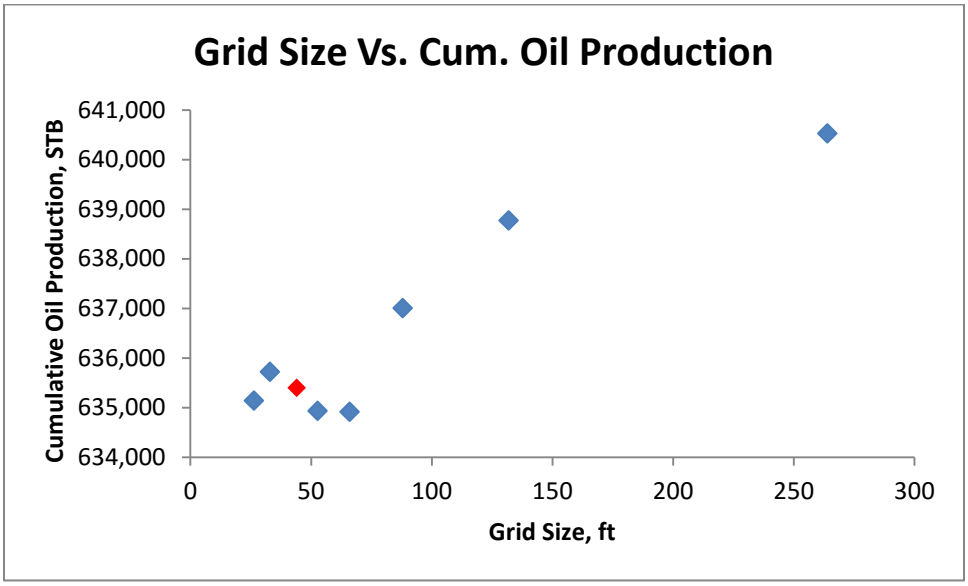

Figure 5-1: Grid Sensitivity Analysis

5.1.3 Reservoir Layering

Reservoir layering is an important topic when it comes to reservoir simulation. A 1-layer model is not capable of depicting certain mechanisms such as gravity effects. In this project, CO_2 is injected continuously in a miscible process and fluid composition changes throughout the injection duration. When CO_2 comes in contact with reservoir fluid, it could lead to higher recovery if it is injected in the bottom layers rather than the top layers of the oil zone. Also, production scenario will differ if the well is producing only from the top layers or the bottom layers, or it is completed in all the layers.

On a similar note, most reservoirs exhibit vertical and lateral heterogeneities due to historical depositional events. However, with limited computational powers and geological data, lateral heterogeneities are very difficult to capture. Vertical heterogeneities can be taken into account using different layers and different properties for each individual layer. At the same time, limited computational powers play the main role in determining how many layers the model should have.

In this project, two, three, and four layers were tested and then two layers were selected as they provided enough complexity and with a reasonable simulation running time.

5.1.4 Reservoir Fluids

During the first stage of the project, fluid data from the literature were used to test the impact of different fluid ranges under continuous CO_2 injection. The fluids used were real fluids from real reservoirs and the data were available in the literatures. The reservoir fluids used initially to follow an approach similar to Parada (2008) and Artun (2008). Table 5-1 shows some of the fluids used by Parada (2008) as well as a modified version of the fluid that was used by Hindi (Hindi et al, 1992).

Table 5-1: Fluid Compositions Used in the Literature for Similar Projects

Component	PVT 1 Black Oil [McCain, 1990)	PVT 2 Volatile Oil [Papp et al, 1998)	PVT 3 Black Oil [Rathmell, 1971)	PVT 4 SPE 24185 [Hindi et al, 1992]*	PVT 5 Parada Heavy Oil
CO2	0.91	0.51	3.2	4.15	0.11
N2	0.16	1.8	0.03	0.42	0.69
CH4	36.47	46.8	27.81	18.13	10.78
C2H6	9.67	8.09	8.21	9.41	0.12
C3H8	6.95	10.91	5.99	8.04	0.42
IC4	1.44	4.26	0.31	1.46	0.3
NC4	3.93	6.86	4.1	4.33	0.32
IC5	1.44	3.71	1.3	1.74	0.29
NC5	1.41	3.81	2.3	2.4	0.26
C6	4.33	4.73	4.62	3.68	0.64
C7+	33.29	8.52	42.13	46.24	86.09
MW	218	156	223	221	532
SG	0.8515	0.782	0.875	0.874	0.925

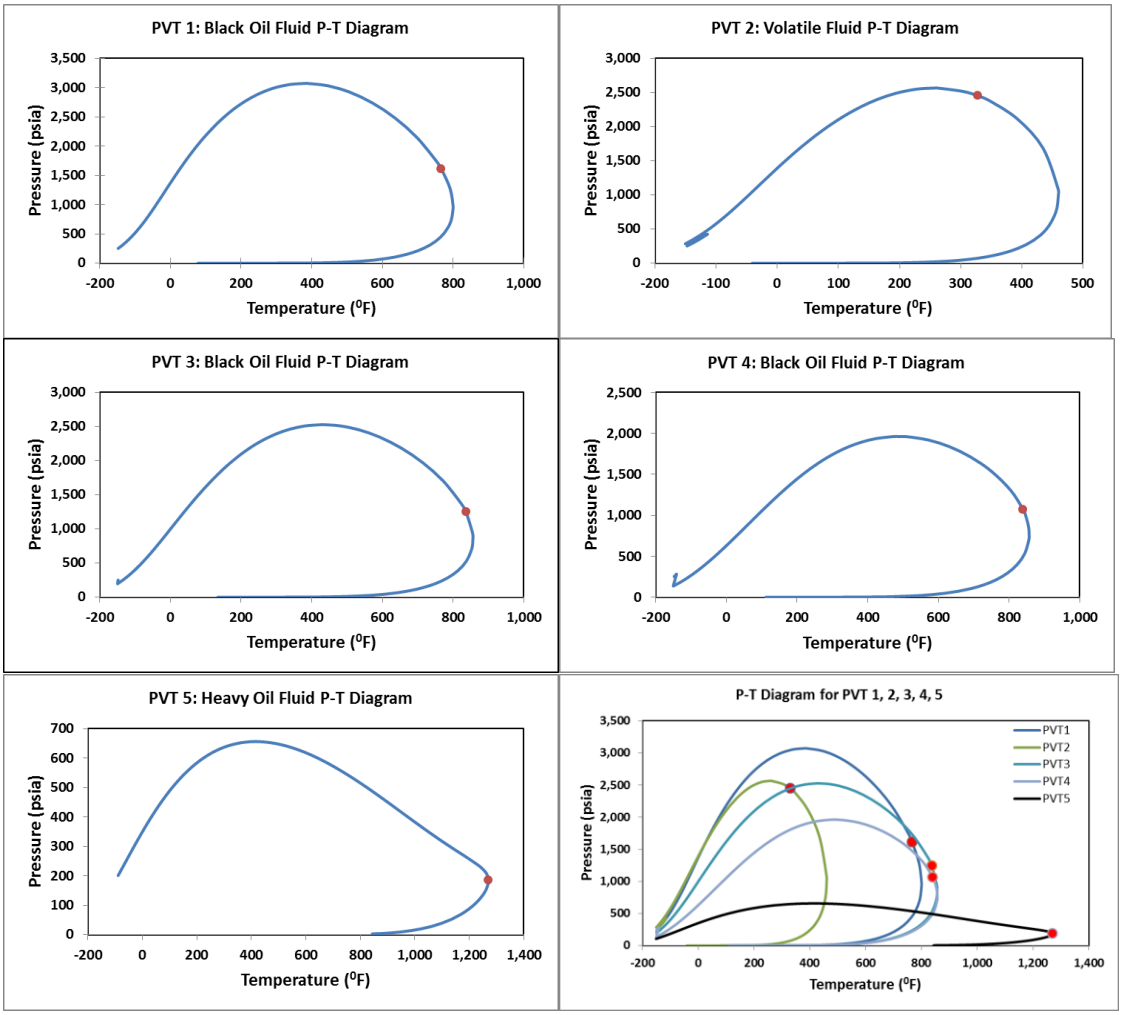

Figure 5-2: Phase Envelopes for PVT1, PVT2, PVT3, PVT4, and PVT5 reservoir fluids

Although reservoirs with very heavy oils are not typically good candidates for CO_2, including them would highlight at which fluid composition is CO_2 injection applicable and under which conditions.

In the literature, CO_2 ANN projects were always created for specific fluid compositions which severely limit the project's applicability. In this project, after gaining enough understanding about the project and the behavior and performance of the five different fluid compositions, the final ANN would be constructed for any fluid composition including any impurities that could be

present in the reservoir fluid such as H_2S. A high range of heavy hydrocarbons are used where heavy hydrocarbons up to 20 atoms (FC20) are included which are then lumped as part of C_{7+} composition.

Phase envelopes provide essential information for any project. They can be constructed once a fluid samples are available. Phase envelopes relate reservoir fluid composition with reservoir temperature and pressure. They can then provide reservoir fluid state at any temperature and pressure. Phase envelopes play a major role in carbon dioxide injection projects. At any temperature and pressure inside the phase envelope, the fluid exhibits two phases while anywhere else outside the phase envelope is a one phase region.

5.1.5 Wettability, Capillary Pressure, and Relative Permeability

Interfacial tension (IFT) forms between immiscible fluids and is a good miscibility indicator. For example, the higher the IFT between two fluids, the less likely for them to become miscible and vice versa.

For any rock, when immiscible fluids come in contact with the rock surface, one fluid adheres more to the surface than the other. The fluid with the stronger attraction is called the wetting phase, and the other fluid is the non-wetting phase. Wettability is a rock property that can be determined by measuring the contact angle between water and the rock surface. A system is considered to be water-wet if the contact angle is less than 90^o and oil-wet if the contact angle is more than 90^o. Figure 5-3 shows a schematic of water-wet and oil-wet systems.

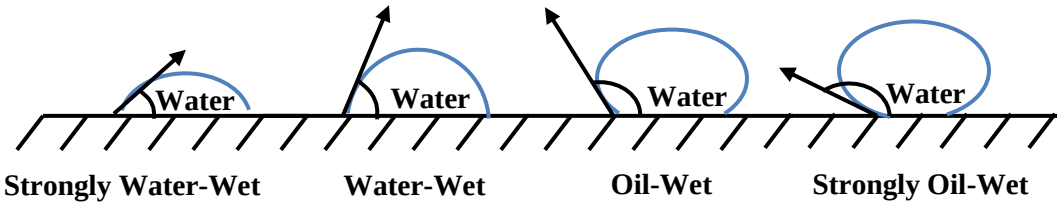

Figure 5-3: Wettability for Different Systems

Capillary pressure occurs across the interface between two immiscible fluids due to the IFT and can be defined as the pressure of the non-wetting phase minus the pressure of the wetting phase. Generally, water is considered to be the wetting phase in an oil-water system while oil is considered the wetting phase in a gas-oil system.

$$P_c = P_{Nonw} - P_w$$

Capillary pressure curves are typically represented by either S-Shaped such as Van-Genuchten or convex like Brooks-Corey (Li et al, 2013). While there is a slight difference between the two methods in the way they show entry pressure, in this research Brooks-Corey model and correlations are used to generate different curves for every single case.

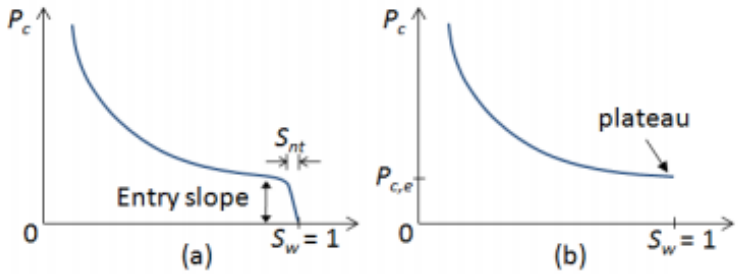

Figure 5-4: Capillary Entry Pressure Representation for Van-Genuchten (Left) and Brooks-Corey (Right) as represented by Li et al. (2013)

Relative permeability is one of the main building blocks for reservoir simulation or any reservoir engineering study. It provides irreplaceable information that relates all the flowing fluids in the

system to the reservoir rock, hence, its importance in reservoir performance and behavior predictions.

Different rock types have different relative permeability curves and the shape of the relative permeability curve is affected by many factors such as reservoir tightness, wettability, and IFT. In enhanced oil recovery projects, interfacial tension effect becomes very important especially in miscible gas injection projects. The decrease in IFT between the fluids means that the fluid properties are becoming the same, which is typically an indication of miscibility. Typically, at very low IFT, the relative permeability shape approaches straight lines (X-shape) and at high IFT the curves gain more curvatures as fluids properties become more distinctively apart.

NOTE: In this research, the effect of IFT and wettability are not modeled explicitly, their effect is included implicitly as part of the final ANN. This is included in the main data set that is used to construct the ANN where every single case has a completely different set of relative permeability and capillary pressure curves.

Chapter 6

ARTIFICIAL NEURAL NETWORK DESIGN PARAMETERS AND DATA GENERATION

Data are the most important part of any project. The debate is always about the abundance, quality, and accuracy of the data. For ANN projects, good quantitative data are the heart of the project. So, a good project requires good data that are representative to the problem that is being studied.

In the oil and gas Industry, real data are typically a big concern mainly due to confidentiality and political problems. In the literature, most authors and researchers do not publish their full data with their findings making it almost impossible to reproduce especially in EOR projects where reservoirs undergo primary and secondary recovery techniques.

To construct an ANN that is reliable and capable of giving good predictions, extensive data beyond any available real data must be present. Also, constructing an ANN for a problem that is not well researched, hardly any data is available. To overcome this major issue, data generation techniques must be used. However, if this method is not used correctly, the quality of the ANN would be as good as the data used to construct it. In this section, we will go over how data was generated for this project and some of the techniques used to ensure validity, applicability, and reality of the data.

6.1.1 Matrix Porosity & Matrix Permeability

Reservoirs around the world have different rock properties. In terms of matrix permeability, reservoirs range from extremely tight ~ 10^{-4} md to high ~100 md. In this study, only low matrix permeability reservoirs (1+ md) and above are included as tight reservoirs and below are not

typically good candidates for enhanced oil recovery projects. A wide range is used to cover a large number of rock groups. For example, the matrix porosity range used in this study starts from 10% porosity, sandstone porosity, which is considered about the economical limit for developing an oil well.

It is important to note that the base model has two layers and the data design parameters generation accounts for each layer's independency from the other layers. For example, the first layer could have a permeability of 200 md while the second layer could have 10 md for permeability. This will allow the ANN to be exposed to different reservoir types and fluid behaviors with that flexibility imposed in generating the data sets. Mixed with fracture properties, that would make the data sets feeding the ANN even more complex.

6.1.2 Fracture Porosity & Fracture Permeability

In fractured reservoirs, fractures contribute significantly to fluid flow. They don't have much storage at all, but typically they have very high conductivity. Different reservoirs have different fracture densities, conductivity, and contrast with matrix permeability. A large number of reservoirs are naturally fractured, but the effects of fractures differ from one reservoir to another. For example, a reservoir could have many small fractures that are not connected or cemented fractures that would have no impact on fluid behavior. On the other hand, some carbonate reservoirs are infested with networks of connected fracture corridors that impact the reservoir fluid behavior completely, hence the term "fracture dominated flow".

In this design parameter, and to account for various fracture scenarios, the conductivity of the fractures varies from very low to very high. The data generation algorithm varies so that the

contrast between matrix permeability and fracture permeability is very low and fractures won't have much impact on fluid flow (relative permeability is different between fractures and matrix). Also, fracture density varies to form highly fractured reservoirs or reservoirs with low fracture density.

6.1.3 Reservoir Temperature

Reservoir temperature affects reservoir fluid composition and state. In a lot of ANN designs, reservoir temperature is generally fixed when it comes to data generation. Initial ANN designs in this research had the reservoir temperature fixed as well as fixed fluid compositions. However, the latest ANN designs include variations in reservoir temperatures and fluid compositions. The effect of reservoir temperature change can be seen on the phase diagram for any specific composition which then describes, along with reservoir temperature, the fluid state at that specific point. Figure 6-1 shows different reservoir fluid states at different temperatures and pressures.

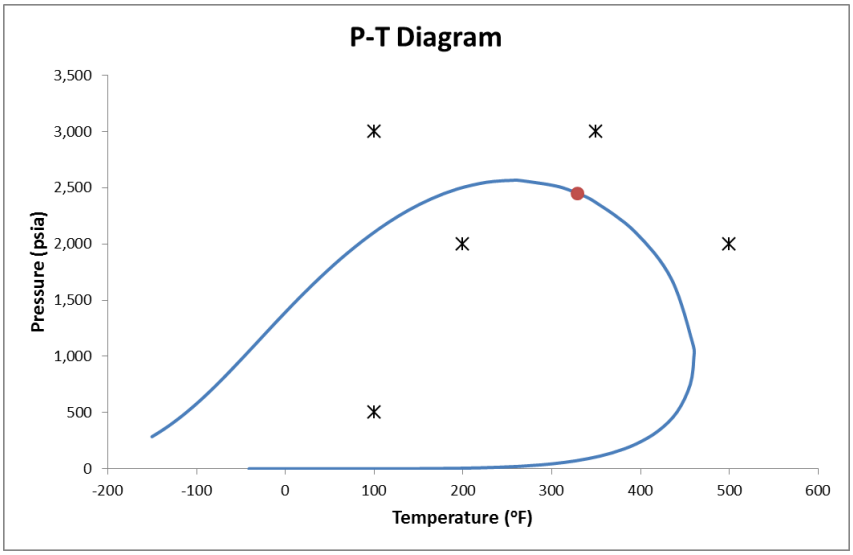

Figure 6-1: P-T Diagram showing different fluid States at various pressures and temperatures

6.1.4 Reservoir Pressure

Similar to reservoir temperature, initial reservoir pressure has more impact. It affects reservoir production as well as the overall development scheme. In this project, initial reservoir pressure affects the type of continuous CO_2 injection whether it would be a miscible injection or immiscible injection at that specific temperature.

6.1.5 Well Spacing

Well spacing is a very important parameter when it comes down to oil recovery. Well spacing differs per reservoir and it is a challenging task to find the optimum well spacing for a particular reservoir. While this study does not go through all factors to determine an optimum well spacing, it does go over a huge range of well spacing and ultimately creates a sensitive relationship that helps determine an optimum spacing for a given reservoir properties. This is a very important feature, which is to determine if one well can do the job of 2 or 3 other wells for the given reservoir.

In this research, well spacing of 17 acres is tested all the way to 217 acres.

6.1.6 Fluid Composition

Fluid composition is a major part of any reservoir study. It determines many factors and affects production based on fluid state at any reservoir pressure and temperature.

In this section, varying fluid composition generation technique is used to generate different fluid composition for every specific case that contributes to the overall data sets. The generation

algorithm changes the composition of every component within the reservoir fluid to get a new fluid every time. It is almost impossible to have the same composition for different cases. What makes this part of the project very important is that, in the previous ANN designs in the literatures, ANN were built for specific compositions due to the fact that it is very difficult to change the reservoir composition and its properties a hundred times, let alone 3,000 times or more.

Initially, ANNs were designed based on 5 specific compositions, each composition had 11 components. While it was for testing purposes, it was actually limiting to only have 5 specific compositions. What makes it difficult to generate new compositions as part of the data sets are the heavy components that are typically lumped to compose the C_{7+}. Compositional fluids are described by their components from Methane up to Hexane and include all the heavy components lumped as part of Heptane plus (C_{7+}). Reservoirs fluids also contain non-hydrocarbon components such as Nitrogen (N_2), Hydrogen Sulfide (H_2S), and Carbon Dioxide (CO_2). Every single component has known properties such as molecular weight (MW), critical temperature (CT), critical pressure (CP), acentric factor (ω), and binary interaction coefficients. These properties are of particular importance due to their part in building the phase behavior model through the Equation of State (EOS). EOS is an analytical representation of any system that relates pressure, temperature, and volume of that system. For example, ideal gas law is a simple equation of state. Constructing and running 11-component fluid through compositional simulator requires heavy computational power, adding to that the changing composition due to carbon dioxide injection, and convergence issues that arise when conducting simulation makes the problem require much higher computational power than available for such a study.

Table 5-1 shows a black oil fluid as described by McCain (McCain, 1990). The table shows the molar composition of each component in the mixture as well as the critical properties, acentric

factor, and molecular weight. The only difference between this mixture and any other mixture would be some additional components, different molar composition, and different C_{7+} lumped components that would yield to different properties.

Table 6-1: McCain's Black Oil Fluid Composition

Component	Molar Composition	Pc (psia)	Tc (^oR)	ω	Mw (lbm/lbml)
CO_2	0.0031	1069.87	547.56	0.23	44.01
N_2	0.16	492.31	227.16	0.04	28.01
C_1	36.47	667.20	343.08	0.01	16.04
C_2	9.67	708.34	549.72	0.10	30.07
C_3	6.95	615.76	665.64	0.15	44.10
IC_4	1.44	529.05	734.58	0.18	58.12
NC_4	3.93	551.10	765.36	0.19	58.12
IC_5	1.44	490.84	828.72	0.23	72.15
NC_5	1.41	489.38	845.28	0.25	72.15
FC_6	4.33	477.03	913.50	0.28	86.00
C_{7+}	33.29	247.29	1360.76	0.63	218.00

In order to make the ANN a universal one, and not just for 5 specific compositions, a compositional fluid generating algorithm is implemented. The algorithm only takes care of lumping the heavy components and getting their corresponding properties. For this purpose, Lee's Mixing Rules (Lee et al. 1979) are used to lump all hydrocarbon components above C_{7+}.

$$\emptyset_i = z_i / \sum^{L} z_i$$

$$M_L = \sum^{L} \emptyset_i M_i$$

$$V_{cl} = \sum^{L} [\emptyset_i M_i V_{ci} / M_L]$$

$$P_{cl} = \sum^{L} [\emptyset_i P_{ci}]$$

$$T_{cl} = \sum^{L} [\emptyset_i T_{ci}]$$

$$\omega_L = \sum^{L} [\emptyset_i \omega_i]$$

Where:

ϕ_i is the normalized mole fraction of the component i in the lumped fraction.

M_L is the Molecular Weight of the lumped C_{7+} fraction.

V_{CL} is the Critical Volume of the lumped C_{7+} fraction.

P_{CL} is the Critical Pressure of the lumped C_{7+} fraction.

T_{CL} is the Critical Temperature of the lumped C_{7+} fraction.

ω_{CL} is the Acentric Factor of the lumped C_{7+} fraction.

The next part would be to implement Lee's mixing rules in the generation algorithm. This algorithm gives flexibility and much more utility as it includes a full library up to HC20 for the user to input their mixture. At the same time, it allows the simulator to run with around 11 components rather than 25 components including non-hydrocarbon components and impurities. The steps below summarize how the algorithm works.

1) All hydrocarbon components and their properties up to HC_{20} as well as H_2S, N_2, and CO_2 are loaded in the generation algorithm's library.
2) A mixture is automatically generated based on ranges given to the algorithm.
3) Lee's mixing rules are applied to lump any component above C_6.

In order to verify the method we are using, and to ensure the accuracy of the algorithm, WinProp, commercial software developed by Computer Modeling Group Ltd. (CMG), is used to compare them to the current algorithm.

Table 6-2: A Synthetic 25 Component Mixture

Comp	Molar Composition	Pc (atm)	Tc(K)	ω	MW (lbm/lbmol)	Vci (m^3/kmol)
H_2S	0.001	88.2	373.2	0.1000	34.08	0.0985
CO_2	0.003	72.8	304.2	0.2250	44.01	0.094
N_2	0.0002	33.5	126.2	0.0400	28.01	0.0895
C_1	0.4	45.4	190.6	0.0080	16.04	0.099
C_2	0.05	48.2	305.4	0.0980	30.07	0.148
C_3	0.06	41.9	369.8	0.1520	44.10	0.203
IC_4	0.07	36	408.1	0.1760	58.12	0.263
NC_4	0.1	37.5	425.2	0.1930	58.12	0.255
IC_5	0.03	33.4	460.4	0.2270	72.15	0.306
NC_5	0.06	33.3	469.6	0.2510	72.15	0.304
FC_6	0.08	32.46	507.5	0.2750	86.00	0.344
FC_7	0.05	30.97	543.2	0.3083	96.00	0.381
FC_8	0.01	29.12	570.5	0.3513	107.00	0.421
FC_9	0.01	26.94	598.5	0.3908	121.00	0.471
FC_{10}	0.01	25.01	622.1	0.4438	134.00	0.521
FC_{11}	0.01	23.17	643.6	0.4775	147.00	0.574
FC_{12}	0.01	21.63	663.9	0.5223	161.00	0.626
FC_{13}	0.01	20.43	682.4	0.5596	175.00	0.674
FC_{14}	0.01	19.33	700.7	0.6048	190.00	0.723
FC_{15}	0.01	18.25	718.6	0.6512	206.00	0.777
FC_{16}	0.01	17.15	734.5	0.6837	222.00	0.835
FC_{17}	0.001	16.35	749.2	0.7286	237.00	0.884
FC_{18}	0.001	15.65	760.5	0.7574	251.00	0.93
FC_{19}	0.002	15.06	771	0.7901	263.00	0.973
FC_{20}	0.0018	14.36	782.9	0.8161	275.00	1.027

Table 6-2 shows a synthetic 25-component mixture that was used to verify the lumping method for C_{7+} between CMG and Lee's mixing rules used in this research. Table 6-3 shows the same mixture but with lumping all the heavy components above C_6 into C_{7+} using CMG.

Table 6-3: A Synthetic 25-Components Mixture represented by 12 Components (WinProp)

Comp	Molar Composition	Pc (atm)	Tc(K)	ω	MW (lbm/lbmol)	Vci (m^3/kmol)
H_2S	0.001	88.20	373.2	0.1000	34.08	0.0985
CO_2	0.003	72.80	304.2	0.2250	44.01	0.094
N_2	0.0002	33.50	126.2	0.0400	28.01	0.0895
C_1	0.4	45.40	190.6	0.0080	16.04	0.099
C_2	0.05	48.20	305.4	0.0980	30.07	0.148
C_3	0.06	41.90	369.8	0.1520	44.10	0.203
IC_4	0.07	36.00	408.1	0.1760	58.12	0.263
NC_4	0.1	37.50	425.2	0.1930	58.12	0.255
IC_5	0.03	33.40	460.4	0.2270	72.15	0.306
NC_5	0.06	33.30	469.6	0.2510	72.15	0.304
FC_6	0.08	32.46	507.5	0.2750	86.00	0.344
FC_{7+}	0.1458	24.18	633.304	0.4582	143.62	0.555

Table 6-4: A Synthetic 25-Components Mixture represented by 12 Components (Lee's Mixing)

Comp	Molar Composition	Pc (atm)	Tc(K)	ω	MW (lbm/lbmol)	Vci (m^3/kmol)
H_2S	0.001	88.20	373.2	0.1000	34.08	0.0985
CO_2	0.003	72.80	304.2	0.2250	44.01	0.094
N_2	0.0002	33.50	126.2	0.0400	28.01	0.0895
C_1	0.4	45.40	190.6	0.0080	16.04	0.099
C_2	0.05	48.20	305.4	0.0980	30.07	0.148
C_3	0.06	41.90	369.8	0.1520	44.10	0.203
IC_4	0.07	36.00	408.1	0.1760	58.12	0.263
NC_4	0.1	37.50	425.2	0.1930	58.12	0.255
IC_5	0.03	33.40	460.4	0.2270	72.15	0.306
NC_5	0.06	33.30	469.6	0.2510	72.15	0.304
FC_6	0.08	32.46	507.5	0.2750	86.00	0.344
FC_{7+}	0.1458	25.01	623.93	0.4582	143.61	0.615

Table 6-3and Table 6-4 show that there is a very marginal difference between the lumped C_{7+} components generated by WinProp (CMG) and Lee's mixing rules. Therefore, the Lee's mixing method is sufficient enough to be used to lump any composition.

The generation algorithm used in this research uses a large list of heavy components (up to HC_{20}). When using Lee's mixing rule to lump the heavy components, we are using a component (C_{7+}) to represent 14 heavy hydrocarbons which gives an error. The proper way to lump heavy components is to lump the similar ones together. This error mainly affects the cricondentherm at very high temperature and not the cricondenbar due to its association with heavy components lumping. Since component lumping is used in this research to minimize the intensive iterative process and equilibrium calculation for all components, and since it only affects the cricondentherm when including very heavy components at higher than usual saturations, this error will be taken into consideration when using the final ANN. Figure 6-2 shows the error between the 25-components mixture described previously and its 11-components mixture representation with lumped C_{7+} component.

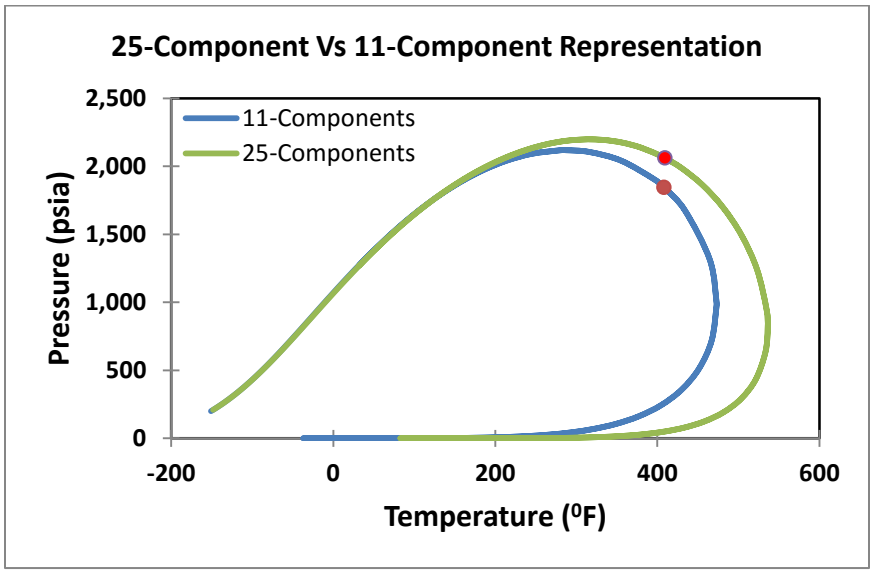

Figure 6-2: Comparison between Synthetic Mixture Representation (25 and 11)

Table 6-5 shows the ranges that are assigned to each component. Notice that all components up to FC6 are assigned a minimum value that is never a zero. This is done to avoid complications when generating various mixtures as the presence or disappearance of some components would not be optimal. So, when a fluid composition is generated, there will always be 12 components, H_2S,

CO_2, N_2, C_1, C_2, C_3, IC_4, NC_4, IC_5, NC_5, FC_6, and lumped C_{7+}. Assigning zero compositions for components heavier than FC_6 doesn't affect the number of components since it would be lumped as part of C_{7+} and the number of components would still be 12 components.

Table 6-5: Components Ranges for Data Generation

Parameter	Min	Max	Units	Notes
H_2S	0.01	0.5	%	
CO_2	0.5	5	%	
N_2	0.5	2	%	
C_1	10	50	%	
C_2	10	30	%	
C_3	0.5	10	%	
IC_4	0.5	5	%	
NC_4	0.5	5	%	
IC_5	0.5	5	%	
NC_5	0.5	5	%	
FC_6	0.5	5	%	
FC_7	0.5	10	%	Lumps into C7+
FC_8	0	10	%	
FC_9	0	10	%	
FC_{10}	0	10	%	
FC_{11}	0	10	%	
FC_{12}	0	10	%	
FC_{13}	0	10	%	
FC_{14}	0	10	%	
FC_{15}	0	10	%	
FC_{16}	0	10	%	
FC_{17}	0	10	%	
FC_{18}	0	10	%	
FC_{19}	0	10	%	
FC_{20}	0	10	%	

6.1.7 Relative Permeability and Capillary Pressure Generation

Relative Permeability: Variations in relative permeability and capillary pressure were not considered in previous ANN studies of this nature. Typically, only one curve is used to describe all kinds of reservoirs. In this research, an intensive algorithm is incorporated to automatically generate different relative permeability curve and capillary pressure. It is almost impossible for

two different cases to share same set. In this section, we will go over how relative permeability and capillary pressure curves are generated and used.

The modified Brooks-Cory correlations, also known as power-law, are used to generate relative permeabilities of oil, water, and gas. Note that these equations are the exact equations used by CMG to generate relative permeability curves, so, no verification is needed.

$$Krow = Krocw * \left(\frac{So - Sorw}{1 - Swcon - Sorw}\right)^{Now}$$

$$Krw = Krwiro * \left(\frac{Sw - Swcrit}{1 - Swcrit - Soirw}\right)^{Nw}$$

$$Krog = Krogcg * \left(\frac{Sl - Sorg - Swcon}{1 - Sgcon - Sorg - Swcon}\right)^{Nog}$$

$$Krg = Krgcl * \left(\frac{Sg - Sgcrit}{1 - Sgcrit - Soirg - Swcon}\right)^{Ng}$$

The modified Brooks-Corey correlations are simple to use once all the variables are known. The following steps show how these correlations are used:

1) The model is assigned values (within the specified range for each parameter) for:
    a. Water relative permeability at Irreducible Oil Saturation (krwiro).
    b. Oil relative permeability at connate water saturation (krocw).
    c. Oil relative permeability at connate gas saturation (krogcg).
    d. Gas relative permeability at connate liquid saturation (krgcl).
    e. Connate water saturation (Swcon).
    f. Critical water saturation (Swcrit).
    g. Residual oil for water-oil table (Sorw).
    h. Irreducible oil for water-oil table (Soirw).
    i. Residual oil for gas-liquid table (Sorg).

j. Irreducible oil for gas-liquid table (Soirg)

2) The relative permeability generation algorithm considers various system types through the exponents N_w, N_{ow}, N_{og}, and N_g. The following shows the exponents used for the systems considered in this study:
    a. Exponents <0.7 indicates channeling
    b. Exponents = 1 indicates the presence of fractures in a fractured system
    c. Exponents = 3 indicates a well sorted rock
    d. Exponents = 3.5 indicates a poorly sorted rock
    e. Exponents = 4 indicates a cemented system
3) Brooks-Corey equations are used to calculate relative permeability at the connate water saturation (water-oil table), or residual oil saturation (gas-liquid table).
4) Saturation increases (or decreases depending on which phase is considered) and new relative permeabilities are calculated using the correlations.

Figure 6-3 illustrates the end points for water-oil relative permeability table and gas-oil relative permeability tables along with the corresponding values for the relative permeabilities at these end points.

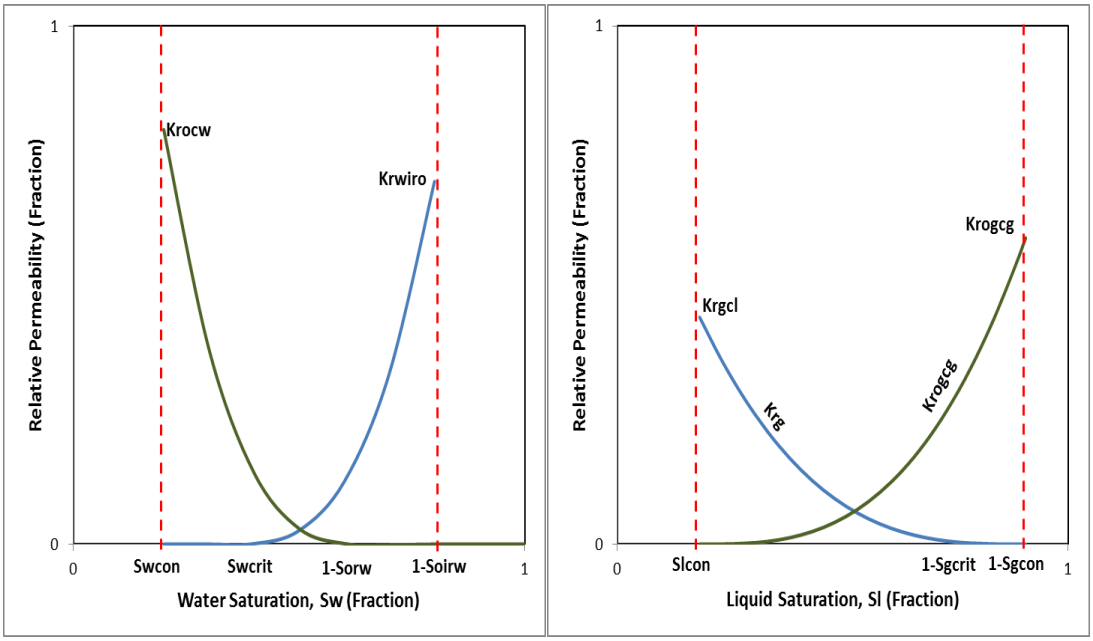

Figure 6-3: End points Saturations for Water-Oil and Gas-Oil Relative Permeability

Capillary Pressure: There are many methods that provide means to generate capillary pressure curves such as Brooks-Corey, Thomeer, J-Leverett, and many others. Since modified Brooks-Corey correlations were used previously for relative permeability curves, their correlations for capillary pressures are used.

$$Pcow = Pce_w * S_w^{*\left(-\frac{1}{\gamma}\right)}$$

$$S_w^* = \left(\frac{Sw - Swirr}{1 - Swirr}\right)$$

6.1.8 Initial Reservoir Water Saturation:

To accommodate various reservoirs, initial reservoir water saturation is used as a variable. Training data sets have different initial reservoir water saturation. No complex algorithm is required to vary the initial reservoir water saturation within a specified range.

6.2.1 Artificial Neural Network Process: The Whole Picture

We previously showed a general ANN, its concept, its components, and its methodology. We also showed the various building blocks for continuous CO_2 injection. Next, we are going to show how everything mixes together to form the ANN for continuous CO_2 injection.

For any ANN, all you need is data with inputs and outputs. If enough, representative field data were available, ANN could be constructed in a relatively short time. On the other hand, representative universal data are extremely difficult to find anywhere, even in the literature. For example, we know the properties of carbonate reservoirs, but we don't have production data for wells producing from carbonate reservoirs. So, we did the next best thing, generated our own data that covers a very wide range of reservoirs and fluids.

One of the outcomes of this research is to construct an ANN with predictive capabilities that can distinguish different reservoir behaviors. The two different reservoir mechanisms depend on the miscibility conditions. This is very difficult to achieve since the ANN only sees inputs and outputs without any additional information about the process itself, unless we create two different ANNs, one for miscible conditions and the other one runs under immiscible conditions which adds another limitation to the final product.

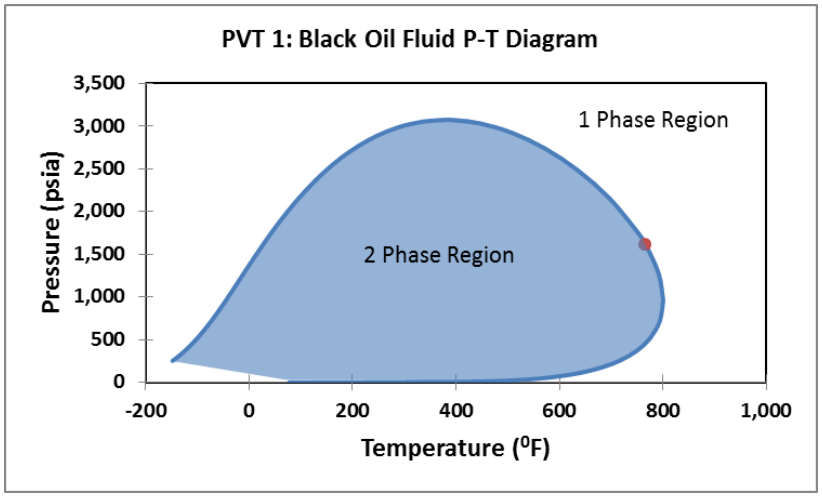

Figure 6-4: Two Phase Region on a Phase Diagram

Figure 6-4 shows the phase envelope for PVT 1. The whole injection process is ruled by the phase envelope and a minimum miscibility pressure. At high reservoir pressure above the two phase region, the process is miscible, but as soon as the pressure drops below into the two phase region, the process becomes immiscible. Highest oil recovery is achieved when the process is miscible where injected CO_2 mixes with oil and forms a single mixture that is lighter than the original mixture and more mobile. In an immiscible process, injected CO_2 only partially dissolves in the oil while the rest stays in the gas phase. While a miscible process recovers more oil, it requires a much higher reservoir pressure than an immiscible process.

In order to create an ANN that is capable of predicting both behaviors, data across the whole phase envelop must be provided for all the various reservoir mixtures. Note that every time there is a new reservoir fluid, its phase envelope could be completely different than the one before it. So, we can solve the problem by:

1) Provide thousands of cases that cover the whole phase envelope.
2) Feed the data to the ANN in stages (Smart feed):
    a. Provide only miscible data sets to the ANN (above the two phase region)

b. Provide only Immiscible data sets to the ANN (inside the two phase region).

c. Combine a and b.

In this research, we are using a smart feed option since we are trying to reduce the number of cases provided due to the heavy compositional simulation requirement. An actual phase diagram is constructed using phase behavior module (PBM) prior to conducting any reservoir simulation. If the initial reservoir pressure and temperature fall outside the two phase region, then the algorithm does nothing and those values would be forwarded to the simulator to run the case. However, if the initial reservoir pressure and temperature happen to fall within the two phase region, then the algorithm adds pressure increments until the two boundary of the phase envelope is felt. After that, a random value of reservoir pressure is assigned between the pressure value at the given temperature and a pressure much higher than reservoir pressure to ensure that we are in the 1 phase region only. Figure 6-5 illustrates how the algorithm works on PVT1 composition. It is also important to note that this process of detecting where the phase boundary and adjusting the initial reservoir pressure is done on every single case in order to generate outputs that are only relevant to miscible CO_2 injection.

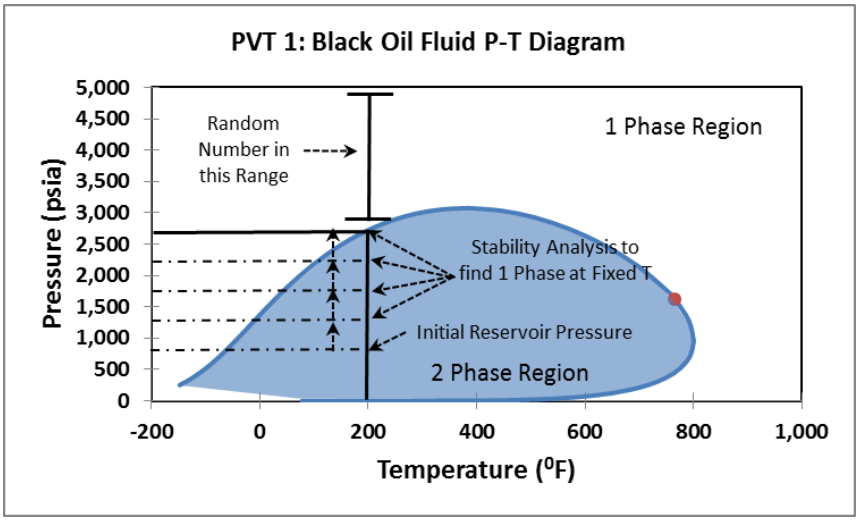

Figure 6-5: Smart Feed Algorithm

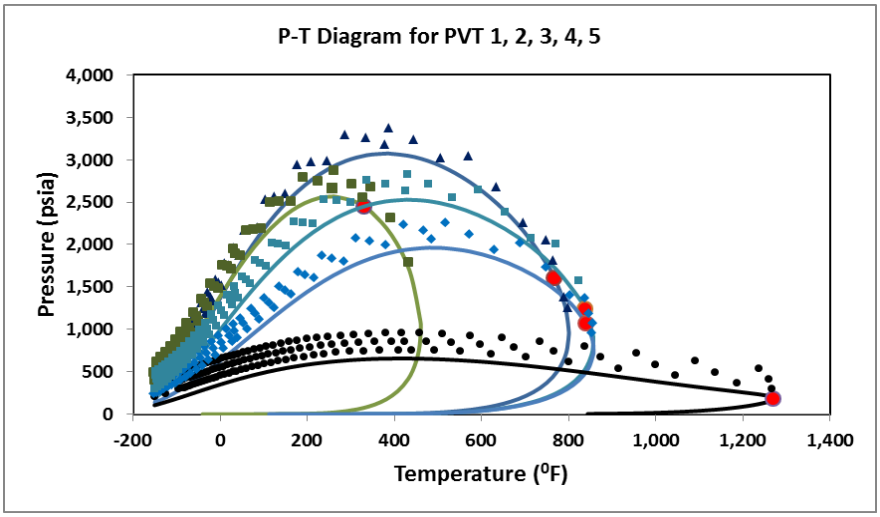

Figure 6-6: Smart Feed or PVT 1, 2, 3, 4, and 5 for Miscible CO_2 Injection

Figure 5-6 shows an example of 5 fluid compositions with initial reservoir distribution pressures for given temperatures. Note that Figure 5-6 is just an illustration as to where the data are located with smart feed and not an actual scenario as every single case has a different composition.

This process of smart feed pre-simulation is a lengthy process and takes much longer time as it is done on every single case. Without smart feed, data generation takes around 30 seconds to generate as much as 6,000 cases. With smart feed, data generation takes around 6 hours.

The following steps summarize how the algorithm works, from the very beginning until the case is about to be submitted to the simulator.

1) Rock properties are chosen from a given range.
2) Fluid composition is chosen from a given range. Up to component HC20.
3) Fluid components above C7+ are lumped, and their properties are calculated.
4) Relative permeability curves are generated using Modified Brooks-Corey.
5) Capillary pressure curves are generated using Brooks-Corey.
6) Phase diagram construction.
7) Check initial reservoir pressure within the phase envelope.
    a. If initial PI is above the two phase region, then proceed to step 8.

b. If Initial reservoir pressure falls within the two phase region, then phase behavior stability analysis are done to find the boundary of the phase envelope at the given temperature.
    i. At fixed T, initial reservoir pressure is increased gradually.
    ii. Stability analysis and check if new pressure with temperature (there is no temperature change) are located within the phase envelope. If yes, repeat the pressure increase at the fixed temperature until phase envelope boundary is reached.

8) Apply a random number between the top of the phase envelope and a higher pressure value to ensure that the database is for miscible cases only.
9) Case is then ready to be submitted to the simulator.

The data generation part of this research is an intensive part. It is very essential to the success of this project that everything is defined thoroughly and carefully. Otherwise, it would be very difficult to find a correlation for the topic at hands.

6.2.2. Minimum Miscibility Correlation Validation

In order to make sure that the data acquired through the developed algorithm is consistent and falls in the miscible region, it is compared against a slim-tube derived correlation. For the algorithm to be successful, the MMP correlation's pressure must be less than the pressures that are assigned to every single case.

Alston et al. (1983) developed a CO_2 MMP correlation as a function of C_{5+} molecular weight, reservoir temperature, and volatile to intermediate mole fraction ratio. The developed correlation reported acceptable MMP predictions for CO_2. For pure CO_2 MMP, Alston et al (1983) reported the following equation:

$$P_{CO2-LO} = 8.78x10^{-4}(TR)^{1.06}(Mc_{5+})^{1.78}(x_{vol}/x_{int})^{0.136}$$

Alston's correlation includes a correction factor for reservoirs with (x_{vol}/x_{int}) that is very different from unity. Most reservoirs have (x_{vol}/x_{int}) close to unity (Alson et al., 1982), so the same equation can be used without the correction term:

$$P_{CO2} = 8.78x10^{-4}(TR)^{1.06}(Mc_{5+})^{1.78}$$

Table 6-6: A Sample of 5 Compositions for Alston's MMP Correlation shows a sample of 5 compositions to find the minimum miscibility pressure using Alston's correlation. The MMP values acquired using Alston's correlation are compared against the values acquired previously through phase behavior diagram. Note that the values acquired through the phase diagram were assigned randomly above the minimum miscibility pressure. So, as long as the phase diagram values are not less than Alston's correlation MMPs, the methodology used is consistent. If the MMP values using Alston's method are higher, then those cases are removed from the data set.

Table 6-6: A Sample of 5 Compositions for Alston's MMP Correlation

Component	Case 1 Composition	Case 2 Composition	Case 3 Composition	Case 4 Composition	Case 5 Composition
H_2S	0.0004	0.0008	0.0003	0.0008	0.0035
CO_2	0.0406	0.0270	0.0070	0.0309	0.0469
N_2	0.0152	0.0056	0.0127	0.0146	0.0112
C_1	0.3729	0.1824	0.4163	0.2936	0.2299
C_2	0.1000	0.0863	0.0655	0.0712	0.0976
C_3	0.0275	0.0650	0.0904	0.0683	0.0575
IC_4	0.0278	0.0382	0.0229	0.0453	0.0306
NC_4	0.0374	0.0410	0.0116	0.0228	0.0118
IC_5	0.0065	0.0475	0.0120	0.0276	0.0299
NC_5	0.0150	0.0251	0.0191	0.0197	0.0115
FC_6	0.0445	0.0474	0.0101	0.0058	0.0382
FC_7	0.0722	0.0797	0.0691	0.0930	0.0168
FC_8	0.0656	0.0189	0.0537	0.0339	0.0862
FC_9	0.0238	0.0991	0.0403	0.0208	0.0210
FC_{10}	0.0592	0.0277	0.0007	0.0003	0.0610
FC_{11}	0.0184	0.0086	0.0968	0.0682	0.0312
FC_{12}	0.0700	0.0279	0.0470	0.0597	0.0998
FC_{13}	0.0031	0.0625	0.0018	0.0636	0.0890
FC_{14}	0	0.0214	0.0227	0.0249	0.0263
FC_{15}	0	0.0198	0	0.0348	0
FC_{16}	0	0.0680	0	0	0
FC_{17}	0	0	0	0	0
FC_{18}	0	0	0	0	0
FC_{19}	0	0	0	0	0
FC_{20}	0	0	0	0	0
C_{7+}	0.3122	0.4337	0.3321	0.3993	0.4314
Temp, ^0F	190	154	174	215	293

Table 6-7 shows the oil volatile fraction (C_1+ N_2) and the intermediate oil fractions (C_2, C_3, IC_4, NC_4, CO_2, and H_2S). These two terms are then used to find which equation to be used as mentioned previously.

Table 6-7: Volatile and Intermediate Fraction Calculation for the 5 Sample Compositions

	Case 1	Case 2	Case 3	Case 4	Case 5
x_{vol}	0.3881	0.1880	0.4289	0.3083	0.2411
x_{int}	0.2337	0.2582	0.1977	0.2393	0.2478
x_{vol}/x_{int}	1.661	0.728	2.170	1.288	0.973

Table 6-8: MMP Values Comparison using Alston's Correlation and the PB Method

	Case 1	Case 2	Case 3	Case 4	Case 5
Alston MMP, psia	1,194	1,082	1,260	1,701	2,237
PB MMP, psia	2,956	1,362	3,755	2,179	3,729

Table 6-8 shows that the MMP values used earlier are consistent with the phase diagram method. This methodology was applied on every single case in the data base that went into building all the various ANNs. There were a few cases that had lower MMP than Alston's correlation and these cases were removed from the data set.

Chapter 7

ARTIFICIAL NEURAL NETWORK DEVELOPMENT

In this section, the development and evolution of various ANN designs are shown. Initially, basic ANN designs for a specific composition and reservoir are shown, and then more complicated and more generalized ones are presented.

During the early stages of the project, some simple ANN configurations were created with as little as 8 neurons. Many parameters and configurations were tested in order to reach a satisfactory ANN that is capable of delivering accurate results that handles a simple purpose.

The major work and development in this section are focused around reservoir fluid composition and how to enable the ANN to handle any reservoir fluid composition. There was extensive testing, tweaking, and manipulations with the ANN around the actual study goal, continuous CO_2 injection. Also, early configurations were designed for specific reservoir fluids (5 compositions that varied between light to heavy oil) and some designed witnessed the water alternating gas approach (WAG).

The main design for continuous CO_2 stayed the same throughout the various ANNs. However, earlier designs included WAG which the most recent designs don't include, but the ANNs structure takes into account the possibility of WAG presence and could be added as part of the main ANN network at later stages. The WAG option has a different index and parameters related to it. The additional parameters describing the WAG process were water injection rate, WAG ratio, and WAG cycle. For a WAG ratio of 0:1, the process has no water and it proceed as a continuous CO_2 injection. For a WAG ratio of 1:1 and higher, the process would switch to a WAG injection rather than continuous CO_2 injection.

6.1 Forward Artificial Neural Networks Proxy (Performance Prediction)

The first ANN development in this project is related to reservoir performance evaluation. This forward proxy requires the user to input all the reservoir properties and the desired injection design parameters. The proxy would then provide oil, and gas production profiles which directly reflect reservoir performance response for the input parameters and the desired injection design. This network design allows the user to check various injection designs as well as study the impact of uncertainty on reservoir properties.

Initial forward designs varied from simple, specific-compositions, specific-reservoirs, to complex universal designs. The simple designs were constructed to learn more about the ANNs and the various behaviors for different input parameters.

Note that bottom-hole flowing pressure (BHFP) in this design is used to control miscibility in all the ANNs in this research.

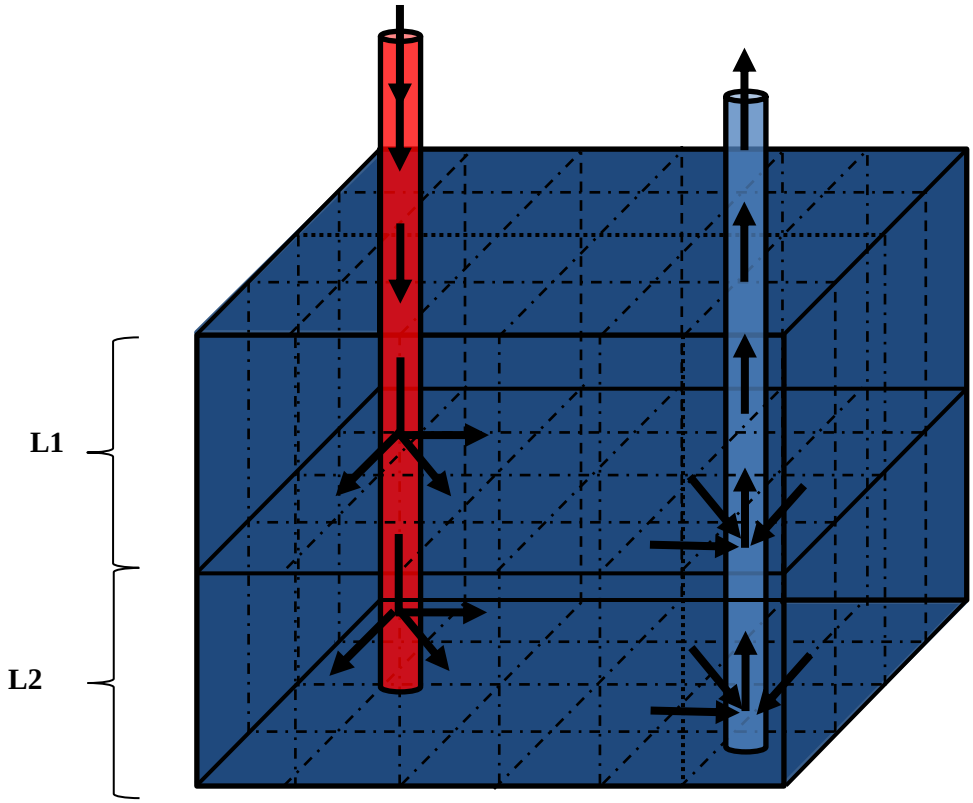

Figure 7-1: Reservoir Simulation Model Concept

ANN Design # 1: Continuous CO_2/WAG Injection, 2-Compsitions, Miscible, Specific Reservoir, 1 Relative Permeability and 1 Capillary Pressure Curve

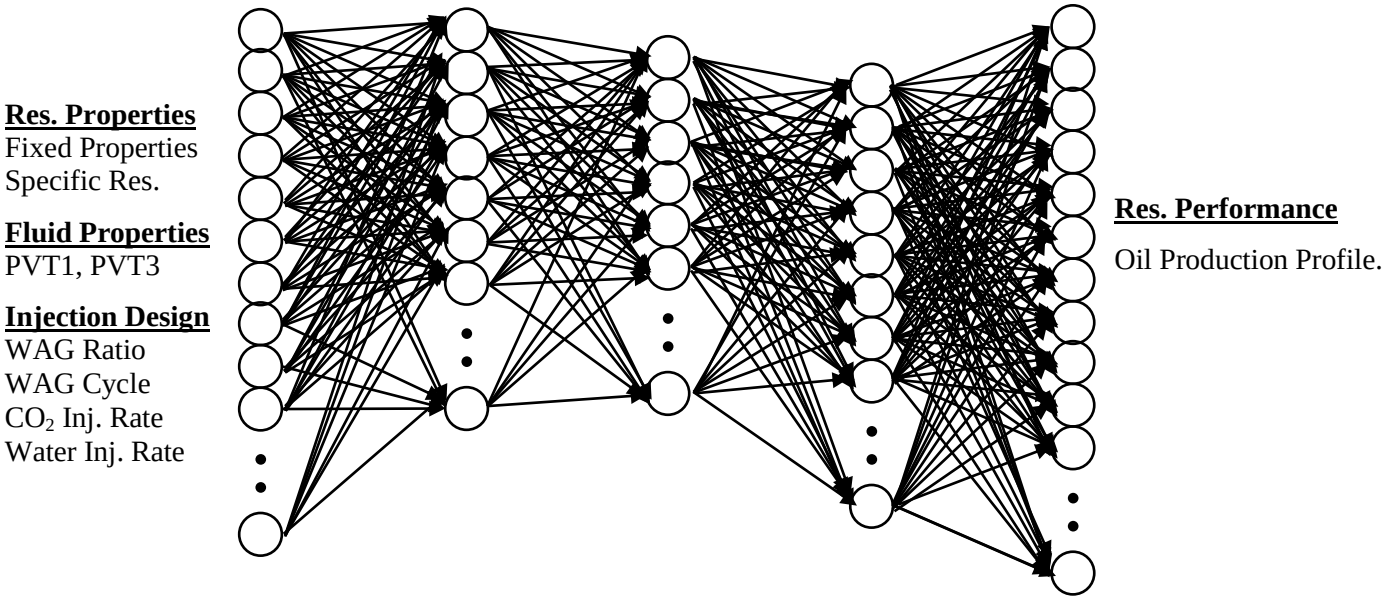

Figure 7-2: Forward ANN design #1 inputs and outputs

ANN design #1 is one of the major initial designs that were constructed with the goal of proof-of-concept. Table 7-1 shows the initial design parameters for ANN design #1.

Table 7-1: Design #1 ANN design parameters

ANN Type	Feed-Forward with Back Propagation
# of Hidden Layers	3
# of Neurons in Hidden Layers	[55,50,44]
Transfer Functions	Logsig, Logsig, Tansig
# Input Neurons	8
# outputs Neurons	122
ANN Target Tolerance	5.E-05
Total Number of Cases	350
% Train Cases	85
% Validation Cases	10
% Blind Testing Cases	5

This design is considered one of the very basic designs for a specific reservoir, relative permeability curve, and capillary pressure curve using two reservoir fluid compositions. One of the features tested within this design was the WAG as an additional option apart from the main continuous CO_2 injection focus.

Design Description:

This is a 20x20x2 reservoir model with grid dimension of 66x66 feet. This grid size was chosen for testing purposes and does not reflect the grid size sensitivity that was done later on to find appropriate grid dimensions that suits the project and its timeline. The model is a dual porosity, dual permeability fractured model using Gilman and Kazemi shape factor. In this design, CO_2 is continuously injected from a dedicated well, while production is done from another dedicated production well. However, CO_2 could be injected alternating with water from the dedicated CO_2 injector.

ANN Design Ranges:

Table 7-2 shows the design parameters specific for this ANN.

Table 7-2: Design parameters for ANN Design #1

Parameter	Value	Units/Notes
Grids	20x20x2	
Grid Dimensions	60	ft
$Kx_m = Ky_m$	20	md
Kz_m	1	md
φ_m	18	%
$Kx_f = Ky_f$	1000	md
Kx_z	10	md
Injection Type	Miscible	
WAG Ratio	**0-3**	0 = Continuous CO_2 Injection
WAG Cycle	**1-6**	Months
Water Injection Rate/D	**500-3000**	Bbls/D
Gas Injection Rate/D	**50,000-600,000**	SCF/D
Simulation Cases	350	
Fluid Compositions	**2**	

Design Reservoir Fluids:

Two black oil compositions were used in this ANN. Table 7-3 shows the fluid compositions for PVT1 and PVT3 that were used in this ANN.

Table 7-3: Reservoir Fluid PVT1 and PVT3 Used in ANN Design#1

Component	PVT 1 Black Oil [McCain, 1990)	PVT 3 Black Oil [Rathmell, 1971)
CO_2	0.91	3.2
N_2	0.16	0.03
C_1	36.47	27.81
C_2	9.67	8.21
C_3	6.95	5.99
IC_4	1.44	0.31
NC_4	3.93	4.1
IC_5	1.44	1.3
NC_5	1.41	2.3
FC_6	4.33	4.62
C_{7+}	33.29	42.13
MW	218	223
SG	0.8515	0.875

Design Analysis and Results

This simple ANN design used a dataset of 350 cases. Miscible continuous CO_2 and WAG injection were tested. Different WAG cycles and ratios were tested under fixed injection rate. This design is reported to highlight the starting point where current existing ANN studies conclude. The performance of the design is measured by how well it performed against blind testing data. Figure 7-3 through Figure 7-7 show the blind testing cases and provide an indication of the overall performance of the ANN. Note that the plots have a different scale reflecting the different responses for the various injection parameters under miscible condition. The average overall errors and average errors post injection are reported on the plots.

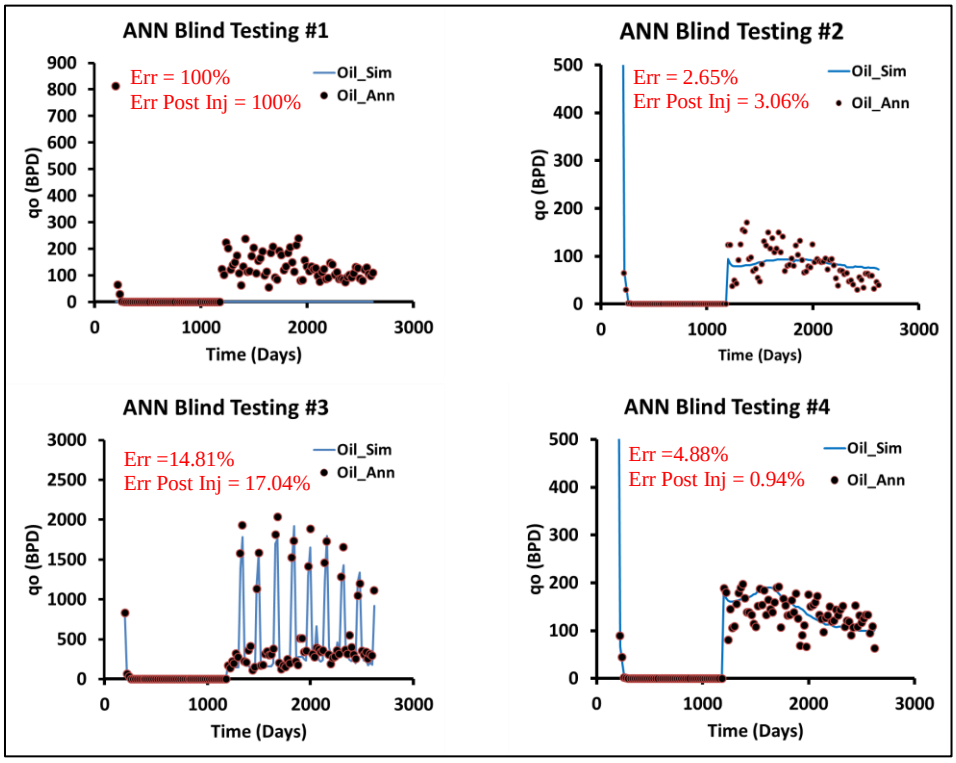

Figure 7-3: Forward ANN#1 Blind Testing Cases 1, 2, 3, 4

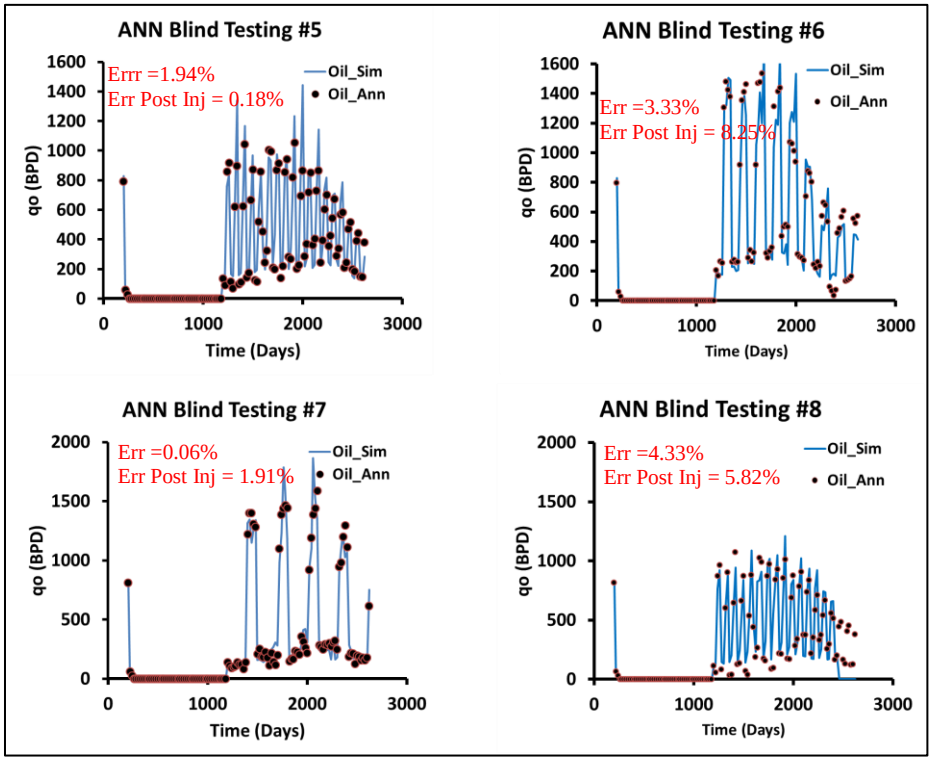

Figure 7-4: Forward ANN#1 Blind Testing Cases 5, 6, 7, 8

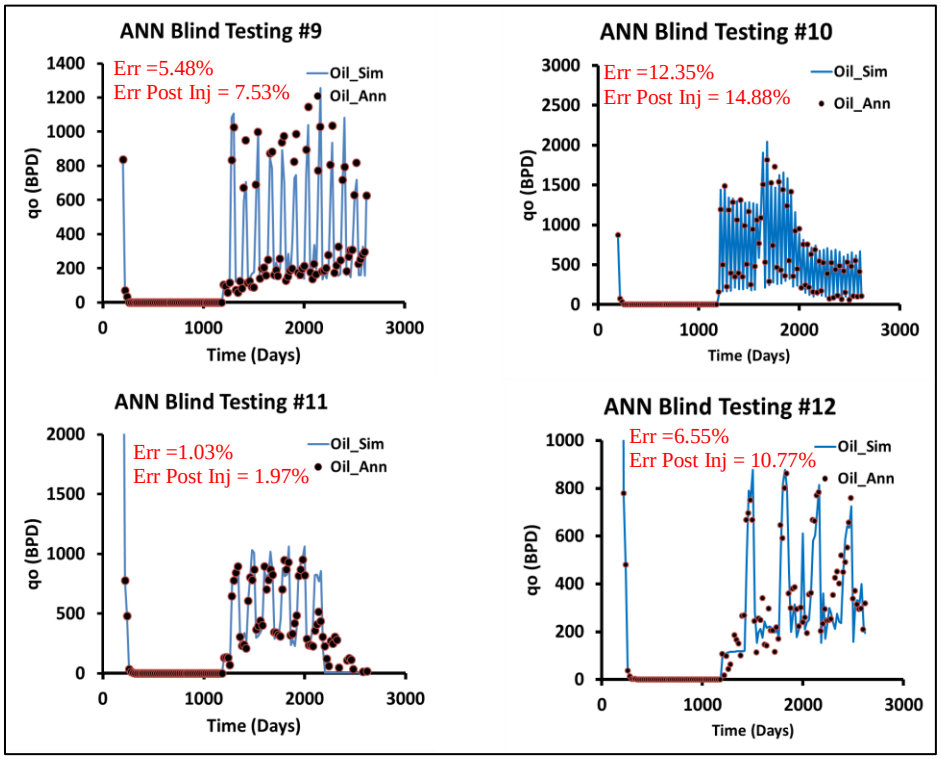

Figure 7-5: Forward ANN#1 Blind Testing Cases 9, 10, 11, 12

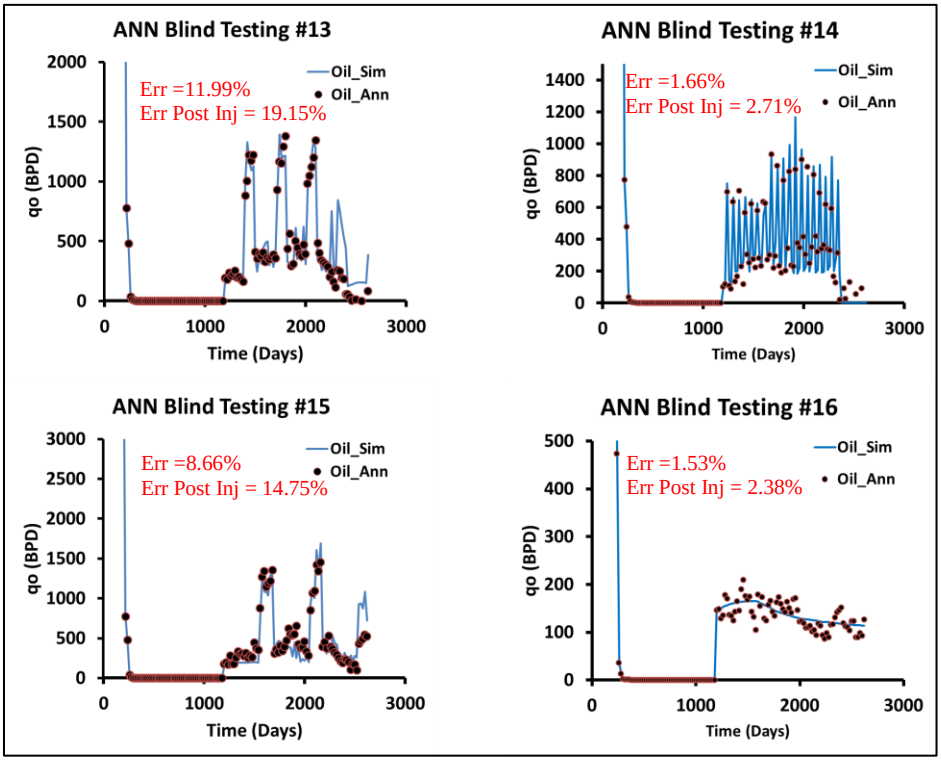

Figure 7-6: Forward ANN#1 Blind Testing Cases 13, 14, 15, 16

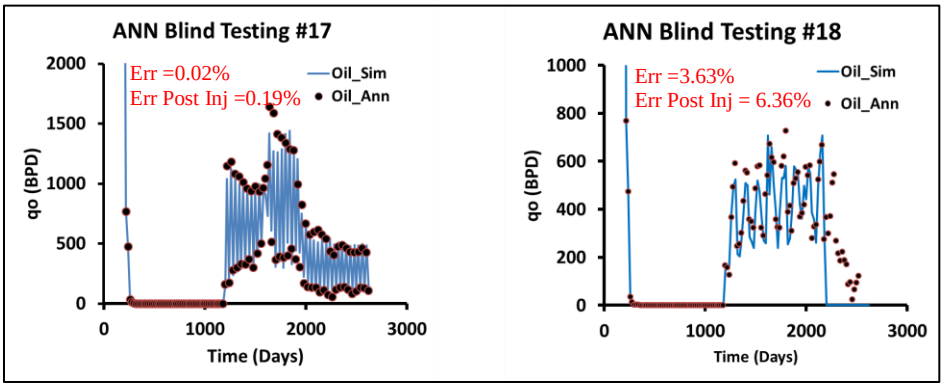

Figure 7-7: Forward ANN#1 Blind Testing Cases 17, 18

Design Error Analysis:

The individual average overall errors and average errors post injection are reported on the blind testing cases. The average overall error and average error post injection for all the blind testing cases are reported in Table 7-4. However, this average error is biased by blind testing case #1 which doesn't produce anything because of low CO_2 injection but the ANN predicts some production for this case.

Table 7-4: Average overall and post injection errors for all the blind testing cases for ANN design #1

Avg Overall Error %	10.23
Avg Error Post Inj %	12.66

Table 7-5 shows the average errors excluding blind testing case#1 and increasing the overall accuracy by around 5%.

Table 7-5: Average overall and post injection errors for all the blind testing cases excluding case #1

Avg Overall Error %	4.95
Avg Error Post Inj %	7.52

Errors alone should not be the only ANN performance indicator as they could easily be misleading. For example, if the target permeability is 2 md, and the predicted value by the ANN is 4 md, the error is 100% and the case is flagged as not good. However, the impact of the 2 md

difference between the actual and predicted values is most likely negligible. On the same note, the error between 7,000 md actual and 7,500 md predicted is 7.14%. However, the difference is 500 md and might contribute to a different behavior than actual.

This initial ANN design is considered good based on two factors:

1) Average error post injection per blind testing case.
2) Overall shape and trend of each blind testing case.

While some blind tests reported average errors above 10%, the overall errors were low and the overall trends for most of the cases were captured successfully. In general, this design was good as a starting point were existing ANN studies of this nature concluded.

ANN Design # 2: Continuous CO_2/WAG Injection, 5 Fluid Compositions, Miscible, Universal Rock Properties, 1 Relative Permeability and 1 Capillary Pressure Curve

Res. Properties

K_m, K_f, φ_m, φ_f,
Fracture Spacing
Well Spacing

Fluid Properties

PVT1, PVT2,
PVT3, PVT4,
PVT5

Injection Design

WAG Ratio
WAG Cycle
CO_2 Inj. Rate
Water Inj. Rate

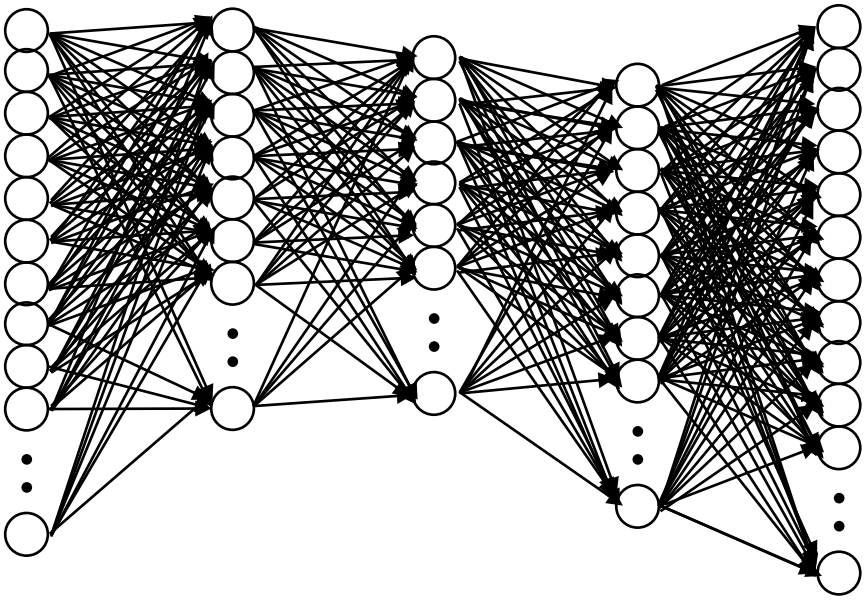

Res. Performance

Oil Production Profile.

Figure 7-8: Forward ANN design #2 inputs and outputs

ANN Design #2 is an evolved design. Initially, only two compositions were used in previous designs. Also, this design includes a wide range of reservoir rock parameters as well as varying monthly CO_2 and water injection rates and varying monthly water injection rate (in case of WAG). Table 7-6 summarizes the network design for ANN design #2.

Table 7-6: Design #2 ANN design parameters

ANN Type	Feed-Forward with Back Propagation
# of Hidden Layers	4
# of Neurons in Hidden Layers	[55,50,44,35]
Transfer Functions	Logsig, Logsig, Tansig, Logsig
# Input Neurons	11
# outputs Neurons	122
ANN Target Tolerance	5.E-05
Total Number of Cases	2000
% Train Cases	85
% Validation Cases	10
% Blind Testing Cases	5

Design Description:

This is a 20x20x2 reservoir model with grid dimension of 66x66 feet. This grid size was chosen for testing purposes and does not reflect the grid size sensitivity that was done later on to find appropriate grid dimensions that suits the project and its timeline. The model is a dual porosity, dual permeability fractured model using Gilman and Kazemi shape factor. In this design, CO_2 is continuously injected from a dedicated well, while production is done from another dedicated production well. However, CO_2 could be injected alternating with water from the dedicated CO_2 injector.

ANN Design Parameter Ranges:

Table 7-7 shows the design parameters specific for this ANN.

Table 7-7: Design parameters for ANN Design #2

Parameter	Value	Units/Notes
Grids	20x20x2	
Grid Dimensions	66	ft
$Kx_m = Ky_m$	20-200	md
Kz_m	$0.01*Kx_m$	md
φ_m	10-40	%
$Kx_f = Ky_f$	1,000-10,000	md
Kz_f	$0.01*Kx_f$	md
φ_f	1	%
Injection Type	Miscible	
WAG Ratio	0-3	0 = Continuous CO_2 Injection
WAG Cycle	1-6	Months
Water Injection Rate/D	500-6000	Bbls/D
Gas Injection Rate/D	600,000-1,500,00	SCF/D
Simulation Cases	3000	
Fluid Compositions	5	
Fracture Spacing	10-40	
Reservoir Size	40 - 500	Acres

Design Reservoir Fluids:

In this ANN, five oil compositions ranging from volatile oil to very heavy oil were used in. Table 7-8 shows the five fluid compositions used in ANN design #2.

Table 7-8: Reservoir Fluids PVT1 through PVT5 Used in ANN Design#2

Component	PVT 1 Black Oil [McCain, 1990)	PVT 2 Volatile Oil [Papp et al, 1998)	PVT 3 Black Oil [Rathmell, 1971)	PVT 4 SPE 24185 [Hindi et al, 1992]*	PVT 5 Parada Heavy Oil
CO_2	0.91	0.51	3.2	4.15	0.11
N_2	0.16	1.8	0.03	0.42	0.69
C_1	36.47	46.8	27.81	18.13	10.78
C_2	9.67	8.09	8.21	9.41	0.12
C_3	6.95	10.91	5.99	8.04	0.42
IC_4	1.44	4.26	0.31	1.46	0.3
NC_4	3.93	6.86	4.1	4.33	0.32
IC_5	1.44	3.71	1.3	1.74	0.29
NC_5	1.41	3.81	2.3	2.4	0.26
FC_6	4.33	4.73	4.62	3.68	0.64
C_{7+}	33.29	8.52	42.13	46.24	86.09
MW	218	156	223	221	532
SG	0.8515	0.782	0.875	0.874	0.925

Note: PVT #4 is modified version of fluid used by Hindi et al. The modified version was used to have the same components for all the five reservoir fluid compositions to provide basis for comparisons.

Design Analysis and Results

What differentiates this ANN from the previous one is that, it has much more neurons than the previous ANN. This ANN accounts for a wide range of reservoirs as well as 3 additional compositions and flexible monthly injection rates. For that reason, around 3000 simulation cases were used to build the data set that eventually went into the ANN. Note that around one half of the 3,000 cases had to be removed after quality-checking the data set as they either didn't run,

didn't produce post injection, or stopped in the middle of simulation. 85% of the cases were used to train the network, 10% for validation, and the last 5% were used later for blind testing.

Figure 7-9 through Figure 7-13 show a sample of the blind testing cases and provide an overall performance of the ANN. The cases in this sample range between good and bad among the 5 PVT compositions. Note that the plots have different scales to reflect all the various inputs of the ANN.

(Note: Appendix E shows all of the 56 blind testing cases.)

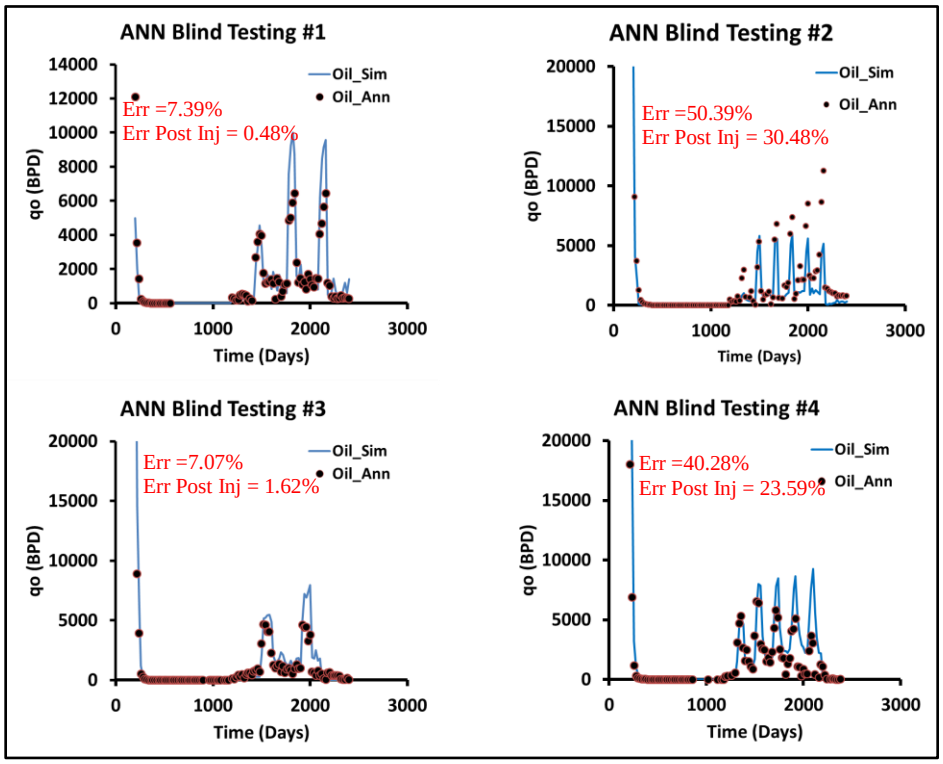

Figure 7-9: Forward ANN#2 Blind Testing Cases 1, 2, 3, 4

It is important to keep in mind that the oil production profiles in ANN design #2 produced much higher rates than the previous design. Also, the early decline period contribute significantly to the overall errors.

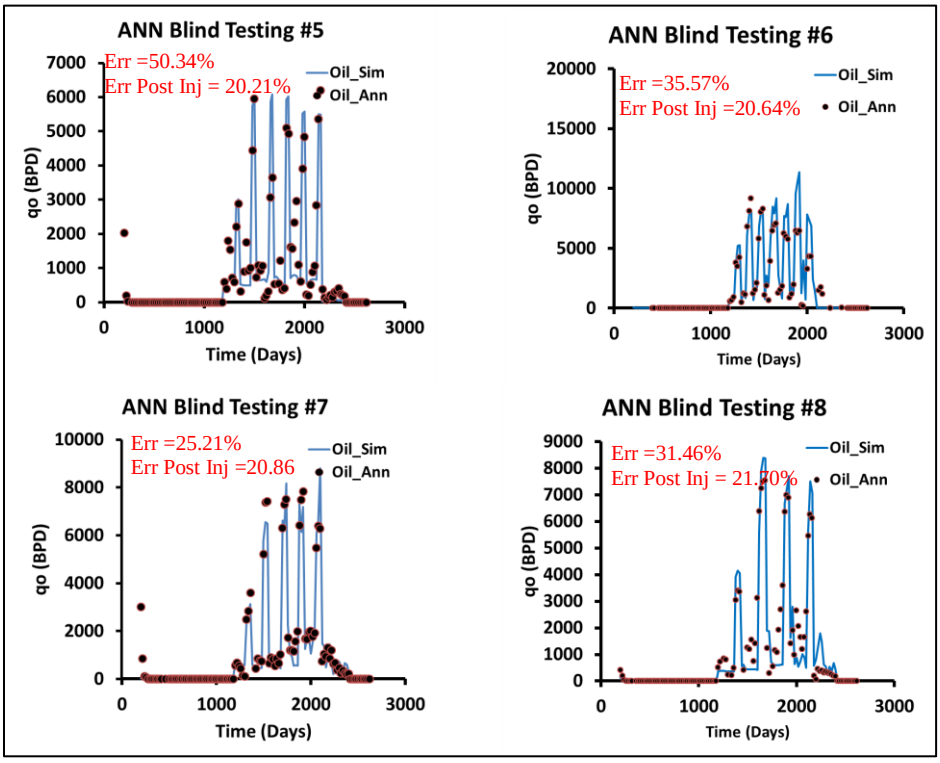

Figure 7-10: Forward ANN#2 Blind Testing Cases 5, 6, 7, 8

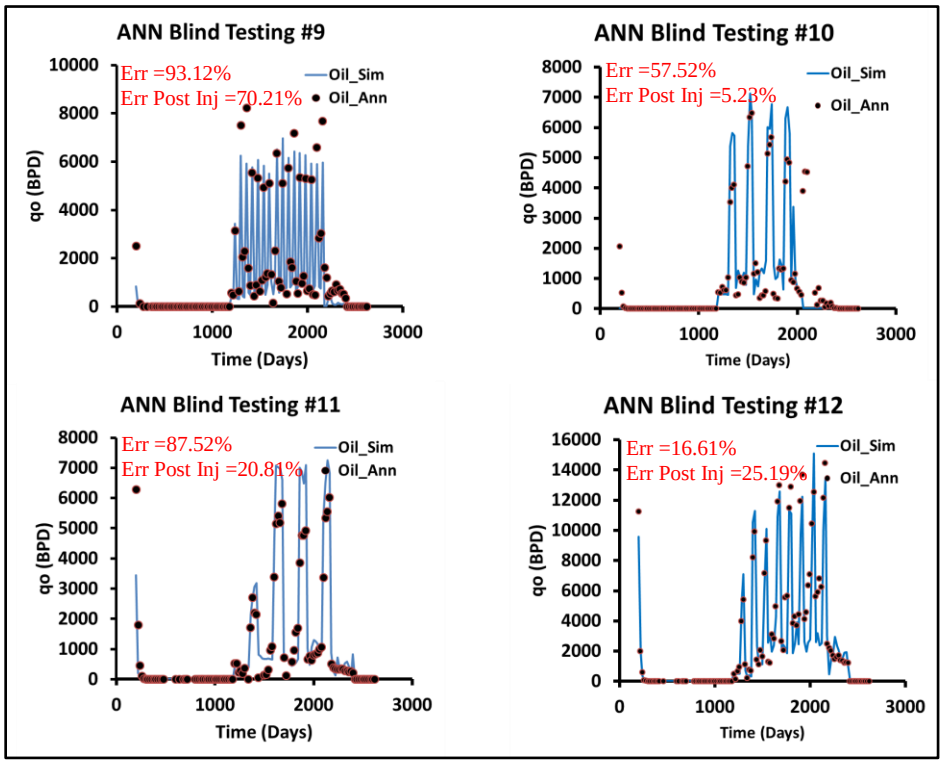

Figure 7-11: Forward ANN#2 Blind Testing Cases 13, 14, 15, 16

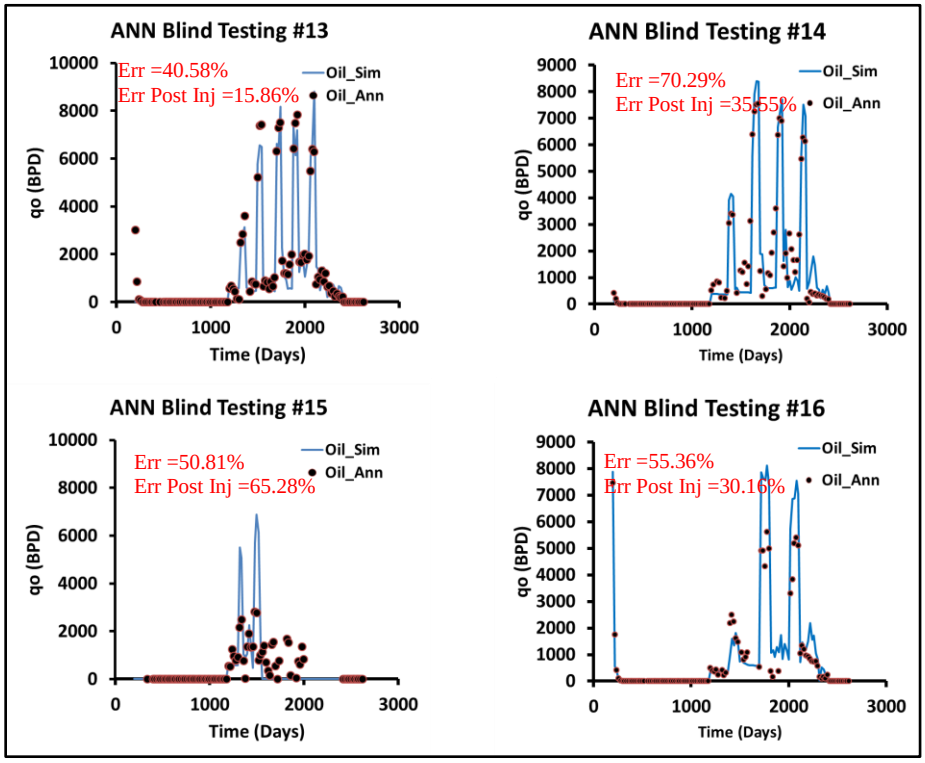

Figure 7-12: Forward ANN#2 Blind Testing Cases 13, 14, 15, 16

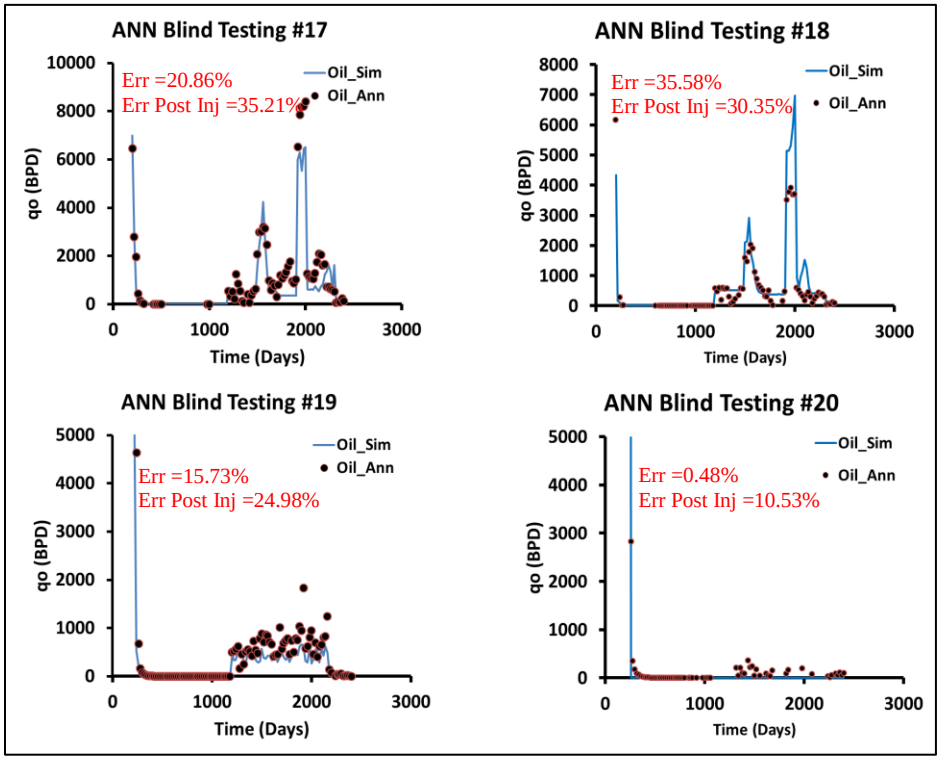

Figure 7-13: Forward ANN#2 Blind Testing Cases 17, 18, 19, 20

Design Error Analysis:

This design has a lot of new features that differentiates it from its previous version. The added features did impact the accuracy of the overall model. The main error contributors are the flexible varying monthly injection CO_2 and water (in case of WAG). Also, three additional reservoir fluids as well as a wide range of reservoir properties are included. The individual average overall errors and average errors post injection are reported on the blind testing cases. The average overall error and average error post injection for all the blind testing cases are reported in Table 7-4. Similar to ANN design #1 the average error is biased by some blind testing cases #1 which do not produce post injection but the ANN predicts some production for these cases.

Table 7-9: Average overall and post injection errors for all the blind testing cases for ANN design #2

Avg Overall Error %	35.15
Avg Error Post Inj %	25.78

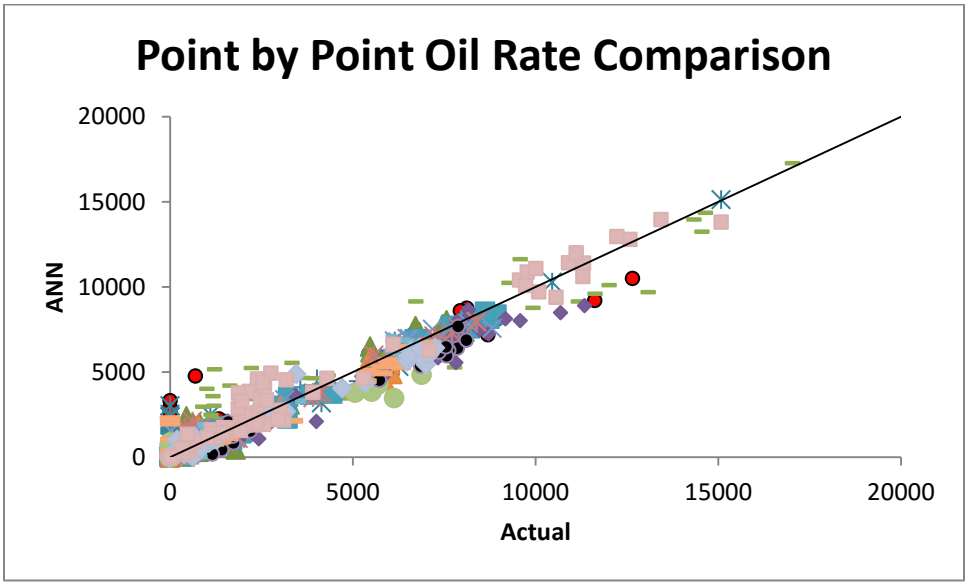

Figure 7-14: Sample blind test monthly oil rate comparison for ANN design #2

Figure 7-14 shows a point by point comparison between the actual monthly oil production rates and the ones predicted by the ANN. The black line represents the best scenario possible. The closer the values from the black line, the better performance the ANN has.

Errors alone should not be the only ANN performance indicator as they could easily be misleading. Also, looking at the plot and capturing the overall trend is not enough. For example, some of the blind testing cases for this design show a close match, however, the small difference between the actual and predicted data contributed to a big error due to high oil production rates. This initial ANN design is considered satisfactory based on:

1) Average error post injection per blind testing case.
2) Overall shape and trend of each blind testing case.
3) Impact of overall errors on the model accuracy.

In this design, some blind tests reported average errors above 20%, but the overall trends for most of the cases were captured successfully. This design is considered satisfactory, but should be fine-tuned more to improve the accuracy of the overall ANN. However, this design is a transitional design and it added a lot of value over the previous simple design. Considering all the new features in terms of 3 additional fluid compositions, varying injection rates for CO_2 and water, and a range of reservoir properties, the ANN design was able to capture most behaviors sufficiently. The value this design adds is still limited due to the limitation imposed by having to choose between five fluid compositions and the specific relative permeability and capillary pressure curves.

ANN Design # 3: Continuous CO_2 Injection, Universal Fluid Composition, Miscible, Universal Rock Properties, Universal Relative Permeability, Universal Capillary Pressure

Res. Properties
K_m, K_f, ϕ_m, ϕ_f,
Thickness
Fracture Spacing
Res. Pressure
Res. Temp
Res. S_W
BHFP
Relative Perm
Cap. Pressure

Fluid Properties
Components:
H_2S, CO_2, N_2,
C1, C2, C3, IC4
NC4, IC5, NC5
FC6, FC7, FC8,
FC9, FC10,
FC11, FC12,
FC13, FC14,
FC15, FC16,
FC17, FC18,
FC19, FC20

Injection Design
CO_2 Inj. Rate
CO_2 Inj. Duration

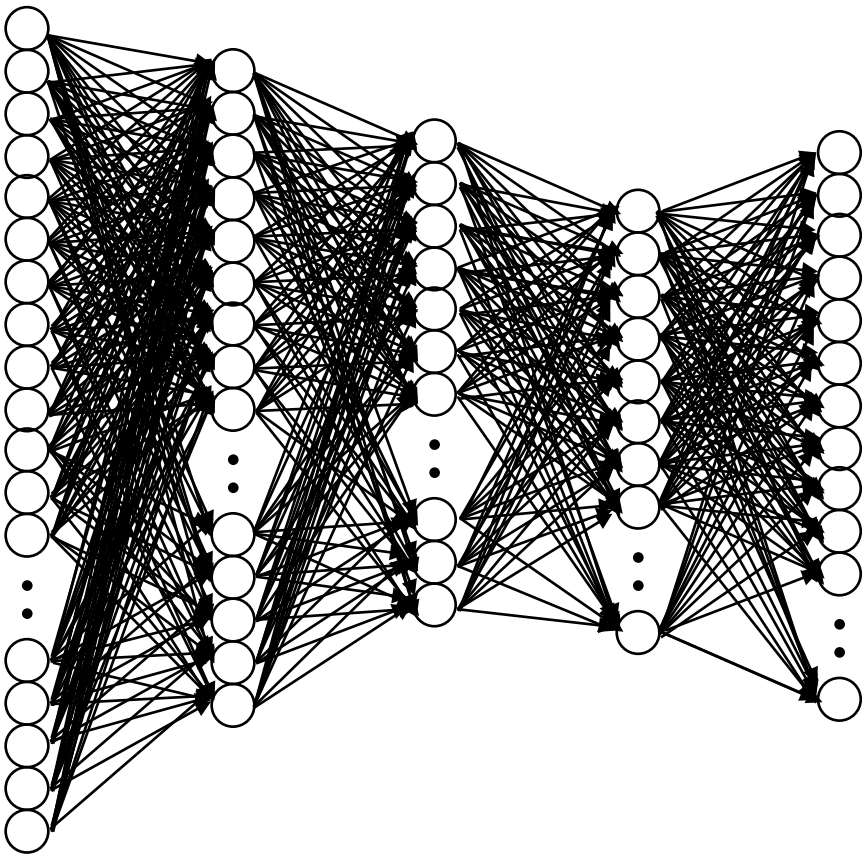

Res. Performance
Oil Production.

Figure 7-15: Forward ANN design #3 inputs and outputs

ANN Design #3 is the most comprehensive and flexible design. It encompasses an extensive number of neurons that represents various reservoir parameters. However, this ANN does not include the WAG option which was a testing parameter in the previously constructed ANNs. WAG was not included in this ANN design due to couple issues that affected the number of cases needed. For example, loss of injectivity issue affected a lot of cases requiring to more data and affecting the overall results for both continuous CO_2 and WAG since at the end, they both would

be part of a single ANN. Running WAG cases affected the run time and contributed to convergence problems. Table 7-10 shows the ANN design #3 network parameters.

Table 7-10: Design #3 ANN design parameters

ANN Type	Feed-Forward with Back Propagation
# of Hidden Layers	4
# of Neurons in Hidden Layers	[50,75,34,70]
Transfer Functions	Logsig, Logsig, Tansig, Logsig
# Input Neurons	106
# outputs Neurons	122
ANN Target Tolerance	5.E-05
Total Number of Cases	2000
% Train Cases	85
% Validation Cases	10
% Blind Testing Cases	5

Design Description:

This is a 20x20x2 reservoir model with grid dimension of 44x44 feet. The 44x44 feet grids were selected even though the 30x30 showed less grid size error, however, the improvements over the 44x44 were very minor but at the expense of run time. The 30x30 grids ran 25% slower than the 44x44 feet grids. The grid size selection was studied in previous sections and the justification of this grid size was explained in previous sections.

The model is a dual porosity, dual permeability fractured model using Gilman and Kazemi shape factor. In this design, CO_2 is continuously injected from a dedicated well, while production is done from another dedicated production well. This design incorporates more features that lift the limitations on fluid composition, relative permeability, and capillary pressure.

ANN Design Parameter Ranges:

Table 7-11: Design Parameters for ANN Design #3

#	Parameter	Min	Max	Units	Notes
1	Gas Inection Rate	6.E+05	2.E+06	SCF	
2	Reservoir Temperature	120	300	^{o}F	
3	Reservoir Pressure	2000	6000	psia	
4	Well Spacing	17	217	Acres	
5	Fracture Perm	1000	10000	md	
6	Fracture Spacing	10	40	Grid/Spacing	
7	Matrix Porosity	10	40	%	
8	Layer 1 Matrix Perm	20	200	md	
9	Layer 2 Matrix Perm	20	200	md	
10	Layer 1 Thickness	20	70	ft	
11	Layer 2 Thickness	20	70	ft	
12	Production Layers	1	2	Production from L1, or L2	
13	H2S Composition	0.01	0.5	%	
14	CO2 Composition	0.5	5	%	
15	N2 Composition	0.5	2	%	
16	C1 Composition	10	50	%	
17	C2 Composition	10	30	%	
18	C3 Composition	0.5	10	%	
19	IC4 Composition	0.5	10	%	
20	NC4 Composition	0.5	10	%	
21	IC5 Composition	0.5	10	%	
22	NC5 Composition	0.5	10	%	
23	FC6 Composition	0.5	10	%	
24	FC7 Composition	0.5	10	%	Lumps into C7+
25	FC8 Composition	0	10	%	
26	FC9 Composition	0	10	%	
27	FC10 Composition	0	10	%	
28	FC11 Composition	0	10	%	
29	FC12 Composition	0	10	%	
30	FC13 Composition	0	10	%	
31	FC14 Composition	0	10	%	
32	FC15 Composition	0	10	%	
33	FC16 Composition	0	10	%	
34	FC17 Composition	0	10	%	
35	FC18 Composition	0	10	%	
36	FC19 Composition	0	10	%	
37	FC20 Composition	0	10	%	
38	C7+ Composition	0	1	%	Lumped Composition
39	BHFP	400	4500	psia	
40	Krw at Irreducible Oil	0.4	1		Krwiro
41	Kro at Connate Water	0.4	1		Krocw
42	Krog at Connate Gas	0.4	1		Krogcg
43	Krg at connate Liquid	0.4	1		Krgcl
44	Connate Water Saturation	0.05	0.4	%	Swcon

45	Critical Water Saturation	0.05	0.4	%	Swcrit = Swcon
46	Residual Oil for Water-Oil	0.05	0.4	%	Sorw
47	Irreducible Oil for Water-Oil	0.05	0.4	%	Soirw = Sorw
48	Residual Oil for Gas-Liquid	0.05	0.3	%	Sorg
49	Irreducible Oil for Gas-Liquid	0.05	0.3	%	Soirg = Sorg
50	Connage Gas Saturation	0.05	0.3	%	Sgcon
51	Critical Gas Saturation	0.05	0.3	%	Sgcrit = Sgcon
52	RelPerm Expononents	0.7	4	Nw, Now, Nog, and Ng	
53	Oil-Water Entry Capillary Pressure	5	30	psia	
54	Oil-Gas Entry Capillary Pressure	5	30	psia	
55	Gamma for Capillary Pressure	1	10		
56	Initial Reservoir Water Saturation	10	40	%	
57	Oil Production Profile	144		Profile Output Parameters	Target

Design Reservoir Fluids:

Handling variations in reservoir fluid compositions are always considered a limiting factor, especially for ANN-related projects. In previous studies, the whole fluid compositions would be referred with a particular name, for example, fluid 1, fluid 2, etc. Therefore, ANN studies were limited to a handful of reservoir fluids and all other fluids would be approximated, which really impacted the accuracy of such studies.

This ANN design incorporates a unique feature that was not included before in previous ANNs nor used in similar studies the literature. This design uses a compositional algorithm that changes reservoir fluid composition in every case inside the data set. The impact of this compositional algorithm is very big. Previously, ANNs were designed using specific fluid compositions just like ANN design #1 and ANN design #2. Using specific compositions limits the ANN and hinders its functionality and purpose. However, the incorporated compositional algorithm makes the ANN usable regardless of the fluid composition which is one of the main factors in EOR projects. The algorithm takes into account components up to heavy hydrocarbon 20 (FC20), and then lumps all the heavy components above C_7 as C_{7+}.

Design Analysis and Results

This design incorporates some new features that were not used in similar studies in the literature. Similar to previous designs, the main success category are the blind testing data For miscible injection cases, around 3000 simulation cases were needed to build the data set. However, after quality-checking the data set, around half the cases was removed as they either didn't run, didn't produce post injection, or stopped in the middle of simulation.

85% of the cases were used to train the network, 10% for validation, and the last 5% were used later for a blind test. The following plots are samples of the blind testing data and they provide an overall performance of the ANN. Note that the plots have different scale to reflect all the various inputs of the ANN.

(Note: Appendix F shows all of the 58 blind testing cases.)

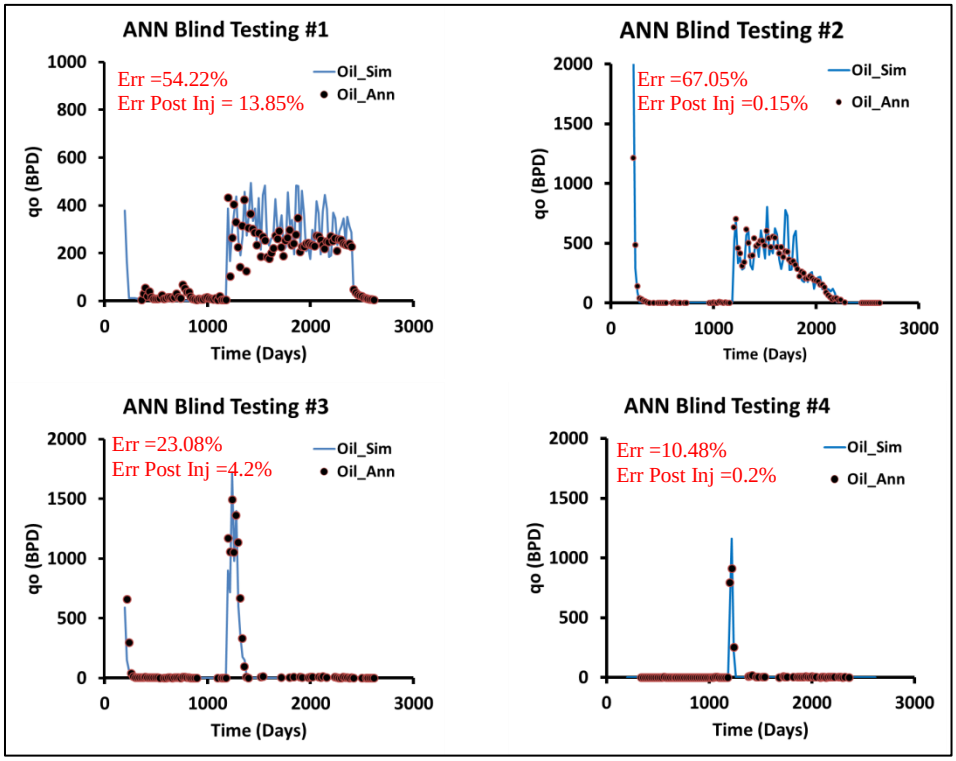

Figure 7-16: Oil Production for Blind Test Cases 1, 2, 3, and 4

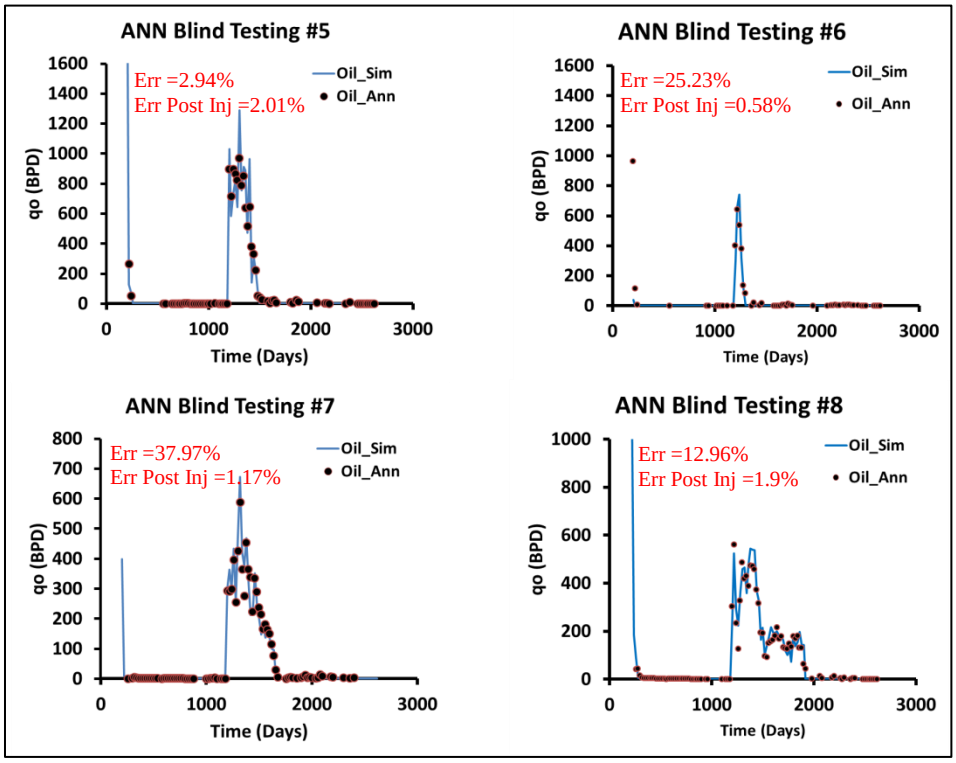

Figure 7-17: Oil Production for Blind Test Cases 5, 6, 7, and 8

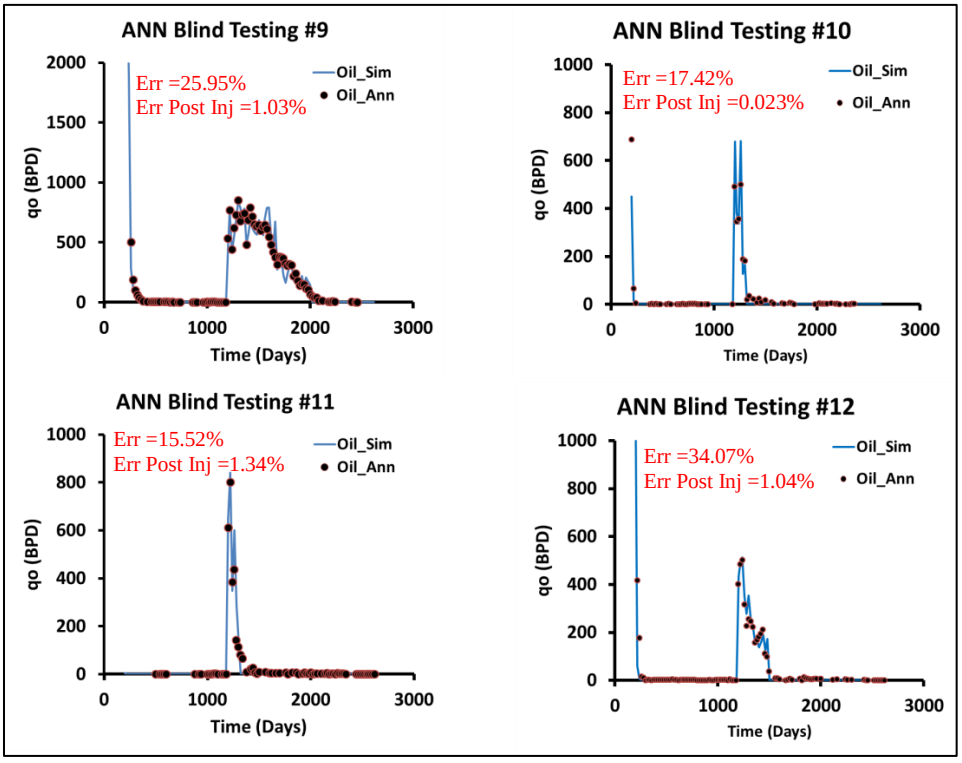

Figure 7-18: Oil Production for Blind Test Cases 9, 10, 11, and 12

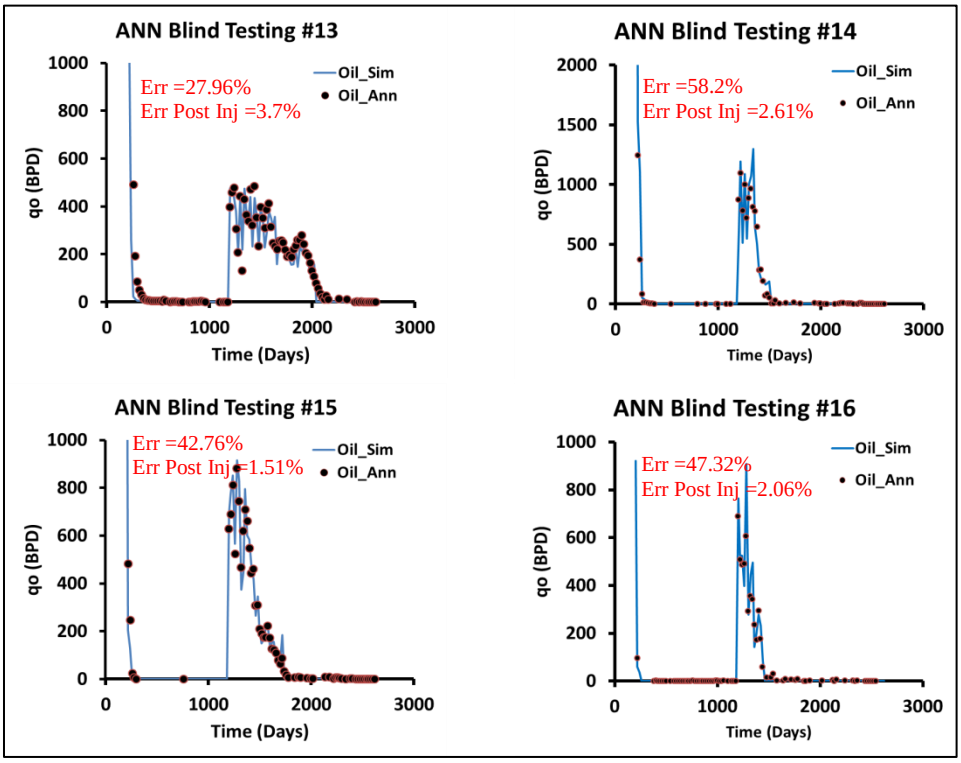

Figure 7-19: Oil Production for Blind Test Cases 13, 14, 15, and 16

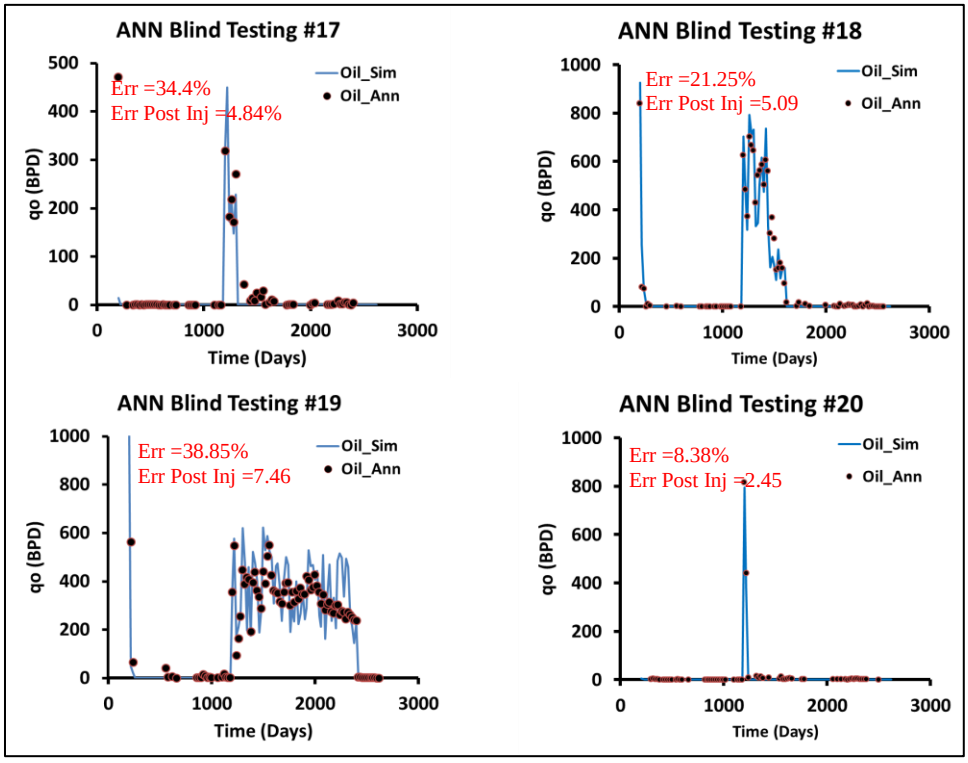

Figure 7-20: Oil Production for Blind Test Cases 17, 18, 19, and 20

ANN design Functional Links:

This major design required a lot of fine tuning and improvements until it reached the final stage. In this design, functional links and data manipulation techniques were used. Taking the log of the outputs and providing the log of some of the inputs as part of the outputs seemed to help the network. Some simple functional links were added on a trial and error basis. However, some complex functional links were required. For those functional links, every input was studied against the target (oil production) for the entire dataset. One of the direct correlations was the cumulative CO_2 injection. A correlation relating the cumulative of both oil and injected CO_2 was then used as an input parameter. Figure 7-21 shows a general correlation between the amount of CO_2 injection and the cumulative oil production in the dataset used for ANN design #3.

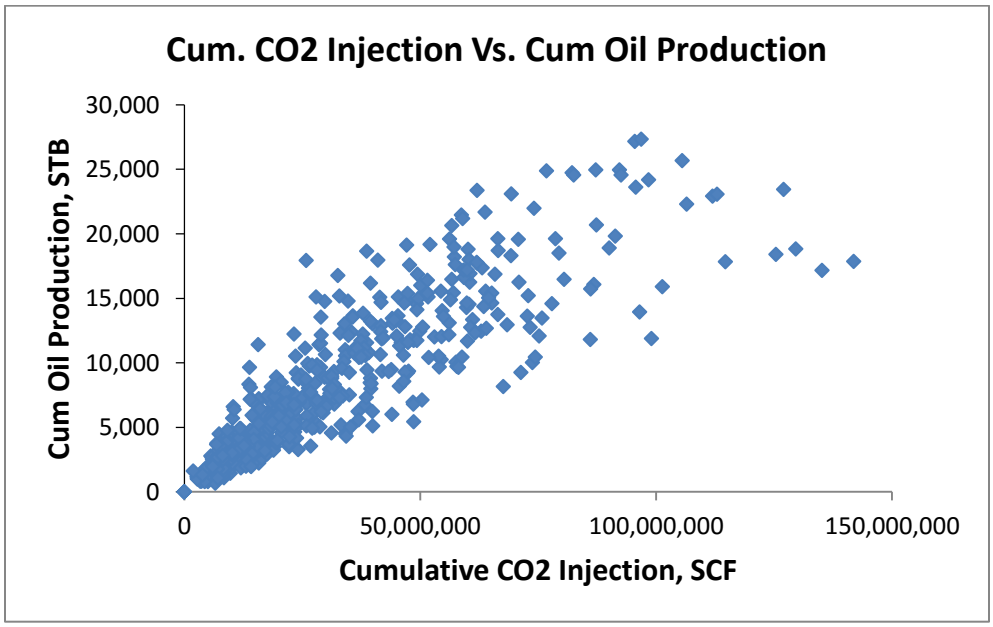

Figure 7-21: Cumulative CO_2 Injection vs. Cumulative Oil Production Correlation for ANN Design #3

Another direct correlation is between cumulative oil production and the product of well spacing and cumulative CO_2 injection, Figure 7-22. An equation was used as an input while on the output the product of well spacing and cum. CO_2 injection is provided.

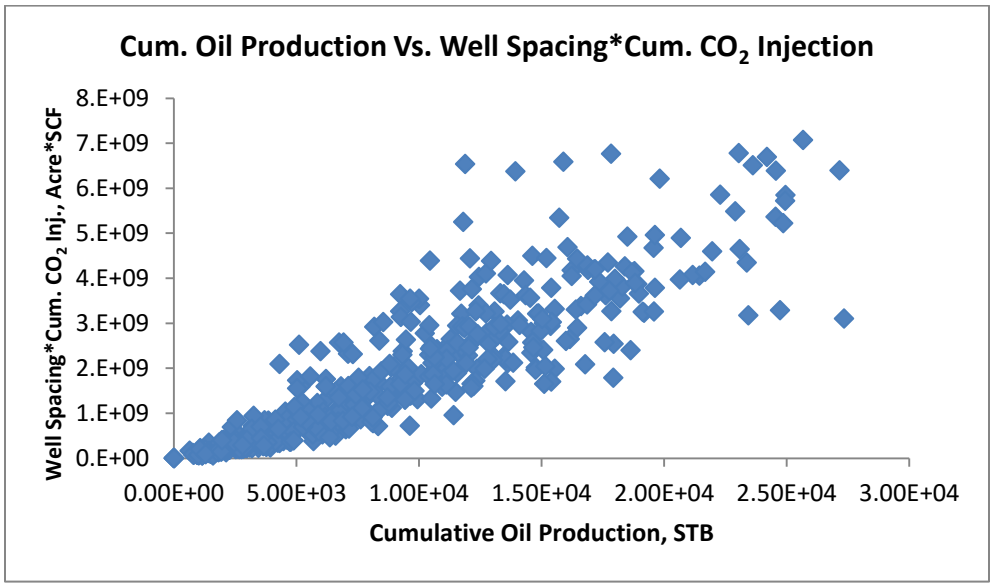

Figure 7-22: Cum. Oil Production vs Well spacing* Cum. CO_2 Injection for ANN Design #3

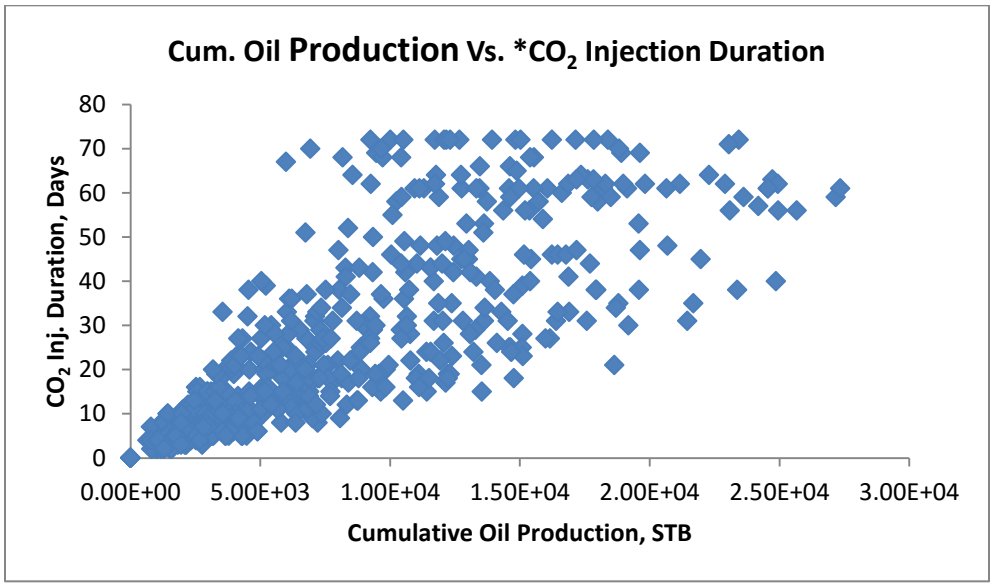

Figure 7-23: Cum. Oil Production vs CO_2 Injection Duration for ANN Design #3

Final data manipulation techniques and functional links are in show in Table 7-12 and Table 7-13 respectively.

Table 7-12: Final Data Manipulation Techniques for ANN Design #3

Data Manipulation	Location
Ln(L1 Matrix Perm.+L2 Matrix Perm.)	Inputs
Ln(Fracture Perm.)	Inputs
Ln(Well Spacing)	Inputs
Ln(L1 Thickness + L2 Thickness)	Inputs
1/Ln(Well Spacing)	Outputs

Table 7-13: Final Functional Links for ANN Design #3

Functional Links	Location
Ln(Well Spacing*Cum. CO_2 Inj.)	Inputs
Pi - BHFP	Inputs
Well Spacing * (L1 Thickness + L2 Thickness)	Inputs
2E-4*Cum. CO_2 Injection + 1,865.4	Inputs
(Cum. CO_2 Injection*Well Spacing+3E8)/231793	Inputs

Design Error Analysis:

This design is considered second generation and much superior to the previous designs. It adds more complexity and functionality through incorporating compositional fluid, relative permeability, and capillary pressure algorithms to account for any reservoir fluid within the provided ranges.

This design surpasses previously constructed ANNs and sets a new benchmark for similar studies in terms of functionality and usability. Previous designs were limited to specific reservoir properties, fluid composition, relative permeability, and capillary pressure while this design is universal to all of these properties.

The individual average overall errors and average errors post injection are reported on the blind testing cases. The average overall error and average error post injection for all the blind testing cases are reported in Table 7-14. Similar to ANN design #1 and ANN design #2, the average overall error is biased significantly by the early decline period which is completely insignificant.

Table 7-14: Average overall and post injection errors for all the blind testing cases for ANN design #3

Avg Overall Error %	33.43
Avg Error Post Inj %	2.86

Figure 7-24 shows a point-by-point comparison between the actual monthly oil production rates and the ones predicted by the ANN. The black line represents the best scenario possible. The closer the values from the black line, the better performance the ANN has.

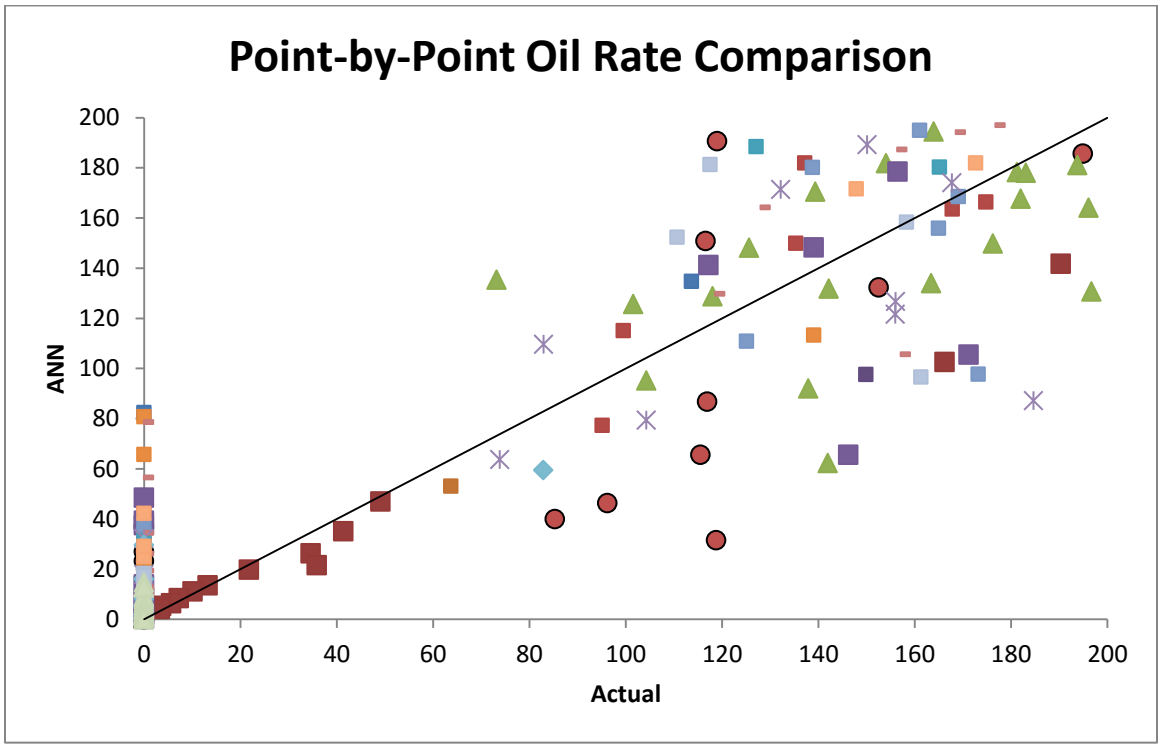

Figure 7-24: Sample blind test monthly oil rate comparison for ANN design #3

The point by point comparison looks exaggerated and does not make sense if compared with the ANN design #2 point-by-point plot. ANN design #2 had much higher rates due to the dominance of the WAG technique in that design and the errors were masked by these high rates. On the other hand, ANN design #3 has low oil production rates contributed exclusively by continuous CO_2.

For example, in Figure 7-24, the average difference of the red circles is around 30 STB, while the same difference in Figure 7-14 from ANN design #2 has a difference of around 3,000 STB. This design is a major milestone in this research. The strength of this ANN is embedded in its flexibility to accommodate a wide range of reservoir fluids, relative permeability data and capillary pressure data under any reservoir temperature. This design was enhanced and manipulated many times in order to come out with the current version as it has all the final features developed.

This ANN design is a successful one, despite the fact that it has a large error on the early decline period which is completely insignificant for this project as the ANN will be used post injection to predict oil production. This final ANN design is considered very reliable based on:

1) Average error post injection per blind testing case.
2) Overall shape and trend of each blind testing case.

Modified ANN Design # 3B: Continuous CO_2 Injection, Universal Fluid Composition, Universal Rock Properties, Universal Relative Permeability, Universal Capillary Pressure

Res. Properties
K_m, K_f, ϕ_m, ϕ_f,
Thickness
Fracture Spacing
Res. Pressure
Res. Temp
Res. S_W
BHFP
Relative Perm
Cap. Pressure

Fluid Properties
Components:
H_2S, CO_2, N_2,
C1, C2, C3, IC4
NC4, IC5, NC5
FC6, FC7, FC8,
FC9, FC10,
FC11, FC12,
FC13, FC14,
FC15, FC16,
FC17, FC18,
FC19, FC20

Injection Design
CO_2 Inj. Rate
CO_2 Inj. Duration

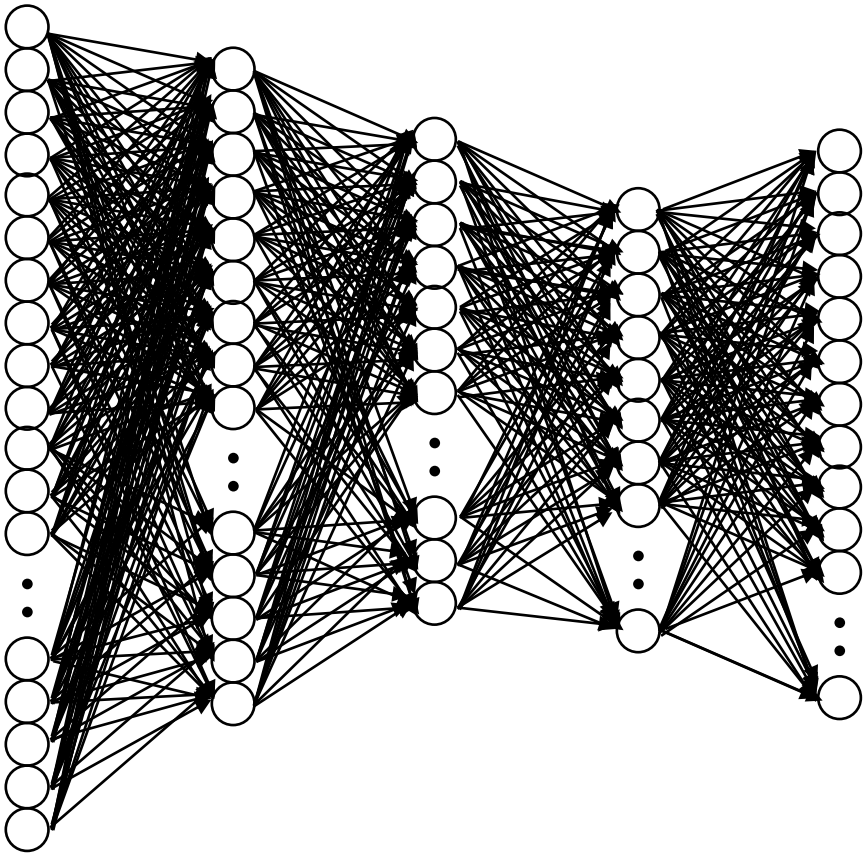

Res. Performance
Oil Production.
Gas Production.

Figure 7-25: Forward ANN design #3B inputs and outputs

Table 7-15: Design #3B network Parameters

ANN Type	Feed-Forward with Back Propagation
# of Hidden Layers	5
# of Neurons in Hidden Layers	[55,50,111,35,30]
Transfer Functions	Logsig, Logsig, Tansig, Logsig, Logsig
# Input Neurons	97
# outputs Neurons	144
ANN Target Tolerance	5.E-05
Total Number of Cases	2000
% Train Cases	85
% Validation Cases	10
% Blind Testing Cases	5

Previous ANN design #3 was the first of its kind where it incorporated various universal parameters and provided a reliable match. However, the target of ANN design #3 was limited to oil production. So, the aim of design #3B is to enhance the previous design and provide a match for gas production profile on top of the oil production profile.

ANN Design Parameter Ranges:

Table 7-16: Design Parameters for ANN Design #3b

#	Parameter	Min	Max	Units	Notes
1	Gas Inection Rate	6.E+05	2.E+06	SCF	
2	Reservoir Temperature	120	300	^{o}F	
3	Reservoir Pressure	2000	6000	psia	
4	Fracture Spacing	10	40	Grid/Spacing	
5	Matrix Porosity	10	40	%	
6	H2S Composition	0.01	0.5	%	
7	CO2 Composition	0.5	5	%	
8	N2 Composition	0.5	2	%	
9	C1 Composition	10	50	%	
10	C2 Composition	10	30	%	
11	C3 Composition	0.5	10	%	
12	IC4 Composition	0.5	10	%	
13	NC4 Composition	0.5	10	%	
14	IC5 Composition	0.5	10	%	
15	NC5 Composition	0.5	10	%	
16	FC6 Composition	0.5	10	%	
17	FC7 Composition	0.5	10	%	Lumps into C7+
18	FC8 Composition	0	10	%	
19	FC9 Composition	0	10	%	
20	FC10 Composition	0	10	%	
21	FC11 Composition	0	10	%	
22	FC12 Composition	0	10	%	
23	FC13 Composition	0	10	%	
24	FC14 Composition	0	10	%	
25	FC15 Composition	0	10	%	
26	FC16 Composition	0	10	%	
27	FC17 Composition	0	10	%	
28	FC18 Composition	0	10	%	
29	FC19 Composition	0	10	%	
30	FC20 Composition	0	10	%	
31	C7+ Composition	0	1	%	Lumped Composition
32	BHFP	400	4500	psia	
33	Krw at Irreducible Oil	0.4	1		Krwiro
34	Kro at Connate Water	0.4	1		Krocw
35	Krog at Connate Gas	0.4	1		Krogcg
36	Krg at connate Liquid	0.4	1		Krgcl

37	Connate Water Saturation	0.05	0.4	%	Swcon
38	Critical Water Saturation	0.05	0.4	%	Swcrit = Swcon
39	Residual Oil for Water-Oil	0.05	0.4	%	Sorw
40	Irreducible Oil for Water-Oil	0.05	0.4	%	Soirw = Sorw
41	Residual Oil for Gas-Liquid	0.05	0.3	%	Sorg
42	Irreducible Oil for Gas-Liquid	0.05	0.3	%	Soirg = Sorg
43	Connate Gas Saturation	0.05	0.3	%	Sgcon
44	Critical Gas Saturation	0.05	0.3	%	Sgcrit = Sgcon
45	RelPerm Expononents	0.7	4	Nw, Now, Nog, and Ng	
46	Oil-Water Entry Capillary Pressure	5	30	psia	
47	Oil-Gas Entry Capillary Pressure	5	30	psia	
48	Gamma for Capillary Pressure	1	10		
49	Initial Reservoir Water Saturation	10	40	%	
50	Oil Production Profile	72		Desired Oil Profile	
51	Gas Production Profile	72		Desired Gas Profile	
52	Well Spacing	17	217	Acres	
53	Fracture Perm	1000	10000	md	Target
54	Layer 1 Matrix Perm	20	200	md	Target
55	Layer 2 Matrix Perm	20	200	md	Target
56	Layer 1 Thickness	20	70	ft	Target
57	Layer 2 Thickness	20	70	ft	Target
58	Production Layers	1	2	Production from L1, or L2	Target

Design Description:

Same as ANN design #3.

Design Reservoir Fluids:

Same as ANN design #3.

Design Analysis and Results

While this design retained the main structure and database of the original design, it required a complete reconfiguration of all the hidden layers and number of hidden neurons in order to match the oil and gas production profiles. Also in this design, the output data for the early decline and shut-in periods were removed which lowered the number of output neurons to almost half of what it used to be. Varying monthly CO_2 injection rate while it added flexibility to the ANN, it also contributed significantly to fluctuations in oil productions, so ANN design #3B runs at a fixed monthly CO_2 injection rate.

Similar to ANN design #3, this design incorporates new features to accommodate a wide range of reservoir properties, fluid compositions, capillary pressure, and relative permeability. This design was capable of predicting oil and gas production profiles for the blind testing cases with a low degree of error.

For miscible injection at fixed CO_2 injection rate, around 2000 simulation cases were needed to build the dataset of which. 85% were used for training, 10% for validation, and 5% were used later for blind testing. However, after quality-checking the data, over half of the data were removed as they didn't run, didn't produce post injection, or stopped in the middle of simulation. Around 700 cases were used to build the dataset for this ANN.

The following plots are samples of the blind tests and they provide an overall performance of the ANN. Note that the plots have different scale to reflect all the various inputs of the blind testing data. (Note: Appendix G shows all of the blind testing cases.)

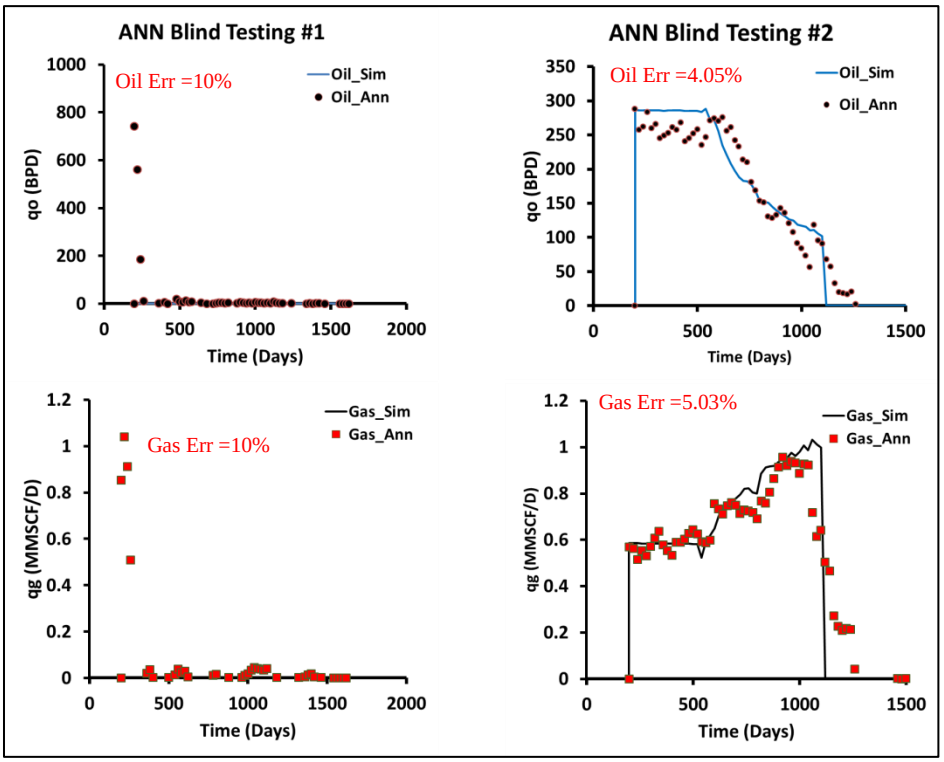

Figure 7-26: Oil and Gas Production for Blind Test Cases 1 & 2

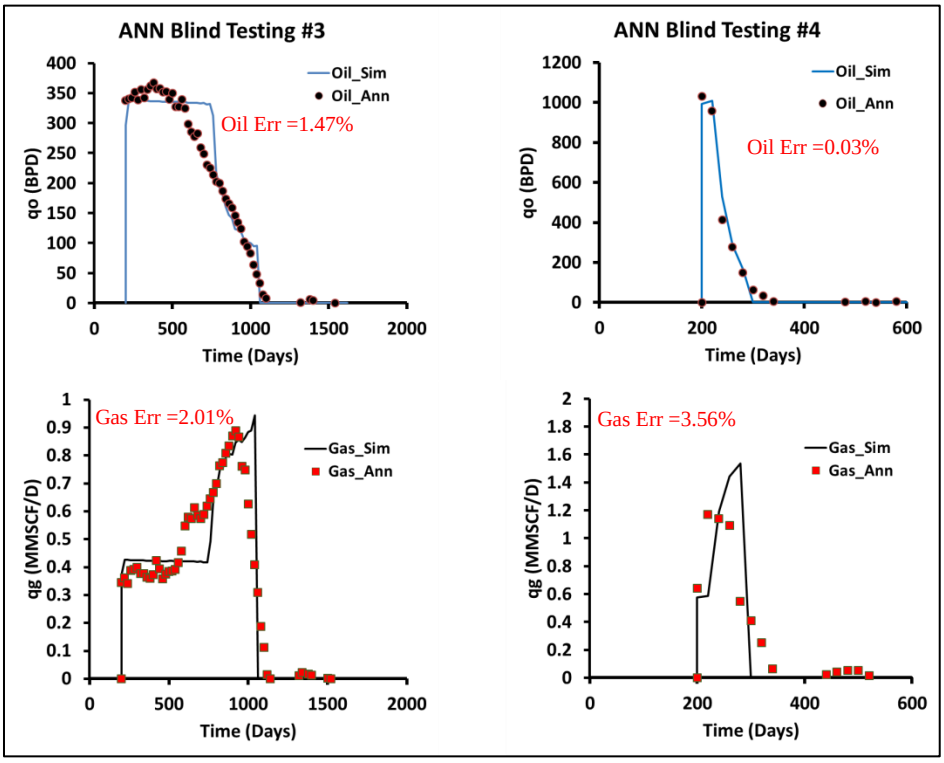

Figure 7-27: Oil and Gas Production for Blind Test Cases 3 & 4

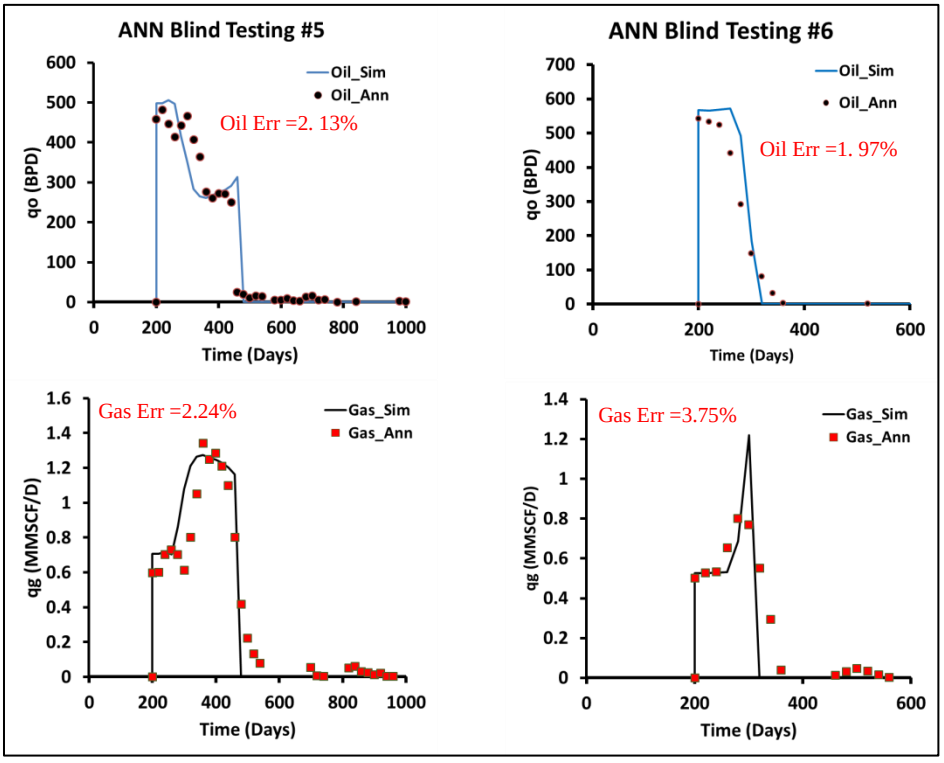

Figure 7-28: Oil and Gas Production for Blind Test Cases 5 & 6

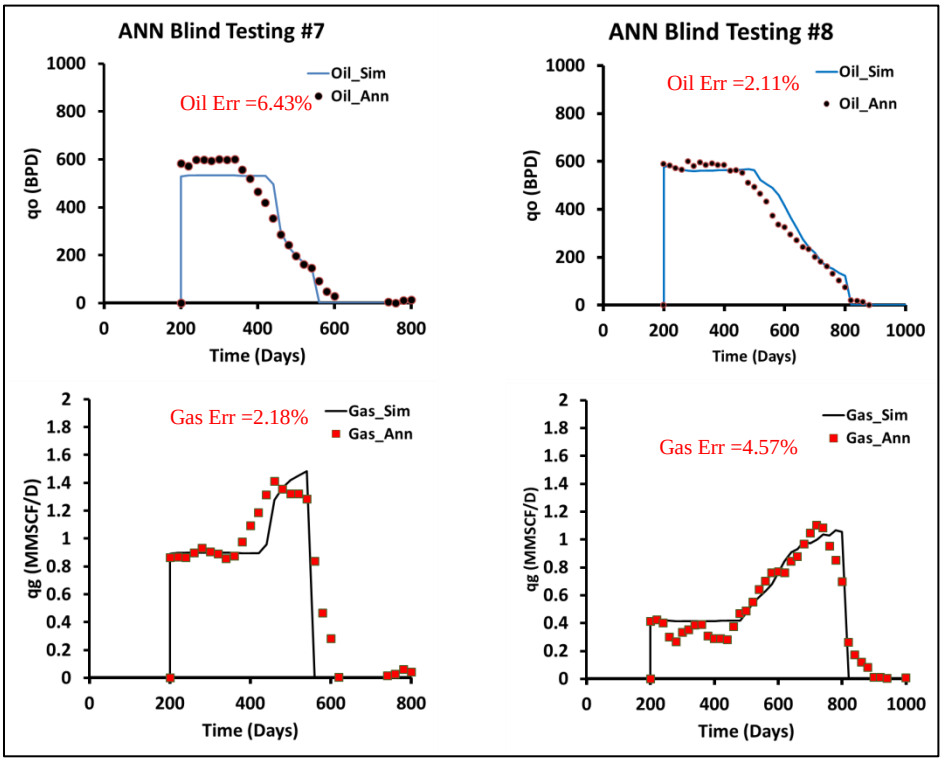

Figure 7-29: Oil and Gas Production for Blind Test Cases 7 & 8

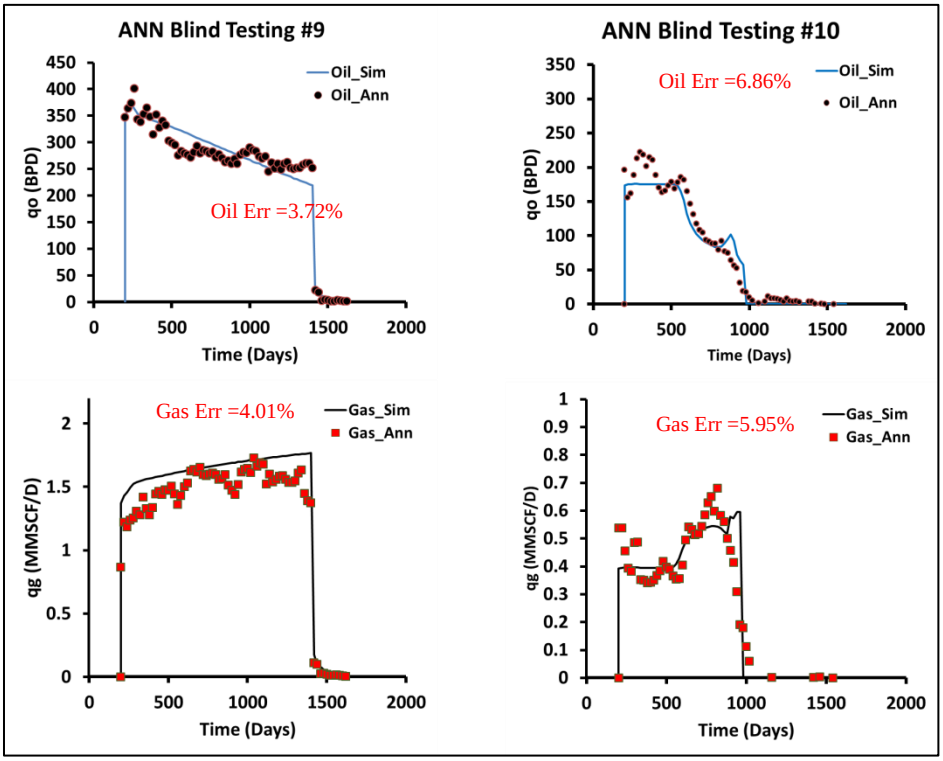

Figure 7-30: Oil and Gas Production for Blind Test Cases 9 & 10

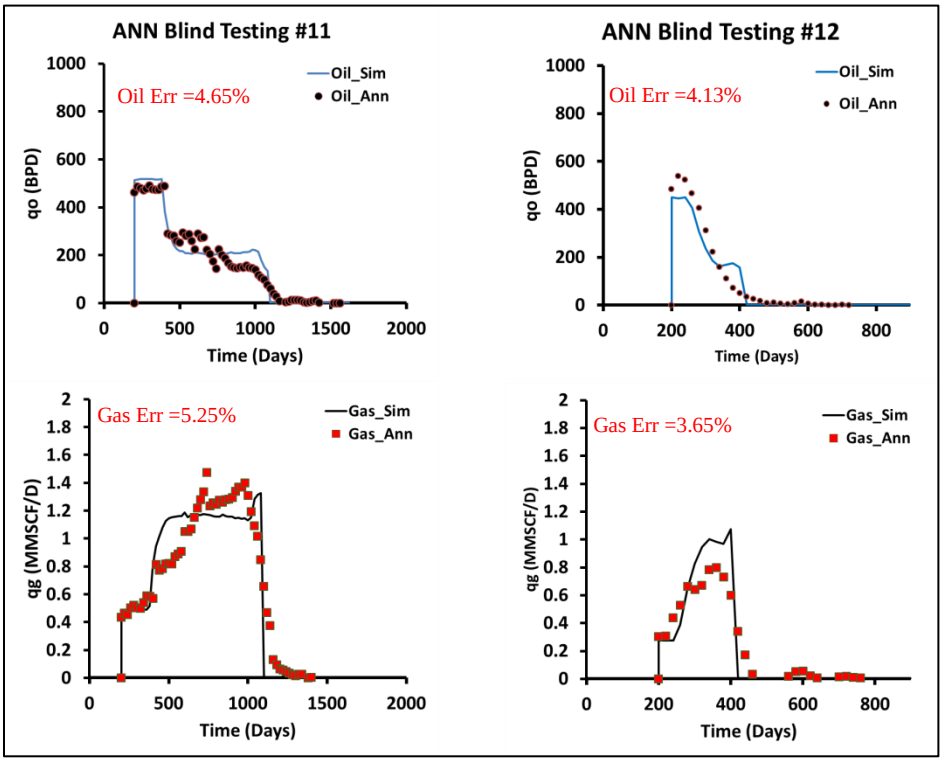

Figure 7-31: Oil and Gas Production for Blind Test Cases 11 & 12

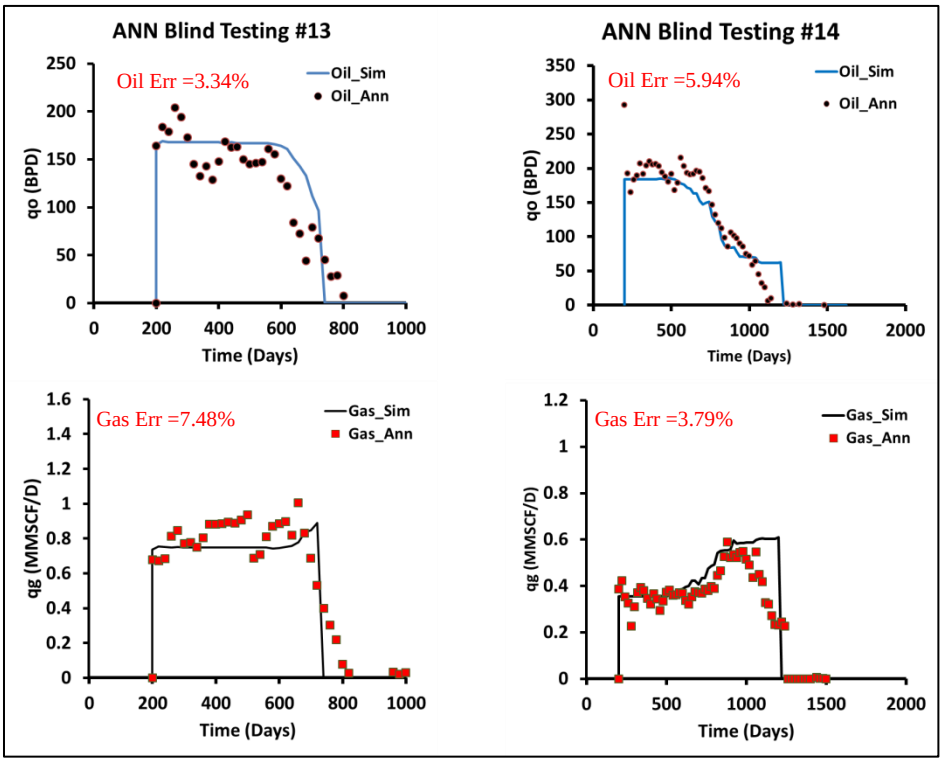

Figure 7-32: Oil and Gas Production for Blind Test Cases 13 & 14

ANN design Functional Links:

Similar to ANN design #3 required a lot of fine tuning and improvements until it reached the final stage. In this design, similar functional links and data manipulation techniques to ANN design #3 were used. Figure 7-33 shows a general correlation between the amount of CO_2 injection and the cumulative oil and gas production in the dataset used for ANN design #3B.

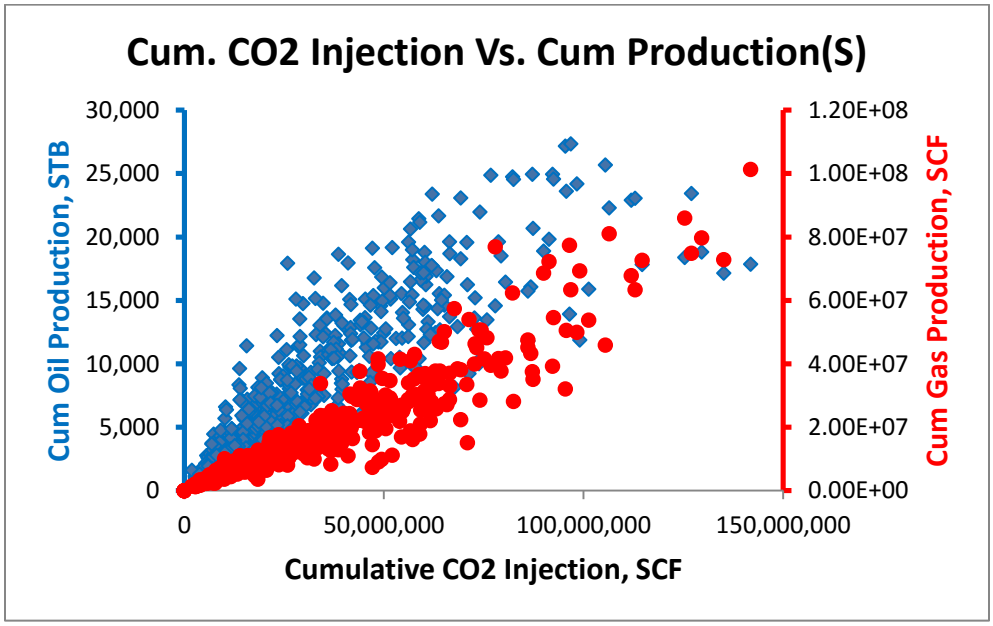

Figure 7-33: Cumulative CO2 Injection vs. Cumulative Oil and Gas Productions for ANN Design #3B

Another direct correlation is between cumulative oil production and the product of well spacing and cumulative CO_2 injection, Figure 7-34. An equation was used as an input while on the output the product of well spacing and cum. CO_2 injection is provided. **Error! Reference source not ound.**Figure 7-34 shows another direct correlation between cumulative oil and gas productions and the injection duration.

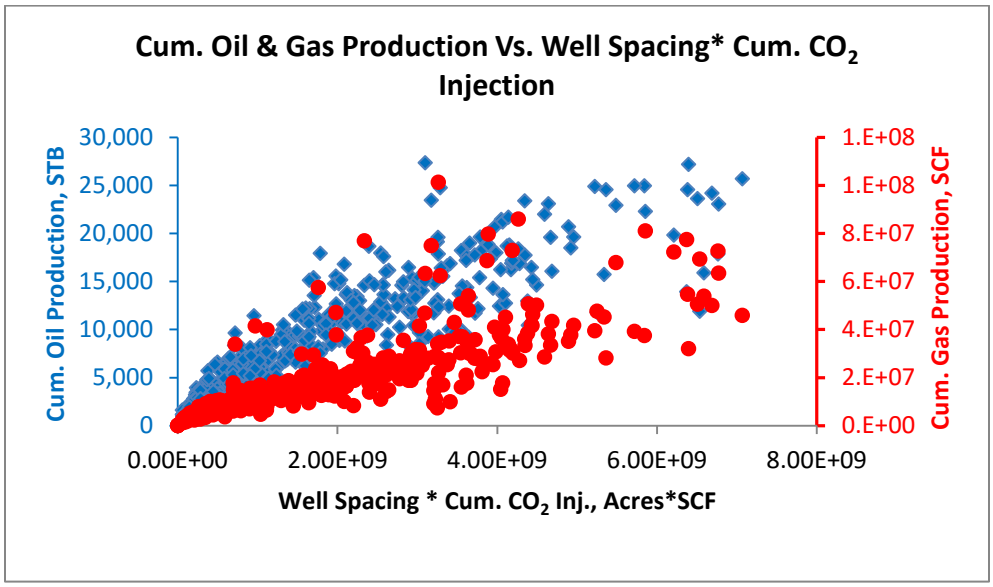

Figure 7-34: Cum. Oil and Gas Productions vs Well spacing* Cum. CO_2 Injection for ANN Design #3B

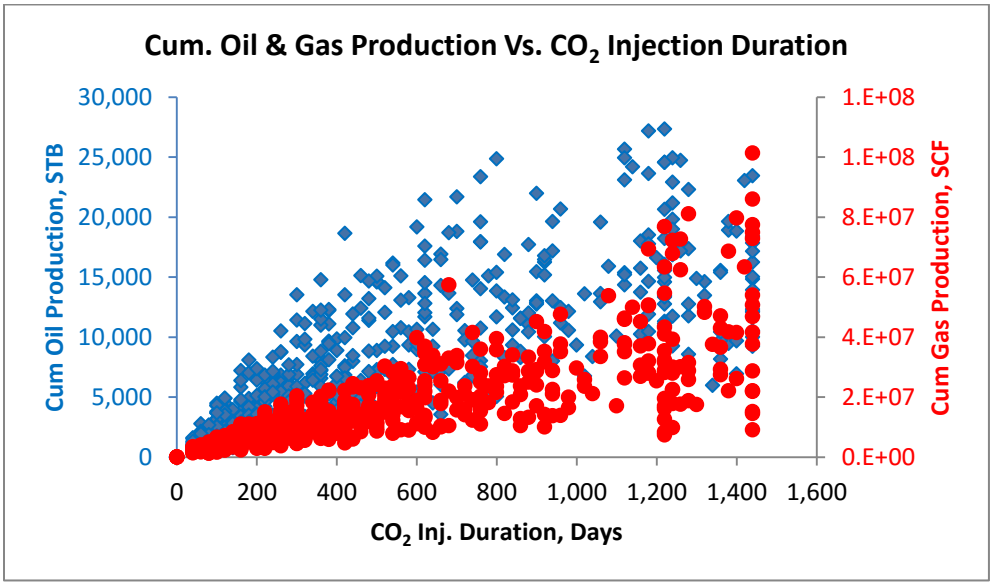

Figure 7-35: Cum. Oil and Gas Production vs CO2 Injection Duration for ANN Design #3B

Final data manipulation techniques and functional links are shown in Table 7-17 and Table 7-18 respectively.

Table 7-17: Final Data Manipulation Techniques for ANN Design #3B

Data Manipulation	Location
Ln(L1 Matrix Perm.+L2 Matrix Perm.)	Inputs
Ln(Fracture Perm.)	Inputs
Ln(Well Spacing)	Inputs
Ln(L1 Thickness + L2 Thickness)	Inputs
1/Ln(Well Spacing)	Outputs
Gas Oil Ratio	Outputs
Removed Early Decline and Shut-in Data	Outputs

Table 7-18: Final Functional Links for ANN Design #3B

Functional Links	Location
Ln(Well Spacing*Cum. CO_2 Inj.)	Inputs
Pi - BHFP	Inputs
Well Spacing * (L1 Thickness + L2 Thickness)	Inputs
Well Spacing/Cumulative CO_2 Injection	Inputs
2E-4*Cum. CO_2 Injection + 1,865.4	Inputs
(Cum. CO_2 Injection*Well Spacing+3E8)/231793	Inputs
Cum. CO_2 Injection*((L1 Matrix Perm+L2 Matrix Perm)+ Matrix Porosity + Fracture Perm)/Fracture Spacing	Inputs
Ln(L1 Matrix Perm+L2 Matrix Perm)+ Matrix Porosity + Fracture Perm)/Fracture Spacing	Inputs

Design Error Analysis:

This design is very similar to its basic version (ANN design #3) with the a few minor differences. The modified design provides reservoir performance in terms of oil and gas, but on the account of the varying monthly injection rate that was present in the previous designs.

The modified design pushes the limit even more by providing gas production on top of the oil production. The individual average overall errors and average errors post injection are reported on

the blind testing cases. The average overall oil and gas error and average error post injection for all the blind testing cases are reported in Table 7-19. This design is different from all the previous design in terms of removing all the early decline and shut-in data. So, the overall error for oil and gas are for the period post-injection.

Table 7-19: Average overall and post injection errors for all the blind testing cases for ANN design #3

Avg Oil Overall Error %	3.63
Avg Gas Overall Error %	4.37

One of the blind testing cases, Figure 7-26: Oil and Gas Production for Blind Test Cases 1 & 2 was assigned a flat error of 10% for oil and gas. While the ANN predicts the rest of the profile reliably, the early prediction period is completely wrong. This behavior was not seen in any of the other blind testing cases.

Figure 7-36 and Figure 7-37 show the point-by-point comparison between the actual monthly oil and gas production rates and the ones predicted by the ANN. The black lines represent the best scenario possible. The closer the values from the black line, the better performance the ANN has.

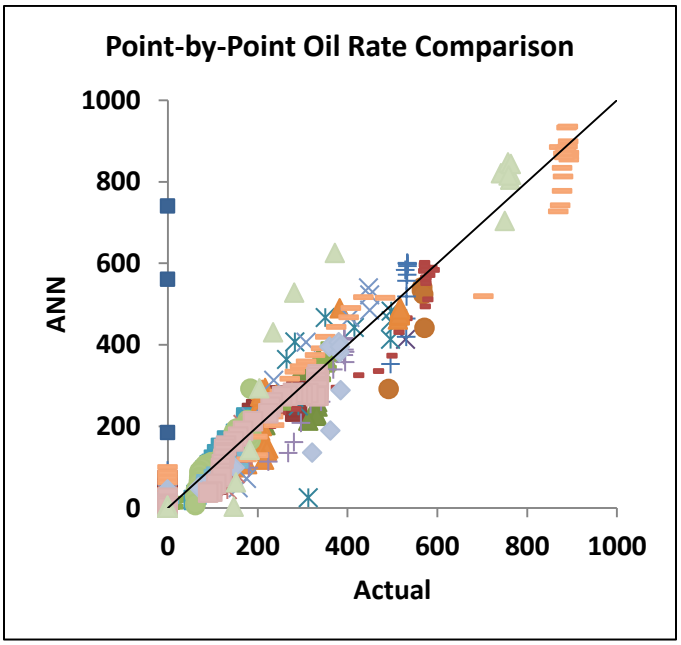

Figure 7-36: Sample blind test monthly oil rate comparison for ANN design #3B

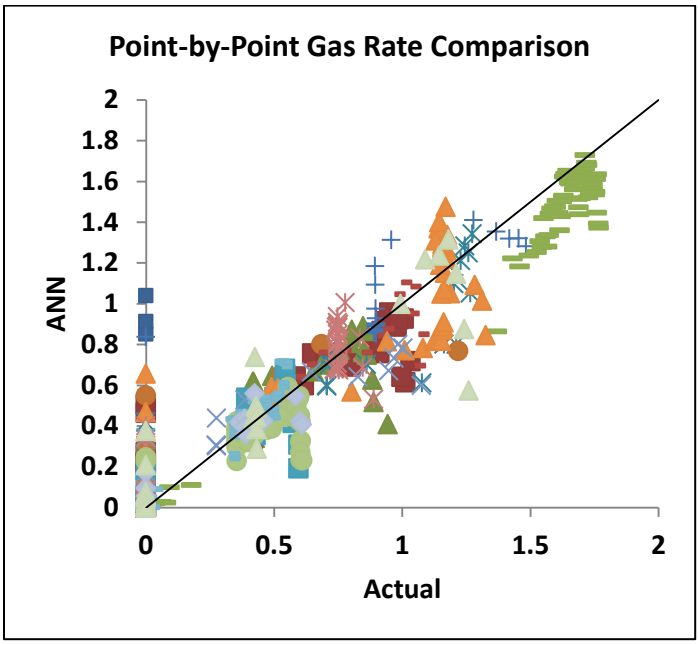

Figure 7-37: Sample blind test monthly gas rate comparison for ANN design #3B

The point by point comparison plots look very good for both oil and gas productions. The oil production profile deteriorated a little bit, but the whole ANN gained good gas production capabilities. Similar to ANN design #3, the oil production rates are small, so the oil plot looks exaggerated.

Final ANN designs have much more input neurons than initial designs which required a much higher number of cases to construct the database. The higher number of cases is essential so the problem does not become ill-posed which would impact the accuracy and validity of the final ANN designs.

This design is another major milestone in this research. The strength of this ANN is embedded in its flexibility to accommodate a wide range of reservoir fluids, relative permeability data and capillary pressure data under any reservoir temperature. This design was enhanced and manipulated many times in order to come out with the current version as it has all the final features developed.

Design ANN-Weight Analysis:

In order to understand the ANN and its response to various neurons throughout the network, some ANN-weight analyses were made. This weight analysis process is studied through looking at the weight of all the neurons from the input layer to the output layer of the configured ANN structure. Figure 7-38 shows an overview of all the weights in forward ANN design #3B.

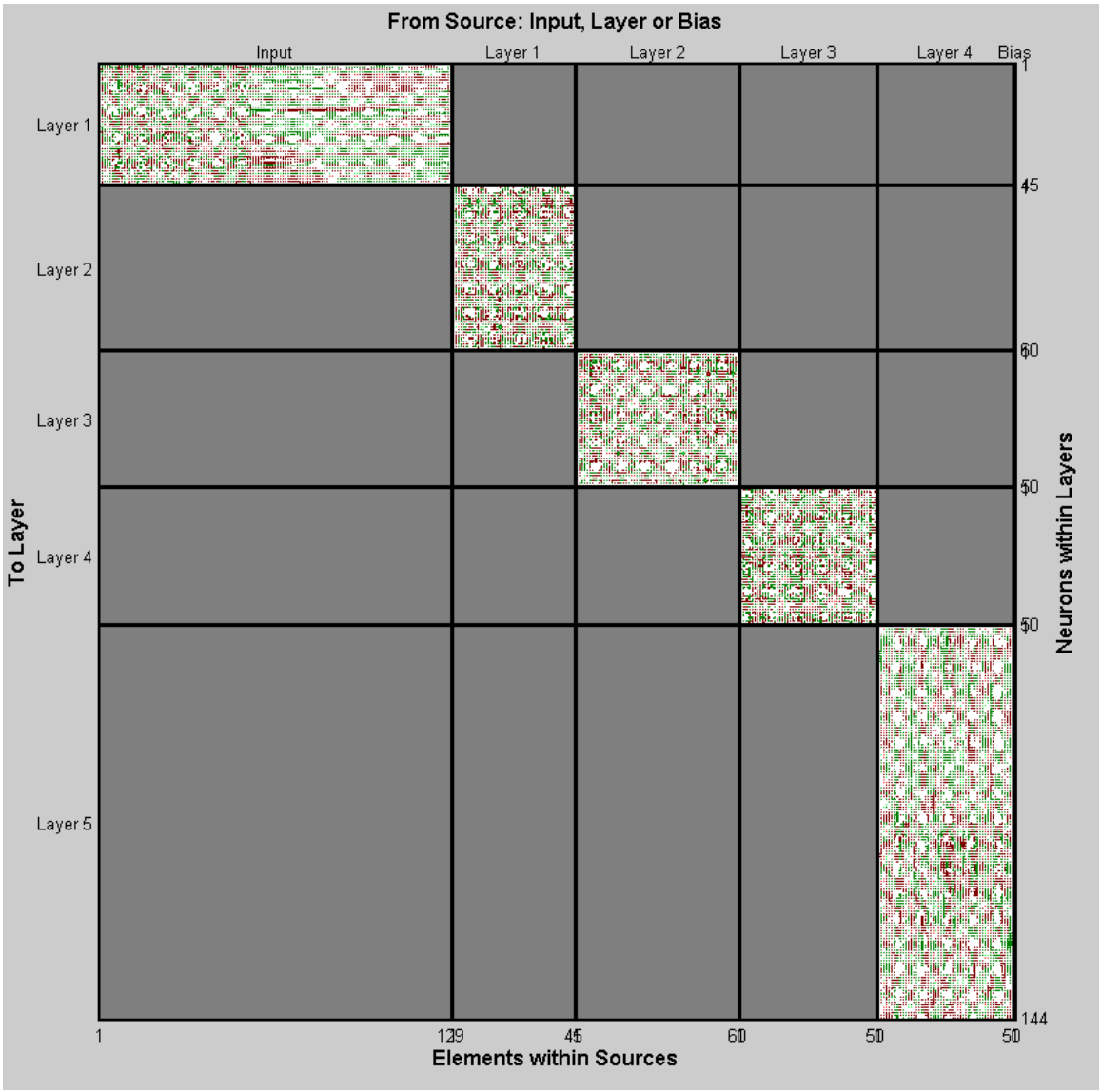

Figure 7-38: ANN design #3B Hinton Diagram between all the layers

The purpose of this procedure is to identify neurons that have weights close to zero so that these neurons can actually be taken out to optimize the network configuration. The weight effect of each neuron is displayed by a magnitude and a sign which is represented by green (+) or red (-).

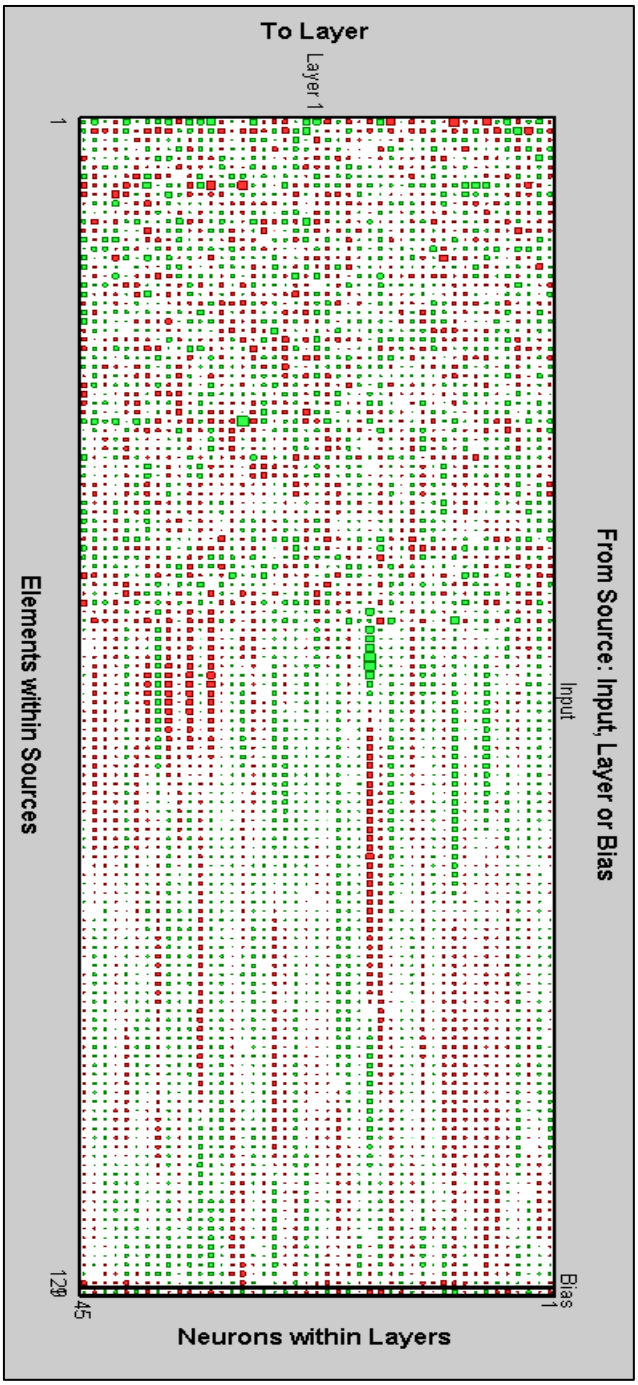

Figure 7-39: ANN design #3B Hinton Diagram between input and first layer neurons

Figure 7-39 shows the Hinton diagram between input and first hidden layer neurons. No apparent trend can be seen by the weights between these layers.

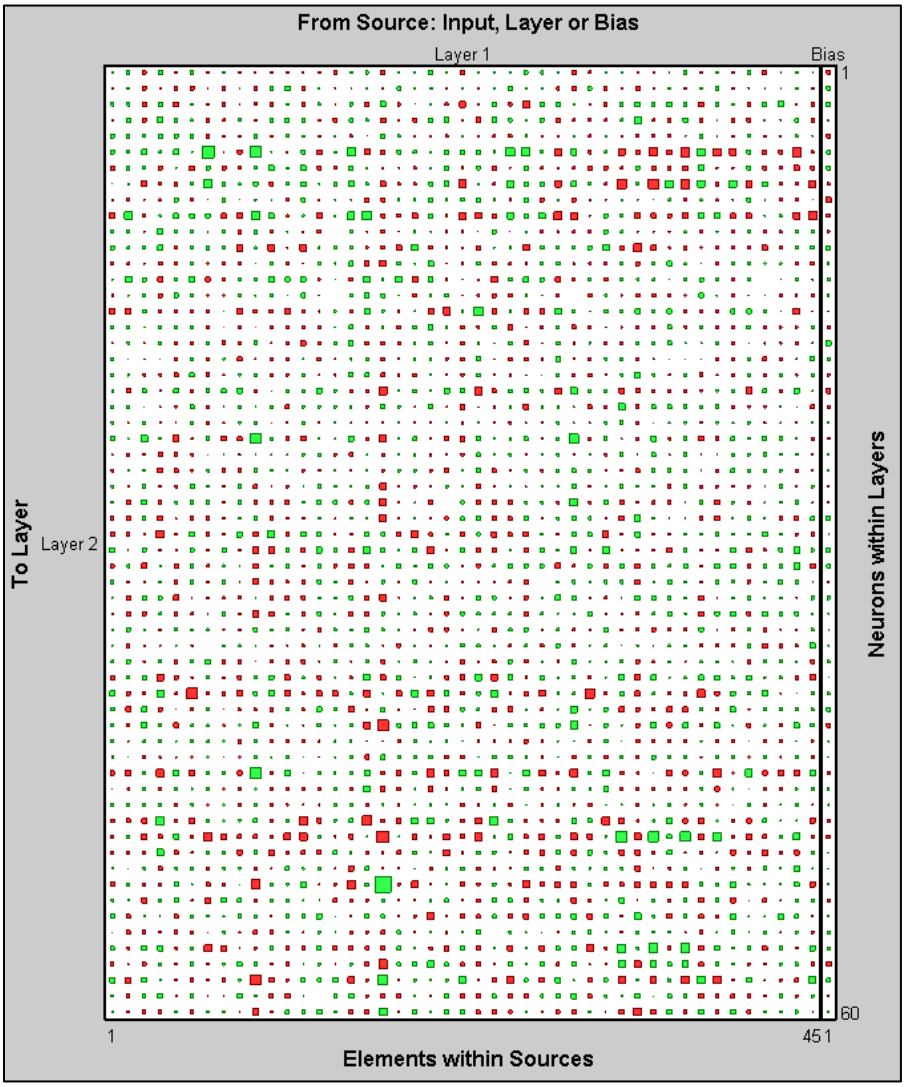

Figure 7-40: ANN design #3B Hinton Diagram between first and second layer neurons

Similar to Figure 7-39, Figure 7-40, Figure 7-41, and Figure 7-42 show the Hinton diagrams between the following layers. No apparent trends are observed by the weights between these layers. Note that the Hinton diagrams look different due to variations in number of neurons in each layer.

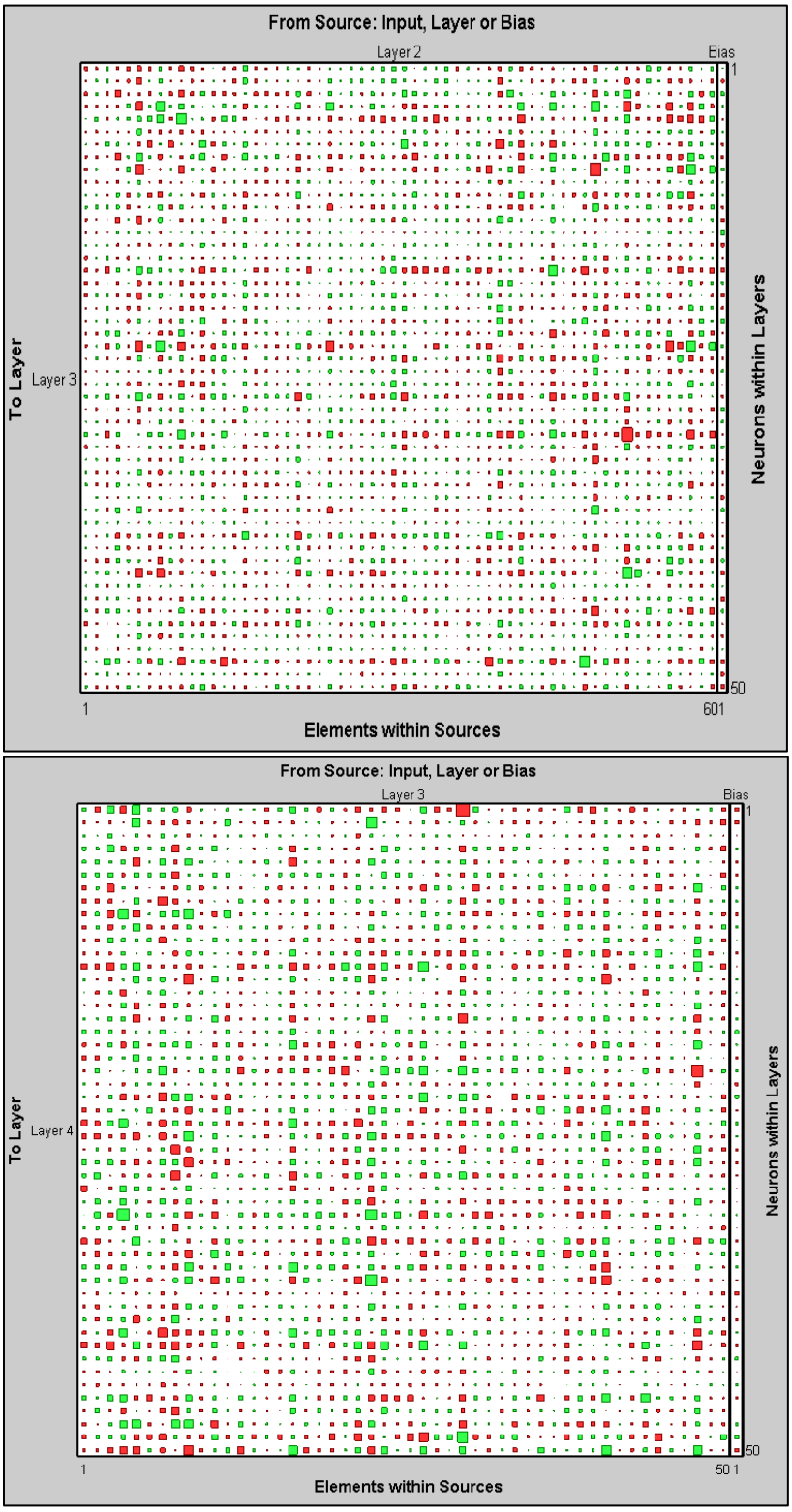

Figure 7-41: ANN design #3B Hinton Diagram between second and third (Above) and between third and fourth (Below) layer neurons

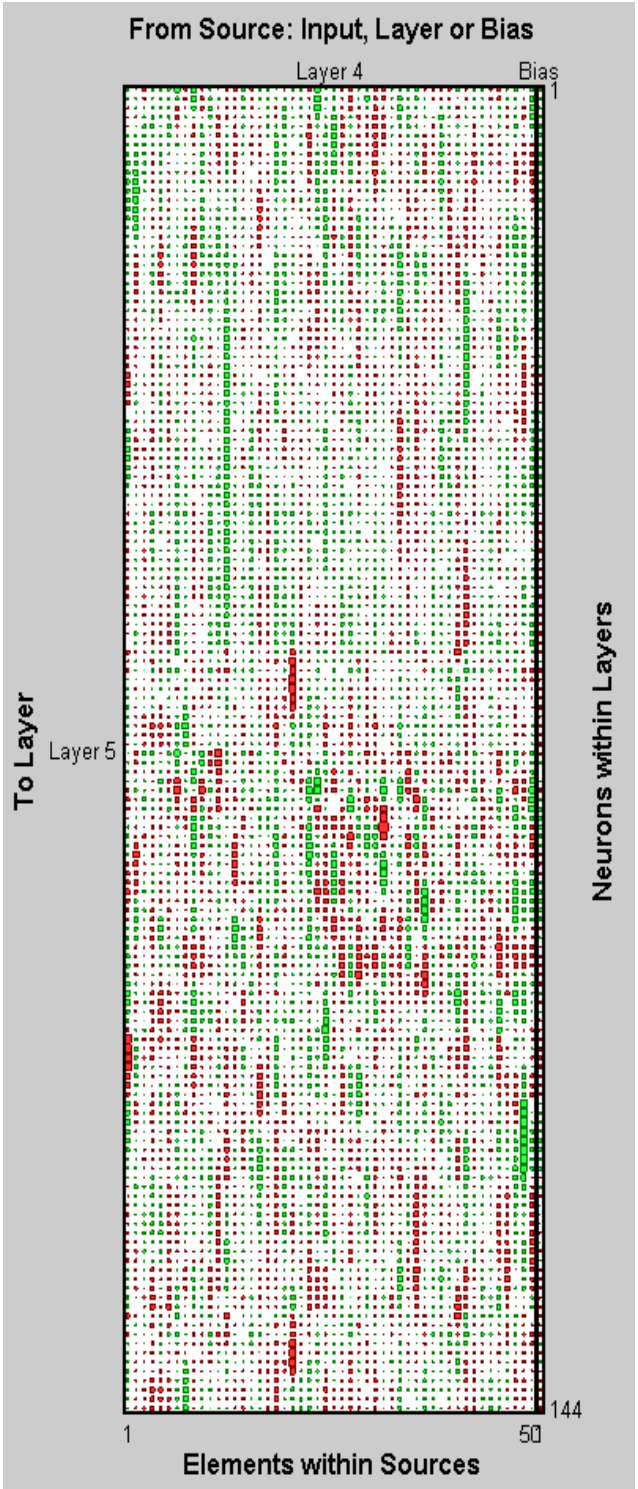

Figure 7-42: ANN design #3B Hinton Diagram between fourth and output layer neurons

In basic ANN configurations, weight influence could be observed and if there are no hidden layers in that particular ANN configuration, the weight influence between input and output neurons can be constructed. However, in complex configurations like in this research, such exercise could not help identify neurons of higher or lower weight influence.

6.2 First Inverse Artificial Neural Networks Proxy (History Match)

The first inverse ANN development in this project provides insights regarding reservoir properties and is referred to in this project as the history match ANN. This inverse proxy uses often known reservoir properties, desired injection design parameters, and oil production profile in order for the proxy to assess and predict uncertain reservoir parameters.

This design is used when a desired oil production profile is sought based on economic analysis that is set by the user. The production profile is then used as an input parameter as well as the known reservoir and parameters for a specific injection scheme.

ANN Design # 1: Continuous CO_2 Injection, Universal Fluid Composition, Miscible, Universal Rock Properties, Universal Relative Permeability, Universal Capillary Pressure

Res. Properties
ϕ_m, ϕ_f,
Fracture Spacing
Res. Pressure
Res. Temp
Res. S_W
BHFP
Relative Perm
Cap. Pressure

Fluid Properties
Components: H_2S, CO_2, N_2,
C1, C2, C3, IC4
NC4, IC5, NC5
FC6, FC7, FC8,
FC9, FC10, FC11,
FC12, FC13, FC14,
FC15, FC16, FC17,
FC18, FC19, FC20

Injection Design
CO_2 Inj. Rate
CO_2 Inj. Duration

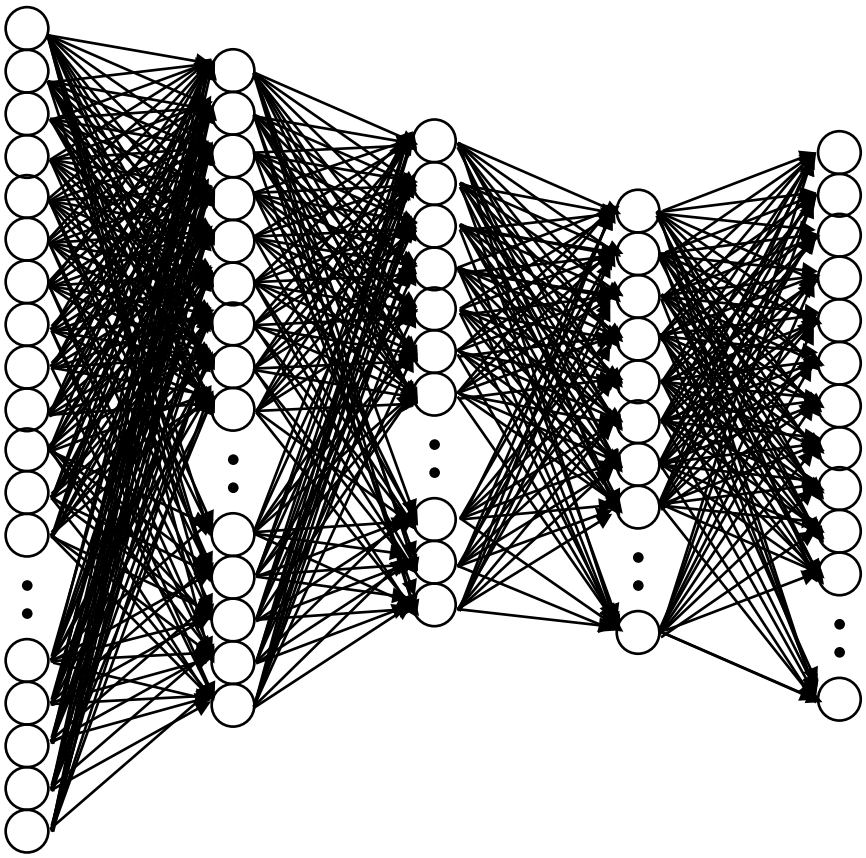

Target Properties
L1 K_m
L2 K_m
K_f
L1 Thickness
L2 Thickness

Figure 7-43: Universal First Inverse ANN Inputs and Outputs

Note that in the development of the 1st inverse ANN, it was not essential to develop starter initial designs as initial forward ANN designs. A lot of lessons were learned from the forward ANN designs regarding data configuration, manipulation and generation as well as ANN construction. This inverse ANN design is the first inverse proxy to the ANN design #3B. This design is the broadest and is inclusive of all the previous designs when it comes to reservoir rock properties, fluid properties, relative permeability data, and capillary pressure data.

Table 7-20:1st Inverse Design network parameters

ANN Type	Feed-Forward with Back Propagation
# of Hidden Layers	3
# of Neurons in Hidden Layers	[35,15, 40]
Transfer Functions	Tansig, Tansig, Logsig
# Input Neurons	52
# outputs Neurons	10
ANN Target Tolerance	5.E-05
Total Number of Cases	2000
% Train Cases	95
% Validation Cases	2
% Blind Testing Cases	3

Design Description:

This is a 20x20x2 reservoir model with grid dimension of 44x44 feet. The 44x44 feet grids were selected even though the 30x30 showed less grid size error, however, the improvements over the 44x44 were very minor but on the expense of run time. The 30x30 grids ran 25% slower than the 44x44 feet grids. The grid size selection was studied in previous sections.

The model is a dual porosity, dual permeability fractured model using Gilman and Kazemi shape factor. In this design, CO_2 is continuously injected from a dedicated well, while production is done from another dedicated production well.

ANN Design Parameter Ranges:

Table 7-21: 1st Inverse ANN Design Parameters

#	Parameter	Min	Max	Units	Notes
1	Gas Inection Rate	6.E+05	2.E+06	SCF	
2	Reservoir Temperature	120	300	^{O}F	
3	Reservoir Pressure	2000	6000	psia	
4	Fracture Spacing	10	40	Grid/Spacing	
5	Matrix Porosity	10	40	%	
6	H2S Composition	0.01	0.5	%	
7	CO2 Composition	0.5	5	%	
8	N2 Composition	0.5	2	%	
9	C1 Composition	10	50	%	
10	C2 Composition	10	30	%	
11	C3 Composition	0.5	10	%	
12	IC4 Composition	0.5	10	%	
13	NC4 Composition	0.5	10	%	
14	IC5 Composition	0.5	10	%	
15	NC5 Composition	0.5	10	%	
16	FC6 Composition	0.5	10	%	
17	FC7 Composition	0.5	10	%	Lumps into C7+
18	FC8 Composition	0	10	%	
19	FC9 Composition	0	10	%	
20	FC10 Composition	0	10	%	
21	FC11 Composition	0	10	%	
22	FC12 Composition	0	10	%	
23	FC13 Composition	0	10	%	
24	FC14 Composition	0	10	%	
25	FC15 Composition	0	10	%	
26	FC16 Composition	0	10	%	
27	FC17 Composition	0	10	%	
28	FC18 Composition	0	10	%	
29	FC19 Composition	0	10	%	
30	FC20 Composition	0	10	%	
31	C7+ Composition	0	1	%	Lumped Composition
32	BHFP	400	4500	psia	
33	Krw at Irreducible Oil	0.4	1		Krwiro
34	Kro at Connate Water	0.4	1		Krocw
35	Krog at Connate Gas	0.4	1		Krogcg
36	Krg at connate Liquid	0.4	1		Krgcl
37	Connate Water Saturation	0.05	0.4	%	Swcon
38	Critical Water Saturation	0.05	0.4	%	Swcrit = Swcon
39	Residual Oil for Water-Oil	0.05	0.4	%	Sorw
40	Irreducible Oil for Water-Oil	0.05	0.4	%	Soirw = Sorw

41	Residual Oil for Gas-Liquid	0.05	0.3	%	Sorg
42	Irreducible Oil for Gas-Liquid	0.05	0.3	%	Soirg = Sorg
43	Connate Gas Saturation	0.05	0.3	%	Sgcon
44	Critical Gas Saturation	0.05	0.3	%	Sgcrit = Sgcon
45	RelPerm Expononents	0.7	4	Nw, Now, Nog, and Ng	
46	Oil-Water Entry Capillary Pressure	5	30	psia	
47	Oil-Gas Entry Capillary Pressure	5	30	psia	
48	Gamma for Capillary Pressure	1	10		
49	Initial Reservoir Water Saturation	10	40	%	
50	Oil Production Profile	72		Desired Oil Profile	
51	Gas Production Profile	72		Desired Gas Profile	
52	Well Spacing	17	217	Acres	
53	Fracture Perm	1000	10000	md	Target
54	Layer 1 Matrix Perm	20	200	md	Target
55	Layer 2 Matrix Perm	20	200	md	Target
56	Layer 1 Thickness	20	70	ft	Target
57	Layer 2 Thickness	20	70	ft	Target

NOTE: Oil and gas production profiles were also provided as part of the input parameters. The oil and gas production profiles used here were generated in the previous ANN designs #3 and 3B. This design shares the same dataset that forward ANN design #3 and #3B used but with different data configuration that suits the nature of the 1st inverse model.

Design Reservoir Fluids:

The 1st inverse design contains all the unique and new features of its forward ANN design (forward ANN design #3). This design uses a compositional algorithm that changes reservoir fluid composition in every case inside the data set. The algorithm takes into account components up to heavy hydrocarbon 20 (FC_{20}), and then lumps all the heavy components above C_7 as C_{7+}.

Design Analysis and Results

One of the main observations regarding the inverse design configurations is that, they are actually more complex than the forward ANN designs. Initial simple ANN configuration would not come close to matching and required a lot of functional links and data manipulation. Even with the extensive use of functional links and data manipulation, the 1st ANN design at its best form had some errors as high as 20% for some of the parameters. There are a few reasons that contributed

to the complexity of this ANN. First, there were no clear direct correlations between any of the input parameters and the target output parameters as can be seen in Figure 7-44 and Figure 7-45.

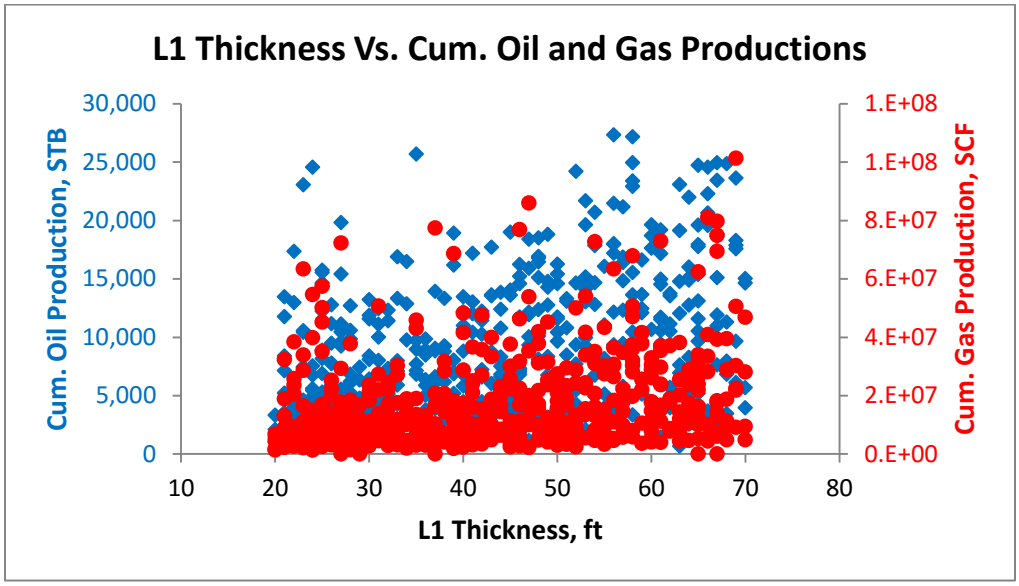

Figure 7-44:L1 Thickness vs. cumulative oil and gas productions relationship

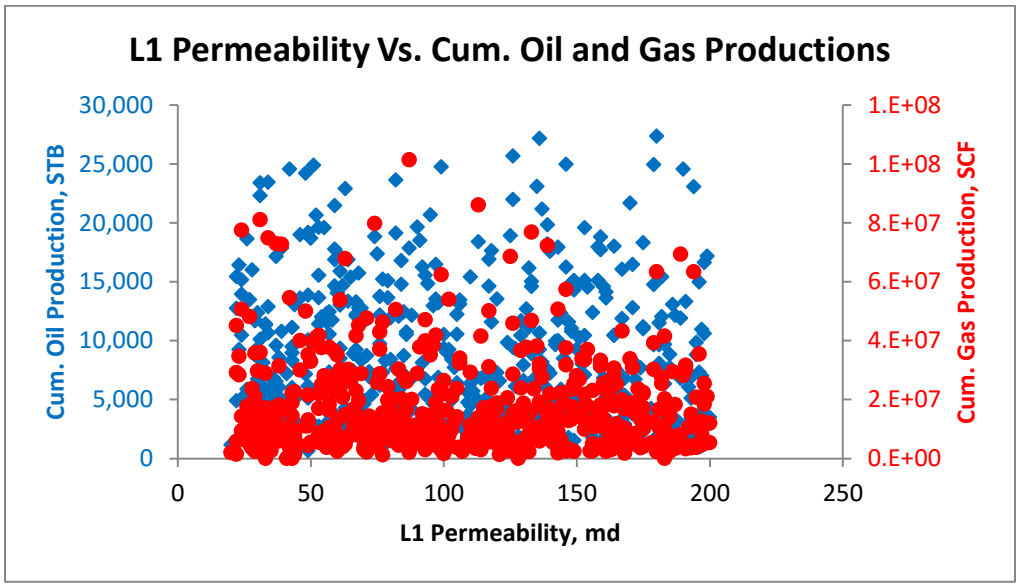

Figure 7-45: L1 Thickness vs. cumulative oil and gas productions relationship

Second, most of the target output parameters didn't have a major impact on the overall performance or the injection process. Finally, the output parameters are not related to each other or follow a certain trend or behavior as is the case for the oil production profile for example. So, the output surface for this ANN is very rough and uneven.

Around 2000 simulation cases were used to build the data set. 95% of the cases were used to train the network, 2% for validation, and the last 3% were used later for a blind test. However, after quality-checking the data, over half of the data were removed as they didn't run, didn't produce post injection, or stopped in the middle of simulation. Around 700 cases were used to build the dataset for this ANN. The following tables are samples of the blind tests and they provide an overall performance of the ANN. (Note: Appendix H shows all of the 10 blind testing cases.) Note that CO_2 injection rate parameter was replaced with cumulative CO_2 injection and CO_2 injection duration as they are more representative of the CO_2 injection amount and has a direct correlation with the oil production and some other parameters.

Table 7-22 shows the output of the first blind testing case in comparison with the actual data.

Table 7-22: 1st Inverse Blind Case #1 Output

Blind Test Case 1 Output Comparison			
Property	**Actual**	**ANN**	**Error**
Frac Perm, md	5,343	4,954	7.28
L1 Matrix Perm, md	175	191	9.14
L2 Matrix Perm, md	35	45	28.57
L1 Thickness, ft	64	60	6.25
L2 Thickness, ft	40	34	15

The first blind test is one of the best cases for the first inverse ANN. Most of the parameters were predicted by the ANN within an acceptable error, except for the thickness of the second layer.

Table 7-23 shows the output of the second blind testing case in comparison with the actual data.

Table 7-23: 1st Inverse Blind Case #2 Output

Blind Test Case 2 Output Comparison			
Property	**Actual**	**ANN**	**Diff**
Frac Perm, md	9681	8063	16.71
L1 Matrix Perm, md	109	97	11.01
L2 Matrix Perm, md	124	103	16.94
L1 Thickness, ft	55	49	10.91
L2 Thickness, ft	37	45	21.62

The second blind test is one of the in-between cases for the first inverse ANN. Most of the parameters were predicted by the ANN at or around the acceptable error of 15% except for the thickness of the second layer.

Table 7-24 shows the output of the second blind testing case in comparison with the actual data.

Table 7-24: 1st Inverse Blind Case #3 Output

Blind Test Case 3 Output Comparison			
Property	**Actual**	**ANN**	**Diff**
Frac Perm, md	7924	8349	5.36
L1 Matrix Perm, md	33	45	36.36
L2 Matrix Perm, md	165	140	15.15
L1 Thickness, ft	32	40	25.00
L2 Thickness, ft	38	33	13.16

The third blind test is also one of the in-between cases for the first inverse ANN. Some of the parameters were predicted by the ANN at or around the acceptable error of 15% except for the thickness of the first layer and the matrix permeability of the first layer.

ANN design Functional Links:

As previously mentioned, this design would not get a close match without the use of functional links. Initial configurations without functional links had over 100% error for most of the parameters.

Similar to forward ANN design #3B required a lot of fine tuning and improvements until it reached the final stage. In this design, similar functional links and data manipulation techniques to forward ANN design #3 and #3B were used.

Table 7-25 shows the final data manipulation techniques used in this inverse ANN. Table 7-26 lists the final functional links used for the first inverse ANN design.

Table 7-25: Final Data manipulation techniques for 1st Inverse ANN#1

Data Manipulation	Location
Cumulative CO_2 Injection	Output
Cumulative Gas Production	Output
Cumulative Oil Production	Output
Removed Early Decline and Shutin-Data	Input

Notice that Table 7-26 shows some of the functional links displaying some constants. Theses constants are not random numbers and were generated as part of a complex correlation that relate cumulative production and injection to some of the target output parameters as similarly used in previous forward ANN designs.

Table 7-26: Final Functional Links used for 1st Inverse ANN

Functional Links	Location
Ln(Gas Oil Ratio)	Output
Ln(Well Spacing*Cum. CO_2 Inj.)	Inputs
Pi - BHFP	Inputs
(L1 Thickness + L2 Thickness)*Frac Perm	Inputs
Well Spacing/Cumulative CO_2 Injection	Inputs
(L1 Matrix Perm+L2 Matrix Perm)* Matrix Porosity + Fracture Perm	Output
Cum. CO_2 Injection/Fracture Spacing	Inputs
4932*Cum Oil Prod-4E6/Cum. Gas Inj.	Inputs
374573*Cum Oil Prod+2E8/Cum. Gas Inj.	Inputs
Ln(408896*Cum Oil Prod+1E8/Cum. Gas Inj.)	Inputs

Design Error Analysis:

The first inverse ANN development in this project provides insights regarding reservoir properties and is referred to in this project as the history match ANN. This inverse proxy uses often known reservoir properties, desired injection design parameters, and oil production profile in order for the proxy to assess and predict uncertain parameters.

This design is used when a desired oil production profile is sought based on economic analysis that is set by the user. The production profiles are then used as input parameters as well as the known reservoir and parameters for a specific injection scheme.

The first inverse ANN proxy couldn't be configured the same way the forward prediction ANN. The impact of all the input parameters on the output parameters was studied and their relationships were used in a trial and error way as part of the base configuration of the first inverse ANN.

The errors for all the blind testing cases are reported in Table 7-27.

Table 7-27: 1st Inverse ANN Average Blind Test Error

Blind Test Errors	
Property	**Avg. Error**
Fracture Perm	33.34
L1 Matrix Perm	24.55
L2 Matrix Perm	19.21
L1 Thickness	14.11
L2 Thickness	18.31

Figure 7-46, Figure 7-47, and Figure 7-48 show the point-by-point comparison between the actual fracture perm, L1 matrix perm, L2 matrix perm, L1 thickness, and L2 thickness and predicted values by the ANN. The black lines represent the best scenario possible. The closer the values from the black line, the better performance the ANN has. In case of fracture permeability, some of the errors were masked by the huge range for this specific property which goes between 1,000 md all the way to 10,000 md.

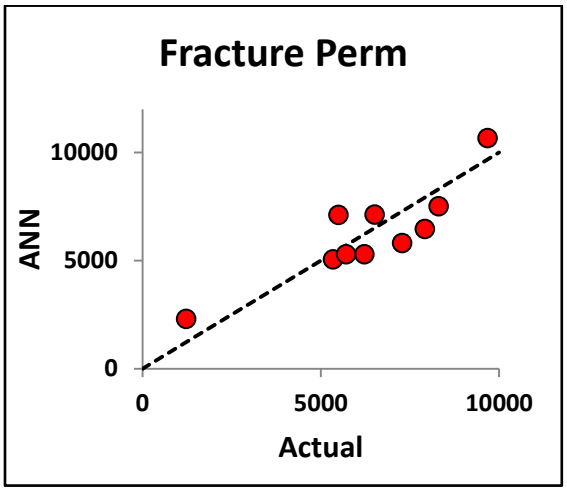

Figure 7-46: First Inverse ANN Performance Plot for Fracture Permeability

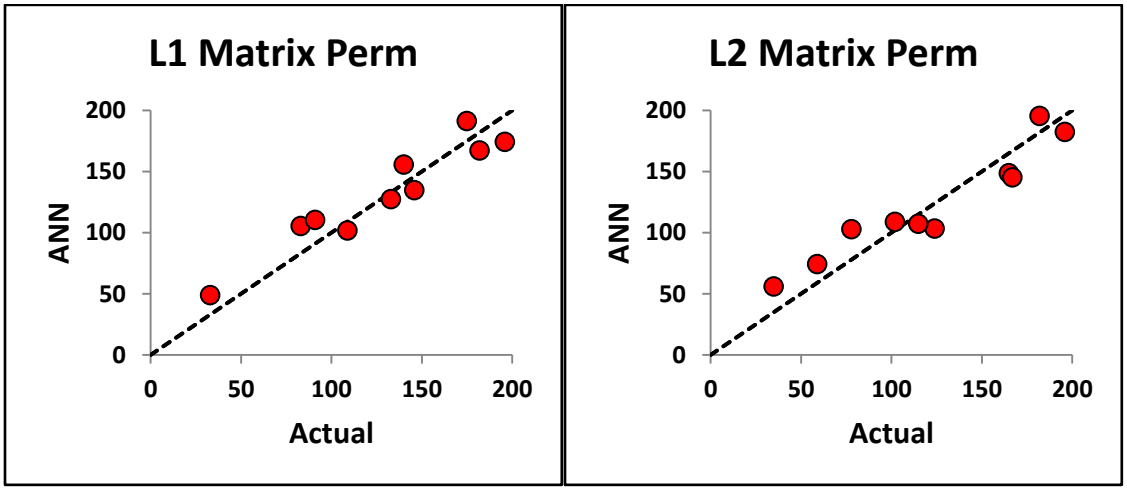

Figure 7-47: First Inverse ANN Performance Plot for L1 & L2 Matrix Permeabilities

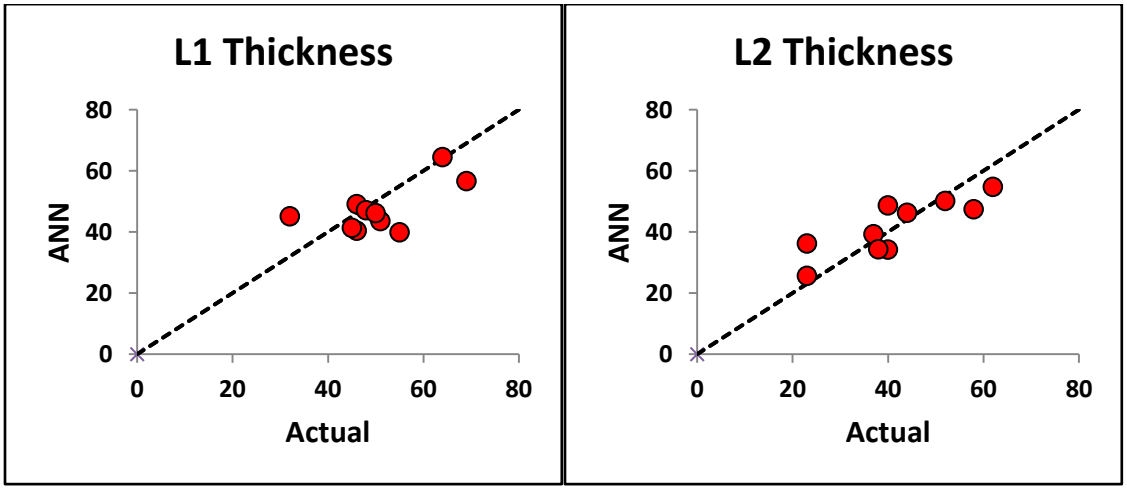

Figure 7-48: First Inverse ANN Performance Plot for L1 & L2 Thicknesses

6.3 Second Inverse Universal Artificial Neural Networks Proxy (Injection Design)

The second inverse ANN design, also known as the injection design ANN, uses the oil production profile as well as reservoir properties that are supplied by the user to provide a proper injection design scheme.

This design helps the engineer to study and evaluate various injection designs for a desired oil production profile.

ANN Design # 1: Continuous CO_2 Injection, Universal Fluid Composition, Miscible, Universal Rock Properties, Universal Relative Permeability, Universal Capillary Pressure

Res. Properties
K_m, K_f, φ_m, φ_f,
Thickness
Fracture Spacing
Res. Pressure
Res. Temp
Res. S_W
BHFP
Relative Perm
Cap. Pressure

Fluid Properties
Components: H_2S, CO_2, N_2,
C1, C2, C3, IC4
NC4, IC5, NC5
FC6, FC7, FC8,
FC9, FC10, FC11,
FC12, FC13, FC14,
FC15, FC16, FC17,
FC18, FC19, FC20

Production Profiles
Oil Production
Gas Production

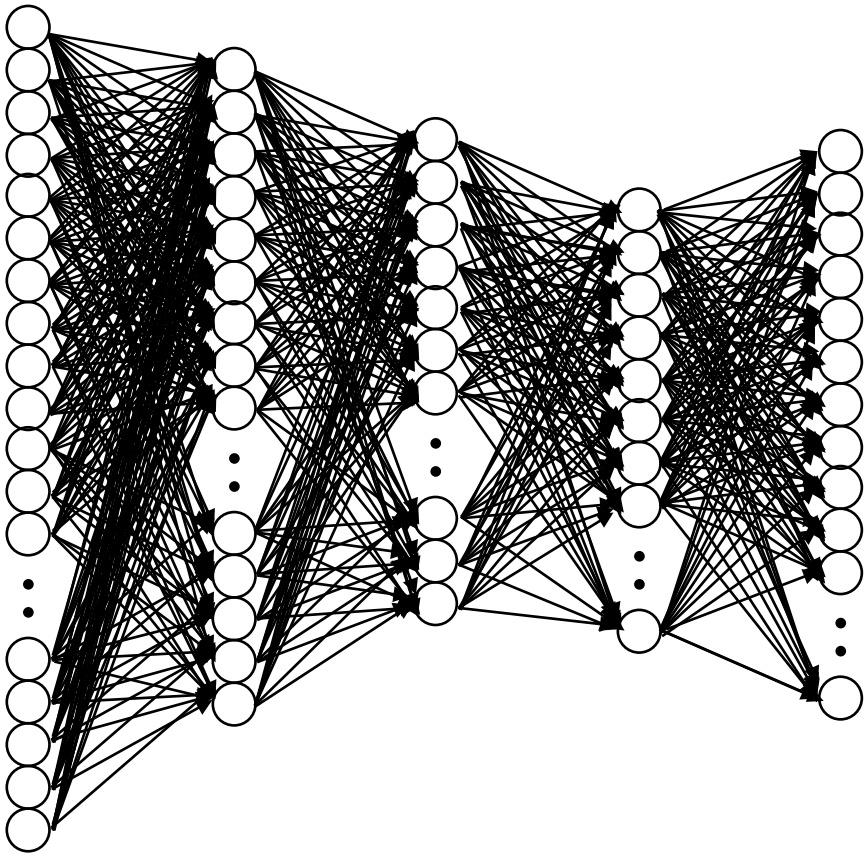

Injection Design
Well Spacing
CO_2 Inj. Rate
CO_2 Inj. Duration

Figure 7-49: Universal Second Inverse ANN Inputs and Outputs

The second inverse ANN design is the second inverse proxy to the ANN design #3B. This design is the broadest and is inclusive of all the previous designs when it comes to reservoir rock properties, fluid properties, relative permeability data, and capillary pressure data. Table 7-28 shows the second inverse network parameters used in this ANN configuration.

Table 7-28: Second Inverse Design Network Parameters

ANN Type	Feed-Forward with Back Propagation
# of Hidden Layers	3
# of Neurons in Hidden Layers	[30,45, 20]
Transfer Functions	Logsig, Tansig, Logsig
# Input Neurons	70
# outputs Neurons	3
ANN Target Tolerance	5.E-05
Total Number of Cases	2000
% Train Cases	85
% Validation Cases	10
% Blind Testing Cases	5

Design Description:

This is a 20x20x2 reservoir model with grid dimension of 44x44 feet. The grid size selection was studied in previous sections.

The model is a dual porosity, dual permeability fractured model using Gilman and Kazemi shape factor. In this design, CO_2 is continuously injected from a dedicated well, while production is done from another dedicated production well.

ANN Design Parameter Ranges:

Table 7-29: 2nd Inverse ANN Design Parameters

#	Parameter	Min	Max	Units	Notes
1	Reservoir Temperature	120	300	^{O}F	
2	Reservoir Pressure	2000	6000	psia	
3	H2S Composition	0.01	0.5	%	
4	CO2 Composition	0.5	5	%	
5	N2 Composition	0.5	2	%	
6	C1 Composition	10	50	%	
7	C2 Composition	10	30	%	
8	C3 Composition	0.5	10	%	
9	IC4 Composition	0.5	10	%	
10	NC4 Composition	0.5	10	%	
11	IC5 Composition	0.5	10	%	
12	NC5 Composition	0.5	10	%	
13	FC6 Composition	0.5	10	%	
14	FC7 Composition	0.5	10	%	Lumps into C7+
15	FC8 Composition	0	10	%	
16	FC9 Composition	0	10	%	
17	FC10 Composition	0	10	%	
18	FC11 Composition	0	10	%	
19	FC12 Composition	0	10	%	
20	FC13 Composition	0	10	%	
21	FC14 Composition	0	10	%	
22	FC15 Composition	0	10	%	
23	FC16 Composition	0	10	%	
24	FC17 Composition	0	10	%	
25	FC18 Composition	0	10	%	
26	FC19 Composition	0	10	%	
27	FC20 Composition	0	10	%	
28	C7+ Composition	0	1	%	Lumped Composition
29	BHFP	400	4500	psia	
30	Krw at Irreducible Oil	0.4	1		Krwiro
31	Kro at Connate Water	0.4	1		Krocw
32	Krog at Connate Gas	0.4	1		Krogcg
33	Krg at connate Liquid	0.4	1		Krgcl
34	Connate Water Saturation	0.05	0.4	%	Swcon
35	Critical Water Saturation	0.05	0.4	%	Swcrit = Swcon
36	Residual Oil for Water-Oil	0.05	0.4	%	Sorw
37	Irreducible Oil for Water-Oil	0.05	0.4	%	Soirw = Sorw
38	Residual Oil for Gas-Liquid	0.05	0.3	%	Sorg
39	Irreducible Oil for Gas-Liquid	0.05	0.3	%	Soirg = Sorg
40	Connate Gas Saturation	0.05	0.3	%	Sgcon
41	Critical Gas Saturation	0.05	0.3	%	Sgcrit = Sgcon
42	RelPerm Expononents	0.7	4	Nw, Now, Nog, and Ng	
43	C7+ Specific Gravity	0	20		
44	Oil-Water Entry Capillary Pressure	5	30	psia	
45	Oil-Gas Entry Capillary Pressure	5	30	psia	
46	Gamma for Capillary Pressure	1	10		
47	Initial Reservoir Water Saturation	10	40	%	

48	Production Layers	1	3	Production from L1, or L2	
49	Oil Production Profile	72		Profile Output Parameters	
50	Gas Production Profile	72		Profile Output Parameters	
51	Well Spacing	17	217	Acres	Target
52	Cumulative CO2 Injection			SCF	Target
53	CO2 Injection Duration			Days	Target

This second inverse ANN design shares the same dataset that the first inverse and forward ANN design #3B used.

Design Reservoir Fluids:

The 2nd inverse design contains all the unique and new features of its forward ANN design (forward ANN design #3B). This design uses a compositional algorithm that changes reservoir fluid composition in every case inside the data set. The algorithm takes into account components up to heavy hydrocarbon 20 (FC_{20}), and then lumps all the heavy components above C_7 as C_{7+}.

Design Analysis and Results

The 2nd inverse design for the forward ANN design #3 could not be developed the same way the forward and 1st inverse designs did. One of the main reasons why that could not be achieved is due to the way the data was designed for the problem that is at hand. Initially, when the forward prediction model was developed, it was developed to allow for gas injection rate to vary every month between a huge gas injection range. The same flexibility that allowed gas injection rate to vary per month, created a very rough injection design surface with very sharp edges that is extremely difficult to correlate to. So, to overcome this issue, the target of this ANN design would be the cumulative gas injection rather than the monthly gas injection rate.

Around 2000 simulation cases were used to build the data set. 85% of the cases were used to train the network, 10% for validation, and the last 5% were used later for a blind test. Table 7-30

through Table 7-32 show a sample of the blind testing cases. (Note: Appendix I shows all of the blind testing cases.)

Table 7-30: Blind Test # 1 and Blind Test # 2 for 2nd Inverse ANN

	Blind T#1			Blind T#2		
	Actual	**ANN**	**Error**	**Actual**	**ANN**	**Error**
Cum. Gas Inj., MMSCF	57.58	57.35	0.40	10.00	10.15	1.50
Injection Duration, D	46.00	37.58	18.30	15.00	12.69	15.40
Well Spacing, Acres	59.00	64.89	9.98	37.00	32.74	11.51

The first two blind tests show good predictability for the second inverse ANN. The error looks inflated for the injection duration. The model does a good job predicting the injection design parameters, Table 7-30.

Table 7-31: Blind Test # 3 and Blind Test # 4 for 2nd Inverse ANN

	Blind T#3			Blind T#4		
	Actual	**ANN**	**Error**	**Actual**	**ANN**	**Error**
Cum. Gas Inj., MMSCF	8.14	7.52	7.62	27.6	27.97	1.34
Injection Duration, D	5.00	3.091	38.18	14.00	16.93	20.93
Well Spacing, Acres	27.00	32.34	19.78	34.00	40.72	19.76

The second two blind tests show satisfactory predictability regardless of the reported high error. The reported error is high because the values predicted are low. The difference between actual injection duration of 5 days and predicted duration of 3 days is around 40%. However, this value is overly exaggerated for both blind tests in Table 7-31.

Table 7-32: Blind Test # 5 and Blind Test # 6 for 2nd Inverse ANN

	Blind T#5			Blind T#6		
	Actual	**ANN**	**Error**	**Actual**	**ANN**	**Error**
Cum. Gas Inj., MMSCF	8.79	13.13	49.37	30.81	32.66	6.00
Injection Duration, D	6.00	12.51	108.50	18.00	21.74	20.78
Well Spacing, Acres	31.00	29.88	3.61	45.00	50.38	11.96

The third set of blind tests show a bad prediction and a good prediction cases. Blind test #5 is predicted wrong, while blind test #6 provides a good match, Table 7-32

ANN design Functional Links:

Similar to the first inverse ANN, this design would not get a close match without the use of functional links. Initial configurations without functional links had over 100% error for most of the parameters.

The second inverse ANN required a lot of fine tuning and improvements until it reached the final stage. In this design, similar functional links and data manipulation techniques to forward ANN design #3B and first inverse designs were used.

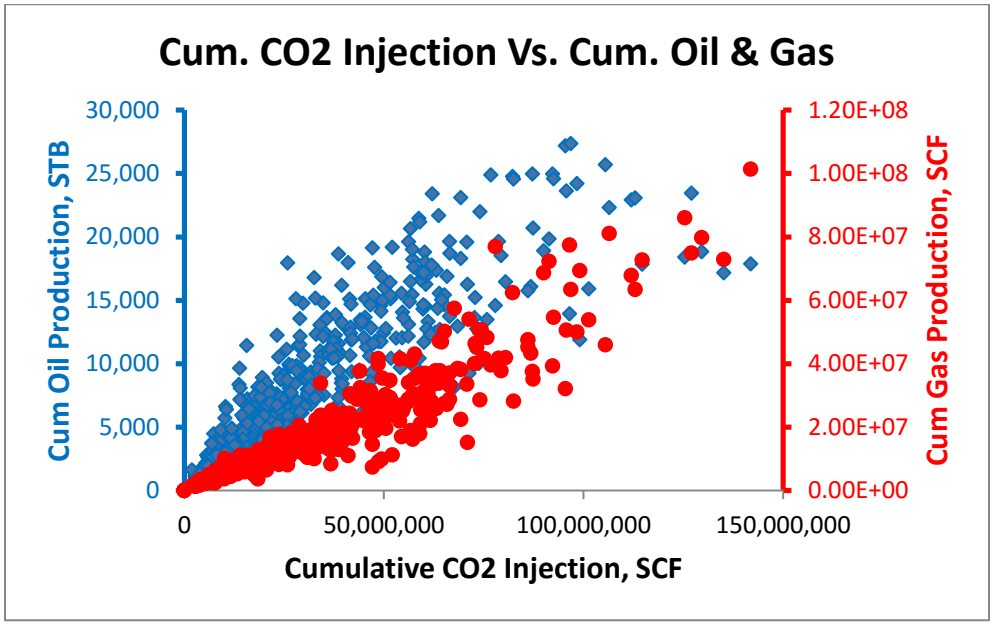

Figure 7-50: Cum. CO2 Injection vs. Cum Oil and Gas Productions

Figure 7-50 shows a direct correlation between the amounts of oil and gas produced to the amount of CO_2 injected. On the same note, Figure 7-51 and Figure 7-52 show some trends between cumulative oil and gas productions CO_2 injection duration, and well spacing.

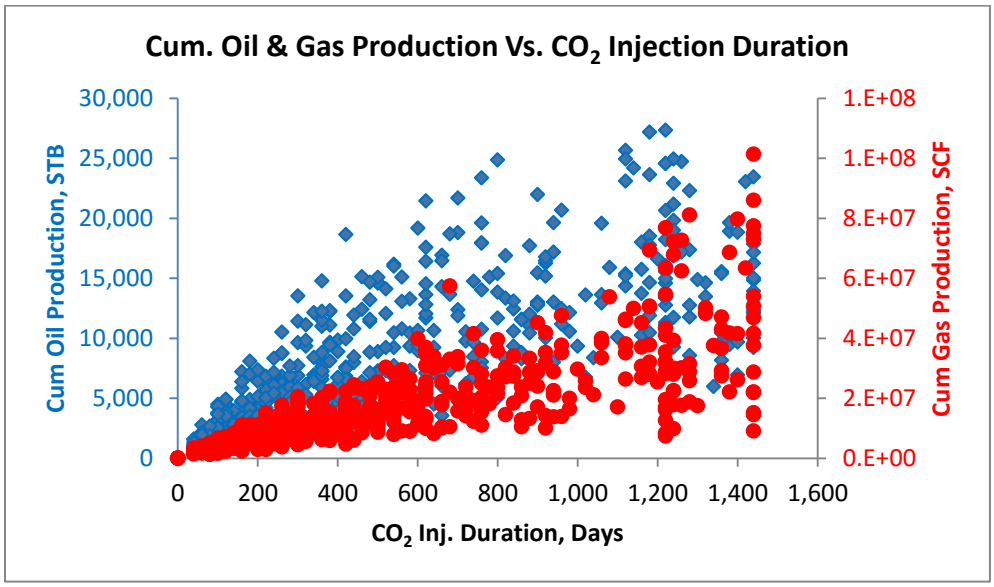

Figure 7-51: Injection Duration vs. Cum Oil and Gas Productions

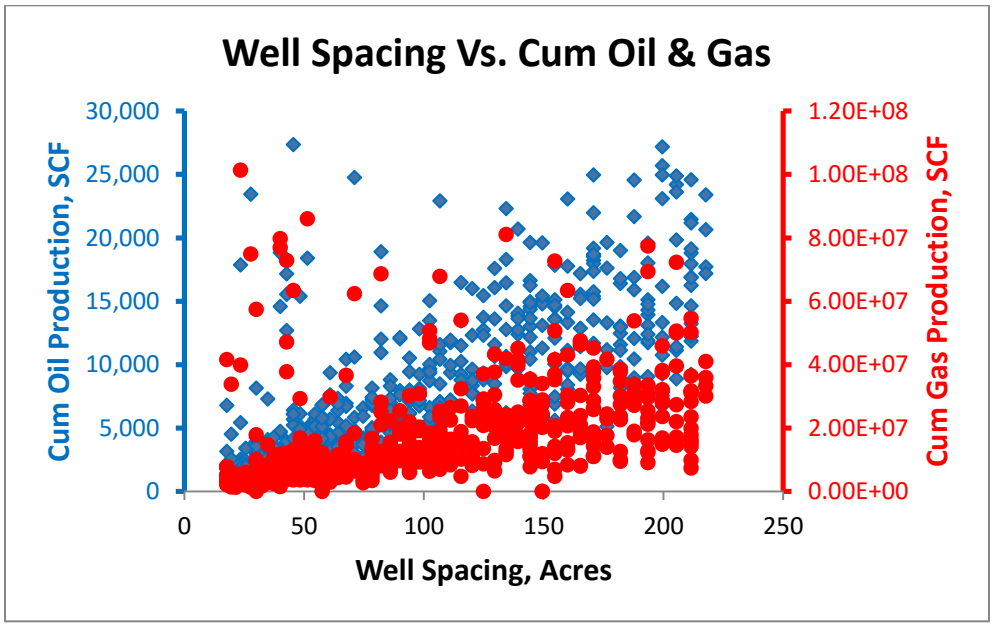

Figure 7-52: Well Spacing vs. Cum Oil and Gas Productions

Table 7-33 shows the final data manipulation techniques used in this inverse ANN. Table 7-34 lists the final functional links used for the first inverse ANN design.

Table 7-33: Final Data manipulation techniques for 2nd Inverse ANN

Data Manipulation	Location
Removed Early Decline and Shut-in Data	Input

Notice that Table 7-34 shows some of the functional links displaying some constants. Theses constants are not random numbers and were generated as part of a complex correlation that relate cumulative production and injection to some of the target output parameters as similarly used in previous forward ANN designs.

Table 7-34: Final Functional Links used for 2nd Inverse ANN

Functional Links	Location
Pi - BHFP	Inputs
(L1 Thickness + L2 Thickness)*Frac Perm	Inputs
Ln(0.0018*Cum Oil Prod)	Inputs
Ln(0.0024*Cum Oil Prod)	Inputs
Ln(0.0036*Cum Oil Prod)	Inputs
Ln(0.0062*Cum Oil Prod)	Inputs
(63.521*Cum Oil Prod-89495)/Cum Oil Prod	Inputs
Ln(0.0062*Cum Oil Prod)- Ln((63.521*Cum Oil Prod-89495)/Cum Oil Prod)	Inputs
Ln((63.521*Cum Oil Prod-89495)/Cum Oil Prod)	Inputs

Design Error Analysis:

The second inverse ANN development in this project provides recommended continuous CO_2 injection design parameters and is referred to in this project as the injection design ANN. This second inverse proxy uses reservoir properties and the desired production profiles and in return, the ANN provides CO_2 injection rate, CO_2 injection duration, and the well spacing.

This design is used to find appropriate injection design parameters for certain oil and gas production profiles for a given reservoir.

The average overall errors for all the blind testing cases are reported in Table 7-35.

Table 7-35: 2nd Inverse ANN Average Blind Test Error

Blind Testing Cases Overall Error	
Property	**Average Error**
Cum. Gas Inj., MMSCF	7.03
Injection Duration, D	23.07
Well Spacing, Acres	10.39

Figure 7-53, Figure 7-54, and Figure 7-55 show the point-by-point comparison between the actual cumulative CO_2 injection, CO_2 injection duration, and well spacing and predicted values by the ANN. The black lines represent the best scenario possible. The closer the values from the black line, the better performance the ANN has. The overall blind tests show good model predictability for the three parameters. It is important to keep in mind that some of those high errors for injection duration are inflated errors for small numbers as previously displayed.

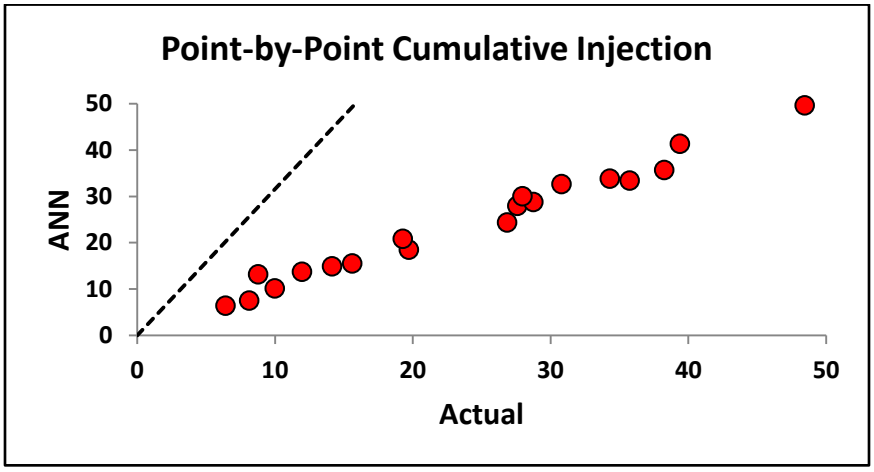

Figure 7-53: Second Inverse ANN Performance Plot for Cumulative Injection

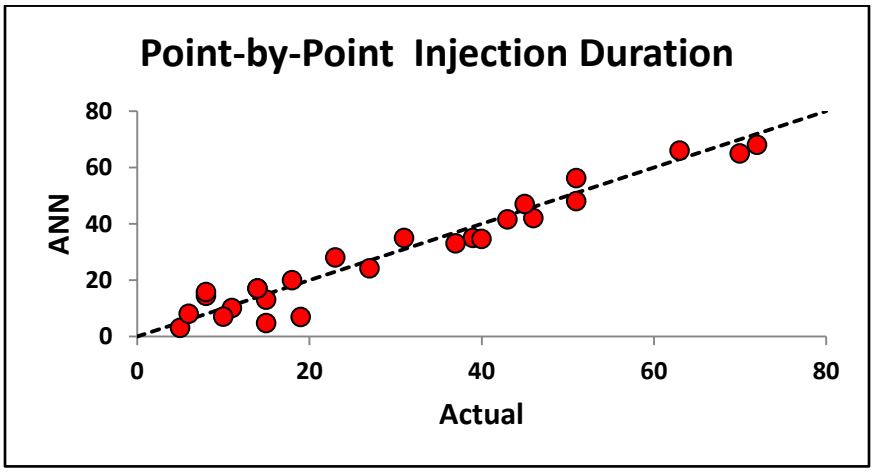

Figure 7-54: Second Inverse ANN Performance Plot for Injection Duration

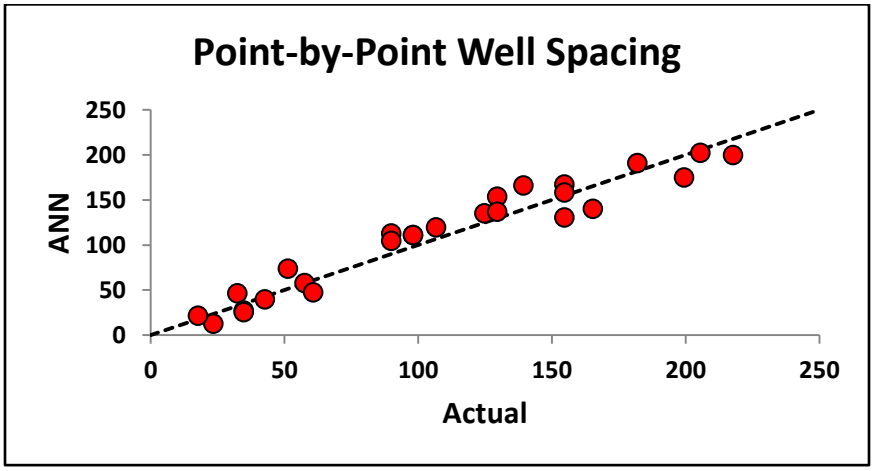

Figure 7-55: Second Inverse ANN Performance Plot for Well Spacing

Chapter 8

RESERVOIR MECHANISM ANALYSIS

This section shows the mechanism inside the reservoir for a sample run that was taken apart in details to ensure that the final ANN reflects our understanding of what goes inside the reservoir. One simulation case will be shown with all the components going inside the simulator and the output given from the simulator. It is important to note that these runs are taken from the data pile that were used in design ANN#3 that were generated using the data generation algorithm described in previous sections.

The reservoir in hand has a good permeability in x and y direction. Vertical permeability is calculated as 1% of the horizontal permeability. Therefore, fluid flow is limited in the vertical direction. Fracture permeability in this case act as major highways with their huge conductivity but extremely low storativity. Similar to vertical matrix permeability, vertical fracture permeability is also calculated as 1% of the fracture horizontal permeability. However, vertical fracture permeability is high allowing vertical fluids movement in the fracture networks.

All the simulation cases in the data set start by depleting the reservoir from the specified reservoir pressure (4,672 psia) until the specified minimum bottom hole flowing pressure (4,172 psia) (BHFP). Miscibility is controlled through minimum BHFP where the reservoir is depleted until the desired miscibility conditions. The production well would then shut-in. CO_2 injection would then start by injecting about 735,000 SCF/D while the producer is on the whole time. When pressure rises above the BHFP due to the injected gas, the producer starts to produce until operational conditions are reached and producer is then shut-in.

Reservoir Matrix Permeability, x, y, z respectively:

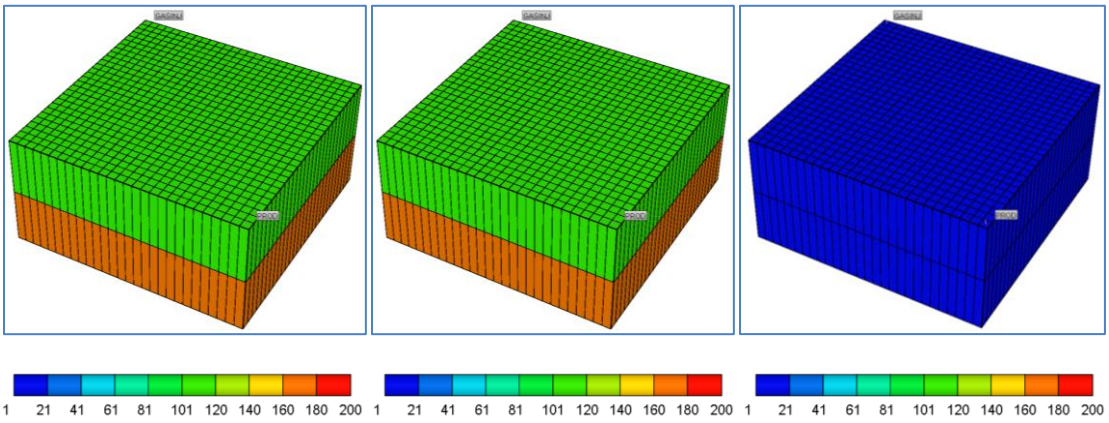

Reservoir Fracture Permeability, x, y, z respectively:

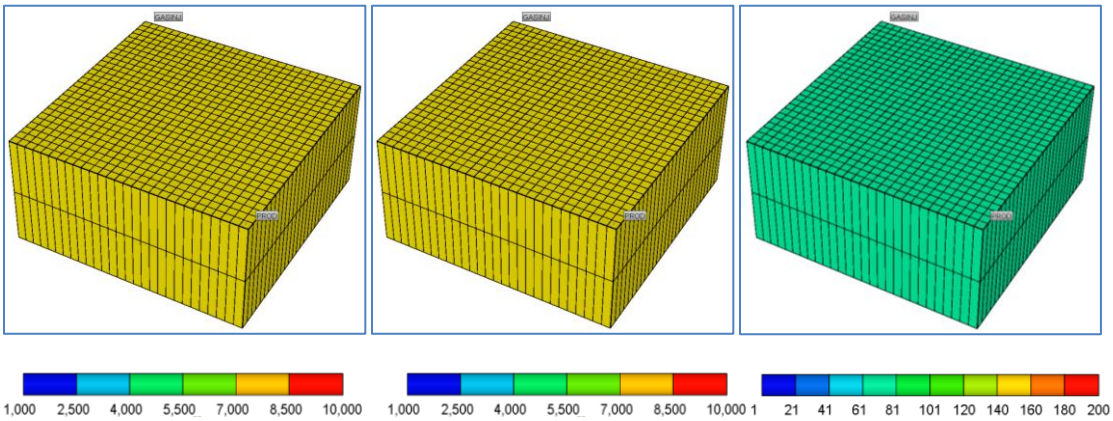

Reservoir Matrix Porosity and Fracture Porosity respectively:

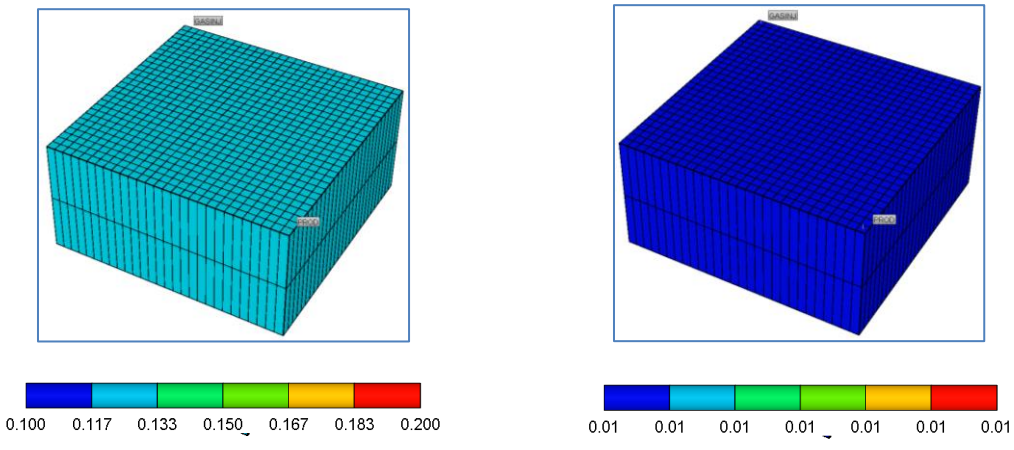

Figure 8-1: Matrix and Fracture Properties for Sample Case

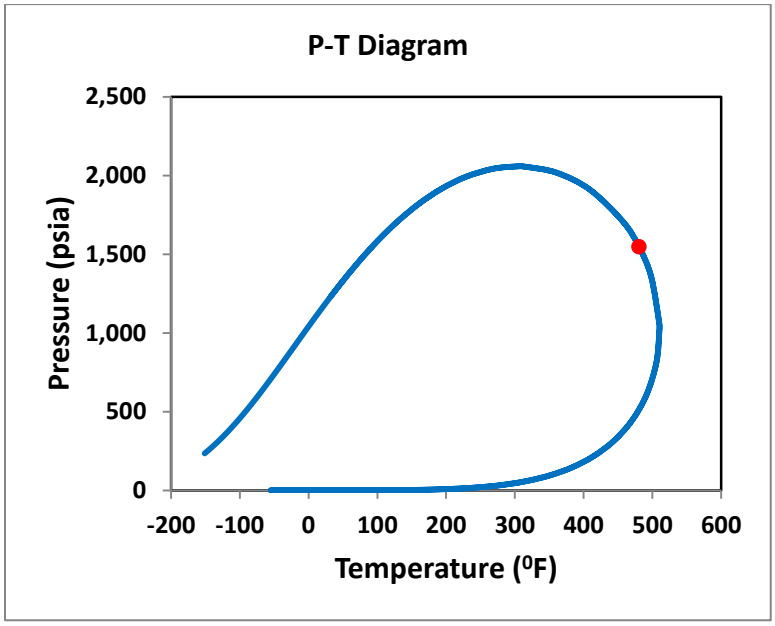

Figure 8-2: Phase Diagram for the Sample Case

Table 8-1: Fluid Composition

Component	Composition
H_2S	0.0002
CO_2	0.0312
N_2	0.0174
C_1	0.2996
C_2	0.1
C_3	0.0672
IC_4	0.0237
NC_4	0.0261
IC_5	0.0472
NC_5	0.0271
FC_6	0.0278
C_{7+}	0.3325
MW	125.90
SG	0.77

Other reservoir information:

Initial Reservoir Pressure: 4,672 psia

Initial Water Saturation: 29.9%

Minimum Bottom Hole Pressure: 4,172 psia

Continuous CO_2 Injection Rate: 734,432 SCF/D

Reservoir Production History: The reservoir starts production in 1/1/1986 and produced a maximum of 23698.1 bbls. The production well was then shut-in due to reaching operational condition (Minimum Bottom Hole Pressure of 4,172 psia). In 1/1/1990 EOR starts by injecting 734,432 SCF/D CO_2 continuously for 4 years.

Figure 8-3 shows the oil production and gas injection profiles for the whole duration since the start of production in 1986 until the end of the EOR project in 1996

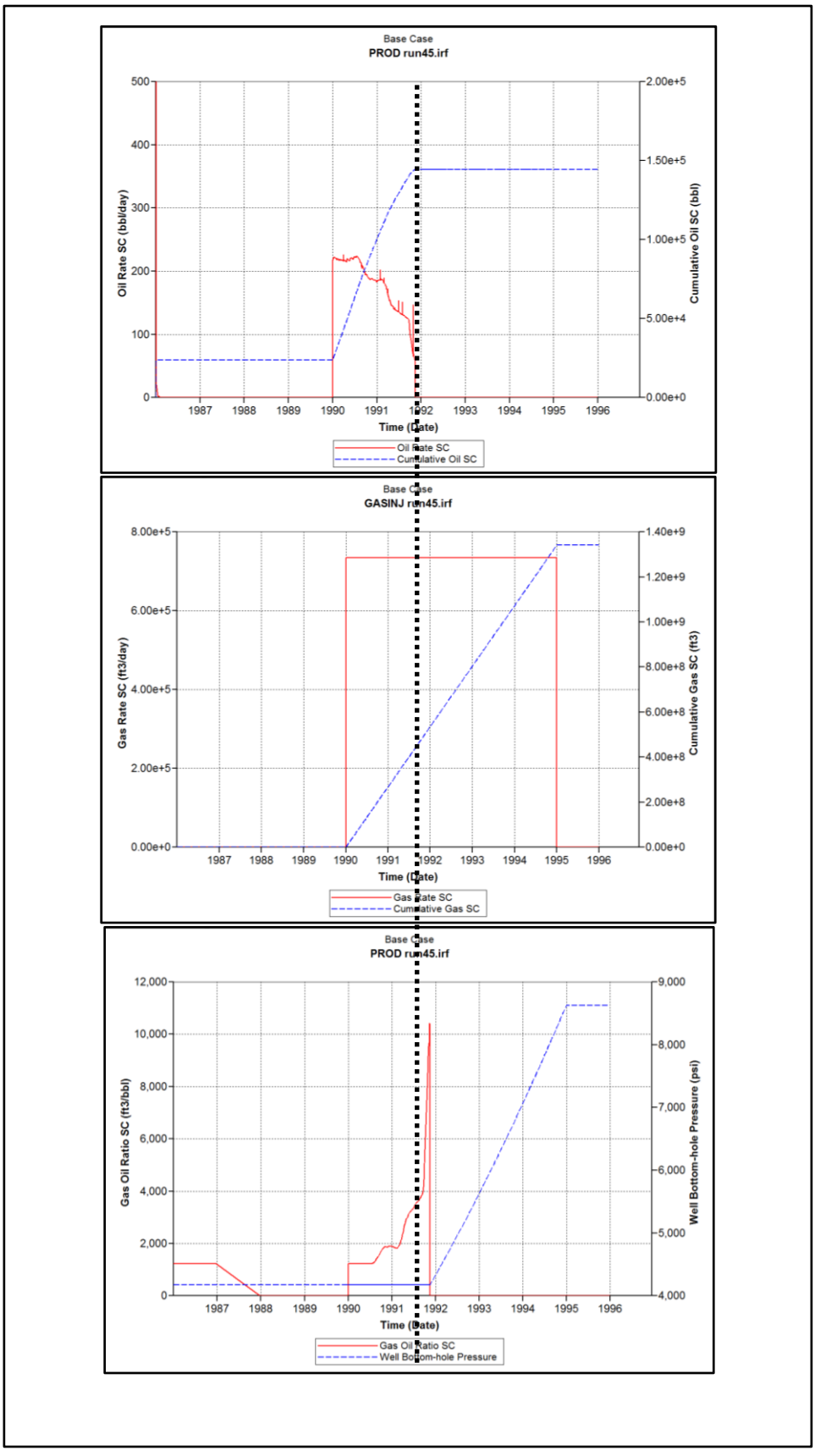

Figure 8-3: Oil and Gas Profiles for the Sample Case

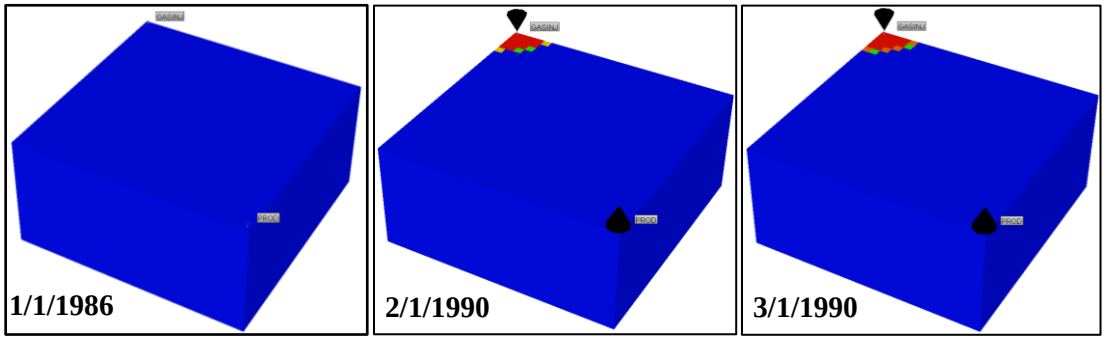

Figure 8-4: Fracture Carbon Dioxide Saturation Starting at 1/1/1986, 1/1/1990, and 3/1/1990

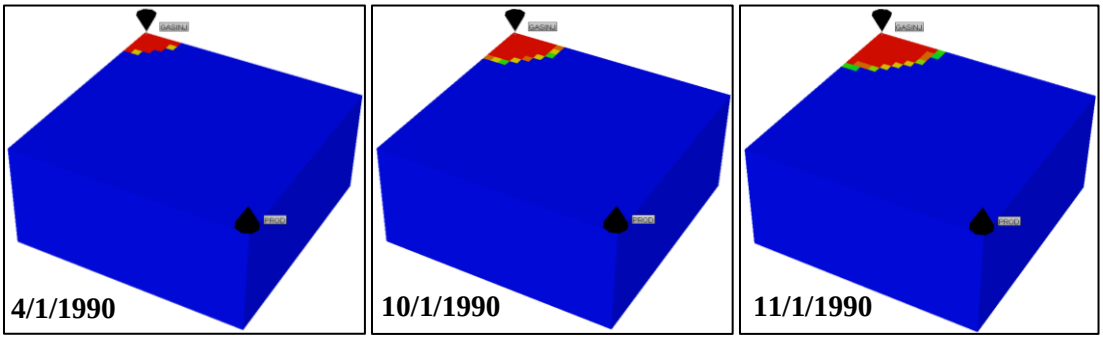

Figure 8-5: Fracture Carbon Dioxide Saturation Starting at 4/1/1986, 10/1/1990, and 11/1/1990

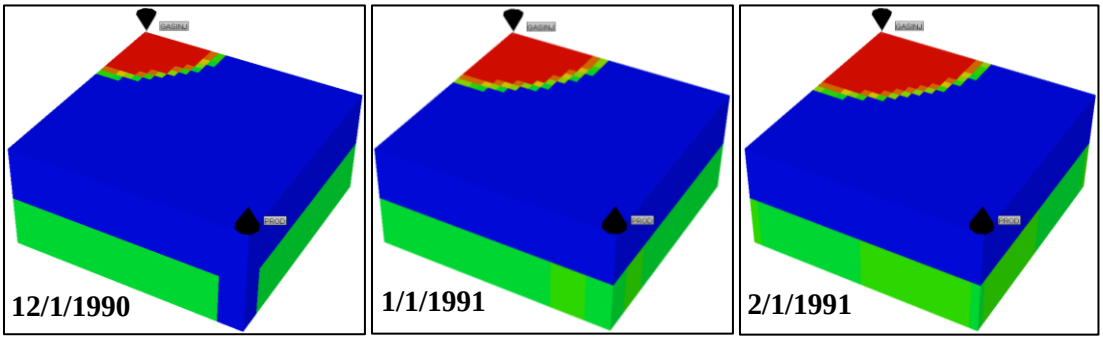

Figure 8-6: Fracture Carbon Dioxide Saturation Starting at 12/1/1990, 1/1/1991, and 2/1/1991

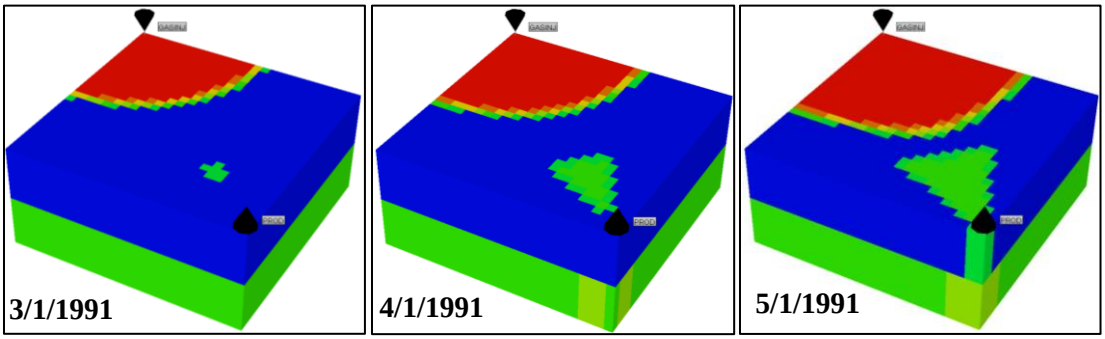

Figure 8-7: Fracture Carbon Dioxide Saturation Starting at 3/1/1991, 4/1/1991, and 5/1/1991

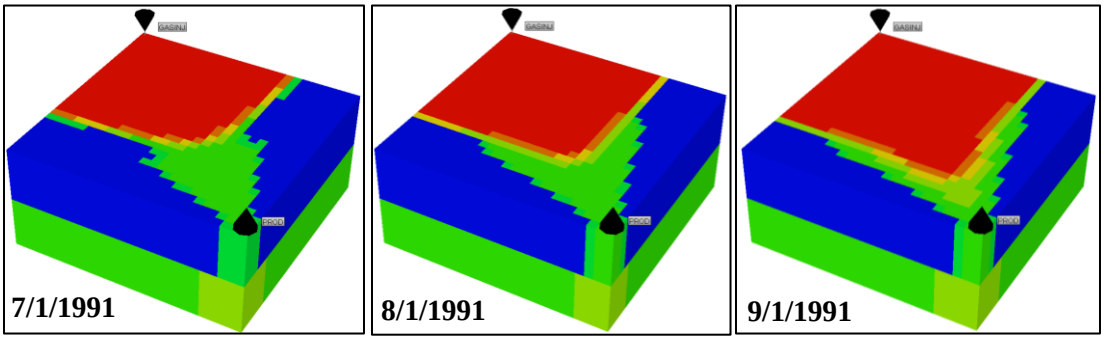

Figure 8-8: Fracture Carbon Dioxide Saturation Starting at 7/1/1991, 8/1/1991, and 9/1/1991

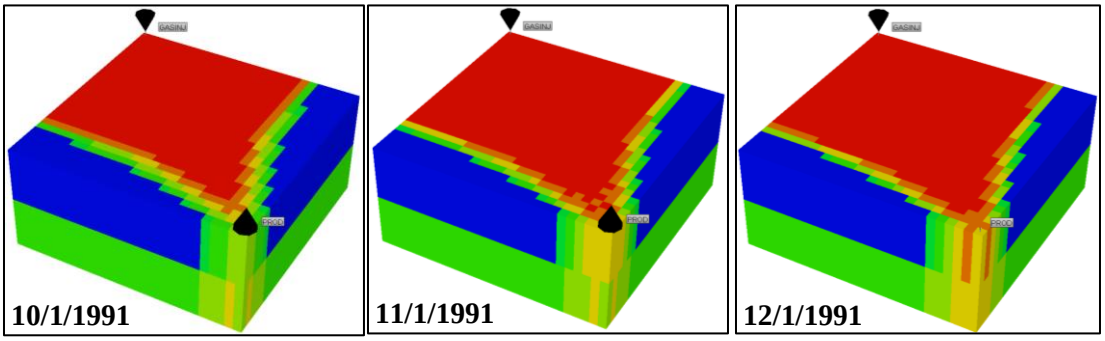

Figure 8-9: Fracture Carbon Dioxide Saturation Starting at 10/1/1991, 11/1/1991, and 12/1/1991

Figure 8-4 through Figure 8-9 show the CO_2 saturation inside the fractures. At 1/1/1986, reservoir pressure declines marking the start of the depletion period and then shut-in once minimum BHFP is reached. CO_2 injection starts at 1/1/1990 and CO_2 saturation starts to rise in the fractures. The saturation profile shows a gradual increase in the top layer followed by CO_2 slumping through the highly conductive fractures to the bottom layer that pushes CO2 to the producer within 1 year of continuous injection. Fractures play different roles as they facilitate early breakthrough as well as exposing reservoir fluid to the injected CO_2 fluid.

In this research, continuous CO_2 injection is done over a period of 4 years which is long enough for CO_2 to breakthrough and reaches operational conditions for different reservoir types and fluids.

Chapter 9

GRAPHICAL USER INTERFACE (GUI)

The main objectives of this research were met when the different ANNs were successfully built and tested against the blind testing cases. However, the ANNs in their final forms are hardly useable by anyone other than the person who developed them. That is simply because of the way the ANNs are developed and the way the data were arranged and used. For example, if a user input a value in the first column for matrix porosity while that value is supposed to be set in another column, the outcome of the ANN will be completely wrong. So, in order to make these ANNs useable and accessible by any one, a graphical user interface was developed. The graphical user interface (GUI) uses the final forms of the forward, first inverse, and second inverse ANNs and present them to the user in a simple fill in the blanks type problem. This chapter highlights the major features in this project through the developed GUIs and provides a simple guide for the user.

NOTE: The GUIs were built using MATLAB GUIDE (2012).

9.1.1 Main Interface Window

The main interface window is the first window the user will see once the program is lunched. The user has 3 ANNs and 3 beneficial tools to choose between, Figure 9-1. The interface states next to each ANNs the type of data needed and it is as the following:

1) Forward Model (**TARGET: Oil and Gas Production Profiles**):
    a. Rock Properties
    b. Fluid Composition
    c. Relative Permeability
    d. Capillary Pressure
    e. Injection Design
2) First Inverse Model (**TARGET: Uncertain Reservoir Properties**):
    a. Known Rock Properties
    b. Fluid Composition
    c. Relative Permeability
    d. Capillary Pressure
    e. Injection Design
    f. Oil and Gas Production Profiles
3) Second Inverse Model (**TARGET: Injection Design Parameters**) :
    a. Rock Properties
    b. Fluid Composition
    c. Relative Permeability
    d. Capillary Pressure
    e. Oil and Gas Production Profiles

The main interface window includes three essential tools to the engineer:

1) Phase Behavior Model (PBM): Provides the phase diagram for any fluid.
2) Lee's C7+ Lumping Method: Lumps all compositions above C6 as part of C7+.
3) Alston et al. MMP Correlation: Provides the user with a good estimate of the MMP for a particular fluid that is undergoing pure CO_2 injection. However, Alston et al. (1983) reports around 7% error using the developed correlation.

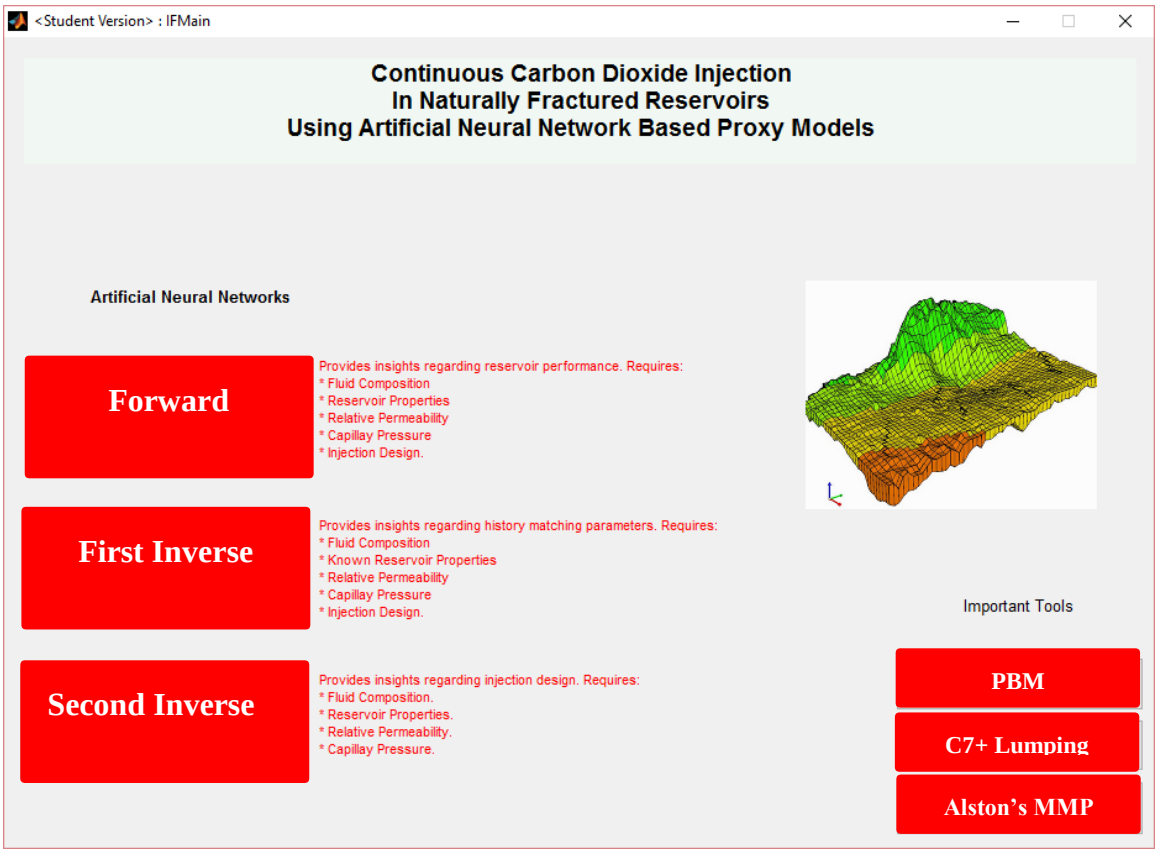

Figure 9-1: GUI Main Window

9.1.2 Forward ANN Window

The forward ANN window is lunched from the main interface window. At first glance, the forward ANN GUI looks overwhelming. However, this actually highlights the strengths and flexibility of this ANN. For example, the user does not have to stick to any particular fluid, reservoir temperature, rock properties, relative permeability, capillary pressure, or injection design. Any reservoir engineer should be able to provide or estimate these data with ease. The forward ANN window has 156 input boxes, but the required data are only 52 for the base case. The other a104 input boxes were implemented to study uncertainty. Figure 9-2 highlights the inputs needed for the main case in question.

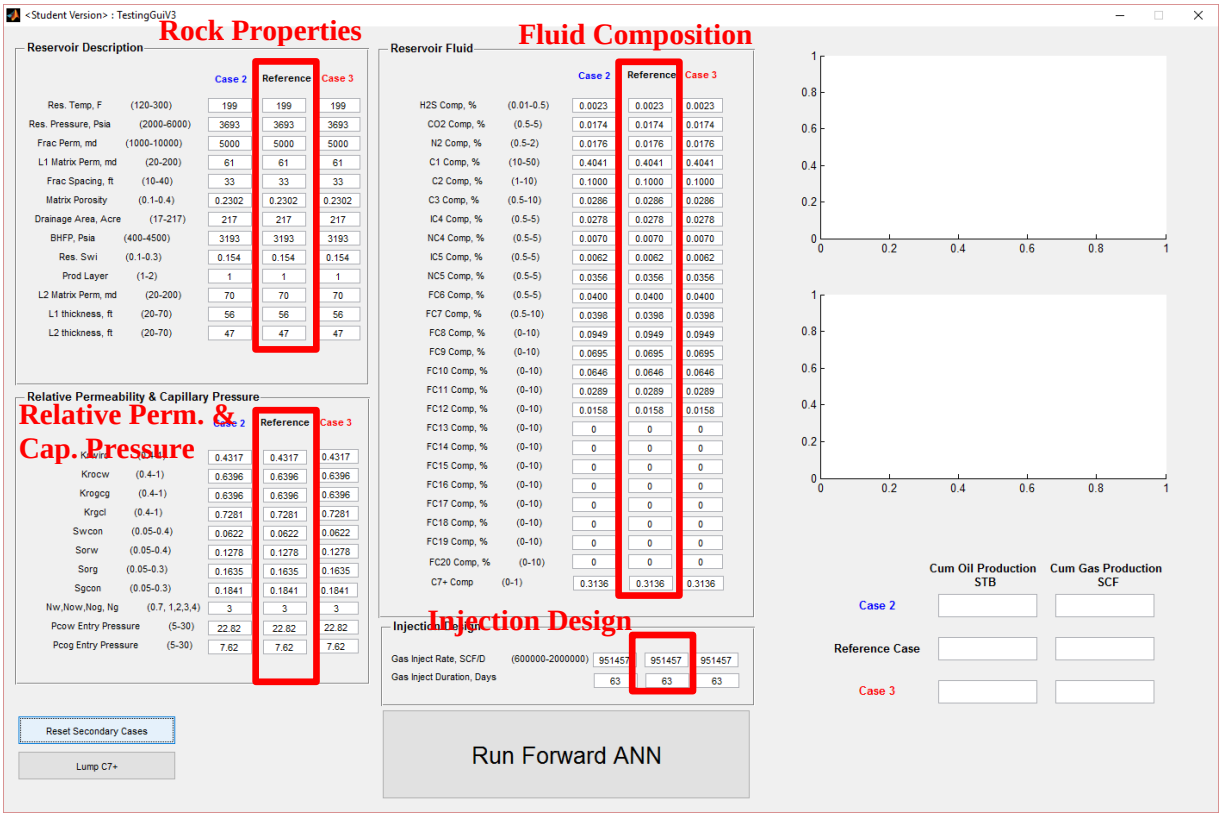

Figure 9-2: Base Case Required Inputs for Forward ANN

Once all the inputs are provided, the user will hit “Run Forward ANN” button and the results will be displayed instantly on the right hand side of the window in the form of oil production rate, gas production rate, and cumulative productions, Figure 9-3.

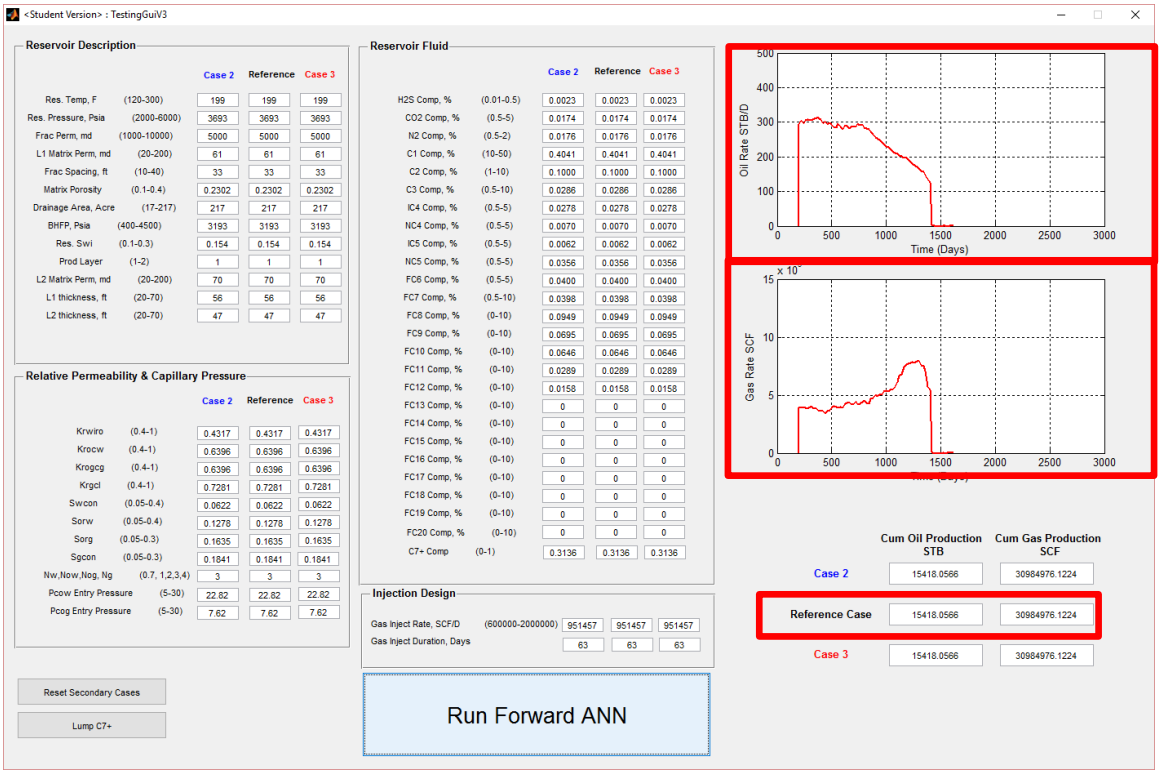

Figure 9-3: Forward ANN Output Area

As mentioned previously, case #2 and case #3 were developed to add more functionality and usability to the ANN. The additional cases provide the engineer with sensitivity analysis on the fly. They also provide uncertainty analysis on any property or combined properties. The results are then displayed promptly on the right hand side of the GUI.

Figure 9-4 shows an example of sensitivity analysis done on fracture permeability while Figure 9-5 shows uncertainty analysis on some parameters. Notice the GUI plots the reference base case in black, while case #2 and case #3 are plotted in blue and red respectively.

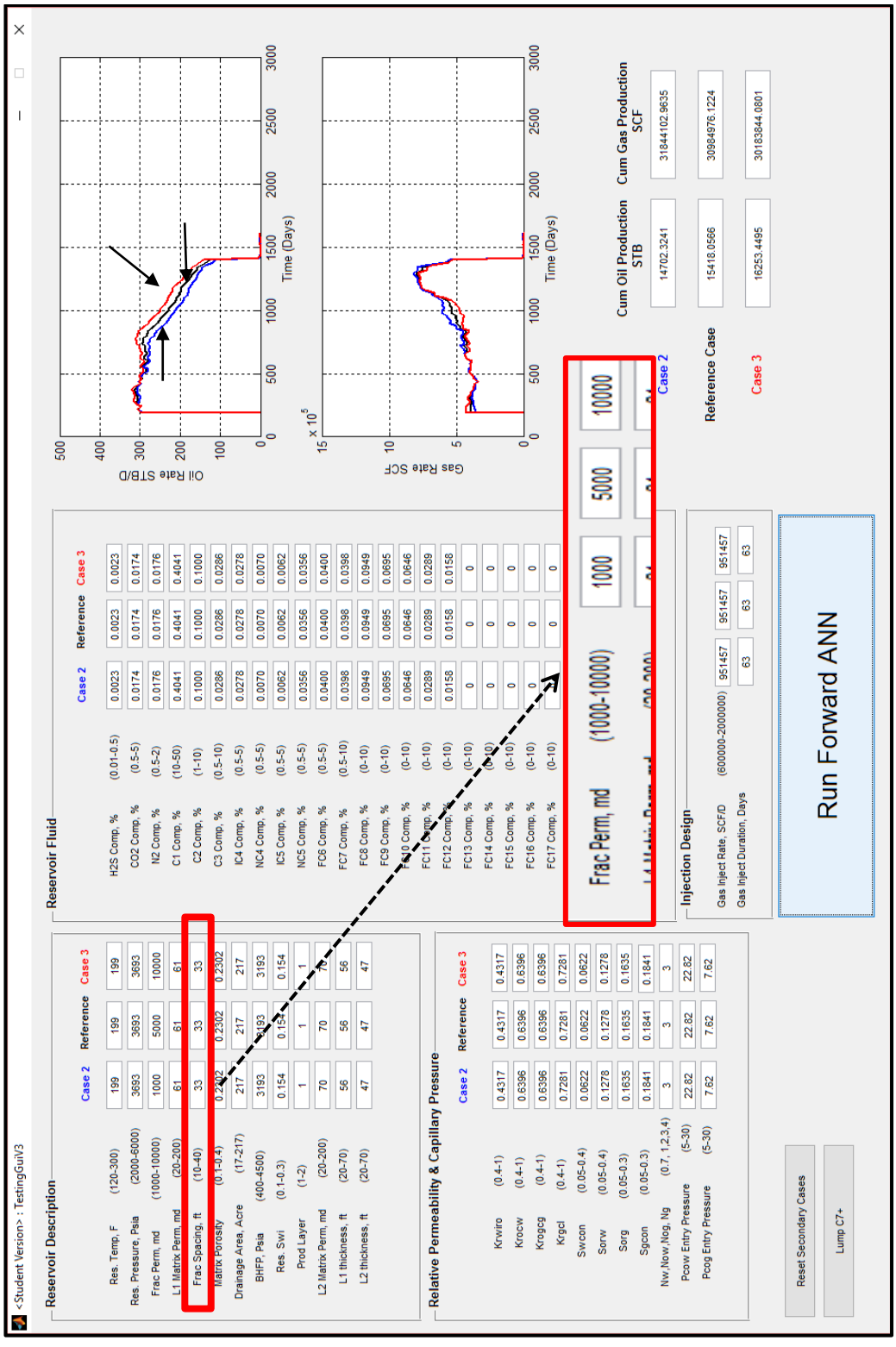

Figure 9-4: Sensitivity Analysis on Fracture Permeability. All other properties are exactly like the base Case

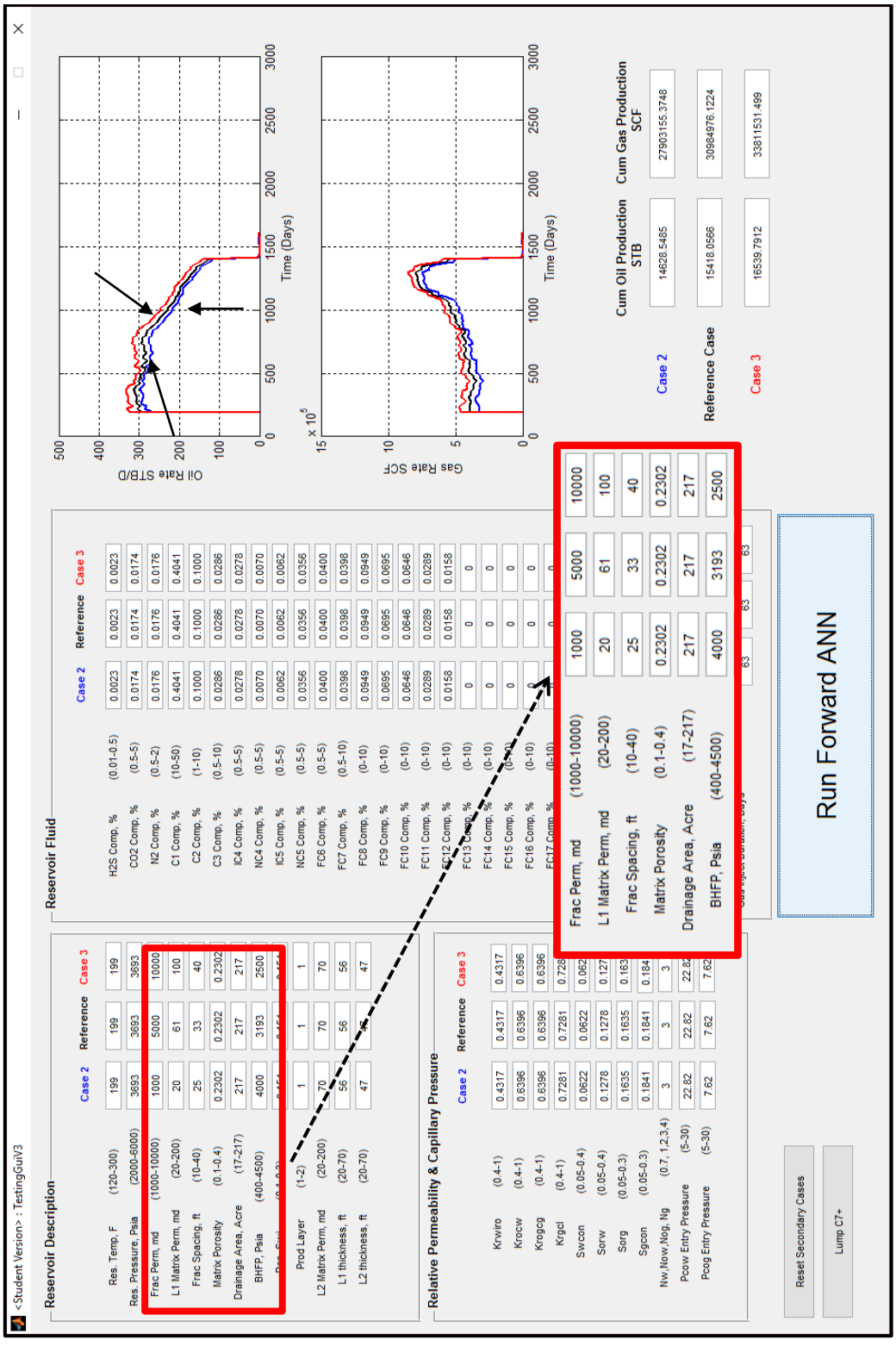

Figure 9-5: Uncertainty Effect of Fracture Perm., L1 Matrix Perm, Matrix Porosity, Drainage Area, and BHFP

Additionally, two beneficial tools are integrated in all of the ANN windows. The first one resets all values and makes them equal to the base reference case. This is very important for sensitivity analysis and when running a single case, otherwise, the user would have to manually reset over 100 values. The second tool is the C7+ lumping tool. So, the engineer would input the reservoir fluid compositions up to heavy hydrocarbon 20 and then press this button which would lump any component above C6 as part of C7+.

Note: The tools implemented in all the windows work independently from all the other GUI windows.

Figure 9-6 highlights the implemented tools in the forward, 1st inverse, and 2nd inverse ANN.

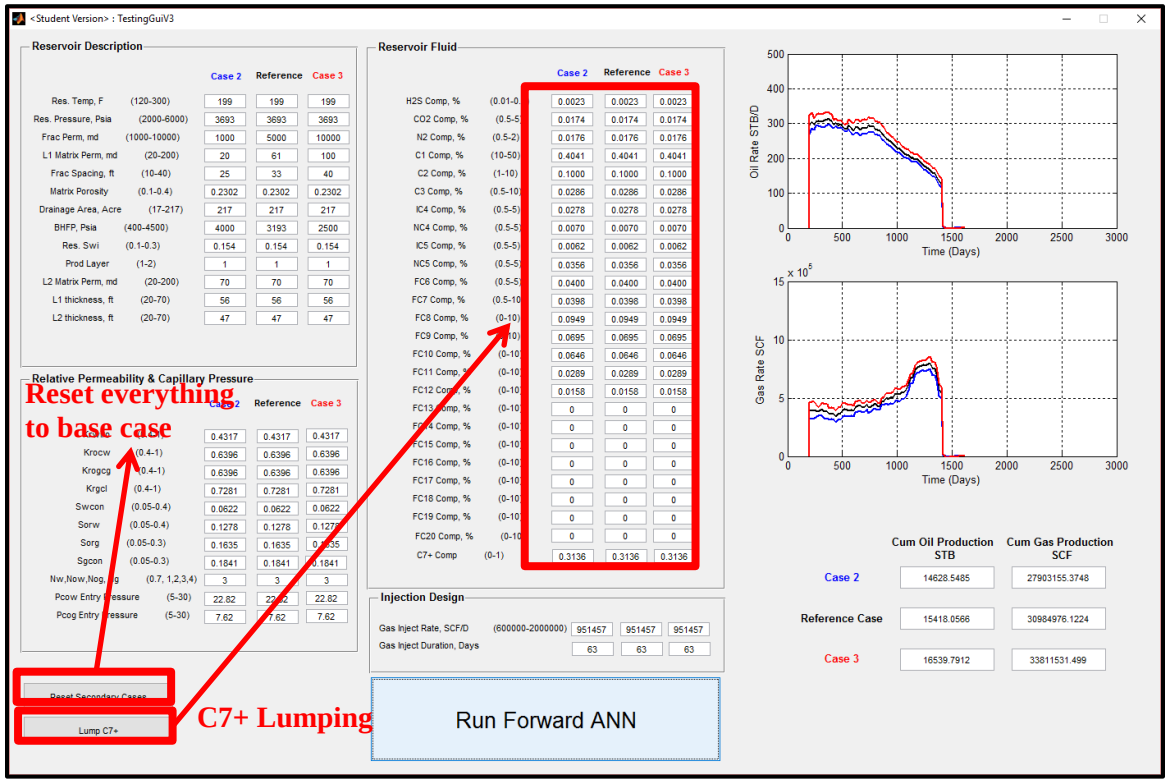

Figure 9-6: Integrated Tools in All GUI Windows, Reset Button and C7+ Lumping Button

9.1.3 First Inverse ANN Window

The first inverse ANN window is lunched from the main interface window. Similar to the forward ANN, the first inverse ANN GUI looks overwhelming at first glance.

The first inverse window has 144 input boxes, but the required data are only 48 for the base case. The other 96 input boxes were implemented to study uncertainty. Figure 9-7 highlights the inputs needed for the main case in question.

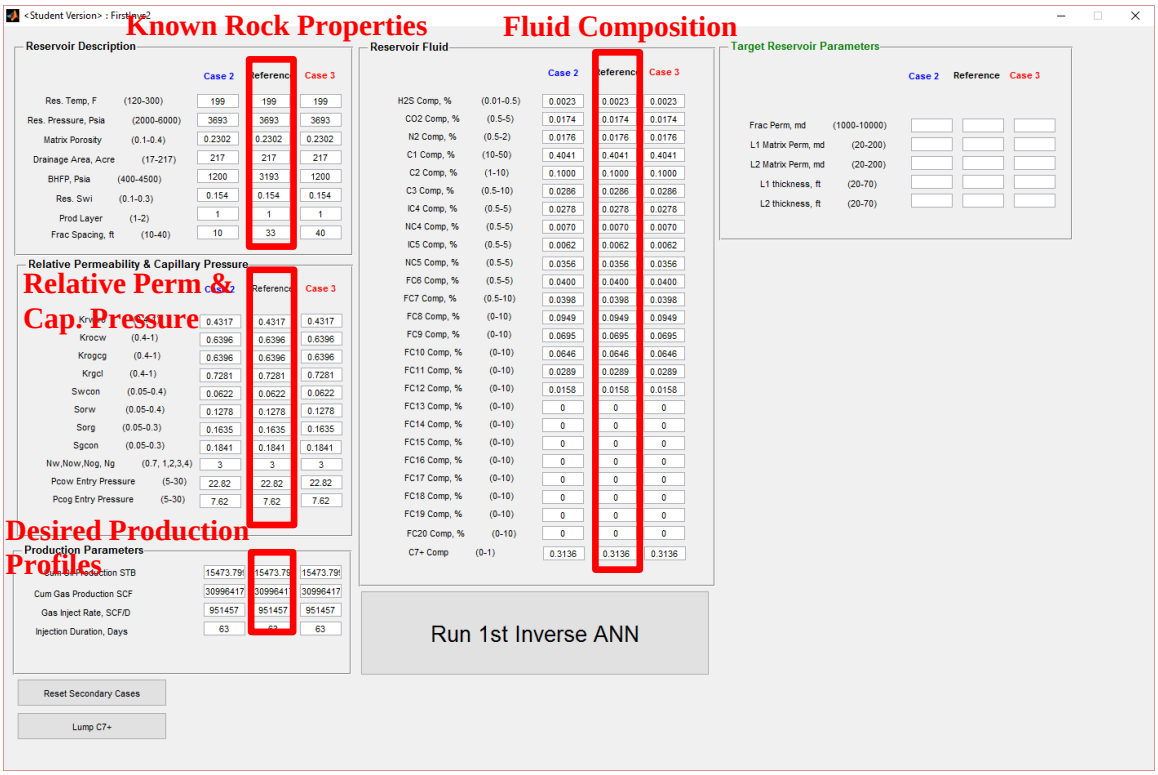

Figure 9-7: Base Case Required Inputs for 1st Inverse ANN

Once all the inputs are provided, the user will hit "Run 1st Inverse ANN" button and the results will be displayed instantly on the right hand side of the window.

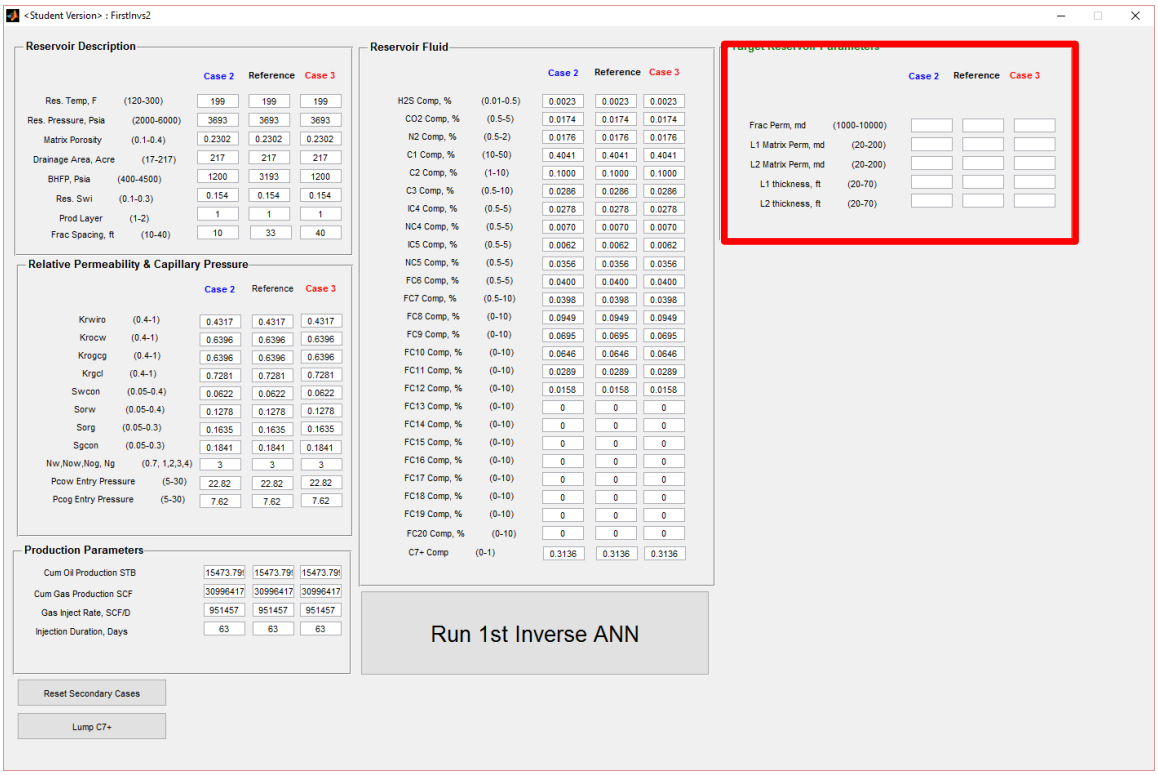

Figure 9-8: 1st Inverse ANN Output Area

Similar to forward ANN GUI window, case #2 and case #3 were developed to add more functionality and usability to the ANN. The additional cases provide the engineer with sensitivity analysis on the fly. They also provide uncertainty analysis on any property or combined properties. The results are then displayed promptly on the right hand side of the GUI.

Figure 9-9 shows an example of sensitivity analysis done on reservoir pressure. The GUI reports the reference base case in black, while case #2 and case #3 are plotted in blue and red respectively.

Figure 9-10 shows an example of uncertainty analysis done on reservoir pressure, matrix porosity, well spacing, and bottom hole flowing pressure. The GUI reports the reference base case in black, while case #2 and case #3 are plotted in blue and red respectively.

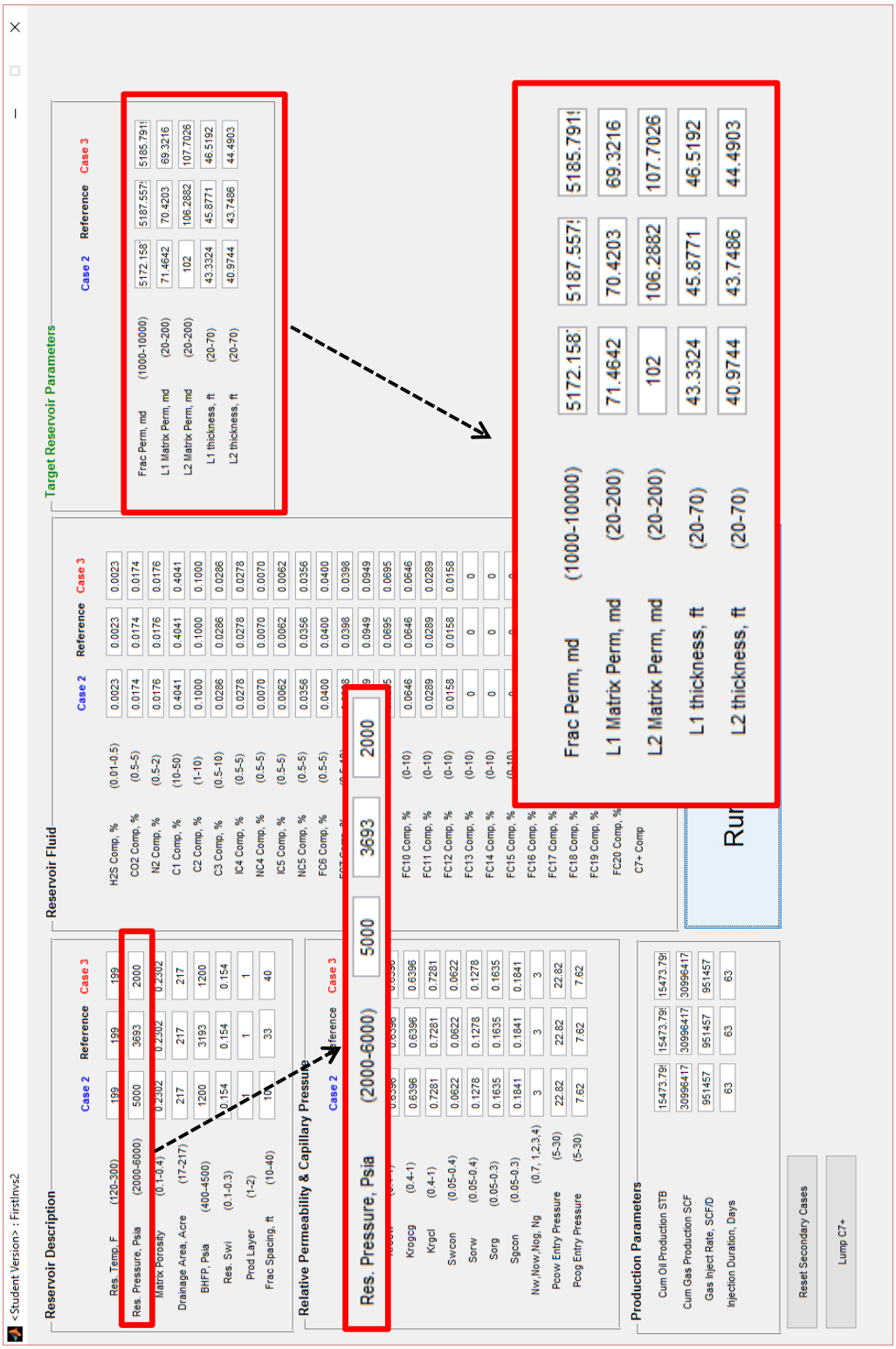

Figure 9-9: Sensitivity Analysis on Reservoir Pressure. All other properties are exactly like the base Case

Figure 9-10: Uncertainty Effect of Reservoir Pressure, Matrix Porosity, Drainage Area, and BHFP

9.1.4 Second Inverse ANN Window

The second inverse ANN window is lunched from the main interface window. It follows the same general theme of the previous GUIs but with different objectives.

The first inverse window has 153 input boxes, but the required data are only 51 for the base case. The other 102 input boxes were implemented to study uncertainty. Figure 9-11 highlights the inputs needed for the main case in question.

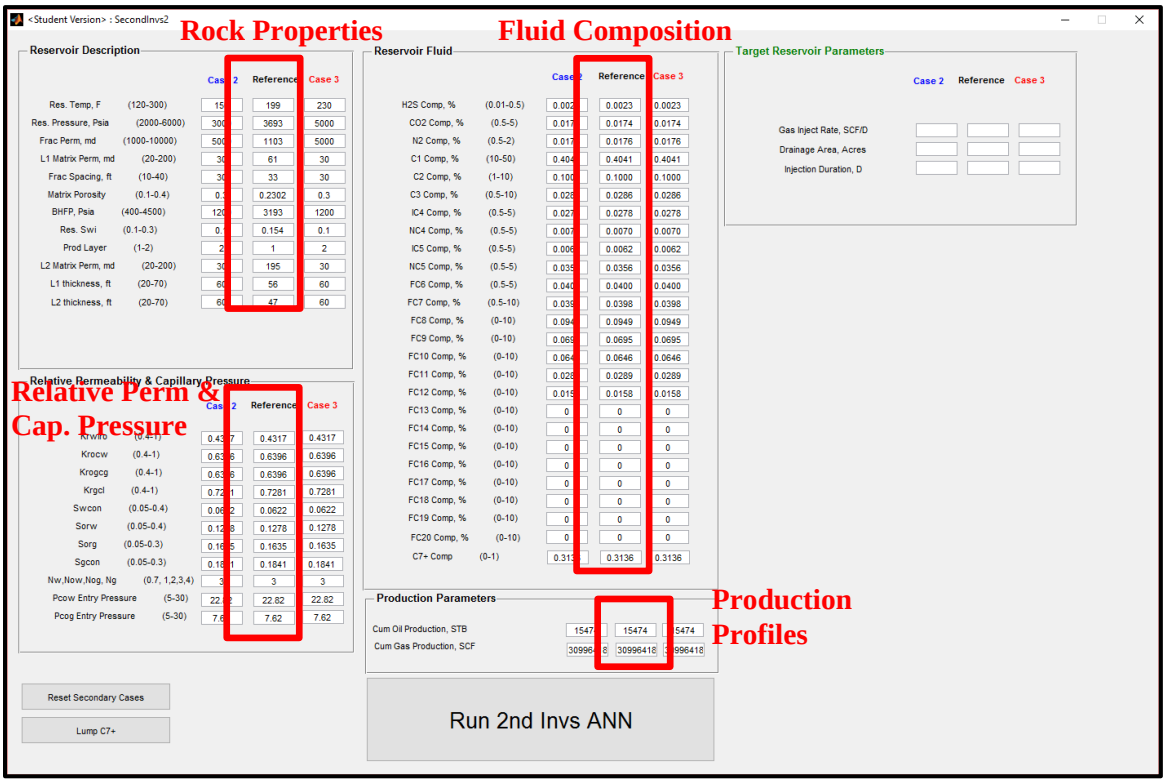

Figure 9-11: Base Case Required Inputs for 2nd Inverse ANN

Once all the inputs are provided, the user will hit "Run 2nd Inverse ANN" button and the results will be displayed instantly on the right hand side of the window.

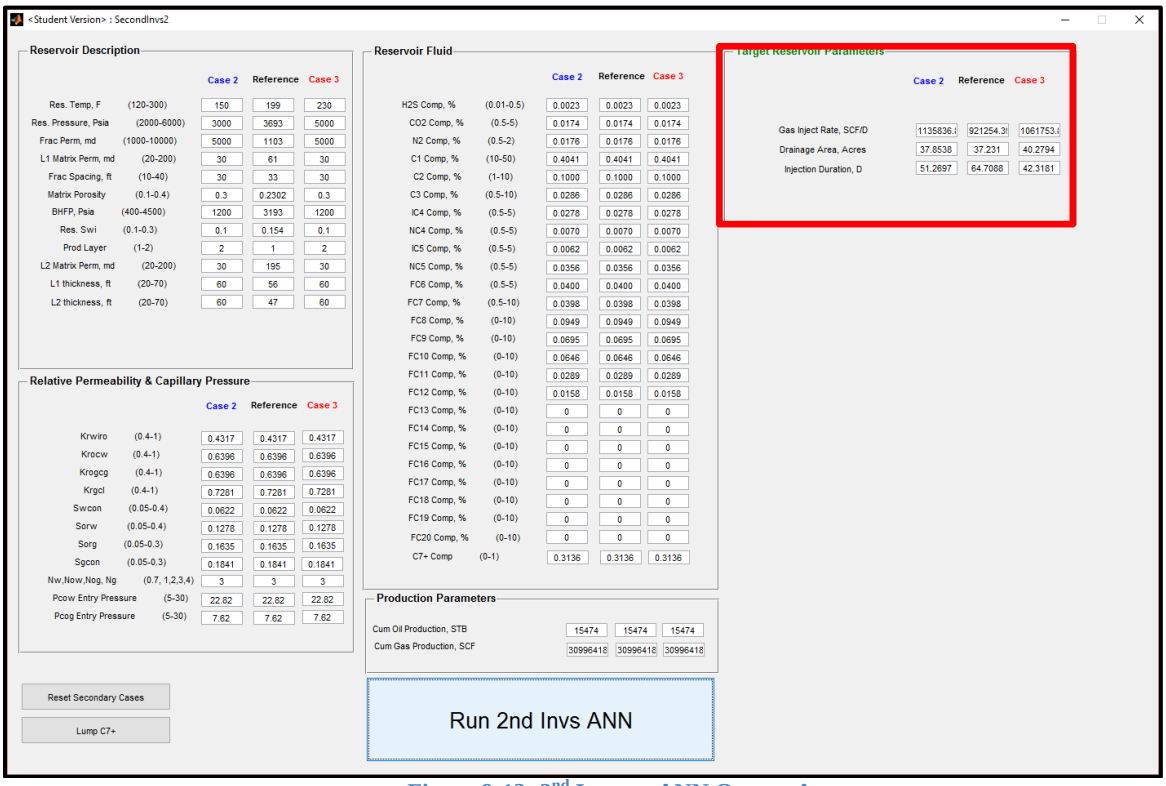

Figure 9-12: 2nd Inverse ANN Output Area

Similar to previous ANN GUI windows, case #2 and case #3 were developed to add more functionality and usability to the ANN. The additional cases provide the engineer with sensitivity analysis on the fly. They also provide uncertainty analysis on any property or combined properties. The results are then displayed promptly on the right hand side of the GUI.

Figure 9-13 shows an example of sensitivity analysis done on fracture permeability. The GUI reports the reference base case in black, while case #2 and case #3 are plotted in blue and red respectively.

Figure 9-14 shows an example of uncertainty analysis done on fracture permeability, L1 matrix permeability, fracture spacing, matrix porosity, and bottom hole flowing pressure. The GUI reports the reference base case in black, while case #2 and case #3 are plotted in blue and red respectively.

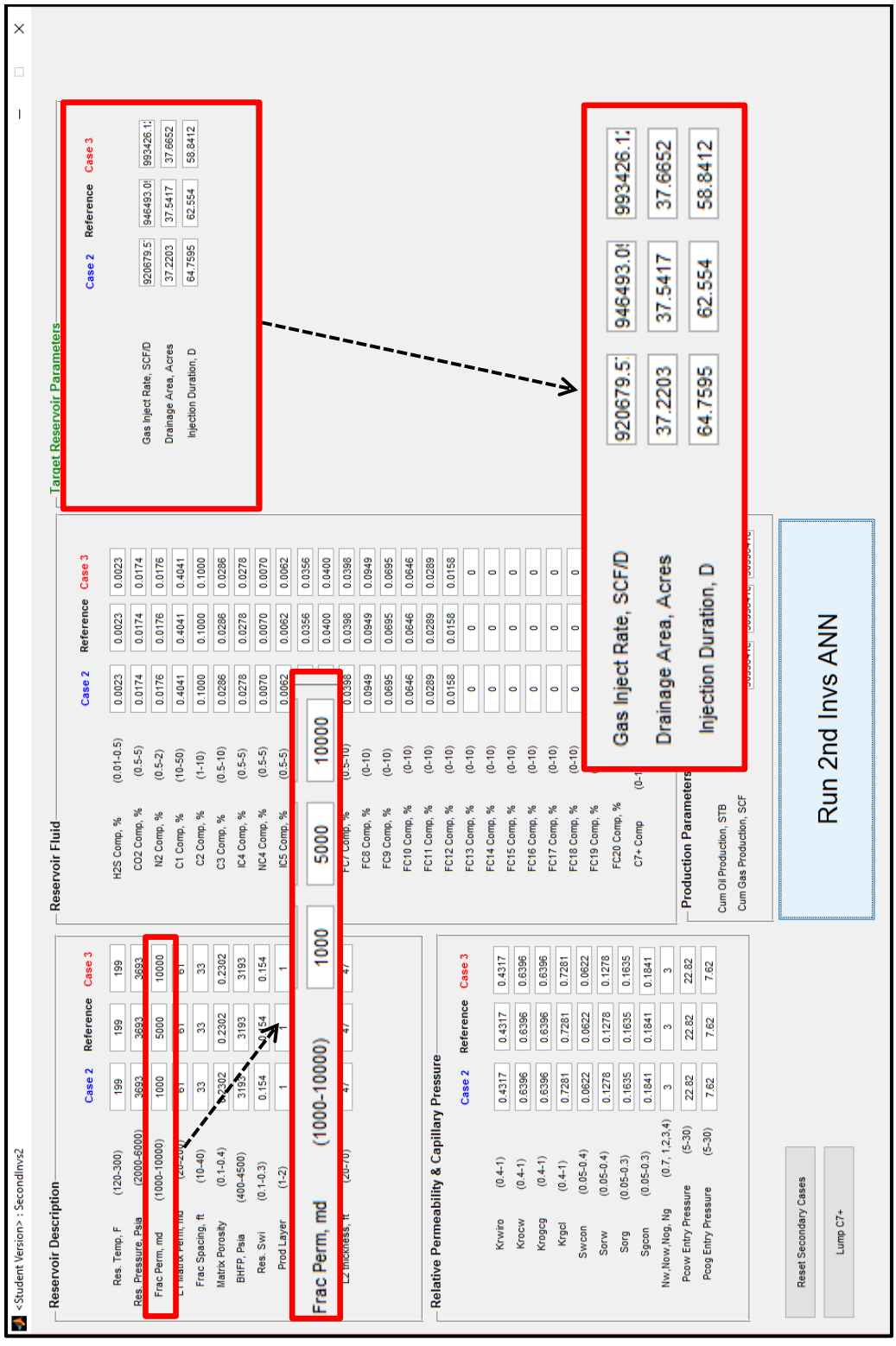

Figure 9-13: Sensitivity Analysis on Fracture Permeability. All other properties are exactly like the base Case

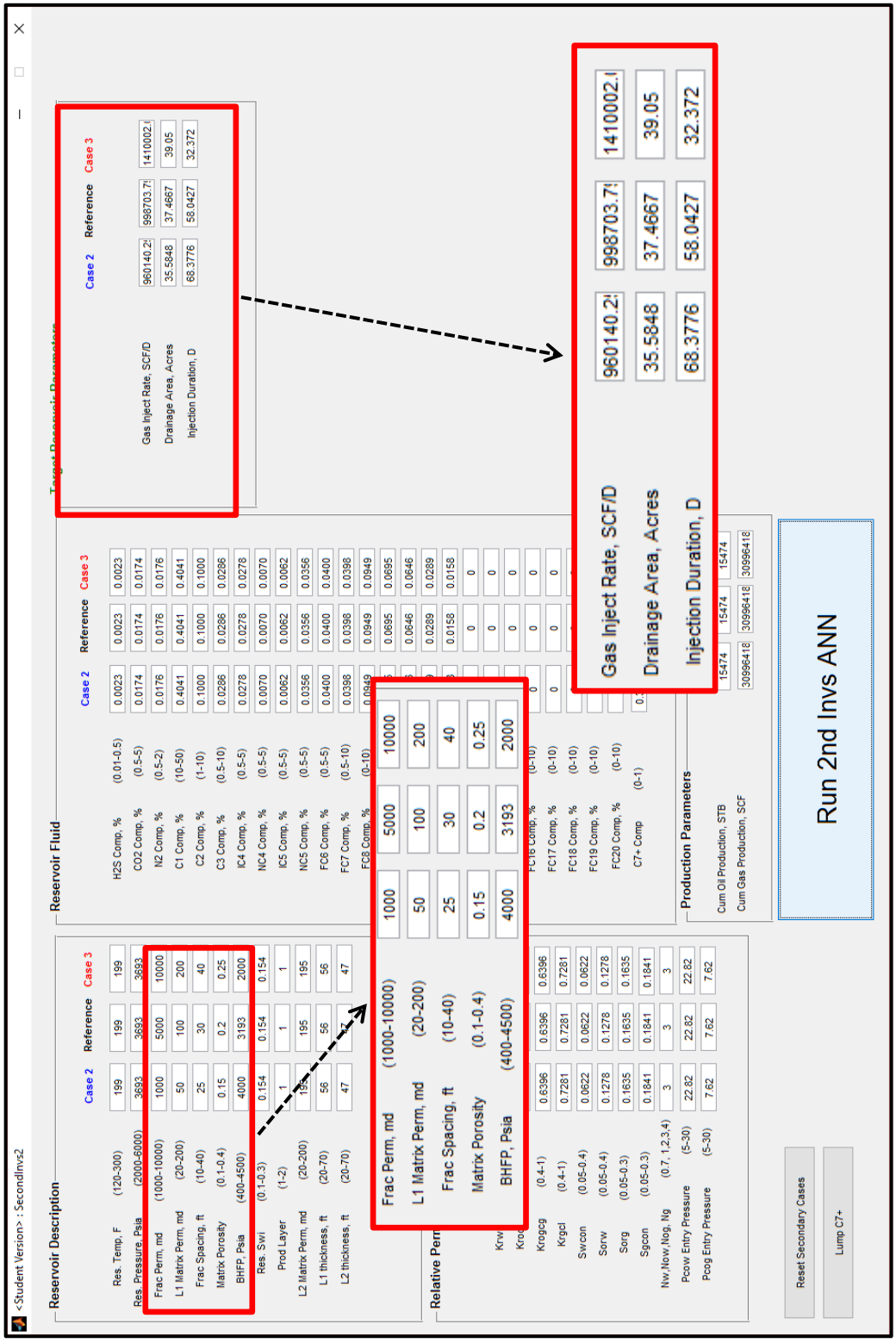

Figure 9-14: Uncertainty Effect of Fracture Perm., L1 Matrix Perm, Fracture Spacing, Matrix Porosity and BHFP

Chapter 10

SUMMARY AND CONCLUSIONS

This research translates a complex, computationally-heavy, EOR project into a powerful uncertainty-equipped universal screening tool. In this research, complex correlations are develop for continuous CO_2 injection in naturally fractured reservoir through the use of artificial neural networks. The correlations embedded in the artificial neural networks were developed gradually from a specific reservoir with specific reservoir fluid composition, capillary pressure, and relative permeability and ended with very complex artificial neural networks for a huge number of reservoirs with any reservoir fluid composition, any capillary pressure, and any relative permeability. These developed networks are second generation networks and are far superior to previous networks that were very limited to specific reservoir properties, fluids, capillary pressures, and relative permeabilities.

The forward prediction network provides reservoir performance assessments on the fly rather than taking months using conventional methods. A particular reservoir might not be a good candidate for continuous carbon dioxide injection, but it shouldn't take a very long time and exhausting every possible scenario to come up with that conclusion. The first inverse network helps the engineer history matching any reservoir by providing insights regarding uncertain reservoir parameters for various production profiles. The second inverse network aims to help the engineer in designing a proper injection scheme for any reservoirs and production profiles.

The artificial neural networks along with established procedures

The developed artificial neural networks mimic a two-well, two-layer, miscible compositional simulation model and provide reliable on the fly reservoir performance, history match insights, and injection design recommendations. A graphical user interface was developed encompassing all three networks as well as essential tools that are essential to the engineer when conducting a

carbon dioxide study. The GUI adds more to the project where it allows the engineer to study parameter sensitivity as well as the effect of uncertainty of single or multiple parameters using forward, first inverse, or second inverse ANNs. The critical parameters that affected the continuous CO_2 injection the most are reservoir fluid composition, fracture permeability, well spacing, bottomhole flowing pressure (BHFP), thickness, and CO_2 injection amount.

The developed ANNs in this research set a new standard in terms by overcoming the limitations imposed by reservoir fluid composition, relative permeability, and capillary pressure.

This research does not approve or disapprove the applicability of continuous carbon dioxide injection in naturally fractured reservoirs. However, the ANNs developed act pre-screening tools that help accelerate the decision making process. These pre-screening tools do not replace current industry standards, methodologies, or protocols but should be treated as complementary tools with predictive capabilities.

Recommendations

This project provides a new benchmark for artificial neural network study. However, it can be further enhanced with the following:

- The main scope of this research is continuous CO_2 injection, but some of the initial ANN designs studied the applicability of water alternating gas and proved very promising.
- The fluid composition in this research goes up to HC_{20}, a further expansion to the list for much heavier HC would expand the range of fluid compositions this fluid could evaluate.
- Every fluid composition in this study includes H_2S, N_2, and CO_2 in very small percentages. While their effects at very small percentages are negligible, it would add more value to have the option to include them or not.
- This study could include an even wider range of reservoir properties.
- Different Well configurations could be studied.
- The methodology developed here could be used on cyclic pressure pulsing and WAG, and all three methods could be developed under a single ANN.
- The GUI could be enhanced with an optimization technique.
- The developed ANNs in this research are only applicable to miscible injection. This could be further expanded to include near miscible condition or multiple contact miscibility cases which could affect WAG projects.
- WAG relative permeability hysteresis effect.
- ANN configurations in this research could be dynamically updated and calibrated with additional data coming from the field. This step requires retraining of the ANNs due to additional outputs that were not initially part of the main configurations.

REFERENCES

Ahmadi, K., and Johns, R. T.: "Multiple Mixing-Cell Method for MMP Calculations", SPE paper 116823 presented at the 2008 Annual Technical Conference and Exhibition held in Denver, Colorado, USA, 21-24 September, 2008.

Artun, E. F. (2008). Optimized Design of Cyclic Pressure Pulsing in Naturally Fractured Reservoirs Using Neural-Network Based Proxy Models. Ph.D. thesis, The Pennsylvania State University, University Park, Pennsylvania.

Barenblatt, G.E., Zheltov, I.P., and Kochina, I.N., "Basic Concepts in the Theory of Homogenous Liquids in Fissured Rocks", Journal of Applied Mathematical Mechanics (USSR), 1960.

Caudle, B. H. and Dyes, A.B., "Improving Miscible Displacement by Gas-Water Injection", Trans., AIME (1958), 213, 281-84.

Christensen, J R, Stenby, E H, Skauge, A, "Review of the WAG field experience", SPE 71203, revised paper 39883, presented at the 1998 SPE International petroleum conference and exhibition of Mexico, Villhermosa, March 3-5, 1998.

Cronquist, C. (1977): 'Carbon Dioxide Dynamic Miscibility with Light Reservoir Oils', Proc. Fourth Annual US DOE Symposium, Tulsa, Oklahoma.

Danesh, A., PVT and Phase Behaviour of Petroleum Reservoir Fluids, Developments in Petroleum Science v. 47, Elsevier, 1998.

Dykhuizen, R. C. (1990). A new coupling term for dual-porosity models. *Water Resour. Res.*, 26, pp 351-356.

Firoozabadi, A., Thermodynamics of Hydrocarbon Reservoirs, Mc Graw Hill, 1999.
Gershenson, C. Artificial Neural Networks for Beginners [Online]

Available at: https://datajobs.com/data-science-repo/Neural-Net-%5BCarlos-Gershenson%5D.pdf[Accessed 20 February 2014].

Gong, B. (2007). Effective Models of Fractured Systems. Ph.D. thesis, Stanford University, Stanford, California

Graupe, D., 2007. *Princeiples of Artificial Neural Networks.* 2nd ed. Hackensack: World Scientific Publishing Co. Pte. Ltd..

Hadlow R.E., Update of Industry Experience With CO2 Injection, SPE 24928, 1992.

Hagan, M. T., Demuth, H. B., and Bearl, M. (1996). "Neural Network Design" (1st ed). Boston, MA: PWS Pub.

Haykin, S. (1998). Neural Networks: A Comprehensive Foundation. Prentice Hall, second edition.

Holm., L.W., (1986). Miscibility and Miscible Displacement. J. Pet. Tech., SPE 15794.

Holm, L. W., and O'Brien, L. J.:"Carbon Dioxide Test at the Mead-Strawn Field", SPE paper 3103 presented at SPE 45th Annual Fall Meeting held in Houston, Oct 4-7, 1970.

Hong, K. C.: "Lumped-Component Characterization of Crude Oils for Compositional Simulation", SPE paper 10691 presented at the SPE/DOE Third Joint Symposium on Enhanced Oil recovery of the Society of Petroleum Engineering held in Tulsa, OK, April 4-7, 1982.

Johnson, J.P. and Pollin, J.S. (1981):' Measurement and Correlation of CO2 Miscibility Pressures', SPE 9790, presented at the SPE/DOE enhanced Oil Recovery Symposium, April 5-8, 1981, Tulsa, Oklahoma.

Kulkarni, M. M. (2003). Immiscible And Miscible Gas-Oil Displacements In Porous Media. MS.C thesis, Louisiana State University, Baton Rouge, Louisiana.

Langston, M. V., Hoadley, S.F., and Young, D.N.:" Definitive CO2 Flooding Response in the SACROC Unit", SPE paper 17321 presented at the SPE/DOE Enhanced Oil Recovery Symposium held in Tulsa, Oklahoma, April 17-20, 1988.

Li, B., Tchelepi, H. A., and Benson, S. M.:" The Influence of Capillary Entry-Pressure Representation on CO2 Solubility Trapping". Available at: www.sciencedirect.com [Accessed 5 August 2014].

McCain, William D.: The Properties of Petroleum Fluids. Second Edition, PennWell Publishing Company, Tulsa, Oklahoma, 1990. ISBN 0-87814-335-1.

Michael A. Nielsen, "Neural Networks and Deep Learning", Determination Press, 2015.

Michelsen, M. and Mollerup, J., Thermodynamic Models: Fundamentals & Computational Aspects, Tie-line publications, Denmark, 2007

Mogensen, K., Hood, P., and Frank, S.: "Minimum Miscibility Pressure Investigations for a Gas Injection EOR Project in Al Shaheen Field, Offshore Qatar", SPE Paper 124109 presented at the 2009 SPE Annual Technical Conference and Exhibition held in New Orleans, Louisiana, 4-7 Octorober, 2009.

Mohaghegh, S. (2000). Virtual Intelligence Applications in Petroleum Engineering: Part 1 - Artificial Neural Networks. J. Pet. Tech., 53(9):64–73. SPE 58046.

Mungan, N, "An evaluation of carbon dioxide flooding", SPE 21762, presented at the SPE Western regional meeting held in Long Beach, CA, March 20-22, 1991.

Murray, M. D., Frailey, S. M., and Lawal, A. S.: " New Approach to CO2 Flood: Soak Alternating Gas", SPE paper 70023 presented at the 2001 SPE Permian Basin Oil and Gas Recovery Conference held in Midland, Texas, 15-16 May, 2001.

National Petroleum Council: Enhanced Oil Recovery, Washington, D.C. (Dec. 1976).

Nelson, R. A. (2001). Geologic Analysis of Naturally Fractured Reservoirs. Gulf Professional Publishing, Boston, Massachusetts.

Orr F.M. and Silva M.K. (1982). 'Equilibrium Phase Compositions of CO2-Hydrocarbon Mixtures: Measurement by a Continuous Multiple Contact Experiment'. Paper SPE 10726 presented at the SPE/DOE Third Joint Symposium on Enhanced Oil Recovery, Tulsa, April 4-7, SCPJ.

Orr, F. M. Jr. (2007): 'Theory of Gas Injection Process', Tie-Line Publications, ISBN 87-989961-2-5.

Parada, C. H. (2008). An Artificial Neural Network Based Tool-Box for Screening and Designing Improved Oil Recovery Methods. Ph.D. thesis, The Pennsylvania State University, University Park, Pennsylvania.

Pedersen, K.S. and Christensen, P.L. Phase Behavior of Petroleum Reservoir Fluids, CRC /Taylor & Francis, 2007.

Ronald, N. A., 2001. Geologic Analysis of Naturally Fractured Reservoirs, Second Edition. Woburn, Massachusetts: Gulf Professional Publishing/Elsevier.

Sandler, S., Chemical, Biochemical, and Engineering Thermodynamics, 4th ed, Wiley, 2006.

Sarma, P., and Aziz, K. (2004). New transfer functions for simulation of naturally fractured reservoirs with dual porosity models, paper SPE 90231 presented at the SPE Annual Technical Conference and Exhibition, Houston, Texas.

Stone, H. (1973). Estimation of Three-Phase Relative Permeability and Residual Oil Data. J. Cdn. Pet. Tech, 12(4):53.

Surguchev., L. M., Korbol., R., and Krakstad., O.S.: " Screening of WAG injection Strategies for Heterogeneous Reservoirs", SPE paper 25075 presented at the European Petroleum Conference held in Cannes, France, 16-18 November, 1992.

Surguchev, L. and Li, L.: "IOR Evaluation and Applicability Screening Using Artificial Neural Networks", SPE paper 59308 presented at 2000 SPE/DOE Improved Oil Recovery Symposium held in Tulsa, Oklahoma, 3-5 April, 2000.

Thomas, L. K., Dixon, T. N., and Pierson, R. G. (1983). Fractured reservoir simulation. *SPE J.*, 23(1), pp 42-54.

Vidal, J. Thermodynamics: Applications in Chemical Engineering and the Petroleum Industry, Editions TECHNIP, Paris, France, 2003.

Warren, J. E. and Root, P. J. (1963). The Behaviour of Naturally Fractured Reservoirs. SPEJ, 3(3):245–255. 426-PA.

Whitson, C. and Brule, M., Phase Behavior, SPE Monograph Volume 20, Henry Doherty Series, 2000.

Yuan, H., Johns, R.T., Egwuem, A.M. and Dindoruk, B. (2005):' Improved MMP Correlation for CO2 Floods Using Analytical Gas Flooding Theory', SPE REE, pp. 418-425.

Yellig, W.F. and Metcalfe, R.S. (1980): 'Determination and Prediction of CO2 Minimum Miscibility Pressures', JPT, pp. 160-168.

Zhou D., Yan M., and Calvin W. M.: "Optimization of a Mature CO2 Flood – From Continuous Injection to WAG", SPE paper 154181 presented at the Eighteenth SPE Improved Oil Recovery Symposium held in Tulsa, Oklahoma, USA, 14-18 April, 2012.

Zimmerman, R. W., Chen, G., Hadgu, T., and Bodvarsson, G. S. (1993). A numerical dual-porosity model with semianalytical treatment of fracture/matrix flow. *Water Resour. Res.*, 29, pp 2127-2137.

Appendix A: Peng-Robinson EOS Derivation

$$(P + \delta_{PAtt})(\tilde{v} - b) = RT$$

$$\delta_{PAtt} = \frac{a\alpha}{\tilde{v}^2 + 2b\tilde{v} - b^2}$$

$$P = \frac{RT}{\tilde{v} - b} - \frac{a \propto}{\tilde{v}^2 + 2b\tilde{v} - b^2}$$

$$P = \frac{RT}{\tilde{v} - b} - \frac{a \propto}{\tilde{v}^2 + 2b\tilde{v} - b^2}$$

$$(\tilde{v}^2 + 2b\tilde{v} - b^2)(\tilde{v} - b) = \frac{RT(\tilde{v}^2 + 2b\tilde{v} - b^2)}{P} - \frac{a \propto (\tilde{v} - b)}{P}$$

$$\tilde{v}^3 - \tilde{v}^2 b + 2\tilde{v}^2 b - 2b^2\tilde{v} - b^2\tilde{v} + b^3 = \frac{RT(\tilde{v}^2 + 2b\tilde{v} - b^2)}{P} - \frac{a \propto (\tilde{v} - b)}{P}$$

$$\tilde{v}^3 - \tilde{v}^2 b + 2\tilde{v}^2 b - 2b^2\tilde{v} - b^2\tilde{v} + b^3 = \frac{RT\tilde{v}^2 + 2RTb\tilde{v} - RTb^2}{P} - \frac{(a \propto \tilde{v} - a \propto b)}{P}$$

$$\tilde{v}^3 + \tilde{v}^2 b - \frac{RT\tilde{v}^2}{P} - 3b^2\tilde{v} - \frac{2RTb\tilde{v}}{P} + \frac{a \propto \tilde{v}}{P} + \frac{RTb^2}{P} - \frac{a \propto b}{P} + b^3 = 0$$

$$\tilde{v}^3 + \tilde{v}^2\left(b - \frac{RT}{P}\right) - \tilde{v}\left(3b^2 + \frac{2RTb}{P} - \frac{a \propto}{P}\right) + \frac{RTb^2}{P} - \frac{a \propto b}{P} + b^3 = 0$$

Now, we convert that to cubic EOS in Z

$$\tilde{v} = \frac{RT}{P}Z$$

$$\left(\frac{RT}{P}\right)^3 Z^3 + \left(\frac{RT}{P}\right)^2\left(b - \frac{RT}{P}\right)Z^2 - \frac{RT}{P}Z\left(3b^2 + \frac{2RTb}{P} - \frac{a \propto}{P}\right) + \frac{RTb^2}{P} - \frac{a \propto b}{P} + b^3 = 0$$

$$Z^3 + \left(\frac{Pb}{RT} - 1\right)Z^2 - \left(\frac{P}{RT}\right)^2 Z\left(3b^2 + \frac{2RTb}{P} - \frac{a \propto}{P}\right) + \left(\frac{P}{RT}\right)^3 \frac{RTb^2}{P} - \left(\frac{P}{RT}\right)^3 \frac{a \propto b}{P} + \left(\frac{b^3 P}{RT}\right)^3 = 0$$

$$Z^3 - \left(1 - \frac{Pb}{RT}\right)Z^2 + Z\left(-\frac{3P^2b^2}{R^2T^2} - \frac{2Pb}{RT} + \frac{Pa \propto}{R^2T^2}\right) - \left(\frac{a \propto P^2 b}{R^3T^3} - \frac{P^2b^2}{R^2T^2} - \left(\frac{bP}{RT}\right)^3\right) = 0$$

$$Z^3 - (1 - B)Z^2 + Z(-3B^2 - 2B + A) - (AB - B^2 - B^3) = 0$$

$$A = \frac{a \propto P}{R^2T^2}$$

$$B = \frac{bP}{RT}$$

Apply criticality condition on Z-Cubic Equation

$$(Z - Z_c)^3 = 0$$

$$Z^3 - 3Z^2Z_c + 3ZZ_c^2 - Z_c^3 = 0$$

$$3Z_c = 1 - B \quad \rightarrow \quad B = 1 - 3Z_c \ldots\ldots\ldots.1$$

$$3Z_c^2 = -3B^2 - 2B + A \ldots\ldots\ldots\ldots.2$$

$$3Z_c^2 = (-3(1 - 3Z_c)^2 - 2(1 - 3Z_c) + A)$$

$$3Z_c^2 = (-3(1 - 6Z_c + 9Z_c^2) - 2(1 - 3Z_c) + A)$$

$$3Z_c^2 = (-3 + 18Z_c - 27Z_c^2 - 2 + 6Z_c + A)$$

$$3Z_c^2 = (-5 + 24Z_c - 27Z_c^2 + A)$$

$$30Z_c^2 + 5 - 24Z_c = A$$

$$Z_c^3 = (AB - B^2 - B^3) \ldots\ldots\ldots\ldots.3$$

$$Z_c^3 = \left((30Z_c^2 + 5 - 24Z_c)(1 - 3Z_c) - (1 - 3Z_c)^2 - (1 - 3Z_c)^3\right)$$

$$Z_c^3 = \left((30Z_c^2 + 5 - 24Z_c)(1 - 3Z_c) - 1 + 6Z_c - 9Z_c^2 - (1 - 3Z_c)^3\right)$$

$$Z_c^3 = 30Z_c^2 + 5 - 24Z_c - 90Z_c^3 - 15Z_c + 72Z_c^2 - 1 + 6Z_c - 9Z_c^2 - 1 + 9Z_c - 27Z_c^2 + 27Z_c^3$$

$$-64Z_c^3 + 66Z_c^2 - 24Z_c + 3 = 0$$

$$Z_c = 0.307401$$

Now substitute back for the value of Z_c to find B and A

$$B = 1 - 3Z_c = 1 - 3 * 0.307401 = 0.077797$$

$$A = 30Z_c^2 + 5 - 24Z_c = 30(0.307401)^2 + 5 - 24 * 0.307401 = 0.457237$$

$$A = \frac{a \propto P}{R^2T^2}, B = \frac{bP}{RT}$$

Appendix B: VLE Flash

$$K_i = \frac{y_i}{x_i}$$

$$g(f_{ng}) = \sum_{i=1}^{Nc} \frac{c_i(K_i - 1)}{1 + f_{ng}(K_i - 1)} = 0$$

$$f_{ng}^{new} = f_{ng}^{old} - \frac{g(f_{ng}^{old})}{g'(f_{ng}^{old})}$$

$$\left| f_{ng}^{new} - f_{ng}^{old} \right| < \varepsilon$$

$$0 < f_{ng} < 1$$

$$\frac{1}{(1 - K_i max)} < f_{ng} < \frac{1}{(1 - K_i min)}$$

$$f_{nl} = 1 - f_{ng}$$

$$Liquid\ \% = 100 * f_{nl}$$

$$Gas\ \% = 100 * f_{ng}$$

$$x_i = \frac{c_i}{1 + f_{ng}(K_i - 1)}$$

$$y_i = K_i x_i = \frac{K_i c_i}{1 + f_{ng}(K_i - 1)}$$

The module starts by loading the initial reservoir temperature and pressure. Next, the model would try to find the gas molar fraction. At the start, an initial value of 0.999 is assigned to the gas molar fraction and Wilsons' correlation is used to find a value for the equilibrium ratio (Ki). Then, substituting in the Rachford and Rice equation, a new value of gas molar fraction is acquired. The initial guess and the new value from the equation are then compared. If they are within the given tolerance, then the model converges and the gas molar fraction is found. If not, then the new gas molar fraction from the Rachford and Rice equation is then used while the

program loops and start with that value as its new starting point. This procedure repeats until the desired value is found (within the specified criteria).

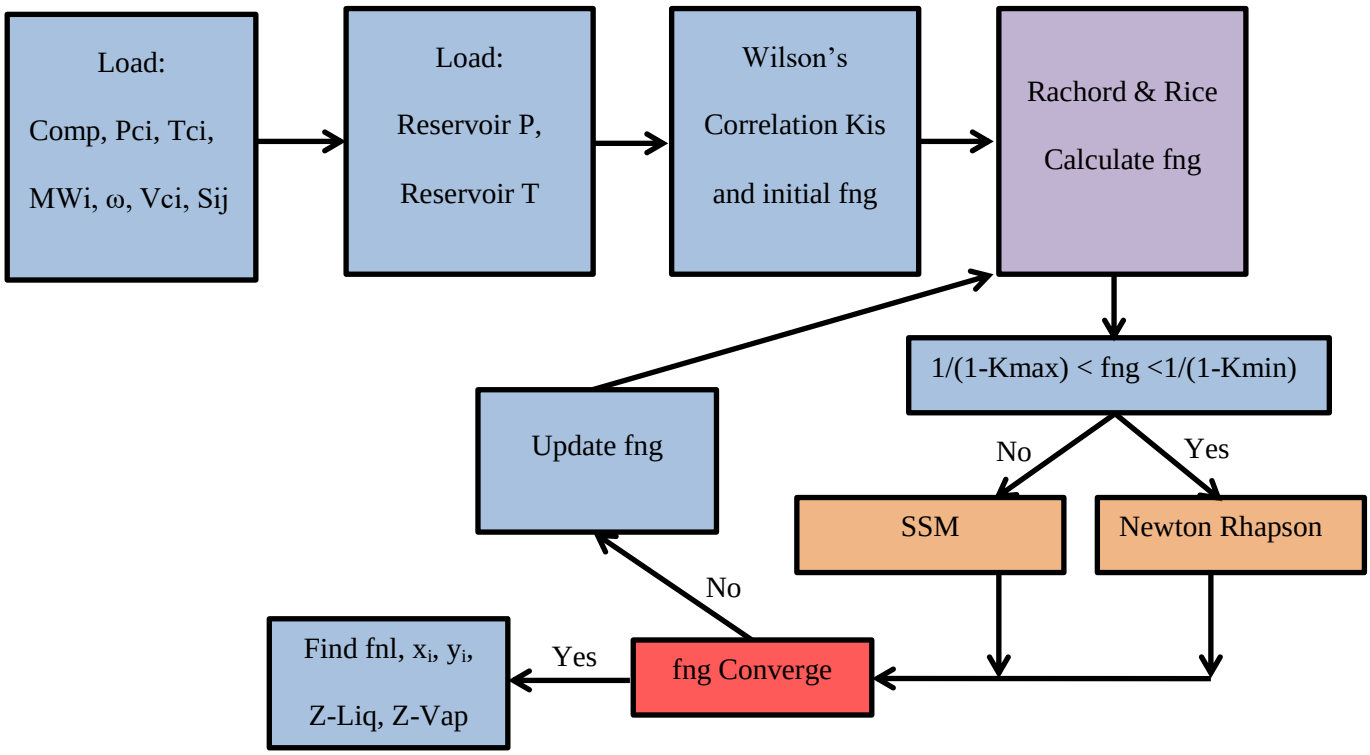

Appendix C: Fugacity Module

$$f_h = f_{gi}$$

$$f_h = Fugacity\ of\ the\ i-th\ component\ in\ the\ liquid\ Phase$$

$$f_{gi} = Fugacity\ of\ the\ i-th\ component\ in\ the\ vapor\ Phase$$

$$\phi_{gi} = \frac{f_{gi}}{y_i P}$$

$$\phi_{gi} = \frac{f_{gi}}{y_i P}$$

$$ln\phi_i = -\ln(Z-B) + \frac{A}{(m_1-m_2)B}\left(\frac{2\sum_{j=1}^{nc} A_{ij}c_j}{A} - \frac{B_i}{B}\right) ln\left[\frac{Z+m_2B}{Z+m_1B}\right] + \frac{B_i}{B}(Z-1)$$

$$A = \sum_i^{nc}\sum_j^{nc} c_i c_j\, A_{ij}$$

$$A_{ij} = \left(1-\delta_{ij}\right)\left(A_i A_j\right)^{0.5}$$

$$A_i = \Omega_{ai}^o\left[1+m_i\left(1-T_{ri}^{0.5}\right)\right]^2 \frac{P_{ri}}{T_{ri}^2}$$

$$B = \sum_{i=1}^{nc} c_i B_i$$

$$B_i = \Omega_{bi}^o \frac{P_{ri}}{T_{ri}}$$

$$\Omega_{ai}^o = 0.457235529$$

$$\Omega_{bi}^o = 0.077796074$$

Appendix D: Phase Stability Module

Vapor-Like Second Phase

$$Y_i = z_i K_i$$

$$K_i = \frac{1}{P_{ri}} EXP\left[3.37(1+\omega_i)\left(1-\frac{1}{T_{ri}}\right)\right]$$

$$S_V = \sum_i^n Y_i$$

$$y_i = \frac{Y_i}{S_V}$$

$$R_i = \frac{f_{zi}}{f_{yi}} \frac{1}{S_V}$$

$$K_i^{(n+1)} = K_i^n R_i$$

Convergence Check:

$$\sum_i^n (R_i - 1)^2 < 1 * 10^{-4}$$

Trivial Solution Check:

$$\sum_i^n (lnK_i)^2 < 1 * 10^{-4}$$

Liquid-Like Second Phase

$$Y_i = z_i / K_i$$

$$S_L = \sum_i^n Y_i$$

$$x_i = \frac{Y_i}{S_L}$$

$$R_i = \frac{f_{xi}}{f_{zi}} S_L$$

Appendix E: Forward ANN Design #2 Blind Testing Cases

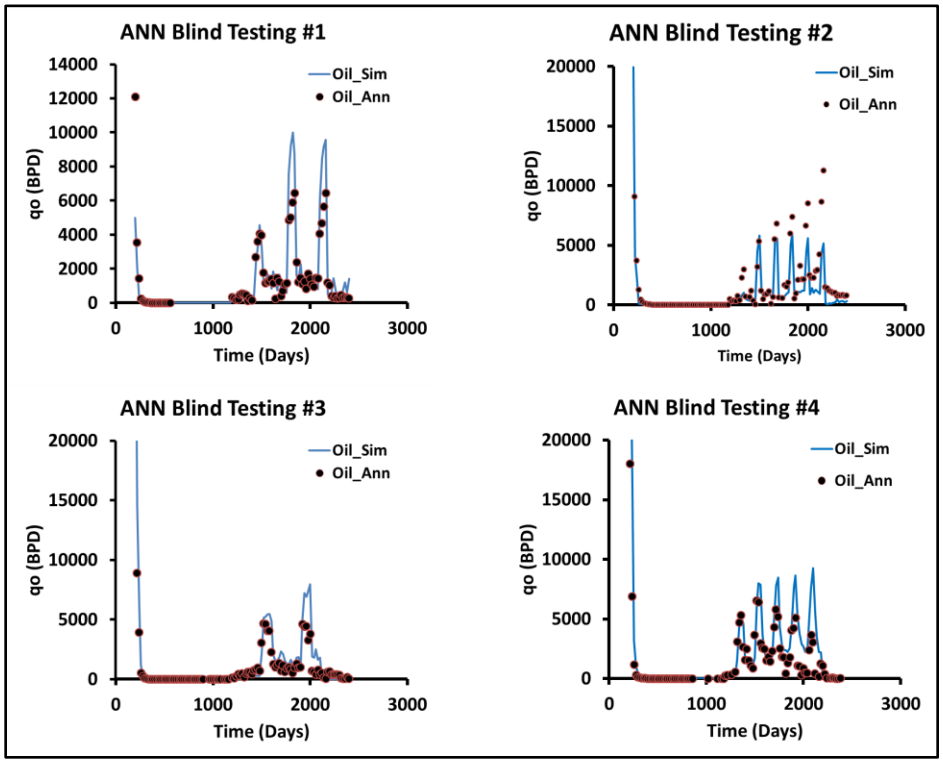

Figure AE- 1: Forward ANN#2 Blind Testing Cases 1, 2, 3, 4

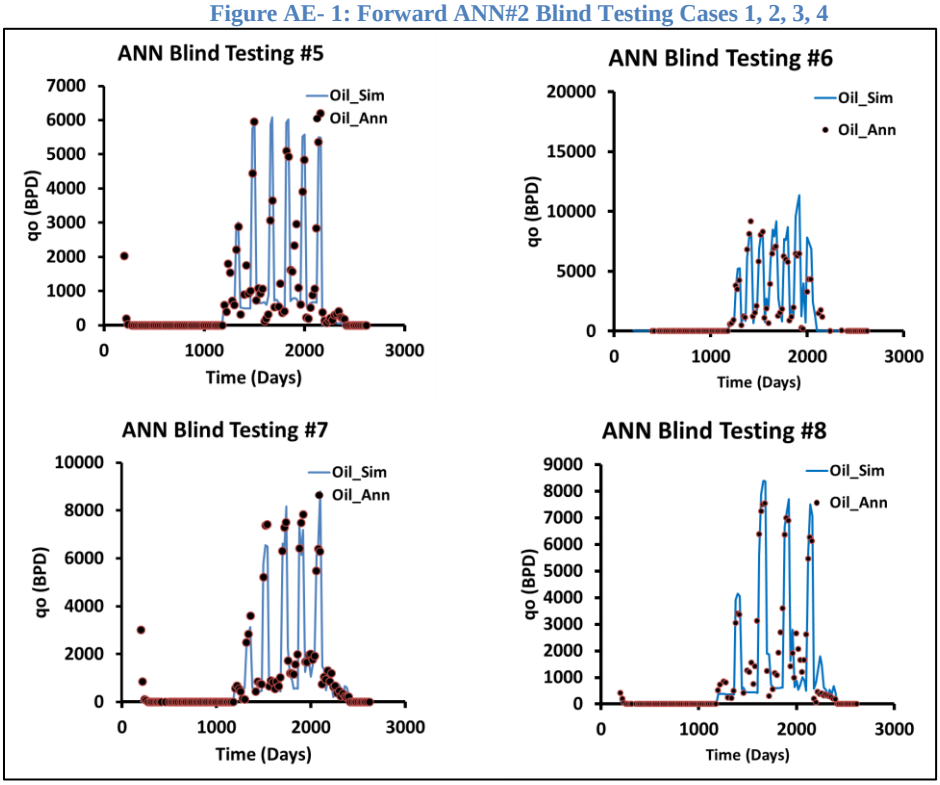

Figure AE- 2: Forward ANN#2 Blind Testing Cases 5, 6, 7, 8

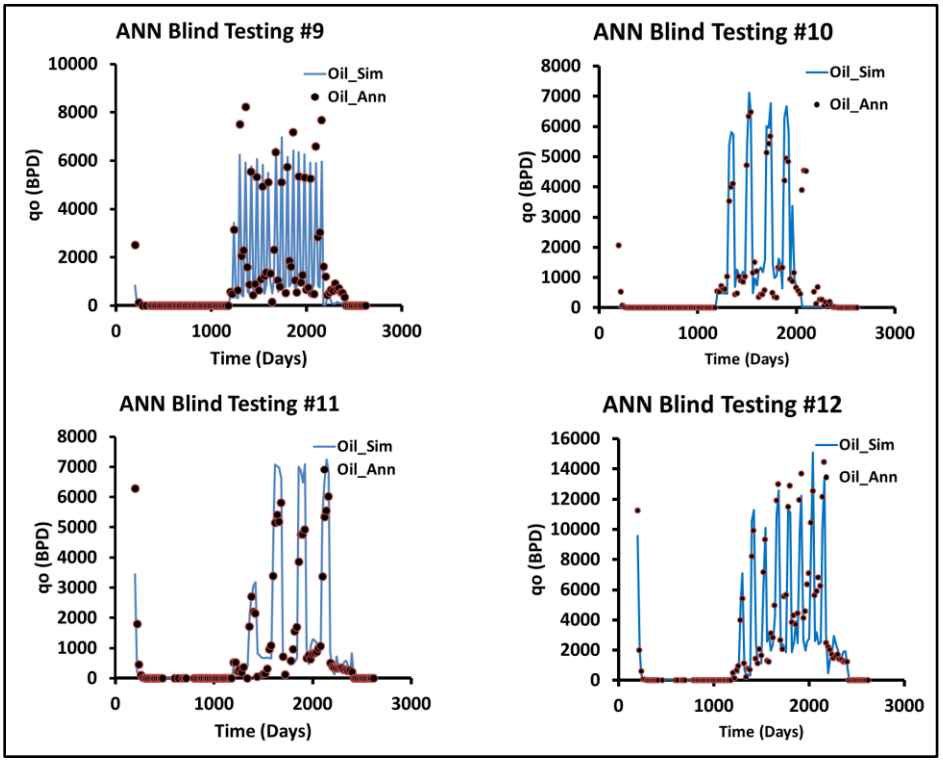

Figure AE- 3: Forward ANN#2 Blind Testing Cases 13, 14, 15, 16

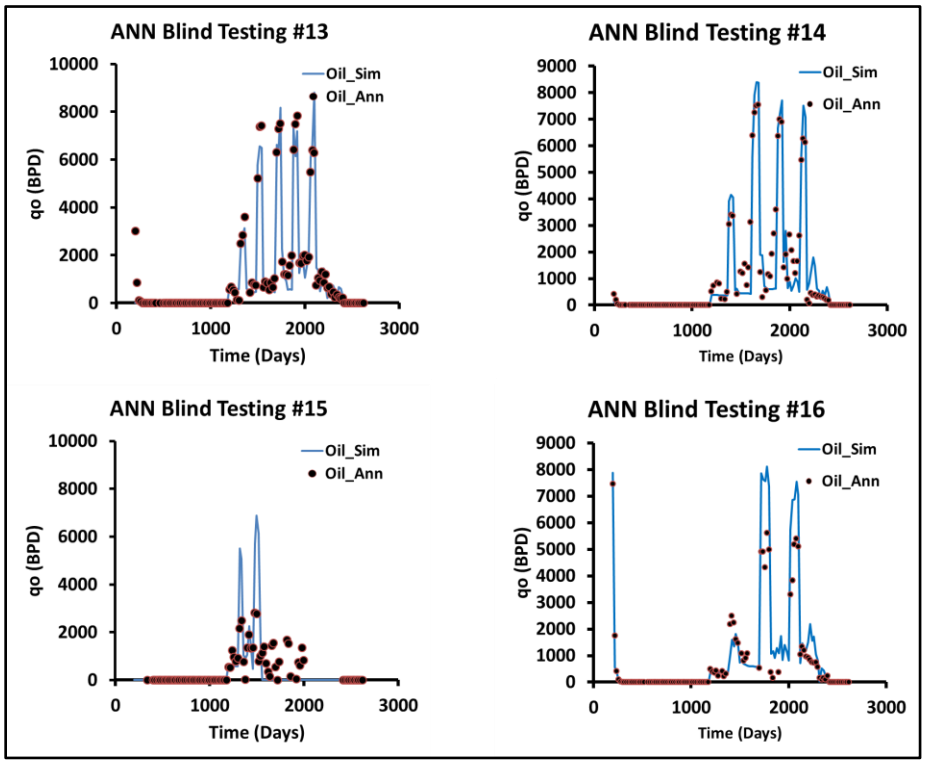

Figure AE- 4: Forward ANN#2 Blind Testing Cases 13, 14, 15, 16

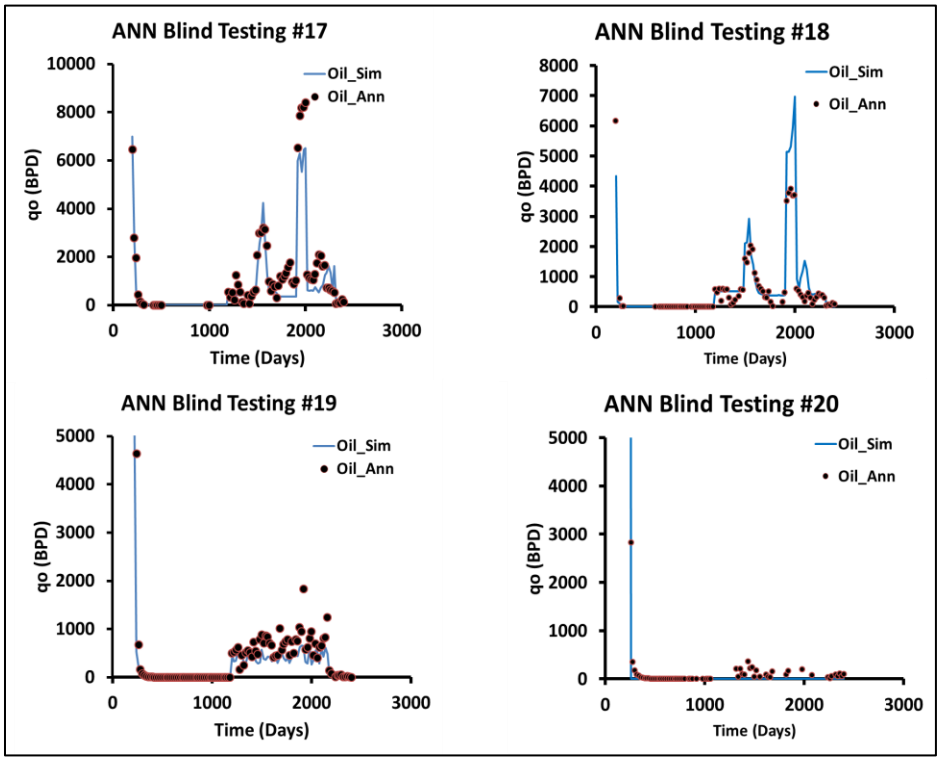

Figure AE- 5: Forward ANN#2 Blind Testing Cases 17, 18, 19, 20

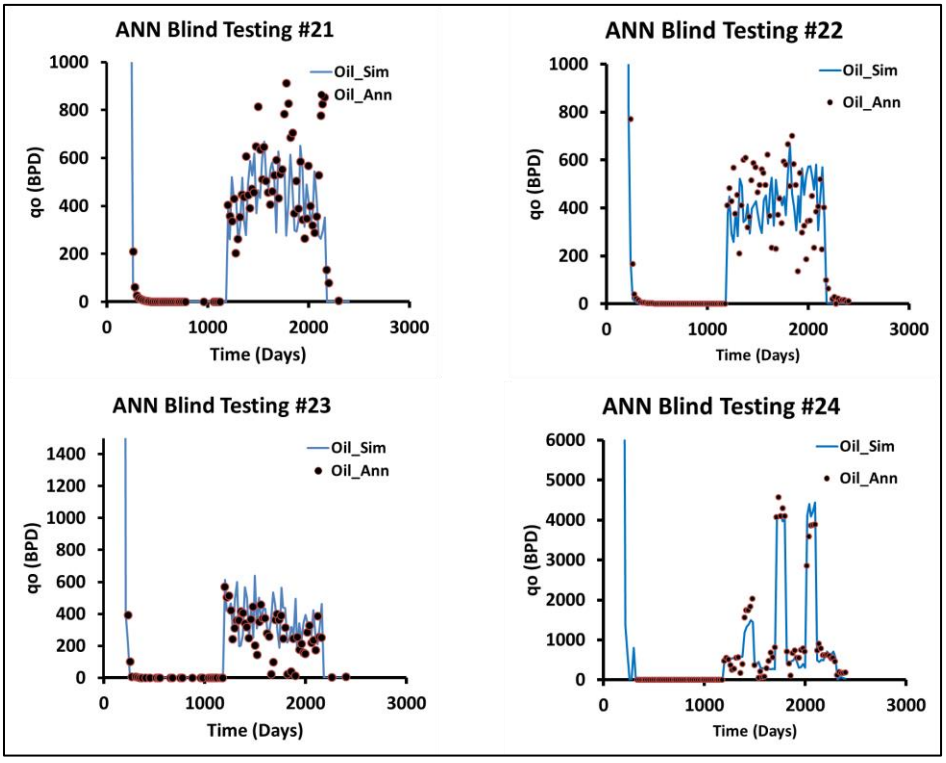

Figure AE- 6: Forward ANN#2 Blind Testing Cases 21, 22, 23, 24

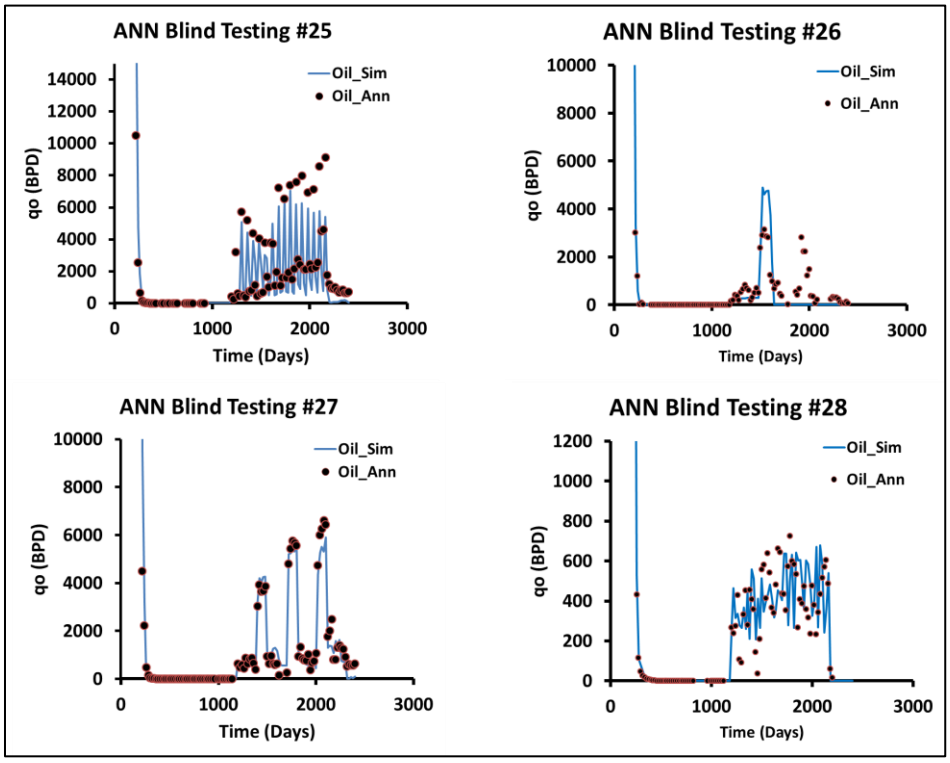

Figure AE- 7: Forward ANN#2 Blind Testing Cases 25, 26, 27, 28

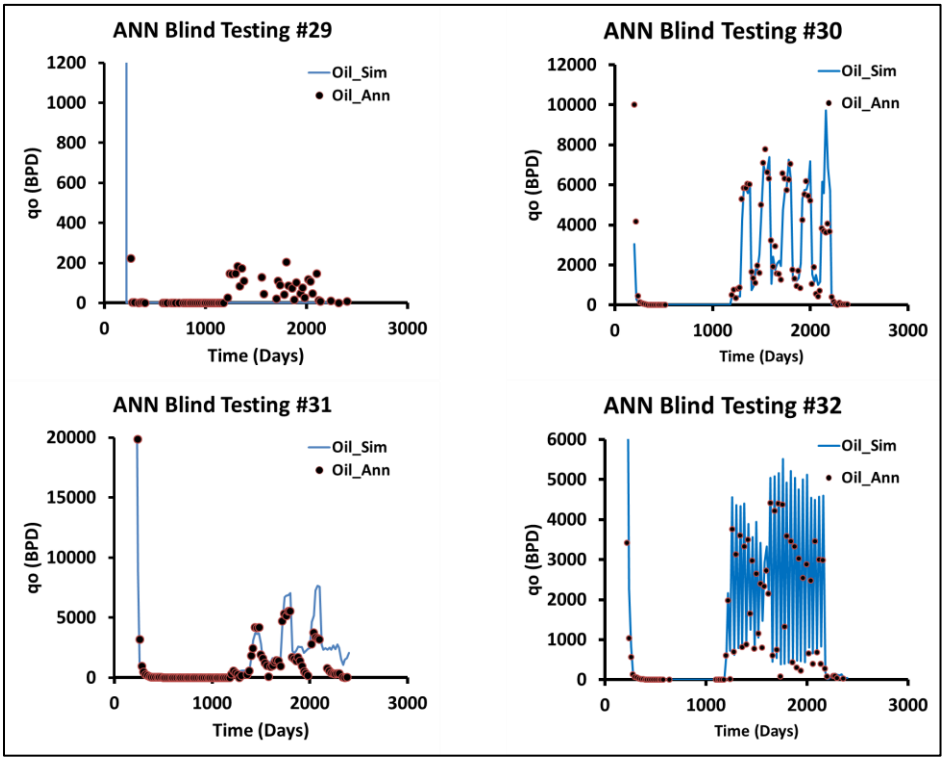

Figure AE- 8: Forward ANN#2 Blind Testing Cases 29, 30, 31, 32

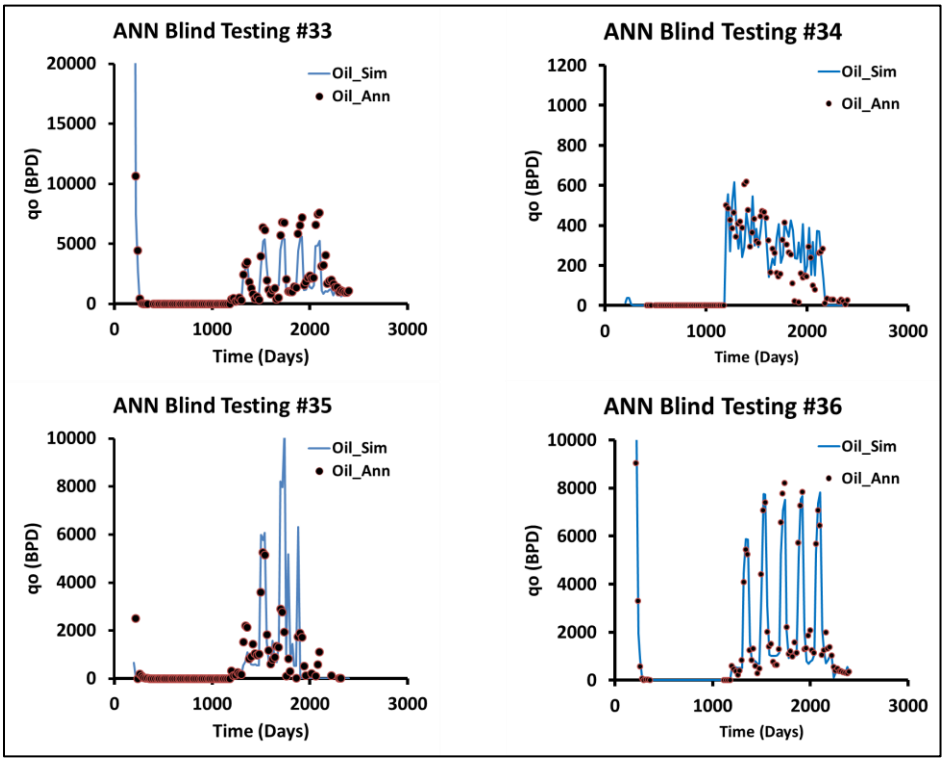

Figure AE- 9: Forward ANN#2 Blind Testing Cases 33, 34, 35, 36

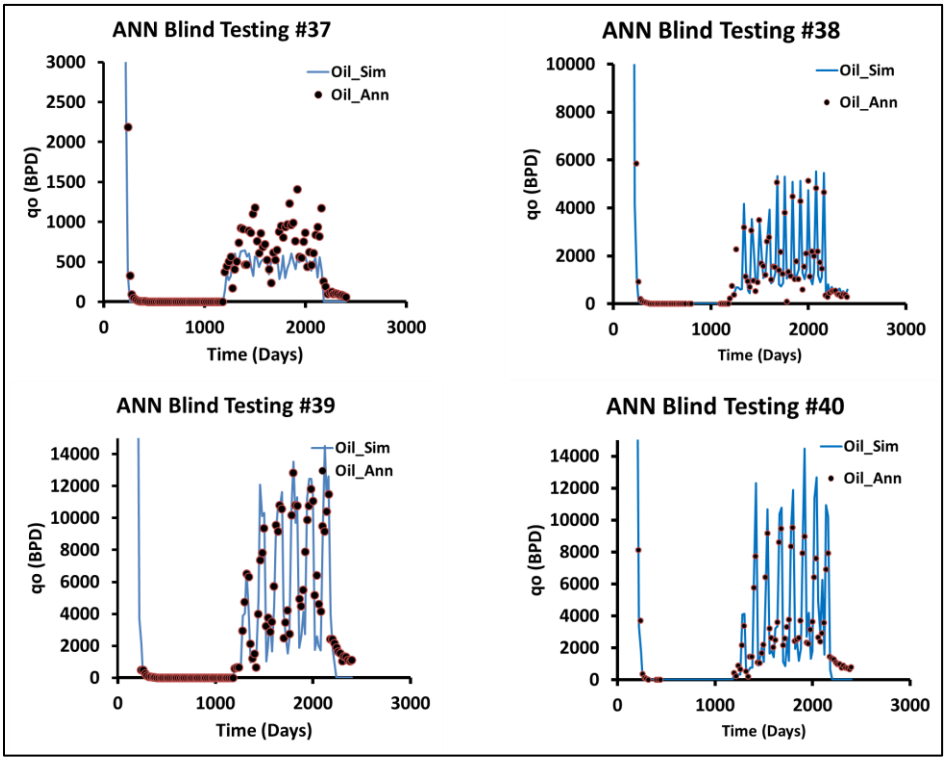

Figure AE- 10: Forward ANN#2 Blind Testing Cases 37, 38, 39, 40

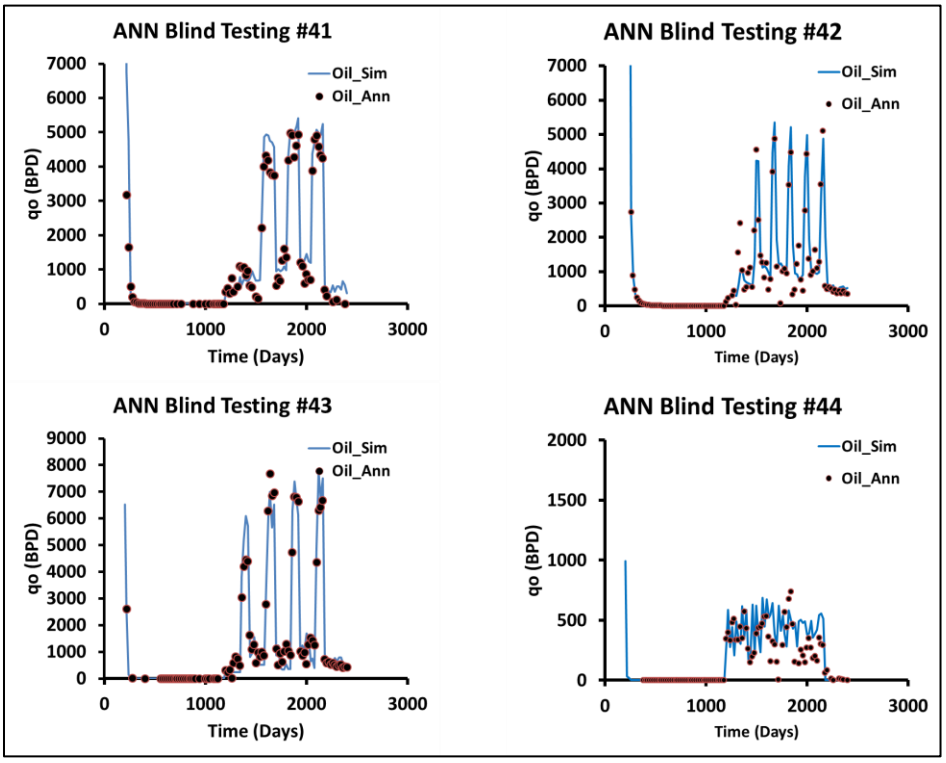

Figure AE- 11: Forward ANN#2 Blind Testing Cases 41, 42, 43, 44

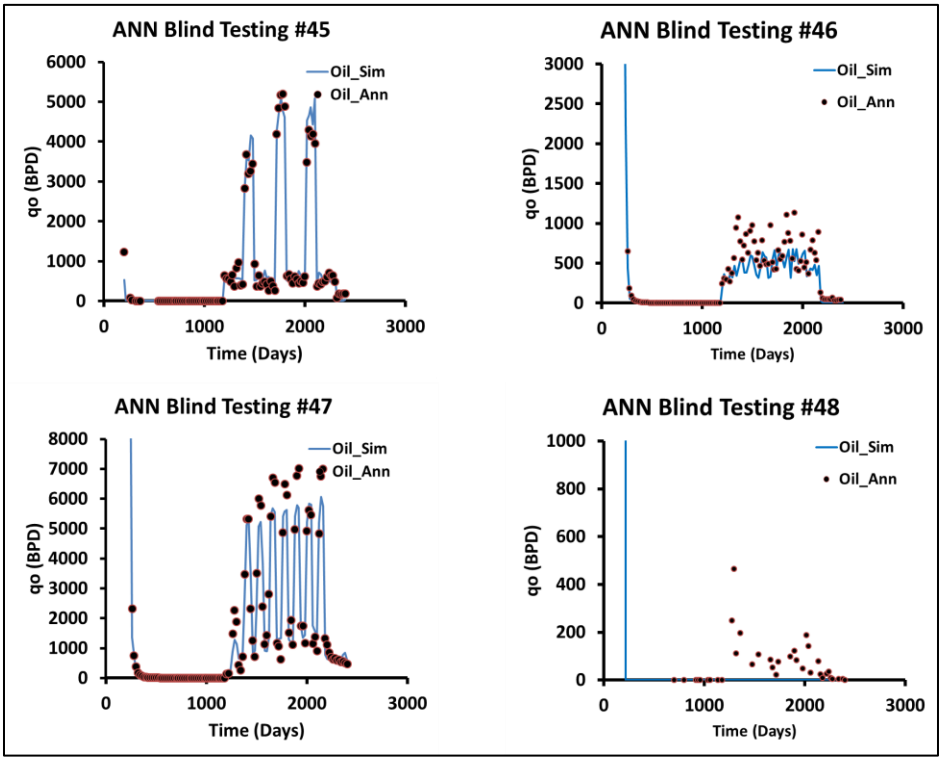

Figure AE- 12: Forward ANN#2 Blind Testing Cases 45, 46, 47, 48

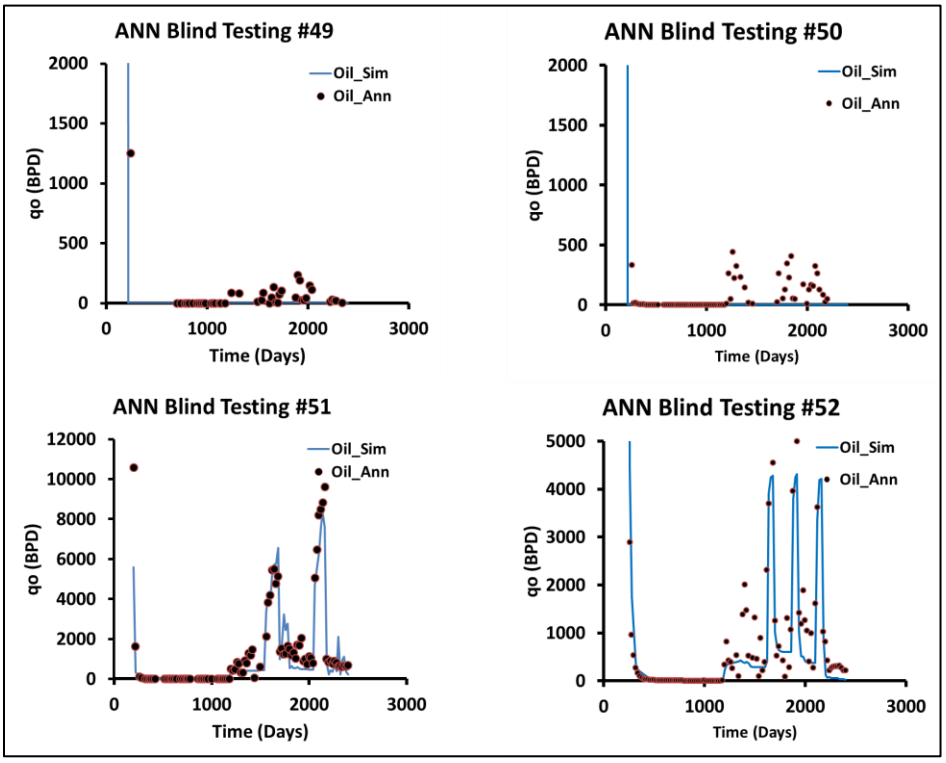

Figure AE- 13: Forward ANN#2 Blind Testing Cases 49, 50, 51, 52

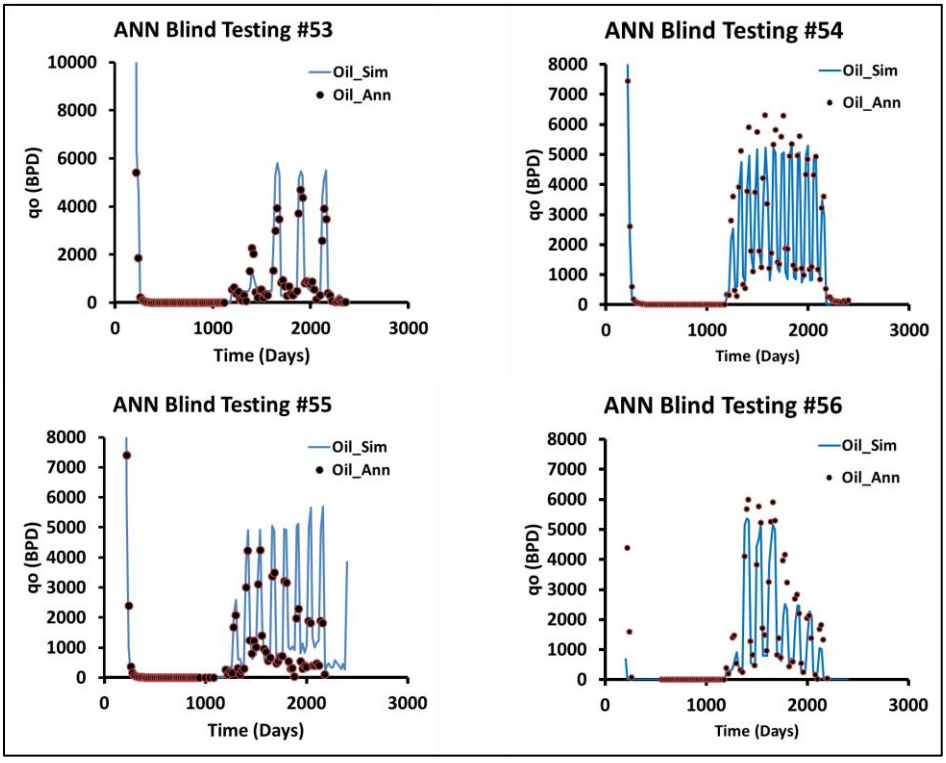

Figure AE- 14: Forward ANN#2 Blind Testing Cases 53, 54, 55, 56

Appendix F: Forward ANN Design #3 Blind Testing Cases

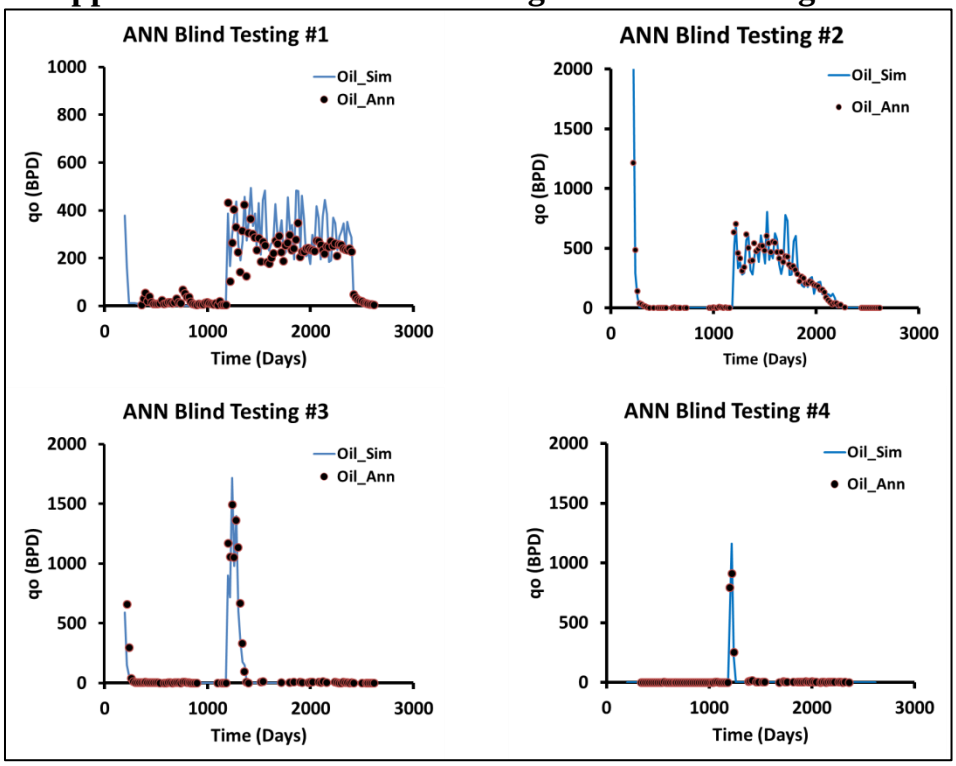

Figure AF- 1: Oil Production for Blind Test Cases 1, 2, 3, and 4

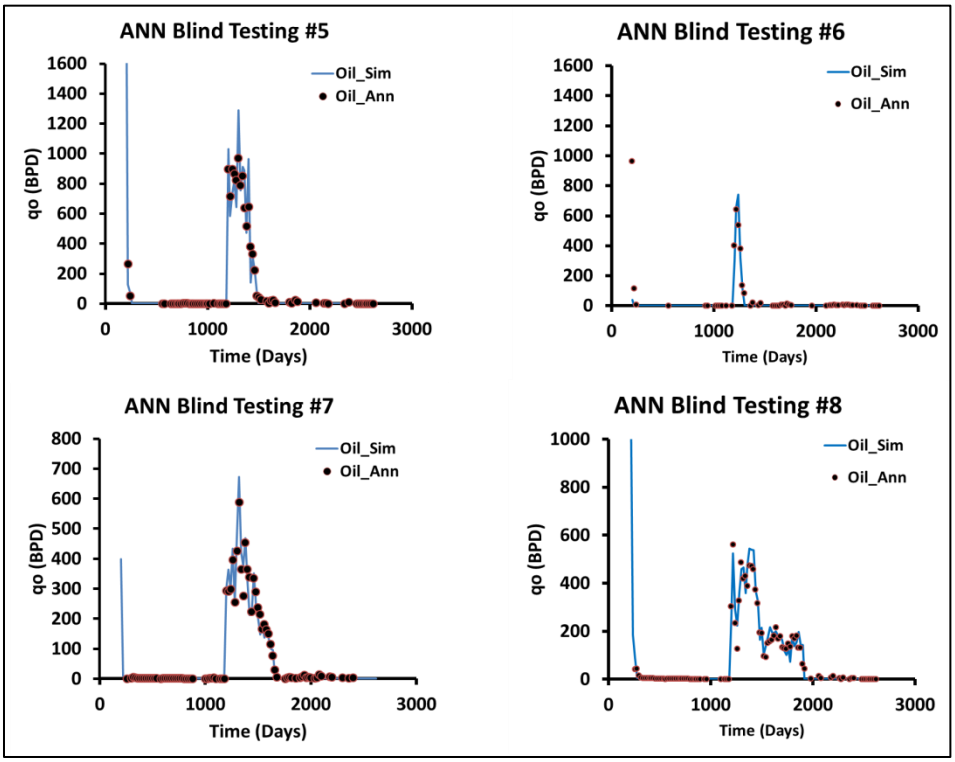

Figure AF- 2: Oil Production for Blind Test Cases 5, 6, 7, and 8

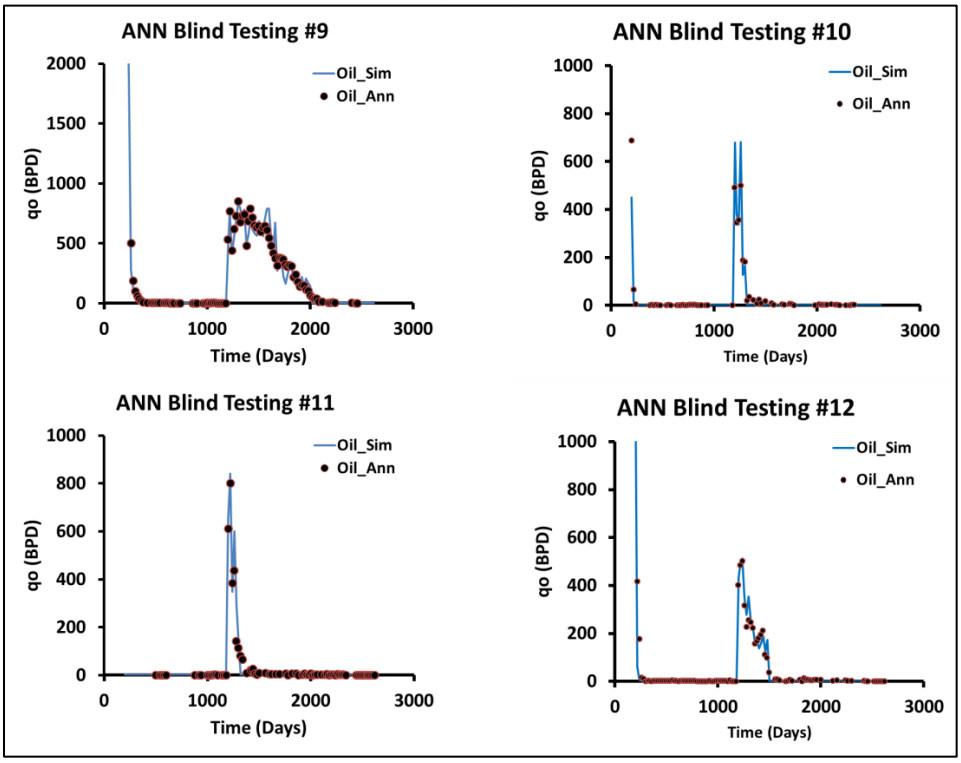

Figure AF- 3: Oil Production for Blind Test Cases 9, 10, 11, and 12

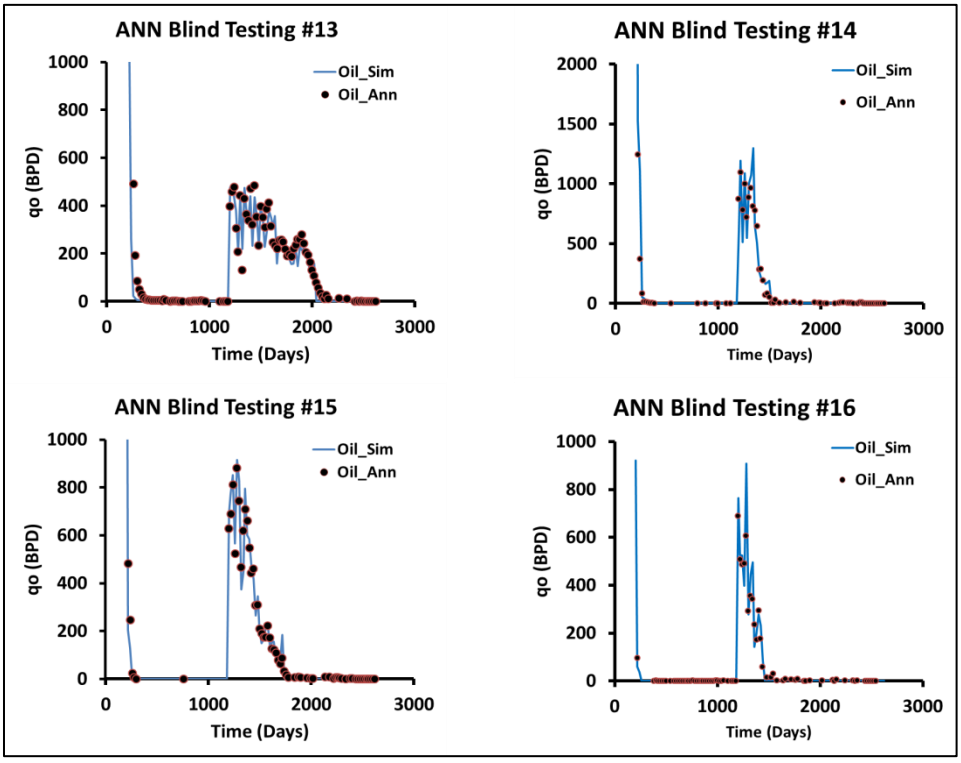

Figure AF- 4: Oil Production for Blind Test Cases 13, 14, 15, and 16

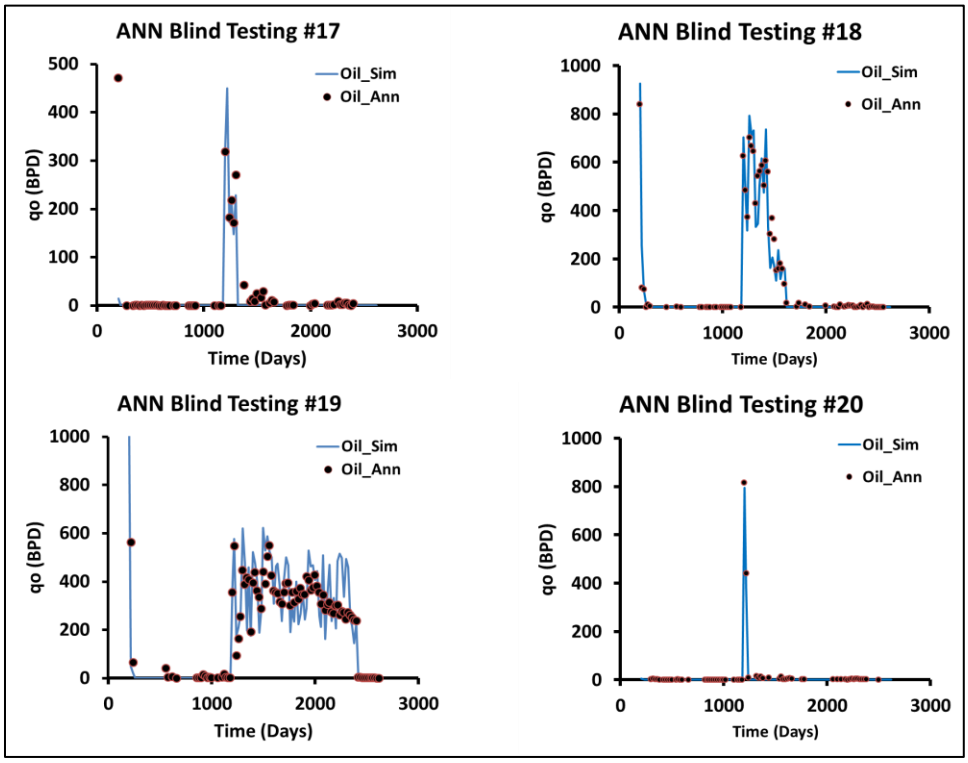

Figure AF- 5: Oil Production for Blind Test Cases 17, 18, 19, and 20

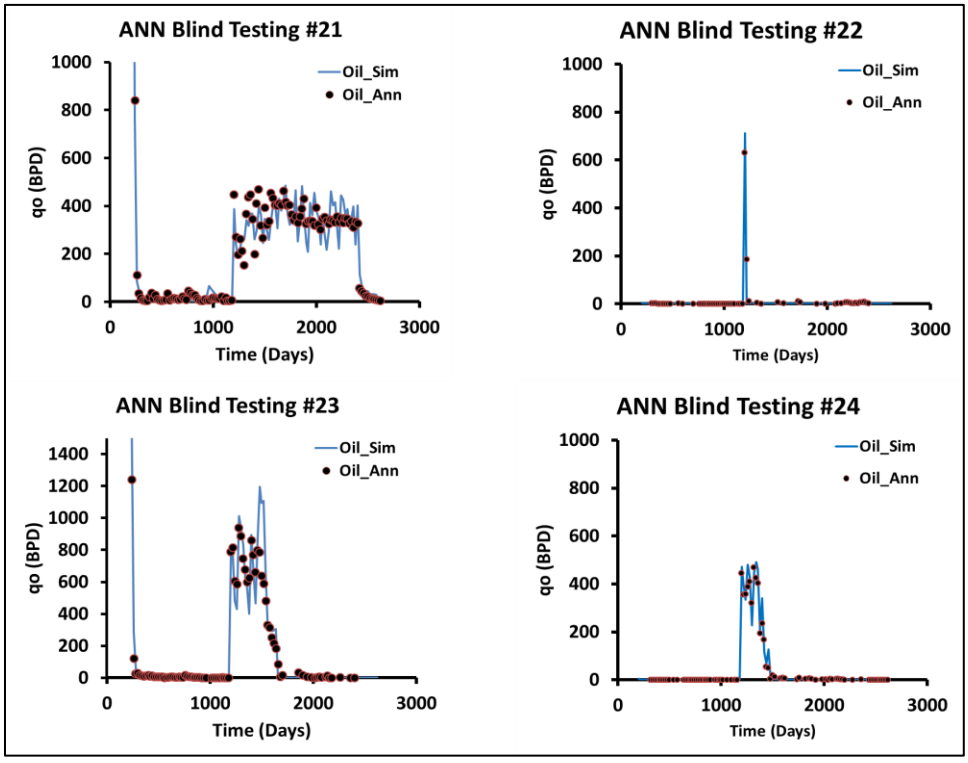

Figure AF- 6: Oil Production for Blind Test Cases 21, 22, 23, and 24

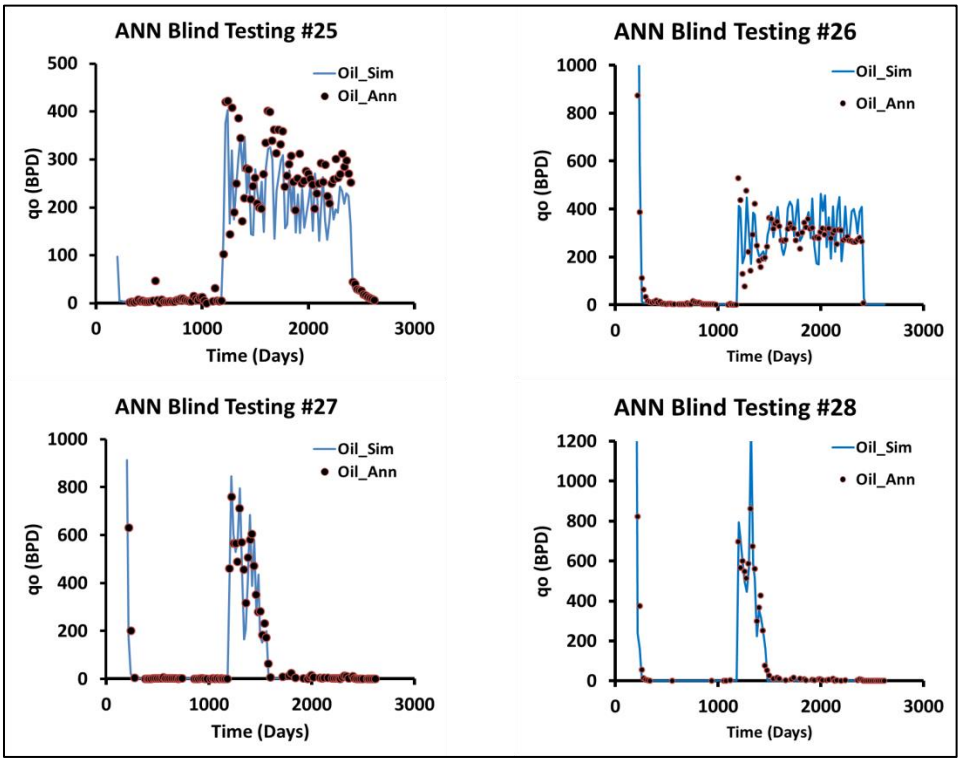

Figure AF- 7: Oil Production for Blind Test Cases 25, 26, 27, and 28

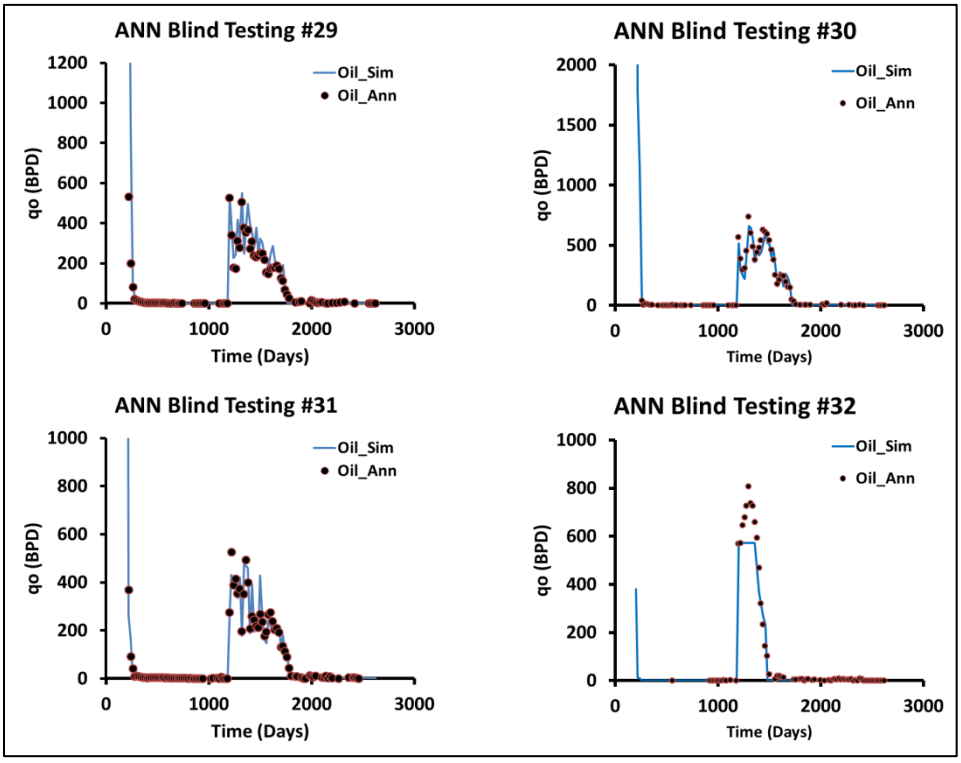

Figure AF- 8: Oil Production for Blind Test Cases 29, 30, 31, and 32

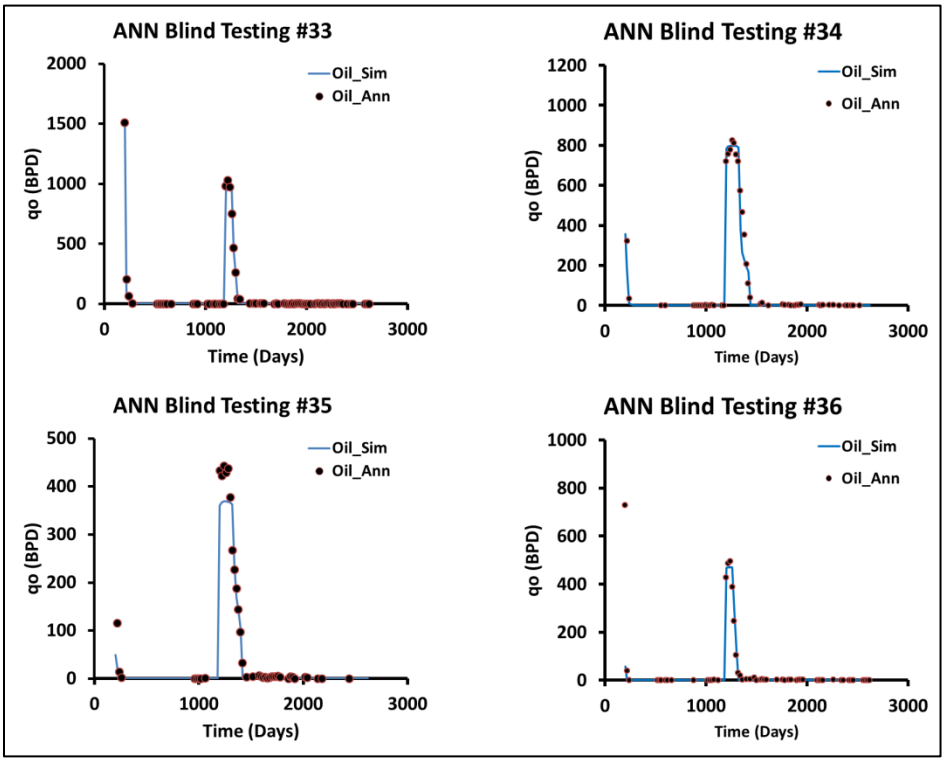

Figure AF- 9: Oil Production for Blind Test Cases 33, 34, 35, and 36

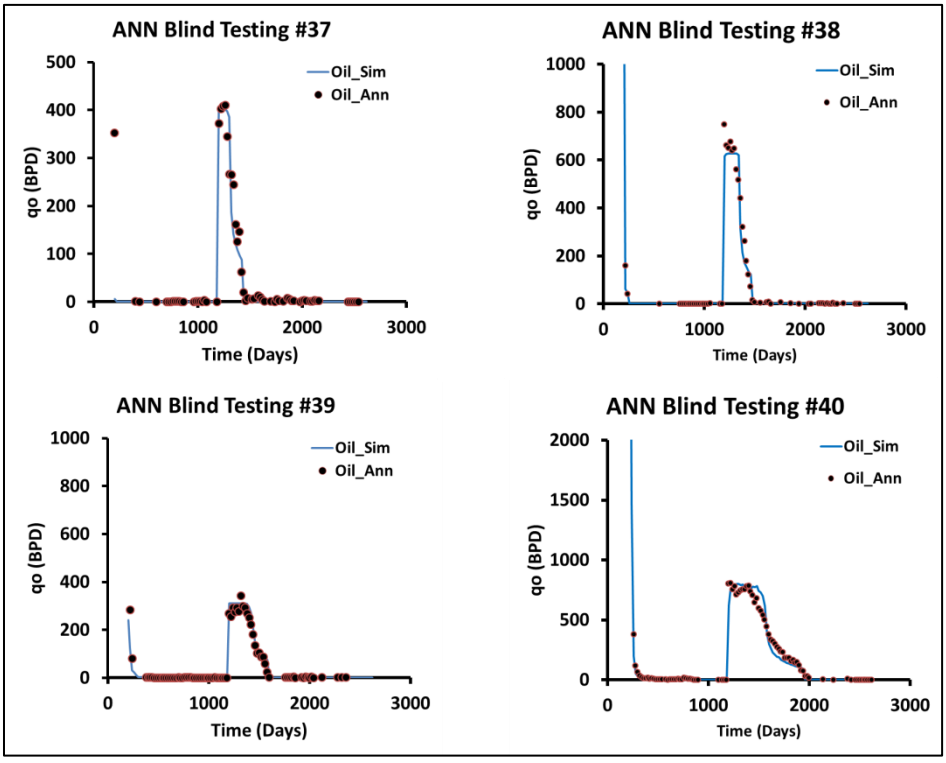

Figure AF- 10: Oil Production for Blind Test Cases 37, 38, 39, and 40

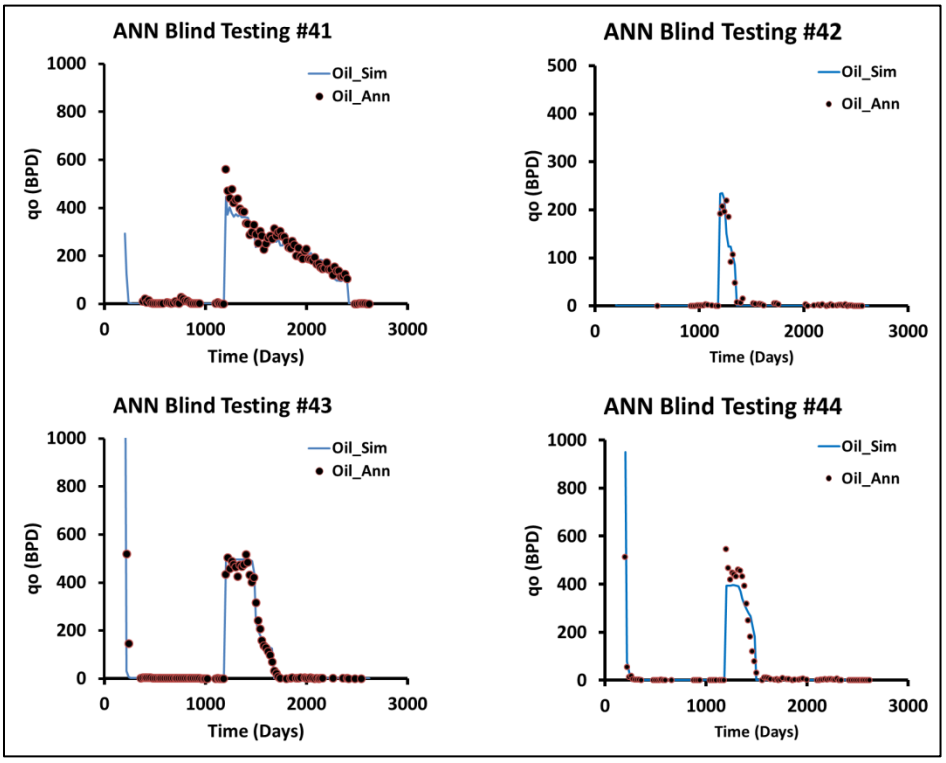

Figure AF- 11: Oil Production for Blind Test Cases 41, 42, 43, and 44

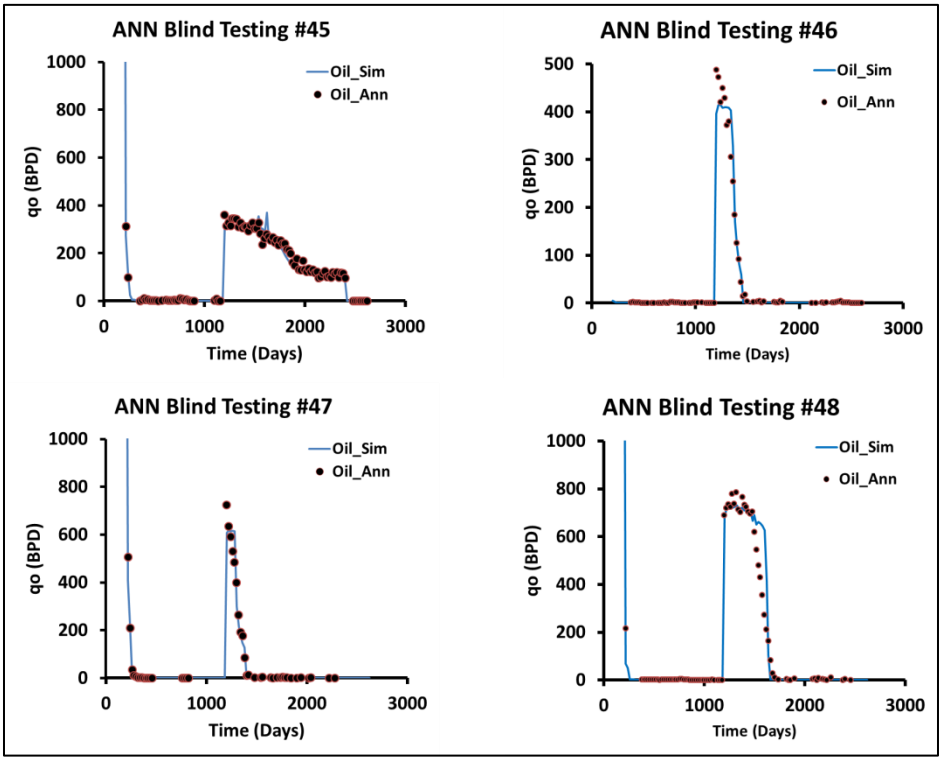

Figure AF- 12: Oil Production for Blind Test Cases 45, 46, 47, and 48

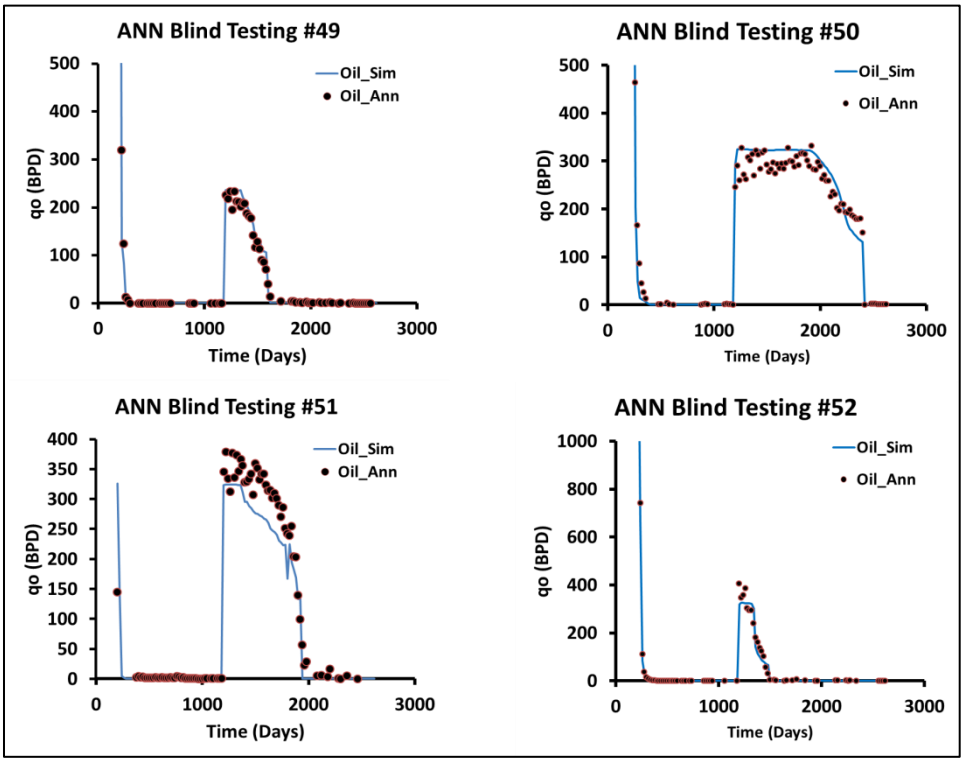

Figure AF- 13: Oil Production for Blind Test Cases 49, 50, 51, and 52

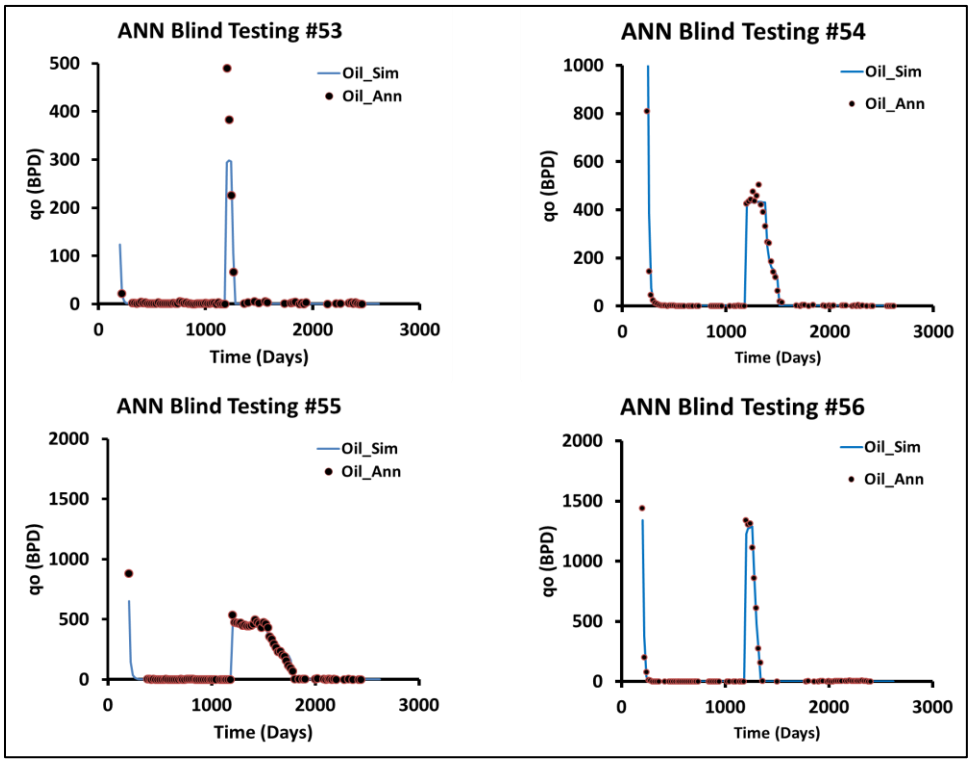

Figure AF- 14: Oil Production for Blind Test Cases 43, 54, 55, and 56

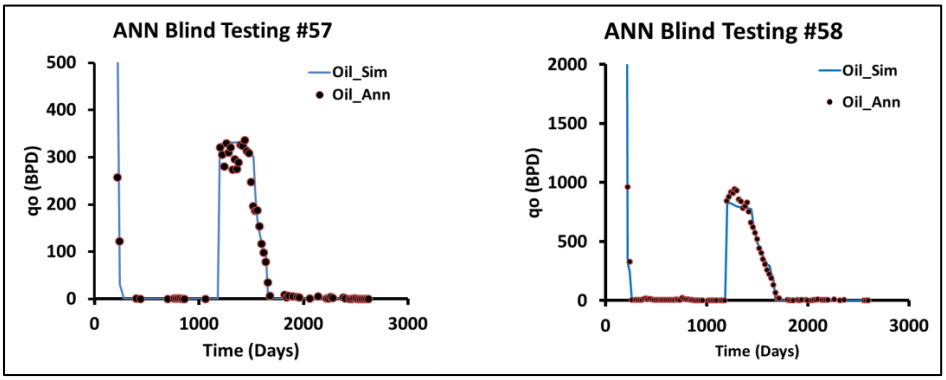

Figure AF- 15: Oil Production for Blind Test Cases 57, and 58

Appendix G: Forward ANN Design #3B Blind Testing Cases

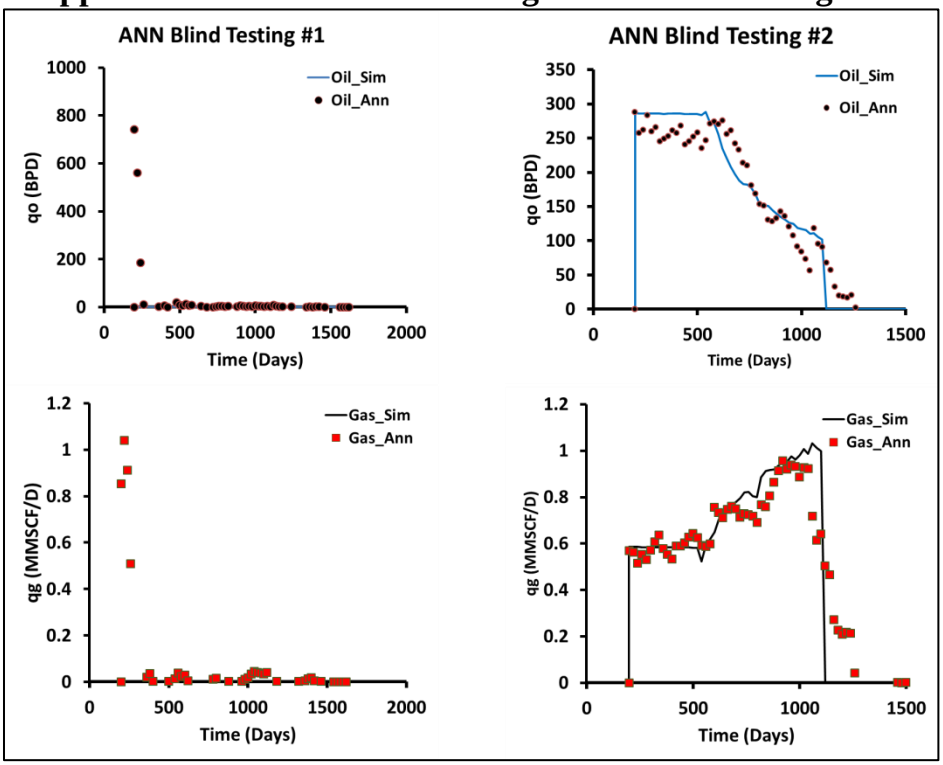

Figure AG- 1: Oil and Gas Production for Blind Test Cases 1 & 2

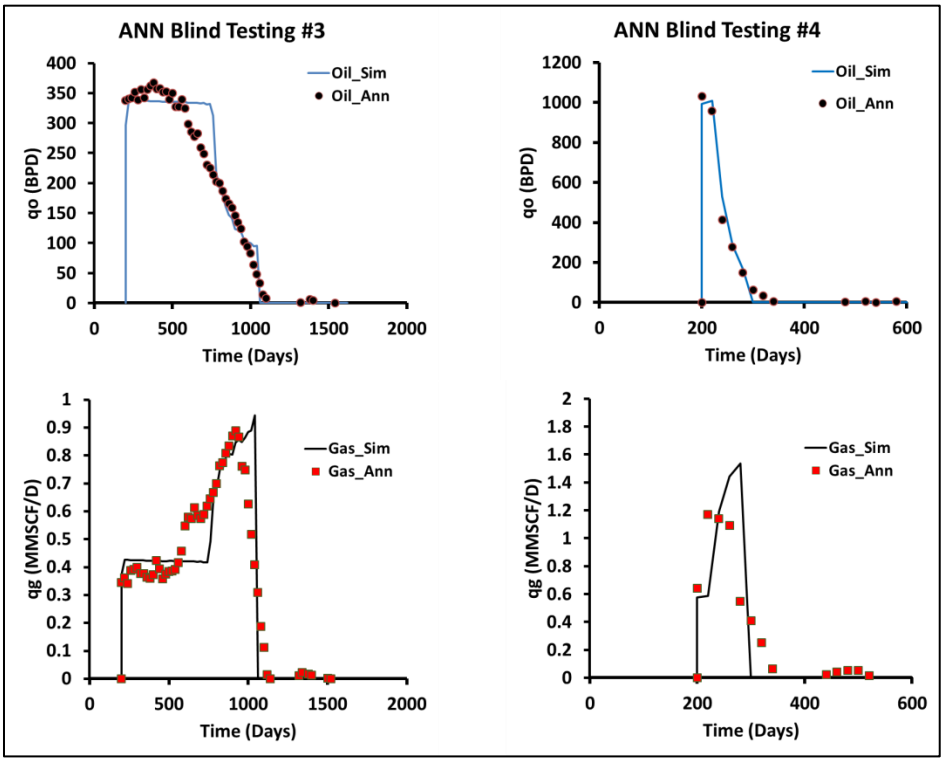

Figure AG- 2: Oil and Gas Production for Blind Test Cases 3 & 4

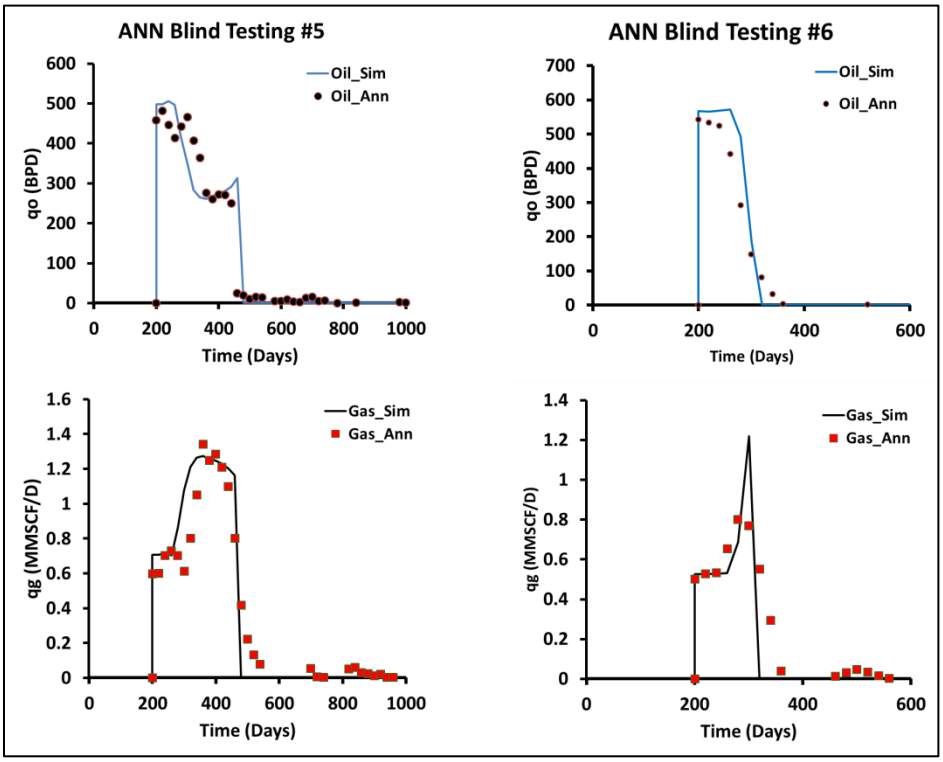

Figure AG- 3: Oil and Gas Production for Blind Test Cases 5 & 6

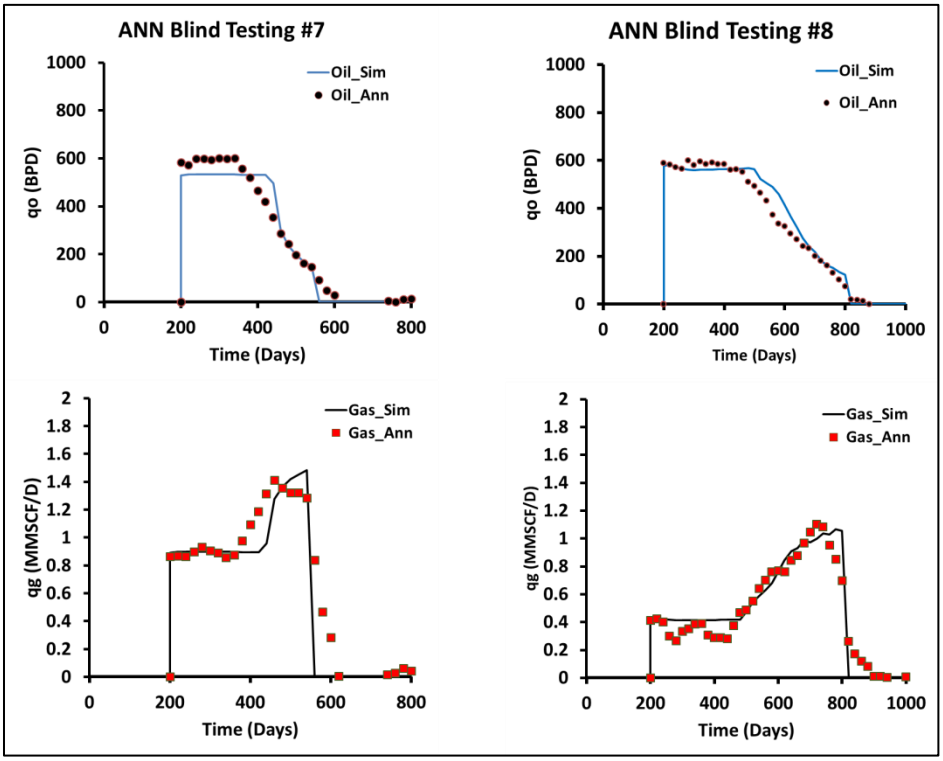

Figure AG- 4: Oil and Gas Production for Blind Test Cases 7 & 8

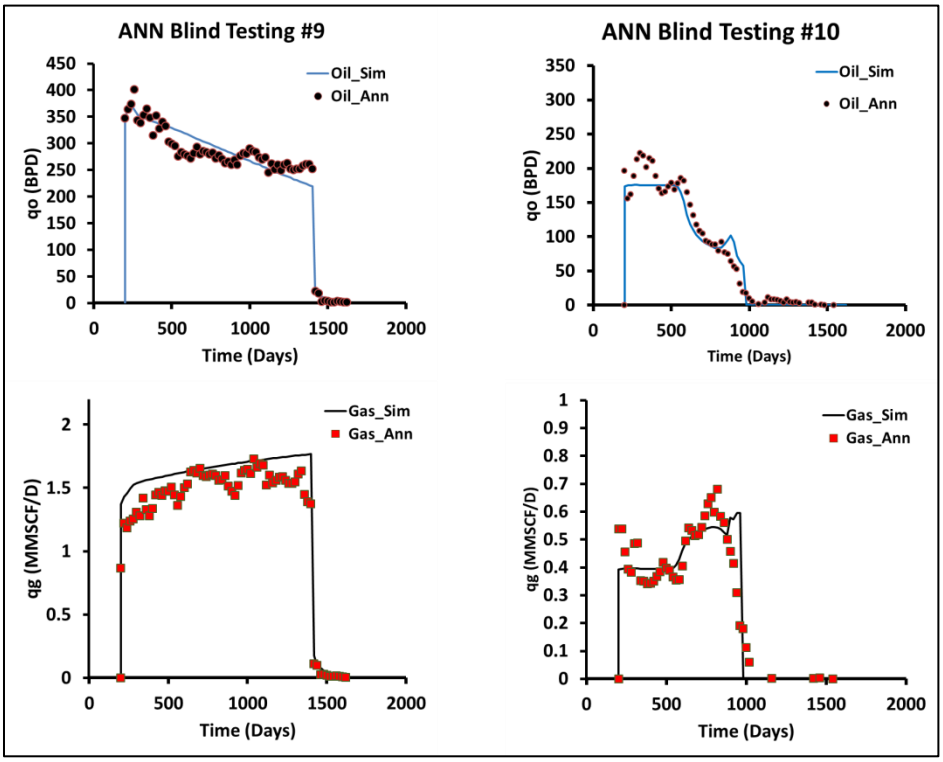

Figure AG- 5: Oil and Gas Production for Blind Test Cases 9 & 10

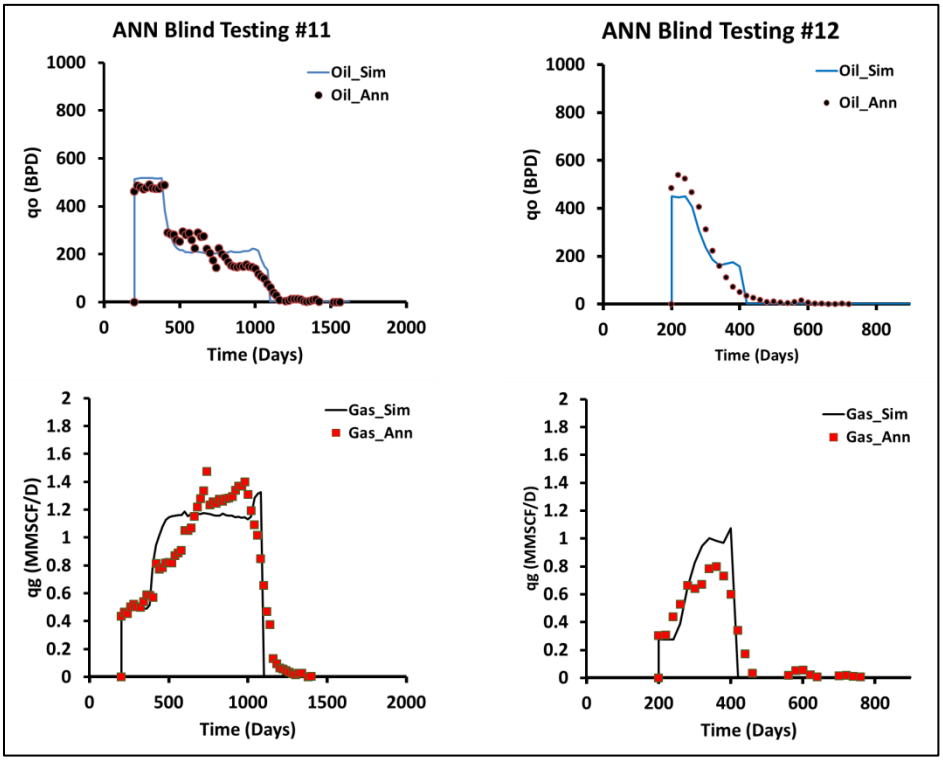

Figure AG- 6: Oil and Gas Production for Blind Test Cases 11 & 12

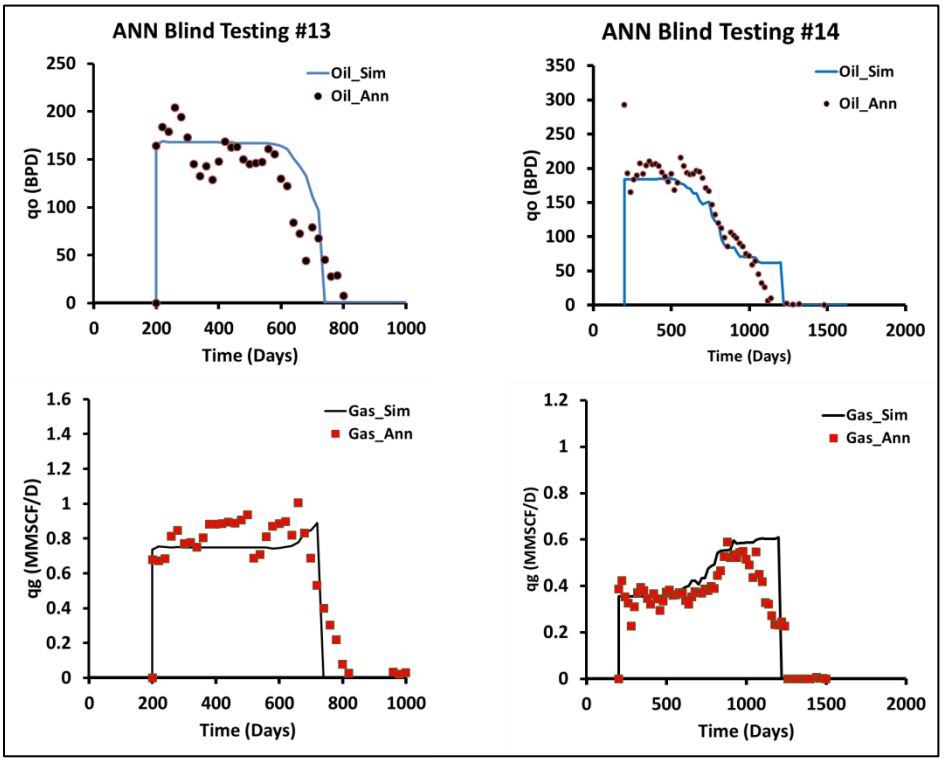

Figure AG- 7: Oil and Gas Production for Blind Test Cases 13 & 14

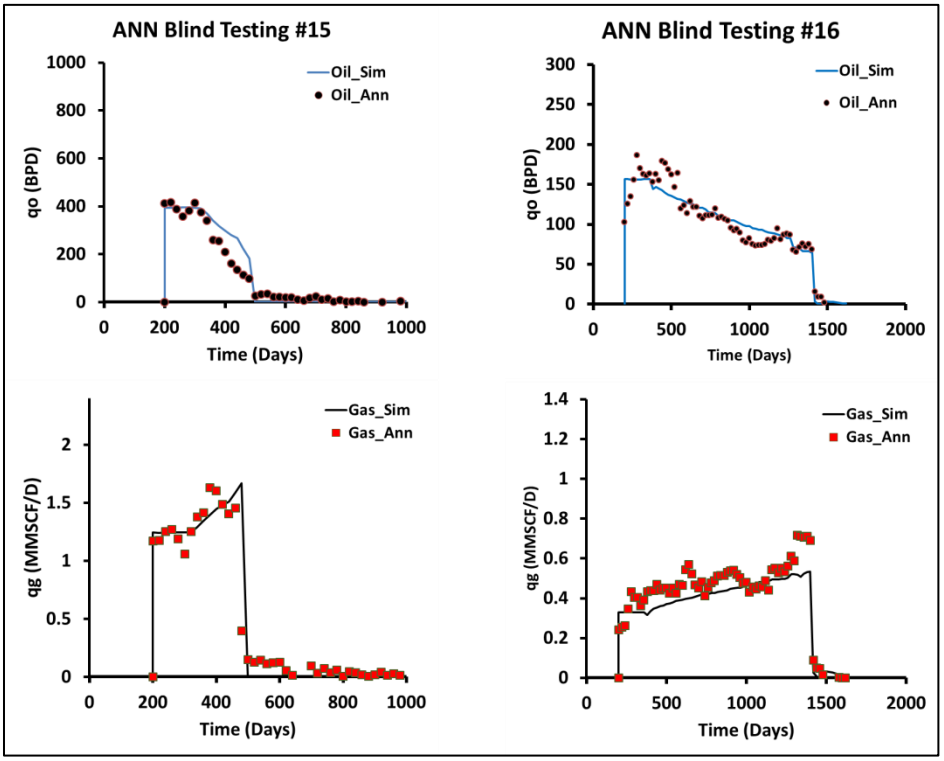

Figure AG- 8: Oil and Gas Production for Blind Test Cases 15 & 16

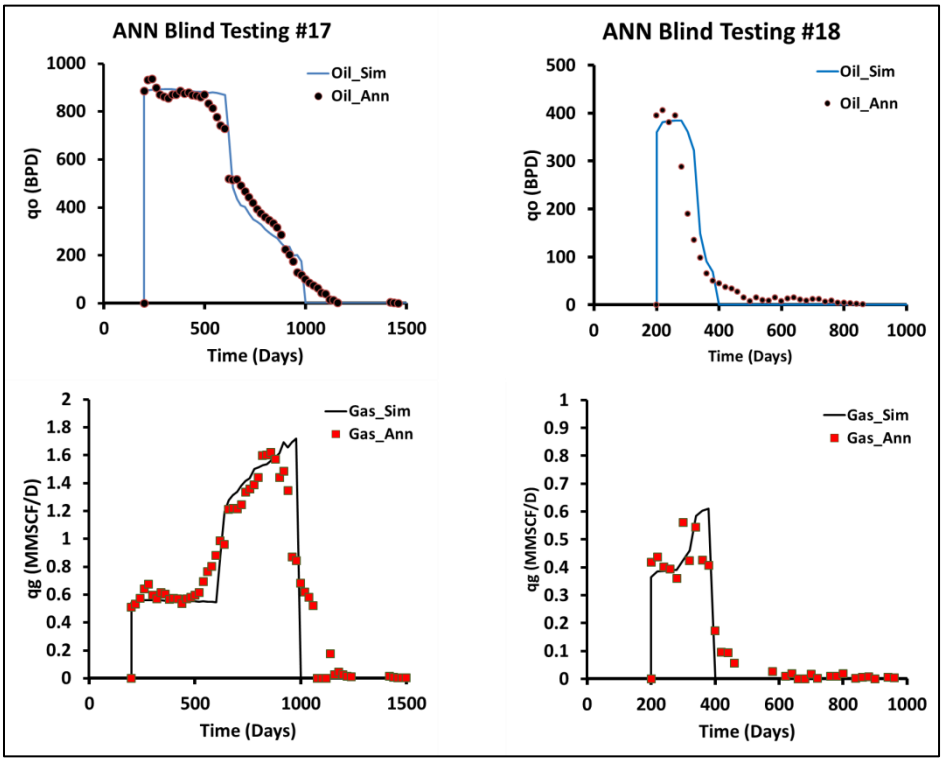

Figure AG- 9: Oil and Gas Production for Blind Test Cases 17 & 18

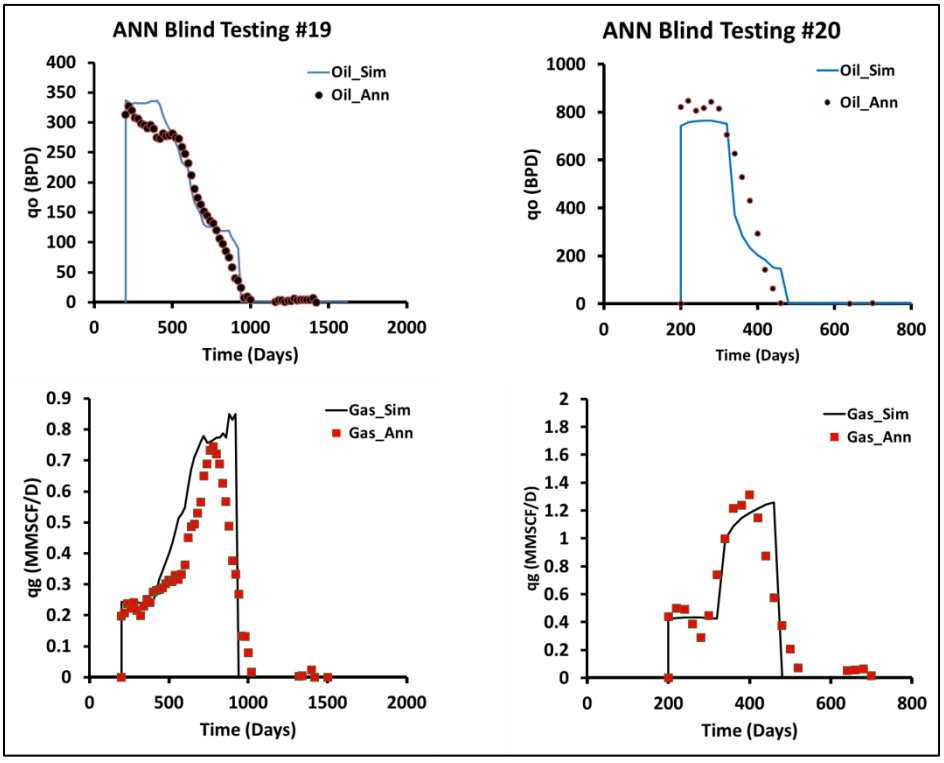

Figure AG- 10: Oil and Gas Production for Blind Test Cases 19 & 20

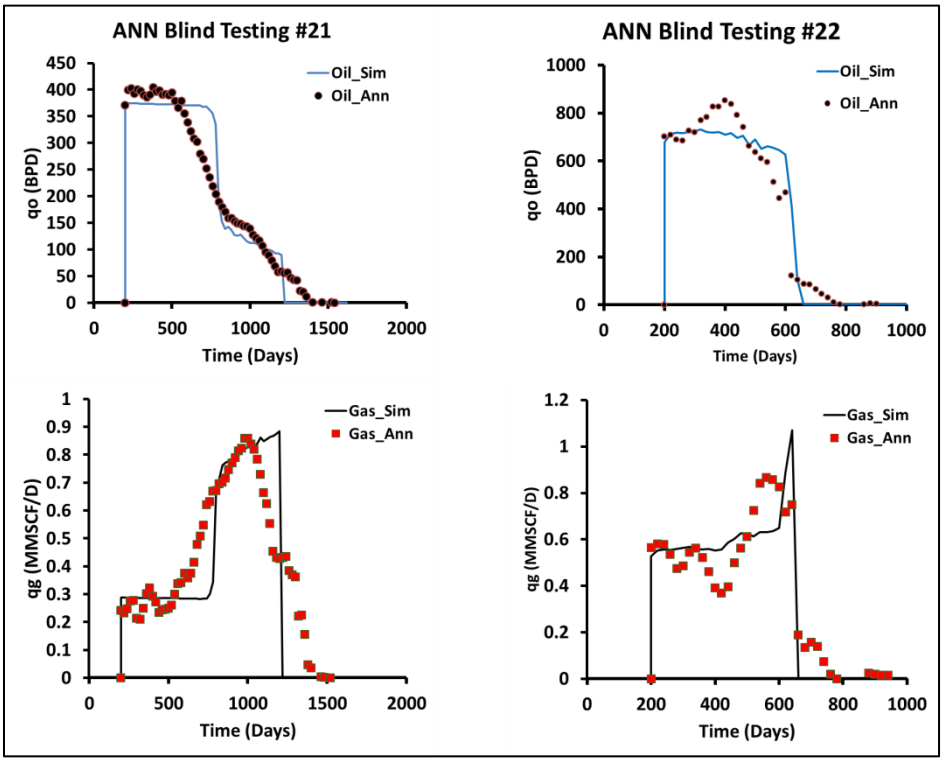

Figure AG- 11: Oil and Gas Production for Blind Test Cases 21 & 22

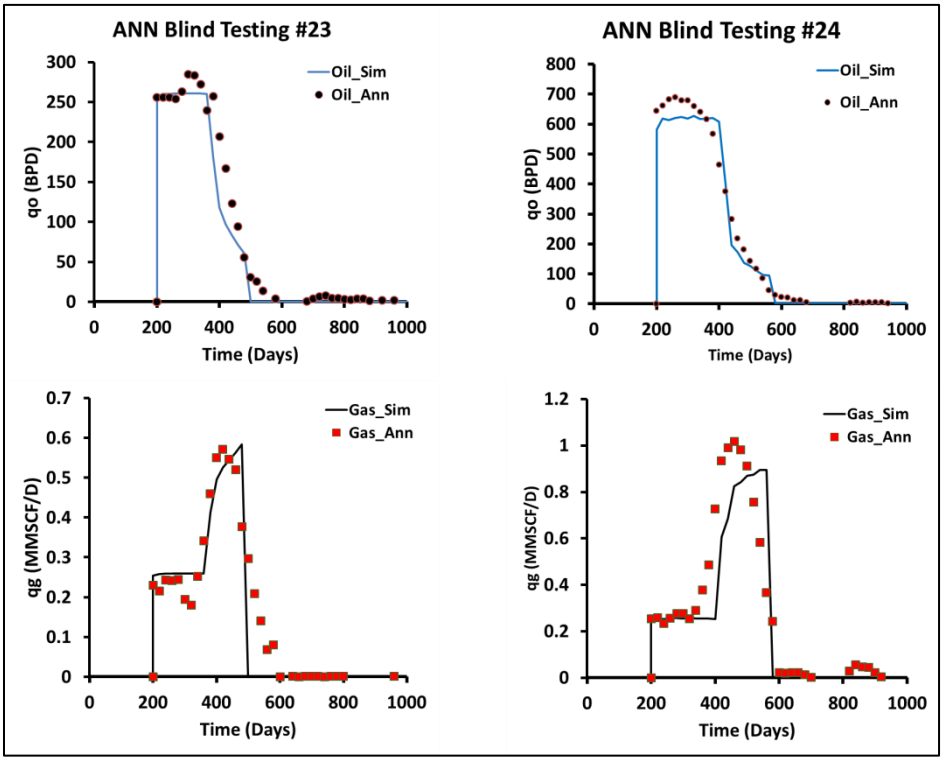

Figure AG- 12: Oil and Gas Production for Blind Test Cases 23 & 24

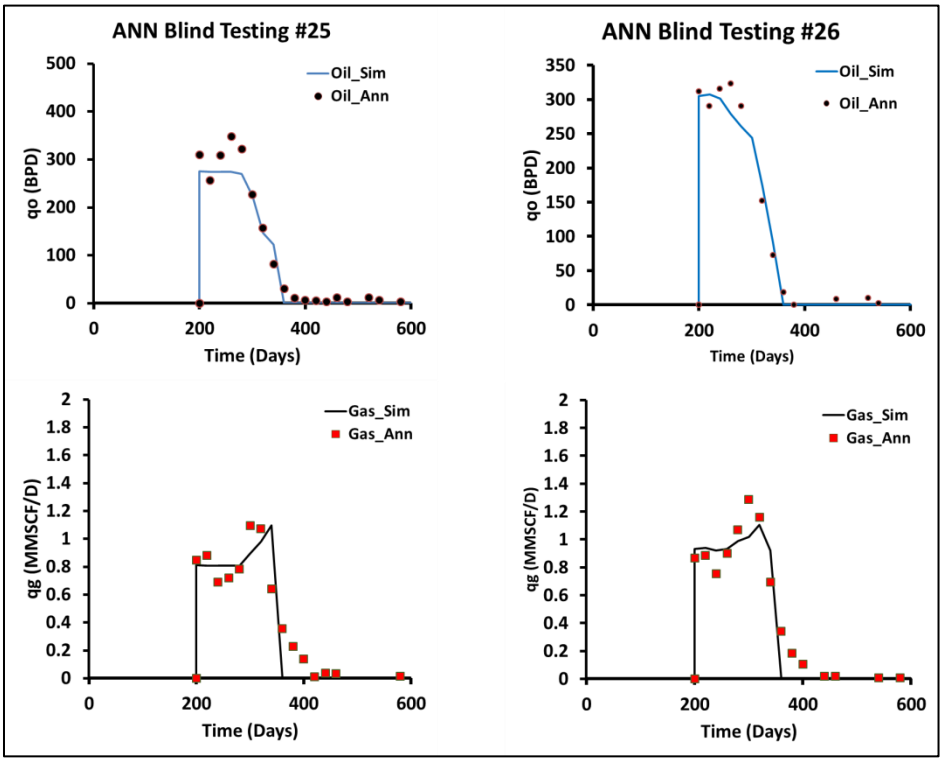

Figure AG- 13: Oil and Gas Production for Blind Test Cases 25 & 26

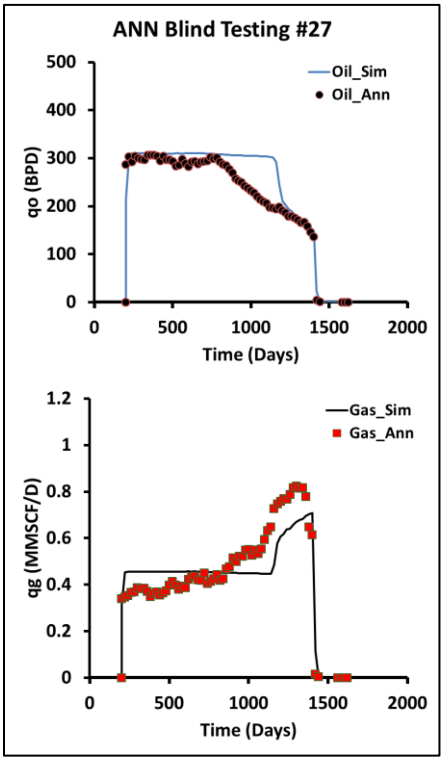

Figure AG- 14: Oil and Gas Production for Blind Test Cases 27

Appendix H: First Inverse ANN Design Blind Testing Cases

Table AH- 1: 1st Inverse Blind Case #1 Output

Blind Test Case 1 Output Comparison		
Property	**Actual**	**ANN**
Frac Perm, md	5,343	4,954
L1 Matrix Perm, md	175	191
L2 Matrix Perm, md	35	45
L1 Thickness, ft	64	60
L2 Thickness, ft	40	34

Table AH- 2: 1st Inverse Blind Case #2 Output

Output Blind Test Case 2 Output Comparison		
Property	**Actual**	**ANN**
Frac Perm, md	9,681	8,063
L1 Matrix Perm, md	109	97
L2 Matrix Perm, md	124	103
L1 Thickness, ft	55	49
L2 Thickness, ft	37	45

Table AH- 3: 1st Inverse Blind Case #3 Output

Blind Test Case 3 Output Comparison		
Property	**Actual**	**ANN**
Frac Perm, md	7,924	8,349
L1 Matrix Perm, md	33	45
L2 Matrix Perm, md	165	140
L1 Thickness, ft	32	40
L2 Thickness, ft	38	33

Table AH- 4: 1st Inverse Blind Case #4 Output

Blind Test Case 4 Output Comparison		
Property	**Actual**	**ANN**
Frac Perm, md	6,508	7,117
L1 Matrix Perm, md	196	174
L2 Matrix Perm, md	196	182
L1 Thickness, ft	46	40
L2 Thickness, ft	23	30

Table AH- 5: 1st Inverse Blind Case #5 Output

Blind Test Case 5 Output Comparison		
Property	**Actual**	**ANN**
Frac Perm, md	6,221	5,486
L1 Matrix Perm, md	133	127
L2 Matrix Perm, md	87	103
L1 Thickness, ft	45	41
L2 Thickness, ft	23	30

Table AH- 6: 1st Inverse Blind Case #6 Output

Blind Test Case 6 Output Comparison		
Property	**Actual**	**ANN**
Frac Perm, md	1,232	1,414
L1 Matrix Perm, md	146	120
L2 Matrix Perm, md	115	107
L1 Thickness, ft	46	49
L2 Thickness, ft	52	50

Table AH- 7: 1st Inverse Blind Case #7 Output

Blind Test Case 7 Output Comparison		
Property	**Actual**	**ANN**
Frac Perm, md	5,498	5,401
L1 Matrix Perm, md	83	115
L2 Matrix Perm, md	167	143
L1 Thickness, ft	51	57
L2 Thickness, ft	62	59

Table AH- 8: 1st Inverse Blind Case #8 Output

Blind Test Case 8 Output Comparison		
Property	**Actual**	**ANN**
Frac Perm, md	8,303	7,010
L1 Matrix Perm, md	91	110
L2 Matrix Perm, md	59	70
L1 Thickness, ft	48	47
L2 Thickness, ft	58	47

Table AH- 9: 1st Inverse Blind Case #9 Output

Blind Test Case 9 Output Comparison		
Property	**Actual**	**ANN**
Frac Perm, md	7,287	6,507
L1 Matrix Perm, md	182	165
L2 Matrix Perm, md	182	173
L1 Thickness, ft	50	46
L2 Thickness, ft	40	49

Table AH- 10: 1st Inverse Blind Case #10 Output

Blind Test Case 10 Output Comparison		
Property	**Actual**	**ANN**
Frac Perm, md	5,713	5,285
L1 Matrix Perm, md	140	126
L2 Matrix Perm, md	102	109
L1 Thickness, ft	69	55
L2 Thickness, ft	44	46

Appendix I: Second Inverse ANN Design Blind Testing Cases

Table AI- 1: Blind Test # 1 and Blind Test # 2 for 2nd Inverse ANN

	Blind T # 1		Blind T # 2	
	Actual Data	ANN Data	Actual Data	ANN Data
Cum Gas Inj., MMSCF	57.58	57.35	10.00	10.15
Injection Duration, D	46.00	37.58	15.00	12.69
Well Spacing, Acres	59.00	64.89	37.00	32.74

Table AI- 2: Blind Test # 3 and Blind Test # 4 for 2nd Inverse ANN

	Blind T # 3		Blind T # 4	
	Actual Data	ANN Data	Actual Data	ANN Data
Cum Gas Inj., MMSCF	8.14	7.52	27.60	27.97
Injection Duration, D	5.00	3.091	14.00	16.93
Well Spacing, Acres	27.00	32.34	34.00	40.72

Table AI- 3: Blind Test # 5 and Blind Test # 6 for 2nd Inverse ANN

	Blind T # 5		Blind T # 6	
	Actual Data	ANN Data	Actual Data	ANN Data
Cum Gas Inj., MMSCF	8.79	13.13	30.81	32.66
Injection Duration, D	6.00	12.51	18.00	21.74
Well Spacing, Acres	31.00	29.88	45.00	50.38

Table AI- 4: Blind Test # 7 and Blind Test # 7 for 2nd Inverse ANN

	Blind T # 7		Blind T # 8	
	Actual Data	ANN Data	Actual Data	ANN Data
Cum Gas Inj., MMSCF	35.74	33.38	141.84	122.47
Injection Duration, D	31.00	42.28	72.00	61.07
Well Spacing, Acres	59.00	54.20	23.00	16.96

Table AI- 5: Blind Test # 9 and Blind Test # 10 for 2nd Inverse ANN

	Blind T # 9		Blind T # 10	
	Actual Data	ANN Data	Actual Data	ANN Data
Cum Gas Inj., MMSCF	26.85	24.32	73.28	65.67
Injection Duration, D	39.00	34.67	45.00	53.16
Well Spacing, Acres	45.00	48.52	56.00	61.11

Table AI- 6: Blind Test # 11 and Blind Test # 12 for 2nd Inverse ANN

	Blind T # 11		Blind T # 12	
	Actual Data	ANN Data	Actual Data	ANN Data
Cum Gas Inj., MMSCF	15.61	15.52	34.31	33.80
Injection Duration, D	11.00	10.13	27.00	24.19
Well Spacing, Acres	20.00	22.01	61.00	47.22

Table AI- 7: Blind Test # 13 and Blind Test # 14 for 2nd Inverse ANN

	Blind T # 13		Blind T # 14	
	Actual Data	ANN Data	Actual Data	ANN Data
Cum Gas Inj., MMSCF	38.27	35.68	28.76	28.75
Injection Duration, D	51.00	45.37	15.00	18.95
Well Spacing, Acres	67.00	54.70	54.00	58.80

Table AI- 8: Blind Test # 15 and Blind Test # 16 for 2nd Inverse ANN

	Blind T # 15		Blind T # 16	
	Actual Data	ANN Data	Actual Data	ANN Data
Cum Gas Inj., MMSCF	48.46	49.64	76.78	73.68
Injection Duration, D	70.00	65.04	40.00	34.57
Well Spacing, Acres	53.00	55.18	68.00	67.48

Table AI- 9: Blind Test # 17 and Blind Test # 18 for 2nd Inverse ANN

	Blind T # 17		Blind T # 18	
	Actual Data	ANN Data	Actual Data	ANN Data
Cum Gas Inj., MMSCF	6.426	6.36	39.39	41.342
Injection Duration, D	10.00	7.91	37.00	29.199
Well Spacing, Acres	36.00	36.01	49.00	51.893

Table AI- 10: Blind Test # 19 and Blind Test # 20 for 2nd Inverse ANN

	Blind T # 19		Blind T # 20	
	Actual Data	ANN Data	Actual Data	ANN Data
Cum Gas Inj., MMSCF	19.74	18.461	54.89	51.369
Injection Duration, D	14.00	18.191	51.00	56.181
Well Spacing, Acres	47.00	49.974	54.00	55.507

VITA

Hassan H. Hamam was born in Jeddah, Saudi Arabia in 1982. He joined Saudi Aramco after high school as part of their exceptional College Preparatory Program (CPP) in 2000. He was then sponsored to get his Bachelor degree in Petroleum and Natural Gas Engineering from West Virginia University. In May 2005, he earned his Bachelor of Science in Petroleum and Natural Gas Engineering. Since getting his Bachelor degree, Hassan held various positions within Saudi Aramco in Dhahran, Saudi Arabia.

In 2008, Hassan was awarded a scholarship by Saudi Aramco to pursue his Master's degree. He earned his Masters of Science in Petroleum and Natural Gas Engineering from Texas A&M University in August 2010. After that, He was recruited to join Aramco's flagship center, the Event Solution Center for Integrated Reservoir Studies. He worked with various experts from all disciplines doing intensive integrated studies. In 2011, he joined Aramco's Technical Development Program (TDP) to become a specialist in real-time simulation.

In 2012, Hassan was awarded another scholarship by Saudi Aramco for his PhD Degree. Since then, he has been a PhD candidate in the Petroleum and Natural Gas Engineering program and is expected to graduate in summer 2016.

Hassan's work experience includes reservoir engineering, production engineering, and reservoir description as well as integrated studies and working with teams of various specialties. He can be reached at Hass1402@gmail.com